CSM Report MT-CWJCR-098-008

Final Progress Report

Contract DAAH04-94-G-0281

Agency Report Number : 32823-MS

High Strength Steel Weldment Reliability : Weld Metal Hydrogen Trapping

submitted to : United States Army Research Office
Materials Science Division
P.O. Box 12211
Research Triangle Park, NC 27709-2211

submitted by : David L. Olson
Principal Investigator
Center for Welding, Joining, and Coating Research
Colorado School of Mines
Golden, CO 80401-1887

February 1998

CSM

CENTER FOR WELDING AND JOINING RESEARCH

Colorado School of Mines
Golden, Colorado 80401

SF 298 MASTER COPY KEEP THIS COPY FOR REPRODUCTION PURPOSES

REPORT DOCUMENTATION PAGE

Form Approved OMB NO. 0704-0188

1. AGENCY USE ONLY *(Leave blank)*	2. REPORT DATE	3. REPORT TYPE AND DATES COVERED
	3/11/98	Final Progress Report :8/1/94-12/31/97

4. TITLE AND SUBTITLE

High Strength Steel Weldment Reliability :
Weld Metal Hydrogen Trapping

5. FUNDING NUMBERS

DAAH04-94-G-0281

6. AUTHOR(S)

David L. Olson

7. PERFORMING ORGANIZATION NAMES(S) AND ADDRESS(ES)

Colorado School of Mines
Center for Welding, Joining, and Coatings Research
Metallurgical and Materials Engineering Dept.
Golden, CO 80401-1887

8. PERFORMING ORGANIZATION REPORT NUMBER

9. SPONSORING / MONITORING AGENCY NAME(S) AND ADDRESS(ES)

U.S. Army Research Office
P.O. Box 12211
Research Triangle Park, NC 27709-2211

10. SPONSORING / MONITORING AGENCY REPORT NUMBER

ARO 32823.6-MS

11. SUPPLEMENTARY NOTES

The views, opinions and/or findings contained in this report are those of the author(s) and should not be construed as an official Department of the Army position, policy or decision, unless so designated by other documentation.

12a. DISTRIBUTION / AVAILABILITY STATEMENT

Approved for public release; distribution unlimited.

12 b. DISTRIBUTION CODE

13. ABSTRACT *(Maximum 200 words)*

The potential use of weld metal hydrogen getters (traps) to increase the reliability of high strength steel weldments was investigated. This research aimed to establish a fundamental understanding of the trapping mechanisms in weld metal and to evaluate the effectiveness of irreversible traps introduced by specific alloying additions, in comparison to the reversible hydrogen trapping by weld metal constituents and solidification substructure. The work involved : (1) fundamental calculations to select most promising elemental trapping additions to be made through the welding consumable, (2) evaluations of hydrogen-contaminated welds to determine the relative amount of hydrogen trapping, (3) evaluations of the influence of welding parameters and practice (multiple-pass welding) on the effective use of weld metal hydrogen gettering, and (4) demonstrations of the potential of using gettering additions to welding consumables to control weld metal hydrogen and thus reduce susceptibility to cold cracking in high strength steel weldments.

14. SUBJECT TERMS

15. NUMBER IF PAGES

16. PRICE CODE

17. SECURITY CLASSIFICATION OR REPORT	18. SECURITY CLASSIFICATION OF THIS PAGE	19. SECURITY CLASSIFICATION OF ABSTRACT	20. LIMITATION OF ABSTRACT
UNCLASSIFIED	UNCLASSIFIED	UNCLASSIFIED	UL

Table of Content

I. Statement of the Problem Studied

This research project focused on better understanding of hydrogen trapping phenomena and applying weld metal hydrogen trapping to improve the resistance to hydrogen cracking in welding of high strength steels. Hydrogen cracking in high strength steel is a crucial problem, which severely limits the reliability and the life-time of many welded structures. The goal of this research is to develop welding consumables which contain trap additions to minimize the content and to control the distribution of diffusible hydrogen; the two requirements which are necessary to prevent hydrogen cracking in high strength steel welding.

Common practices to prevent hydrogen cracking in steel weldments include pre- or post-weld heat treatment, the use of non-cellulosic electrodes with proper baking, and edge preparation. These practices are applied to assure that the hydrogen concentration is below the critical concentration for hydrogen cracking, especially at temperatures below 100° C. Particularly for high strength steel weldments, high concentration of hydrogen can be localized in region of stress concentration. This localized hydrogen concentration can easily reach the critical concentration for hydrogen cracking, even though the nominal concentration of the weld joint is low below 2 ml H_2/100g-metal. Such a condition requires a very low and impractical allowable contamination of hydrogen in the welding environment. It has also been observed that the pre-heat treatments and improper post-weld heat treatments enhance the development of localization of hydrogen in high strength steel welds. Therefore, new solutions to hydrogen cracking in high strength steel welding must involve a substitution to the heat treatment practices and must offer a greater tolerance for hydrogen contamination in the environment.

Hydrogen trapping offers a solution to the prevention of hydrogen cracking through an accelerated reduction of diffusible hydrogen during welding cooling cycle. The significant of this trapping mechanism is that diffusible hydrogen can be reduced without the need of an extensive heat treatment. Strong and finely distributed hydrogen traps will capture hydrogen atoms during welding cooling cycle, giving a much less chance for

hydrogen to migrate and accumulate in region of stress concentrations. In the presence of strong traps, the nominal content of residual hydrogen may be higher than that content without traps. However, hydrogen concentration will be much more uniformly distributed and still below the critical diffusible hydrogen concentration for hydrogen cracking. Such a condition, that implies a more tolerance to hydrogen contamination in the welding environment, adds to the advantage of applying hydrogen traps in hydrogen management of high strength steel welding.

II. Summary of the Most Important Results

A comprehensive literature review about hydrogen trapping in steel weldment has led to a compilation of very useful information about the microstructural dependence of hydrogen cracking in general and about prospective hydrogen traps for high strength steel welding application in particular. This literature review has been finalized and is being submitted for publication in the Journal of International Materials Review (see Appendix 1).

Also included in this review paper, a summary of electronic structure calculations that have been done to evaluate several prospective hydrogen traps in high strength steel. These selected traps were ranked based on their values of binding energy with hydrogen atoms. By electronic structure principles, the binding energy is calculated from the integral reduction of free energy of the steel-trap-hydrogen system as the hydrogen atom incrementally approaches a trap site. Using this criterion, Ce_2O_3 was predicted to be the most effective trap, followed by TiC, Y_2O_3, VC, NbC, and finally Mo_2C.

In accordance with the literature survey completed in this study, rare earth metals have been recognized as the most potential elements to form strong hydrogen traps in steel. Neodymium and yttrium have been selected as the trapping additions to be introduced to the weld pool during the gas metal arc (GMA) welding process. These additions were introduced as $Fe_{17}Nd_2$ and Fe_2Y compounds, inserted as powder ingredients in filled metal-cored GMA wire electrodes. The production of these ferroaddition powders were

made at CSM. Both of the trap additions have demonstrated a significant reduction of diffusible hydrogen content relative to a reference wire electrode that does not contain such additions. This result has been presented in the annual AWS convention 1997, in Los Angeles, and is shown in Figure 1.

In Figure 1, the trap additions were shown to perform consistently at different levels of hydrogen contamination in the GMA welding (argon) shielding gas. With the presence of trap additions in the weld metal, as much as 600 ppm, more than 50 percent reduction of diffusible hydrogen has been achieved. The most promising result, shown in this figure, is the reduction from 4.5 to 1.5 ml H_2/100 g-metal, when welding with 0.1 pct. hydrogen in the shielding gas. A further investigation, which is described in the next paragraph, found that both traps, associated with neodymium and yttrium, have high values of binding energy. However, yttrium was found to yield higher recovery during the arc welding process than that recovery of neodymium (Figure 2). Also, since yttrium forms a richer yttrium compound with iron than neodymium does, higher density of trap addition can be easily inserted to the wire electrode if the ingredient is Fe_2Y.

A criteria of designing a proper addition of hydrogen traps through welding consumables has been formulated through the use of numerical calculation of hydrogen diffusion in steel weld metal containing traps. These calculations predict the amount of diffusible hydrogen as a function of temperature during welding cooling cycle. Proper trapping additions should reduce the amount of diffusible hydrogen rapid enough so that the hydrogen levels at hydrogen cracking susceptible temperature (100-300° C) is below the critical limit. These calculations demonstrated that this requirement can be achieved with a proper combination of several factors such as the trap-hydrogen binding energy, martensite start temperature, trap concentration, and welding cooling rate. The preferred trap addition, according to this model, should have a high binding energy. High binding energy is necessary to provide accelerated reduction of diffusible hydrogen, especially in steel with low martensite start temperature, as well as to minimize release of hydrogen from the trap sites during multi-pass welding (see Appendix 2). With a more accurate data on the characteristic of specific trap additions, this model will be used to determine

the optimum amounts of trap additions in welding consumables and the corresponding conditions in welding parameters and practices for high strength steel.

Characteristic of specific trap additions has been assessed through the use of the hydrogen thermal desorption analysis. This experimental set-up, which comprises a special temperature ramping – gas chromatographic system, analyzes the release of hydrogen from various trap sites during a constant rate heating of the weld samples. The methodology applied in this analysis provides an easy way to evaluate a specific trap without interference from other traps coexisting in the weld samples. The results of this analysis, which is the hydrogen evolution rate as a function of temperature, can be curve-fitted for assessment of a specific trap characteristics. As shown in Figure 3, the hydrogen evolution of iron weld metal with neodymium additions was contrasted with an iron weld metal free of strong traps. The different between the two evolution curves is that the presence of a hydrogen evolution peak around 873 K from the neodymium containing sample which is not present in the reference sample. This high temperature peak indicates the presence of high binding energy traps associated with neodymium. Similar results for yttrium additions to iron weld metal is also shown in Figure 4. Hydrogen evolution peaks in Figure 4 occurred at lower temperatures than those peaks in Figure 3 because of the slower heating rate applied when collecting data for Figure 4. By using different heating rate the binding energy for a specific hydrogen trap can be determined by the Kessinger's analysis (see Appendix 3).

Results from the hydrogen desorption analysis, especially Figure 3, also showed that, during re-heating, the strong trap sites impeded hydrogen release from weak trap sites such as grain boundaries, while the strong traps themselves released hydrogen only at high temperature ranges. These effects are beneficial in multi-pass welding. Further, the amount of hydrogen released from strong traps containing weld metal is higher than that sample free of strong traps. This observation verifies that the reduction of diffusible hydrogen shown in Figure 1 is due to the presence of strong trap addition in the weld metal.

Focus officer progress report for the TTCP project on hydrogen management in steel weldment for defense application is included in the appendices (see appendix IV). Next TTCP workshop will be held from 6th to 8th October 1998, at CANMET, Ottawa, Ontario, Canada.

III. Figures

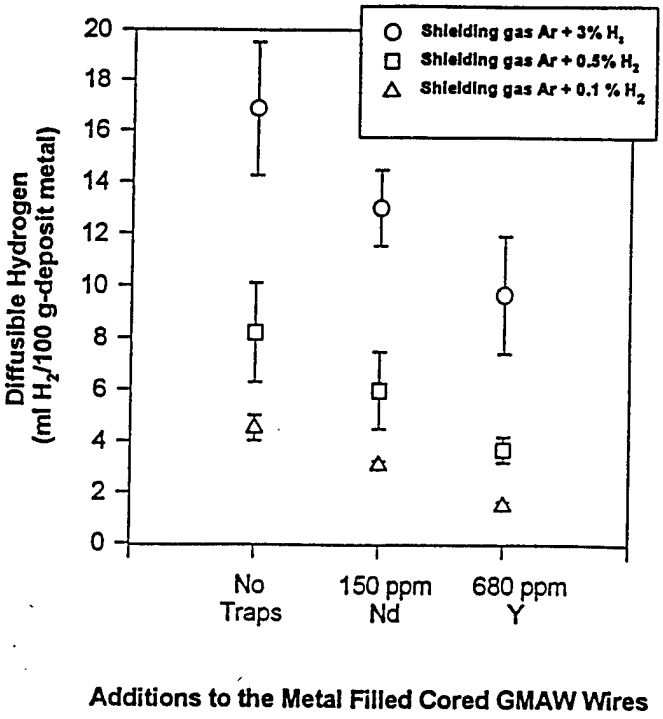

Figure 1. The effect of trap additions to the amount of diffusible hydrogen of weld samples welded with GMA welding process at nominal heat input of 1.5 kJ/mm.

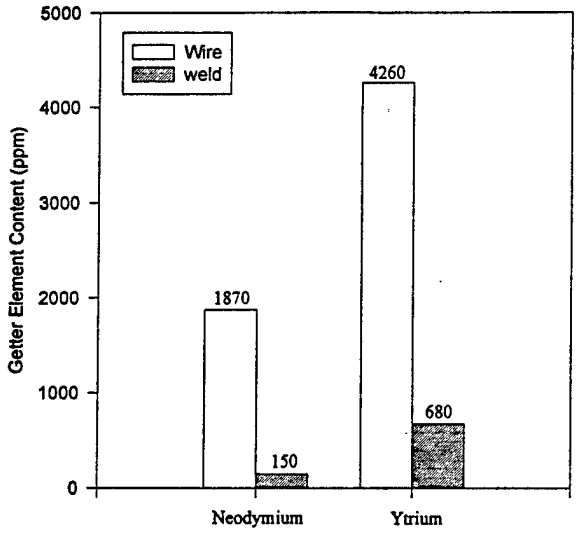

Figure 2. The content of trap additions in the filled metal cored wire (white) and in the weld sample (grey).

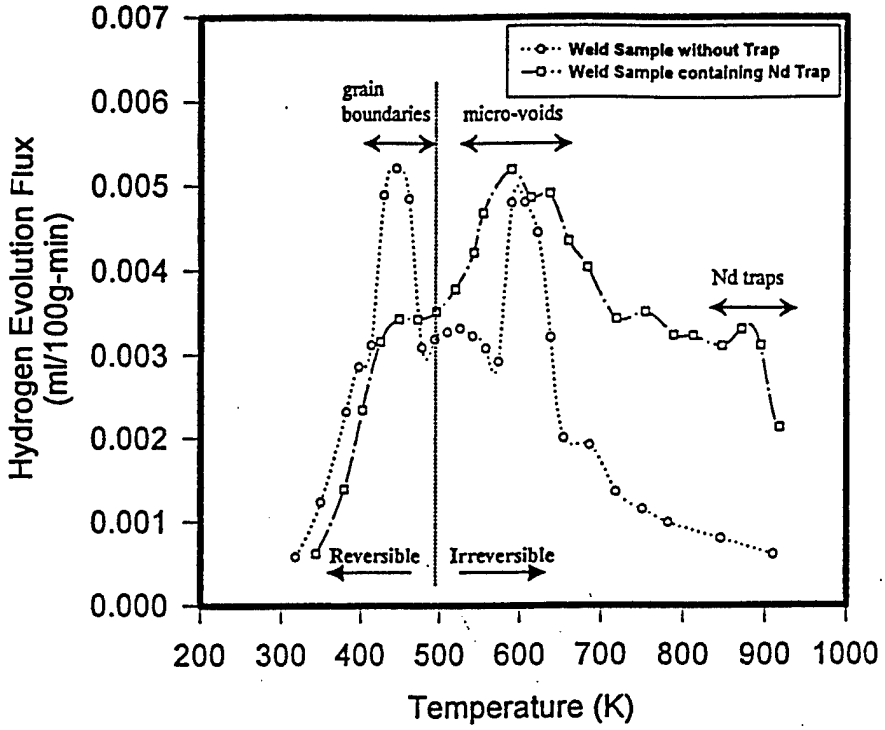

Figure 3. Hydrogen evolution curves from non-isothermal analysis of weld sample free of deep traps and weld sample containing neodymium deep traps. The peak at 373 K is the hydrogen released from grain boundaries, at 575 K from micro-voids and at 873 K from neodymium associated trap sites

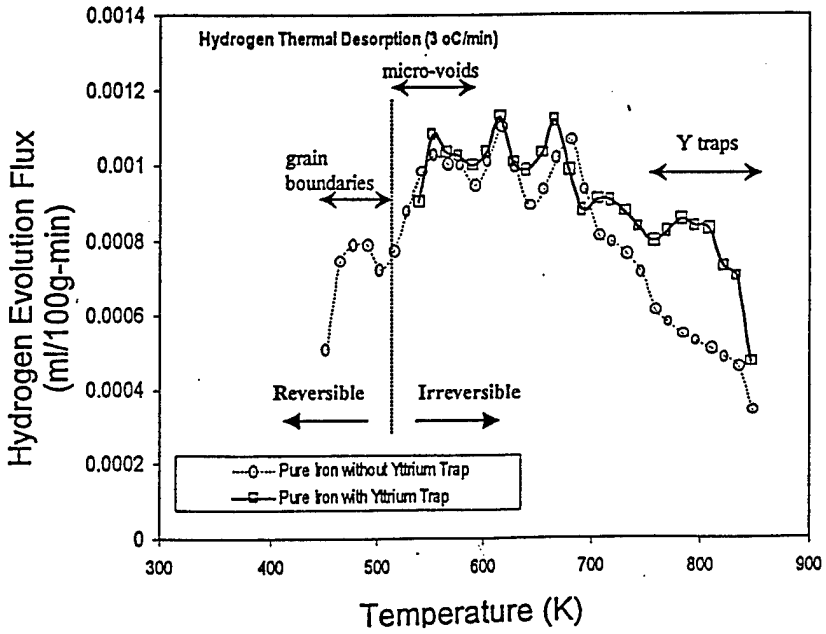

Figure 4. Hydrogen evolution curves from non-isothermal analysis of weld sample free of deep traps and weld sample containing yttrium deep traps. The peak at 373 K is the hydrogen released from grain boundaries, at 575 K from micro-voids and at 873 K from yttrium associated trap sites.

IV. List of Publications, Technical Reports, and Invited Presentations :

1. I. Maroef, D.L. Olson, M. Eberhart, G.R. Edwards, and C. Lensing: "Weld Metal Hydrogen Trapping", is being submitted for publication in International Materials Review(1998).
2. D.L. Olson, I. Maroef, C. Lensing, R.D. Smith, W.W. Wang, S. Liu, T. Wildeman, and M. Eberhart: "Hydrogen Management in High Strength Steel Weldments", in Hydrogen Management in Steel Weldments (ed. J.L. Davidson and D.L. Olson), Proc. of Joint Sem., Oct 1996, DSTO Australia and WTIA, pp. 1-19 (1996).
3. I. Maroef, D.L. Olson, and M. Eberhart: "Weld Metal Hydrogen Trapping", presentation in the AWS Annual Meeting, paper 14B, April 1996, Chicago, IL (1996).
4. C.A. Lensing, I. Maroef, and D.L. Olson: "Hydrogen Trapping in Ferrous Weld Metal", presentation in the AWS Annual Meeting, paper 24A, April 1997, Los Angelos, CA (1997).
5. D.L. Olson : "Application of Metallurgical Concept to Develop Advanced High Strength Steel Welding Consumables", keynote paper, published abstract of the 8th Israeli Metallurgical Conference, March 18th 1997, Beer Shiva, Israel (1997).
6. I. Maroef, C.A. Lensing, and D.L. Olson:"Evaluation of Hydrogen Trapping for Hydrogen Management in Ferrous Alloy Welding", to be presented in the AWS Annual Meeting, paper 5C, April 1997, Detroit, MI (1997).
7. I. Maroef, D.L. Olson, and G.R. Edward: "Hydrogen Assisted Cracking in High Strength Steel Weldments", to be presented in the Int. Conf. of 'Welding and Related Technologies for the XXIth Century' Nov. 1998, Kiev, Ukraine (1998).
8. D.L. Olson : "Hydrogen Management in Steel Welding", Monterray Tech., 20th March 1997, Monterray, Mexico (1997).
9. J.L. Davidson and D.L. Olson : editors "Hydrogen Management in Steel Weldments", pp 1-181, ISBN 0-7311-0809-4, Conf. Proc. (sponsored by US Army Research Office), WTIA, Brighton, Australia (1997).
10. D.L. Olson : "Use of Hydrogen Traps for Hydrogen Management in Steel", US Army Benet Laboratories Seminar, 9th Oct. 1997, Watervretet, NY (1997)

V. List of Participating Personel :

1. Prof. David. L. Olson, Principal Investigator
2. Prof. Mark Eberhart, Research Scientist
3. Iman Maroef, Ph.D. Student

Appendix I

Draft of the Manuscript for Publication

in

the Journal of International Materials Review

"Weld Metal Hydrogen Trapping".

WELD METAL HYDROGEN TRAPPING

I. Maroef, D.L. Olson, M. Eberhart, G.R. Edwards, and C. Lensing
Center for Welding, Joining, and Coating Research
Colorado School of Mines
Golden, Colorado 80401-1887
USA

ABSTRACT

Review of hydrogen trapping in steel will be given. Effectiveness of hydrogen trapping through selective alloying to reduce hydrogen cracking susceptibility will be evaluated. The relationship of weld metal microstructure and interstitial contents on effective introduction of hydrogen trapping elements will be discussed.

1. INTRODUCTION

Common practices to prevent hydrogen cracking in high strength steel weldments include pre- or post-weld heat treatment, the use of non-cellulosic electrodes with proper baking, and edge preparation. Heat treatment has been necessary to control the welding cooling rate to allow for sufficient hydrogen removal as well as to control the heat affected zone (HAZ) hardness. The higher the strength of the steel, the lower the acceptable weld hydrogen content, even to levels as low as one to two ml H_2/100 g deposit metal [1,2]. With proper selection and use of welding consumables, a minimal hydrogen content can be introduced to the weld pools. However, non-uniform distributions of hydrogen in weldment have been found detrimental, especially for welds requiring very low acceptable hydrogen content [3]. This situation will become a more crucial problem with the welding of ever higher strength steels.

Non-uniform hydrogen distribution across the weldment can result from poorly matched welding consumables and base metal compositions [4]. Stress-induced hydrogen diffusion and hydrogen transport by dislocation sweeping are also factors generally considered to be responsible for localized accumulation of hydrogen at stress concentration regions [3,5]. Dislocation sweeping in weld joints will be operative if the hydrogen cracking mechanism is dominated by localized plasticity [6]. Through implant tests of high strength steel, localized plasticity in the form of microvoids has been shown to occur by Gedeon and Eagar [7].

Recent scientific approaches supported by FEM calculation have made it possible to predict the proper heat treatments that can prevent an undesirable hydrogen distribution in critical weld joints [8]. However, such methodologies require costly testing programs and tight temperature controls as well as control of welding parameters. Such controls are frequently found to be impractical and complicated. Therefore, new approaches to hydrogen management in steel welding, based on more fundamental metallurgical understanding and predictions, need to be investigated.

Approaches for mitigating hydrogen cracking by metallurgical modification, including alloy additions, have been discussed [9,10]. One of these approaches is to

employ hydrogen trap sites in the weld metal. The purpose of introducing hydrogen trap sites is to force a redistribution of absorbed hydrogen, partitioning it between lattice sites and trap sites, so that the critical hydrogen concentration required to induce interfacial decohesion at potential crack initiation sites cannot readily be obtained. In addition, the presence of deep trap sites will minimize the operation of dislocation sweeping by reducing the probability of hydrogen-dislocation interaction, which is the origin of hydrogen induced microplasticity observed in steel. Hydrogen atoms which occupy interstitial sites are generally termed diffusible hydrogen atoms. They are considered detrimental because they have much more chance to travel and accumulate at any region of stress concentration than those hydrogen atoms trapped in deep trap sites. This review addresses the feasibility of using weld metal hydrogen trapping as a means to assist in hydrogen management in high strength steel welds, and thus reduce the susceptibility to hydrogen cracking.

1.1. Hydrogen Assisted Cracking in High Strength Steel

Hydrogen assisted cracking (HAC) is defined as the hydrogen-induced reduction of the fracture toughness of a metallic alloy or steel [11]. It is often manifested by the delayed failure of steels, pre-charged with hydrogen, and can even occur under circumstances where the fracture surface shows no evidence of brittleness. The nominal fracture stresses are usually low, and often less than stresses experienced by the metal at various times before failure occurs [12].

Phenomenology of delayed failure in high strength steels is summarized in Figure 1 [13]. The notch tensile strength (upper critical stress (UCS)) is less than a normal value and directly reflects the loss of ductility due to hydrogen. There is also a lower critical stress (LCS), below which failure does not occur and above which failure occurs after a significant time. This phenomenon is well known as the static fatigue limit. The static fatigue limit is sensitive to hydrogen, in that its value increases with decreasing hydrogen concentration. In addition to sensitivity to hydrogen content, the critical stresses are also found to be a function of the environment, temperature, and microstructure.

Under constant stress loading, the crack initiates once some critical concentration of hydrogen (c_K) has been reached [14]. In an attempt to explain this observation, Troiano [15] suggested that this critical hydrogen concentration corresponded to a critical applied stress that overcomes the hydrogen-degraded cohesive strength of the material at the initiation site. Beachem [16], in his model, suggested an interrelationship between the critical stress intensity factor (K_c), the critical hydrogen content (c_K) and HAC deformation mode, in a microscopically small volume of crack tip material.

As shown in Figure 2, with a constant loading, a material with certain hydrogen content will fracture intergranularly when the stress intensity factor is low. This low stress fracture is the most energetically favorable process because it involves the least amount of plastic deformation. As the stress intensity increases with longer crack length, crack propagation proceeds quasi-cleavage (which require more plastic deformation), followed by microvoid coalescence. Increasing hydrogen content at the crack tip has the effect of decreasing the stress intensity factor necessary for each of these fracture processes to occur. Gedeon and Eagar [7], working to substantiate the Beachem theory for high strength steel welds, showed (Figure 3) that, at high hydrogen concentration, intergranular fracture will still occur during high stress intensity loading. This observation differs slightly from the original Beachem model, where microvoid coalescence was the predicted fracture mode at both high hydrogen concentration and high stress intensity factor.

Investigation of the kinetics of crack growth in high strength steel exposed to hydrogen gas usually reports the velocity – mode I stress intensity ($v - K$) plot as shown in Figure 4 [17–19]. Three-stage log velocity vs. K dependence is generally observed, both for internal hydrogen-induced cracking and for the case where the hydrogen source is external [20]. The onset of stage I, usually characterized by intergranular cracking, effectively defines the environmental threshold stress intensity, K_{th}, which corresponds to the lower critical stress (LCS) in Figure 1. The value of K_{th} for a given steel exposed to gaseous hydrogen at pressure P_{H2} decreases with log P_{H2} [21]. In stage II, the crack growth rates are found to be stable and quite insensitive to stress intensity over a wide range, indicative of an independent rate controlling process [22]. As K approaches the

critical value for failure (K_c), the crack growth velocity v increases rapidly and again becomes dependent on K (stage III). K_c is the fracture toughness or critical stress intensity for initiation of crack propagation in dry air.

The characteristic of hydrogen, which sets it apart from other embrittling elements, is its rapid diffusivity. The diffusion coefficient of hydrogen in iron is several orders of magnitude larger than that of other elements. Consequently, hydrogen transport is a prominent factor of hydrogen-induced crack growth kinetics. The velocity in stage II (Figure 4) varies with temperature as shown in Figure 5. The apparent decline in embrittlement at temperatures above and below 300 K, as characterized by crack growth rates, has been confirmed [23,24]. This decline in crack growth rate is explained by the slow hydrogen diffusion process at low temperatures and by the low hydrogen occupation at stress concentration sites at higher temperatures.

1.2. Proposed Mechanisms of Hydrogen Assisted Cracking

No single theory has been accepted as explaining all hydrogen degradation phenomena. In particular, the mechanisms responsible for hydrogen assisted cracking, HAC, are thought to be different for metals that are hydride formers such as titanium, zirconium, and niobium, as comapred to metals that are non-hydride formers such as aluminum, iron, nickel, and copper [25].

Westlake [26] proposed that cracking in hydride formers proceeds by stress induced hydride formation near the crack tip. In this model, stable hydride precipitates are believed to be induced by the tensile stress field at the crack tip [27] and these hydride precipitates act as embrittling sites. Propagation of cracks is thought to involve repeated formation and breakage of the brittle hydride precipitates [28].

There is no consensus as to the mechanism of HAC in the metals that are not hydride formers. Several authors have reviewed the mechanisms proposed for HAC in the non-hydride formers [6,25,29]. Both experimental and theoretical investigations have been variously interpreted as supporting radically different views of the mechanism thought to be responsible for hydrogen embrittlement. Some investigators have proposed

that hydrogen embrittlement results from hydrogen-induced weakening of metallic bonds at crack tips. Still others have proposed that hydrogen-induced plasticity is the origin of HAC.

Of the many theories advanced as an explanation of hydrogen embrittlement, one of the oldest is the thermodynamically based pressure theory. Here, cracking is attributed to the large internal pressures required to supersaturate a crack tip with hydrogen. The large triaxial stress-state at the tip of growing cracks creates an excess free volume to which hydrogen atoms readily diffuse. For these hydrogen atoms to remain in solution at the crack tips, large internal pressures are thermodynamically required. This mechanism also nicely explains the origins of helium embrittlement and seems to be applicable in low strength steels [30]. However, this mechanism has been questioned as explaining the origins of embrittlement in high strength steels by internal hydrogen charging, especially at low hydrogen gas pressure [31–34].

Petch and Stables [35] proposed that hydrogen, adsorbed on the free surfaces created by crack propagation, reduces the surface energy. Hence, this adsorption decreases the work of fracture and enhances cracking. Although this mechanism may be operating in a few cases, it cannot explain the commonly observed HAC characteristics such as discontinuous crack propagation [29]. Also, it has been wrongly argued that this mechanism cannot explain why other species such as oxygen, which adsorb more strongly than hydrogen, do not embrittle metals [30]. Clearly the effect of oxygen or any other strongly absorbing species could be to stabilize boundaries and crack tips to a greater degree than they stabilize fracture surfaces.

More recently, principles have been developed for the evaluation of impurity segregation effects on cohesion in terms of relative adsorption properties to the interface and the free surfaces created by fracture [36]. These principles attribute HAC to a decrease in the decohesion energy. The decohesion energy γ_{int} is related to the Griffith - like separation of one side of an interface relative to the other in a common notation involving surface and boundary energies ($\gamma_{int} = 2\gamma_s - \gamma_b$). Thus a segregant, hydrogen in particular, will tend to embrittle either by raising the boundary energy (crack tip energy)

or through a lowering of surface energies. Rice, and coworkers have applied these principles to explain hydrogen and temper-embrittlement phenomena in steels [37,38].

Wang has found experimental support for some of these principles in his studies of the interfacial cracking of Fe-3%Si bicrystals [39] designed to test theoretical predictions on the importance of hydrogen mobility. Rice and Wang has also shown that the ductile versus brittle transition of a solid, under hydrogen environment, is controlled by the ductility of the bulk and the cohesion of internal interfaces, $2\gamma_{intf}$ [40]. Competition between the two factors yields a peak in toughness during the experimental measurement of temperature-dependent toughness of Fe-Si alloys charged with hydrogen, as shown in Figure 6. While the toughness of bulk bcc metals increases with increasing temperature, the embrittlement intensity (reduction in toughness caused by hydrogen segregation to internal interfaces), is thought to increase with time and temperature.

To explain this behavior, a model has been proposed to describe the transient nature of hydrogen embrittlement. Susceptibility to hydrogen embrittlement was shown to increase with time and temperature due to the reduction of interfacial cohesion as hydrogen atoms segregate to internal boundaries [41]. This model was developed based on the thermodynamic analysis of Hirth and Rice [42] and the McLean model for kinetics of segregation [43]. An embrittlement intensity factor was calculated (as a function of interfacial free energy and temperature); this factor is shown in Figure 7 to increase with time and temperature.

Still others have proposed that hydrogen atoms act to decrease the cohesive force between metal atoms. These proposals are based on the model of Rice and Thomson in the early 70s to explain the competition between ductile and brittle fracture in general [44]. They suggested that ductile/brittle behavior was determined at the tips of atomically sharp cracks. When a material is subjected to a tensile load, there will be a tensile force acting to extend the crack and a resolved shear stress on planes inclined to the crack tip. Within the Rice and Thomson model, the competition between these two stresses determines whether a material responds in a brittle or ductile fashion. If the bond strength across the crack tip is exceeded before the shear strength of the bond across the shear planes, then the material will fail in a brittle fashion. On the other hand, if the bond

shear strength is reached first, a dislocation will nucleate, blunting the crack tip. Using this general theory for ductile versus brittle response, hydrogen has been seen as inducing brittle behavior by lowering the bond strength at the crack tip. This explanation should be compared to the previous proposed mechanism in which hydrogen was believed to lower the bond energy.

Others have also proposed a bond strength mechanism. Troiano, et. al [45] proposed that hydrogen dissolved in a steel would diffuse into and concentrate in the triaxial tensile stress region ahead of a crack tip, weakening the cohesive force between metal atoms. When a critical combination of stress and hydrogen concentration is reached, nucleation of a microcrack within the plastic enclave occurs. The microcracks then propagate backward to join with the main crack, manifesting themselves as the discontinuous crack propagation that has been demonstrated by resistivity measurements [15]

On the basis of fractographic evidence, Beachem [16] and others have proposed that sufficient concentration of hydrogen dissolved in the lattice just ahead of the crack tip lowers the work required for fracture by enhancing dislocation motion. This phenomena is termed hydrogen enhanced local plasticity (HELP). In iron with sufficient purity, softening behavior has been observed under specific conditions of hydrogen presence, at temperature near and below ambient [46-48]. Several reasons for this softening phenomena have been suggested [47]. A more impressive softening effect caused by hydrogen was demonstrated on single crystal iron whiskers subjected to dynamic hydrogen charging, which is done using cathodically generated hydrogen [49]. Simultaneous straining and hydrogen charging of iron whiskers reduce flow stress at low deformation, and significantly increase strain hardening at large deformation. Moreover, the total elongation at fracture of the hydrogen charged whiskers relative to uncharged ones is considerably increased, as shown in Figure 8. Enhancement of screw dislocation velocity and multiplication of dislocations due to hydrogen have been observed in nickel and iron. Interactions of the generated dislocations may explain the hardening behavior which follow the initial softening [46].

Reduction of flow stress in hydrogen softening of iron has been explained as a result of the enhancement of screw dislocation motion in the presence of hydrogen. Experimentally, this enhancement of screw dislocation velocity has been demonstrated by Birnbaum et. al by their in situ TEM observation of metal deformation [50]. There are two classes of thought regarding softening in iron. First, hydrogen atoms are thought to interact with edge dislocations and to facilitate kink nucleation on screw dislocations [51,52], which in turn enhances screw dislocation motion. Even though this explanation appears to reconcile observations on the influence of hydrogen internal friction experiments [53,54], it is not the only origin of softening because the presence of hydrogen does not affect only the thermal component of flow stress, σ^*, as it would if kink nucleation is enhanced. Some experimental results have shown that reduction of flow stress in the presence of hydrogen is greater than σ^* , which is also accompanied by different strain and orientation dependence than σ^* [49]. The second class of thought explains that segregation of hydrogen atoms to dislocations relaxes the dislocation stress field [55]. This relaxation provides elastic shielding between dislocation elastic centers and reduces the internal stress component of flow stress.

A model for local enhancement of plasticity of hydrogen charged metal has been recently proposed based on the hydrogen shielding effect [56]. This effect is assumed to facilitate dislocation pile-up interactions by the quick climb of edge segments which enables dislocation loops to overcome pile-up barriers. The non-conservative motion of dislocation associated with this process will be accompanied by generation of vacancies, as supported by experimental observation that shows formation of voids along slip bands at the local plastically deformed regions [57].

Softening is not the only consequence of interaction between hydrogen and dislocations. Hardening, or increase in flow stress and strain hardening rate, has also been observed in hydrogen charged iron, and usually occurs at high strain levels following hydrogen-induced softening. Suppression of cross slip of dislocation by hydrogen is suggested as the reason for this behavior [58], a conclusion which is indirectly supported by the planar dislocation pile-ups [59] and thinner slip bands morphologies [60] experimentally observed in pure iron. It was suggested that either the low probability for

a simultaneous jump of hydrogen atoms and dislocations onto another slip plane or the easy formation of kinks on screw dislocations was the possible cause for suppression of dislocation cross slip [49,61].

In the presence of impurities, dislocations interact not only with hydrogen but also with the impurity atoms, resulting in hardening effects. In an alloy system, the softening effect will reappear when the hydrogen concentration exceeds the impurity concentrations so that intrinsic dislocation-hydrogen interaction is re-established. Transition from hardening to softening in iron with lesser purity as the hydrogen fugacity increases was suggested by Kimura et.al. [62] and is schematically presented in Figure 9, which maps the boundary between the mode of hydrogen-dislocation interaction (line A) as well as that of the hydrogen induced damage (line B). Whether hydrogen damage occurs due to hardening or softening depends on the combination of impurity and hydrogen content.

With the seemingly contradictory phenomena observed to accompany HAC, much theoretical effort has been directed toward discriminating between the decohesive energy mechanism and the bond strength mechanism. Among those investigators supporting the decohesive energy mechanism are Olson and Freeman, whose numerous studies [63] show a consistent correlation between embrittling potency and γ_{int}. On the other hand, Eberhart et al. [64] argue that the mechanism for hydrogen embrittlement must lie in changes of bond strength, not work of fracture. They further suggest that if any correlation exists between γ_{int} and brittle behavior, it is the result of a secondary correlation and should not be interpreted as a confirmation of the cohesive energy mechanism.

Eberhart [65,66] has also pointed out that a lowering of bond strength would have the concomitant effect of lowering the energy for dislocation motion. As such, the tendency for hydrogen to embrittle would be determined by the concentration profile of hydrogen along a grain boundary or other virtual fracture surface. If hydrogen were sharply segregated to the boundary, it would act predominantly to decrease the cohesive force across the boundary, manifesting brittle phenomena. Alternatively, a more slowly

varying concentration profile could act to preferentially lower interatomic shear strength and hence lower the barrier to dislocation nucleation and propagation.

Oriani [11] has also suggested that the decohesion and the localized slip model are not fundamentally competitive, but rather complementary, with both models manifesting a somewhat different aspect of the same disturbance of the metallic bond caused by hydrogen. Which aspect is manifested in any experiment probably depends upon the relative mix of Mode I and Mode II loading [67]. If a significant amount of Mode II loading exists, then enhancement by hydrogen of highly localized dislocation production would be significant. That a hydrogen-induced decrease in metallic bond strength also provides an adequate explanation for the observed enhanced dislocation mobility provides a strong argument in favor of this mechanism for HAC.

1.3. Characteristics of HAC in High Strength Steel Welding

Traditionally, hydrogen assisted cracking in steel welding is considered to occur when all the necessary conditions for cracking are fulfilled simultaneously. These conditions encompass the combination of diffusible hydrogen content, restraint stress, hardness or susceptible microstructure, and a temperature ranging between –100 and 100° C [1]. However, hydrogen cracking in high strength steel welding requires further considerations. The high strength level of this class of steel results in high restraint stresses, which are non-uniformly distributed within the weld joint, a condition which requires very low nominal hydrogen content.

The concomitant effect of localized hydrogen concentration and high restraint stress gives rise to crack initiation at regions of stress concentration within the weld joint. Stress concentrations are located at inclusion interfaces, at grain boundaries, and at the weld fusion line. These locations may be either in the heat-affected zone (HAZ) or in the weld metal (WM), depending upon how hydrogen, stress, and hardness are distributed within the weld joints.

Commonly, hydrogen cracking occurs in the heat-affected zone (HAZ). The crack initiates near the fusion zone, at the regions with the highest stress intensity factor.

However, in recent years, the development of cleaner HSLA steels led to HAC in the weld metal, rather than in the HAZ [68]. To explain this situation, the locations of HAC in weld joints have been related to the non-uniformity of both hydrogen and stress distribution, developed during the cooling cycle after welding. Non-uniformity in distributions of hydrogen or stress is usually a result of variations of temperature and composition across the weldment. Graville [72] has modeled the hydrogen transport across a weldment and has shown the possibility of hydrogen localization in the region of the fusion line. Evidence of this non-uniform hydrogen distribution has been shown by Tarlinski [69], using a laser beam spot fusion technique coupled with mass spectrometric analysis of evaporative hydrogen, as shown in Figure 10. This distribution has also been reported by Olson et. al. [10] using laser-induced breakdown spectroscopy (LIBS).

One common case of non-uniform hydrogen distribution across the weldment is the result of unmatching compositions between the weld metal (WM) and the heat-affected zone (HAZ). Poorly matched welding consumables and base metal composition can create this condition. During the cooling cycle of the welding process, austenite-to-martensite phase transformations in the weld metal and in the heat-affected zone do not take place at the same temperature. Hence, within a certain temperature range, hydrogen transport across the weldment proceeds across two different phases. As a result of much slower hydrogen diffusivity in austenite compared to diffusivity in martensite or ferrite [70], a non-uniform distribution of hydrogen across the weldment may result [71,72]. Another cause for such a non-uniform distribution is a difference in thermal history of the weld metal as compared to the heat affected zone.

Wang et.al. [73] calculated the hydrogen concentrations across the weldment to substantiate a conceptual model, introduced by Granjon [71], that describes how the austenite-to-ferrite (or austenite-to-martensite) phase transformation in steel weldments affects the hydrogen distribution. In this study, the location with the highest calculated hydrogen content was compared to the locations of crack sites obtained from hydrogen cracking tests. Two cases are illustrated. First, as shown in Figure 11, the austenite-to-martensite transformation occurs at a higher temperature in the weld metal than in the heat-affected zone. In this situation, diffusible hydrogen accumulates in the heat-affected zone just under the fusion line and, as verified by experimental data, where underbead

cracking occurs in the heat-affected zone. In the alternate situation, shown in Figure 12, the martensite transformation in the heat-affected zone occurs at a higher temperature than in the weld metal. It is possible, in this case, that the major fraction of the initial diffusible hydrogen remains in the weld metal and thus promotes crack initiation in the weld metal. To minimize the susceptibility to HAC, alloying additions to welding consumables must be selected to achieve a martensite start temperature which is slightly higher in the weld metal than that temperature in the heat-affected zone. Satisfying this condition is expected to alleviate the non-uniformity of hydrogen distribution in weldments as well as to facilitate the maximum rate of hydrogen transport away from the weld metal to the base plate.

Alternate hydrogen cracking locations within weldments have also been illustrated by Matsuda et. al. [74]. In their illustrations, the variation of hydrogen concentration with time in the weld metal was assumed to be different from that variation in the HAZ, as shown in Figure 13. This difference may be caused by the difference in the thermal history of the weld metal as compared to that of the heat-affected zone. The corresponding time dependent critical stresses for HAC in both regions are shown in Figure 14. As shown, low weld metal hardness will cause cracking to occur in the heat-affected zone, since the critical stress for HAC in the weld metal will always be higher than the value of stress being applied to the weld joint. On the other hand, for high weld metal hardness, the crack will initiate in the weld metal, since the critical condition for HAC in the weld metal is satisfied before that condition is met in the heat-affected zone.

1.4. Role of Microstructure in HAC : Diffusible Hydrogen and Hydrogen Trapping

The major goal in preventing HAC in high strength steel is to reduce the amount of hydrogen. However, the nature of hydrogen transport, as affected by the variations of chemical composition and stress across the weldment, gives rise to non-uniform hydrogen distribution. The worst situation for HAC occurs when a localized accumulation of hydrogen is located at the weakest microstructural feature in the weld joint. Hence, an understanding of the microstructural dependence of HAC in steel

weldments is necessary to design a weld microstructure that possesses high resistance to hydrogen cracking.

A microstructural dependence of HAC is indicated by the fact that cracks initiate at certain defect interfaces having the lowest critical hydrogen concentration for HAC , c_K . To prevent crack initiation, it is necessary to keep the actual hydrogen concentration residing at the defect interfaces (c_T) lower than their critical hydrogen concentration (c_K). Delayed failure may be experienced when hydrogen atoms diffuse or are transported by other means to these interfaces. For maximum resistance to hydrogen cracking, one would like to keep the diffusible hydrogen (c_L), as low as possible. This situation will help prevent actual hydrogen concentration at defect interfaces from reaching critical values.

By conventional electrochemical permeation techniques, Pressouyre and Faure [75] conducted a quantitative analysis of the critical hydrogen concentration necessary to induce HAC. This technique provided a gradient of total hydrogen content (c_T + c_L) within the sample thickness so that a critical concentration c_K could be deduced for a particular defect from the position of its first crack occurrence. Figure 15 shows the effect of the total hydrogen concentration (c_T + c_L) on the crack occurrence for three kinds of defects with different c_K values. No crack was found in the sample if the actual hydrogen content was below the critical value, as indicated in Figure 15E.

Mitigating hydrogen cracking by alloy additions has been discussed [9]. Briefly, these explanations include :

1) promoting adhesion at solid-solid interfaces by displacing decohesion-enhancing elements and consequently raising the critical hydrogen level c_K,

2) inducing interfacial segregation of elements, which displace hydrogen from interfaces;

3) reducing hydrogen absorption, thereby lowering both the dissolved and segregated hydrogen concentration in the lattice; and

4) employing hydrogen trap sites.

The purpose of introducing hydrogen trap sites is to force a redistribution of absorbed hydrogen, partitioned between lattices sites and trapping sites, so that the critical hydrogen concentration, c_K, required to induce interfacial decohesion is not readily obtained at the same hydrogen fugacity.

By employing other defects that have high c_K values and strong defect-hydrogen interactions, it is possible to minimize the amount of diffusible hydrogen (c_L) in the lattice. These traps are especially beneficial in the presence of stress concentrations, so that localization of hydrogen at low c_K defects can be minimized. The ability to intelligently choose alloying elements requires an understanding about c_K values of various defects and the interaction between defects and hydrogen in term of capturing or releasing hydrogen atoms.

2. HYDROGEN TRAPPING.

In steel, hydrogen is not homogeneously distributed. Hydrogen will be found not only in the host lattice, but also segregated to atomic and microstructural imperfections such as vacancies, solute atoms, dislocations, grain boundaries, voids, and second phase particles. In these localized regions, the mean residence time of a hydrogen atom is considerably longer than in a normal interstitial lattice site. In the extreme case, these regions are sinks which retain the atom even during thermo-mechanical loading. The generic term for this phenomenon is hydrogen trapping and these localized regions are designated as hydrogen trap sites [76,77]..

A prominent effect of hydrogen trapping is to decrease the apparent hydrogen diffusivity [78] in steel at temperatures below 200° C. The ability of a trap site to hold a hydrogen atom is associated with the hydrogen - trap binding energy. A trapped hydrogen atom must acquire an energy substantially greater than the lattice migration energy to escape the trap and to contribute to the measured diffusivity. Since HAC depends on hydrogen diffusivity, hydrogen trapping influences the kinetics of hydrogen embrittlement and may play a beneficial role in hindering the embrittlement mechanism.

The other effect of trapping is to increase the apparent hydrogen solubility. When charged with a fixed external hydrogen chemical potential, the steel will not only absorb hydrogen to fill the interstitial lattice sites, but will also absorb additional hydrogen atoms to occupy the traps. Below the saturation limit, traps may confer some resistance to hydrogen embrittlement through the reduction of diffusible hydrogen. However, when saturated, these traps may prove detrimental because of localized embrittlement at the trap site-lattice interface. Also, saturated traps may release hydrogen atoms during deformation, which in turn raises the concentration of diffusible hydrogen. During the welding process, hydrogen atoms are absorbed, and the weld metal becomes supersaturated with hydrogen during the cooling cycle. If sufficiently large numbers of trap sites are present, the excess hydrogen will fill these sites to a level well below their saturation limit. In this situation, the trap sites are beneficial and should confer a

resistance to hydrogen embrittlement, providing their size and distribution do not otherwise promote fracture.

2.1. Characteristics of Traps

The strength of a trap site, i.e. the fraction of time a hydrogen atom resides in that trap site, depends on the binding energy, E_B, of the hydrogen atom to the trap. To qualitatively describe the strength of a trap site, a single hydrogen-trap interaction may be written as a first-order reaction :

$$[H] + T = H_T$$

where [H] is the diffusible hydrogen concentration, T is the trap site, and H_T is the trapped hydrogen concentration. The energy associated with the reaction is the hydrogen-trap binding energy, E_B. Hydrogen atoms may then be considered as being either released from, or captured by, the trap sites until equilibrium is reached. The kinetics of hydrogen trapping, which involves release from and capture by a trap site, has been derived by McNabb [79] as follows :

$$\frac{\partial \phi}{\partial t} = \kappa c_L (1-\phi) - \rho\phi \qquad (1)$$

where ϕ is the fraction of traps occupied at time t, c_L is the diffusible hydrogen concentration , and κ and ρ are the rate constants for the capture and release of hydrogen, respectively. The ratio of κ to ρ (κ/ρ) is proportional to $exp(E_B/RT)$ [78].

The significance of the McNabb-Foster parameters κ and ρ have been discussed in depth by several authors [80,81]. The release rate constant, ρ, is interpreted to be related to the trap binding energy by [82] :

$$\rho \approx \nu_T . \varphi(Z) . \exp\left[\frac{(-(E_B + E_S))}{kT}\right] \qquad (2)$$

neglecting the entropy factor, which is the order of unity. E_S is the saddle point energy which includes the activation energy for a jump between normal lattice sites, and ν_T is the

vibration frequency of the trapped hydrogen atom. The function $\varphi(Z)$ is given by $\varphi(Z) = (1 - e^{-Z})/Z$, where $Z = \frac{h.\nu_T}{kT}$ and h is Planck's constant.

Oriani [80], by applying the bimolecular theory of Waite [83], assumed a model in which each trap can hold only one hydrogen atom which is trapped when diffusing into a small volume within a distance r_o of an empty trap site. He interpreted the relationship between κ and ρ as $\kappa/\rho = 4\pi.r_o.\lambda^2.\exp(E_B/kT)$, assuming that the vibration frequency of hydrogen at a lattice site, ν_L, is the same as that at a trap site, $\nu_T \approx \nu_L = \sqrt{E_L/2m\lambda^2} \approx 10^{13} s^{-1}$, where m is the mass of hydrogen and λ is the diffusive jump distance. Estimations of the values of κ and ρ from experimental data are limited. From iron-titanium alloys, Pressouyre and Bernstein [84] reported the value of κ to be of the order of 10^{-24} to 10^{-23} cm^3/s.

If E_B is small, the corresponding traps are referred to as reversible traps and can act either as hydrogen sinks, which capture hydrogen atoms from weaker traps, or as sources, which deposit hydrogen atoms to stronger traps. On the other hand, large E_B give rise to traps which are termed irreversible traps. These traps normally will not release hydrogen. Examples of reversible traps in iron-base alloys are titanium atoms, low angle grain boundaries, or dislocations, while examples of irreversible traps are high angle grain boundaries and titanium carbonitride particles [85]. A schematic representation of the two types of traps is shown in Figure 16, where E_{BR} denotes the binding energy of reversible trap and E_{BI} for irreversible ones.

In general, reversible traps have release rate $\rho \neq 0$ and at steady state :

$$\frac{d\phi_\infty}{dt} = 0, \qquad \phi_\infty = \frac{kc_{L\infty}/\rho}{1 + kc_{L\infty}/\rho} \tag{3}$$

where the subscript ∞ indicates steady state. With $\rho \neq 0$, a reversible trap will not be saturated and an equilibrium between reversibly trapped and lattice hydrogen can be assumed. For weak traps ($\kappa/\rho << 1$), the equilibrium fraction of occupation becomes $\phi_\infty^R = kc_{L\infty}/\rho$. A reversible trap can approach saturation ($\phi_\infty^R \approx 1$) only if $c_{L\infty}$ is very

large. On the other hand, irreversible traps, given sufficient time and hydrogen content, will always reach saturation ($\phi_\infty^I = 1$), independent on the amount of diffusible hydrogen. Saturation of irreversible trap sites was experimentally observed when titanium microalloyed HSLA steel was externally charged with hydrogen in a permeation experiment [86]. Multi polarization of the steel showed that only the reversible traps relinquished their hydrogen on removal of the hydrogen from the steel and the strongly irreversible trap sites retained their hydrogen.

2.2. Various Trap-Hydrogen Interactions

At long range relative to the atomic spacing, a hydrogen atom interacts with defects in crystals through its elastic strain field. At short range, it interacts chemically through localized bonding with matrix atoms [87]. Since it is difficult to make a distinction among the various distinctive chemical interactions, the local interactions are described phenomenologically in terms of a binding energy to the defect, and usually only one trap energy level is assigned to the defect.

Values of the binding energies for various hydrogen traps in ferrous alloys [77,88,89] are listed in Table 1 in the order of increasing trap-hydrogen binding energies. The binding energy of 60 kJ/mol–H for an edge dislocation or a grain boundary is generally regarded as the upper limiting value for a reversible trap. With this energy, a reversible trap effectively captures hydrogen atoms around 400 K and reaches saturation at 200 K. At room temperature, reversible traps do not reach saturation. Therefore, they contribute to the reduction of apparent hydrogen diffusivity due to the effect of local equilibrium between trap site and lattice site. As shown in Table 1, inclusions that constitute transition elements far to the left of iron in the periodic table usually exhibit high degrees of irreversibility (E_B > 60 kJ/mol-H)

Table 1. Hydrogen trapping in Iron. Reference state H in perfect lattice

Trap Site	Binding Energy (kJ/mol)	Assessment Method	Ref.
H-dislocation elastic stress field	0 – 20.2	calculated	90
H-dislocation core (screw)	20 – 30	calculated	91
H-dislocation	26	thermal analysis	92
H-dislocation core (mixed)	59	permeation	93
H-grain boundary	18 – 20	thermal analysis	92
H-grain boundary	49	thermal analysis	94
H-grain boundary	59	permeation	93,95
H-free surface	70	permeation	96
H-free surface	95	permeation	97
β-NiAl *	27	permeation	9
H-PdAl interface *	34	permeation	9
H-Fe-oxide interface	47	thermal analysis	98
H-AlN interface	65	permeation	99
H-MnS interface	72	thermal analysis	100
H-Al_2O_3 interface	79	thermal analysis	101
H-Fe_3C interface	84	permeation	95,102
H-TiC interface	87	thermal analysis	103
H-TiC interface	95	permeation	14
H-Nd	129	calculated	104

* Matrix element is precipitation hardened martensitic stainless steel.

Assessment of a definite binding energy from a particular trap is difficult, not only due to limitations in experimental measurements, but also due to the simultaneous effect of the different origins of trap site-hydrogen interactions. Another source of error may also come from the fact that several types of traps are present during measurement. [88,105].

In contrast to traps, there are other microstructural defects which exhibit repulsive interactions with hydrogen atoms. These defects are termed anti-traps or blocks. Examples of blocking elements in steel can be associated with the solute elements or inclusions that constitute elements which are to the right of iron on the periodic table.

Contributions to the trap binding energy include three specific types of interactions: electronic, stress field, and interfacial interactions.

Electronic interactions

It has been proposed that the electrons of the hydrogen atoms will increase the electronic density state of the d bands of transition metals, increasing the repulsive forces between atoms. This interaction is the basis for the hydrogen embrittlement due to reduction of decohesion energy proposed by Troiano [15]. Any defect that introduces an electron vacancy in the iron d-shell electron level is thought to attract hydrogen to achieve local neutrality. For solute atoms in iron, attractive interaction will then exist when the impurity is located to the left of iron in the periodic table. Attractive interactions between these elements and hydrogen has been correlated with the increase of hydrogen solubility in liquid solution of iron when these elements present as solute atoms, as shown in Figure 17 [106]. On the other hand, solute atoms which lie to the right of iron will be characterized by repulsive interactions. When present as solute atoms, these elements reduce hydrogen solubility in liquid solution of iron, as also shown in Figure 17.

Shirley and Hall [107] substantiated the particular nature of solute-hydrogen electronic interactions, as determined by their position relative to iron in the periodic table. They assumed that the binding energy was the sum of the elastic and the electronic interactions. The elastic interactions were calculated by a stress tensor analysis and the

electronic interactions were approximated by Z .V_{host}, where Z is the difference in the number of valence electrons between the solute and the host, while V_{host} is a measure of the screening ability of the host. V_{host} was approximated as 0.08 eV according to data obtained from niobium and vanadium. The estimated values were shown to agree with the experimental data, as either attractive or repulsive depending on the sign of Z, which is dependent upon the solute atom position in the periodic table.

In solid iron, the situation is rather complicated and a simple correlation between hydrogen solubility and ternary additions has not been easily established. For instance, Schwarz and Zitter [108] reported that the hydrogen solubility in iron at 400 to 1000 °C was increased by the addition of carbon, silicon, manganese, nickel, and chromium in that order, which is in disagreement with the result for liquid iron shown in Figure 17. It was suggested that, in addition to the electron/atom ratio, the chemical affinity of hydrogen for the alloying element, which may be associated with chemical bonding formation, should also be taken into consideration [109] to better understand the hydrogen-solute atom interactions.

Troiano [15] related the nature of 3d band filling by electrons of solute atoms to the propensity of hydrogen embrittlement in nickel-base alloys. His model has been confirmed experimentally where hydrogen embrittlement has been found to decrease with a small addition of iron (fewer 3d electrons) to nickel but increases with a small addition of copper (more 3d electrons), as shown in Figure 18.

The electronic interaction between solute atoms and hydrogen has also been expressed macroscopically as thermodynamic interactions in the formulation of an interaction coefficient , ε_H^i in Fe-H-i systems [110–112], where

$$\varepsilon_H^i = \left[\frac{\partial \ln \gamma_H}{\partial X_i}\right] \tag{4}$$

and

$$\ln \gamma_H = \ln \gamma_H^0 + \sum \varepsilon_H^i X_i \tag{5}$$

where γ_H is the activity coefficient of hydrogen, γ_H^0 is the value of γ_H at infinitely dilute solution, and X_i is the atom fraction of solute atom *i*.

Attractive interactions result from a negative ε_H^i and hence a reduction of the activity coefficient of hydrogen in solution is attained in the presence of the solute atom i. This reduction of activity coefficient indicates an increase in binding energy between hydrogen and other elements in solution. In contrast, a repulsive interaction exists whenever ε_H^i is positive. Values of ε_H^i for liquid iron have been reported at 1600^{o} C [111]. Using these values, Pressoyure [104] calculated the hydrogen - substitutional atom binding energies based upon the known experimental values of the binding energy between titanium and hydrogen *E(Ti:H)*, i.e.

$$\frac{\varepsilon_H^i}{\varepsilon_H^{Ti}} \approx \frac{[\exp(-E(i:H)-1]}{-E(Ti:H)} \tag{6}$$

Such calculation have been shown to be suitable to model substitutional atoms as trap sites.

For higher hydrogen concentrations, the H-H interaction becomes important. The onset of H-H interactions and phase transitions at higher hydrogen concentration is among the most difficult problems of statistical mechanics [113]. Only a simple mean field or quasichemical approach has been used to account for H-H interactions, where a term is added to the chemical potential which is proportional to the hydrogen concentration

$$\mu = \mu_{id} + \Omega c \tag{7}$$

μ_{id} is the chemical potential without H-H interaction, Ω corresponds to an interaction energy between hydrogen atoms, and c is the hydrogen concentration. The above expression should gain more consideration as a trap site reaches saturation wherein the local hydrogen concentration at the trap site (c=c_T) becomes significantly higher than the nominal hydrogen content in the lattice.

Efforts to predict the electronic bonding characteristics of hydrogen in bcc iron with the presence of trap sites, through electronic structure calculations, have recently been initiated. Itsumi and Ellis, using the self-consistent Discrete Variational method (DV-Xα) investigated the effect of a vacancy [114] and a grain boundary [115] on the Fe-H bond strength.

Eberhart in [10] postulated an orbital model to rationalize the effectiveness of traps in bcc iron. Through this model it is argued that the binding energy of hydrogen to traps is largely determined through the Fermi energy orbital topology at the trap-bcc iron interface. Fermi energy interface orbitals of bcc iron are largely of π-character parallel to the interface and δ-character perpendicular to the interface. Whereas effective traps, e.g. TiC, are characterized by interface Fermi orbitals which are of σ-character perpendicular to the interface. Eberhart suggested that these different orbital characters do not allow for overlap to form an energetically stable interface, with the trap providing "dangling bonds" or more accurately unsatisfied orbital character in the interface region. Hydrogen atoms can effectively overlap with these unsatisfied orbitals, in a process similar to the saturation of organic molecules. This overlap lowers the energy of these trap orbitals to energies well below the Fermi level, stabilizing the interface. Effective traps are then seen within this model to be those traps that are characterized by σ-bonding perpendicular to an interface.

Based on symmetry arguments, Eberhart further provided a criterion allowing one to estimate, from bulk electronic structure calculations, which materials are likely to provide σ-bonds perpendicular to an interface with bcc iron. The crystal field splitting of the transition metal d-orbitals (determined from the energy difference between the d-orbitals at the Γ-point of a band calculation) and the position of the Fermi energy with respect to these orbitals is the only information required for these predictions. An optimal trap should display a near degeneracy of all the d-orbitals with a Fermi energy lying just above the point of degeneracy, i.e. the d-band is just beginning to fill. Using this criterion the following estimates of trapping efficiency for several inclusions in steel were made, Ce_2O_3 was predicted to be the most effcetive trap followed by TiC, Y_2O_3, VC, NbC, and finally Mo_2C.

Stress field interactions

In the presence of inclusions or lattice defects such as dislocations or large substitutional atoms, the lattice can be distorted in such a way that a tensile stress is produced around the defects. This stressed region has more free volume for interstitial

atoms, hence, a hydrogen atom trapped by these stress fields. Accordingly, hydrogen concentrations in the tensile stressed region will be higher than those in the lattice sites. The concentration of hydrogen, c_T, occupying a stressed lattice is given by the following equation [80] :

$$c_T = c_L \exp\left(\frac{V_H \sigma}{RT}\right) \tag{8}$$

where, V_H is the partial molar volume of hydrogen in the lattice, σ is the hydrostatic stress $= 1/3(\sigma_1 + \sigma_2 + \sigma_3)$, and c_L is the equilibrium concentration of hydrogen in unstressed lattice. In a similar fashion, repulsive interactions between defects and hydrogen atoms can be explained by the presence of a compressive stress around the defect.

The nature of elastic interactions between defects and hydrogen atoms have been reviewed by Puls [87] and Hirth [116]. Binding of solute atoms to defects in general has been reviewed by Fiore and Bauer [117] and particularly between hydrogen and dislocations has also been discussed in length by Hirth and Carnahan [118] and Wolfer and Baskes [119]. In these studies, hydrogen is assumed to interact only with the hydrostatic stress field. In the case of an edge dislocation this component of the stress is given by:

$$\sigma = \frac{\mu b(1+\nu)\sin\varphi}{3\pi(1-\nu)r} \tag{9}$$

where r and φ are cylindrical coordinates referenced to the dislocation line, μ is the shear elastic modulus, ν is the Poisson's ratio and b is the Burger's vector. The binding energy between hydrogen atoms and dislocations is deduced from the relaxation of elastic energy when hydrogen atom segregates to the dislocation stress field. This relaxation changes the elastic stress field volume by $\delta\upsilon = V_H(1+\nu)/3(1-\nu) = 1.22$ *cc/mole*, with V_H as the partial molar volume of hydrogen in iron. The binding energy is thus:

$$W = p.\delta\upsilon = \frac{\beta \sin\theta}{r} \tag{10}$$

Interfacial interactions

It has been observed that most deep trapping elements have very limited solubility in iron because of their high reactivity. Instead, these potential hydrogen traps exist in iron as inclusions or precipitates, such as oxides, carbo-nitrides, intermetallic inclusion, etc. In such cases, their trap strength will depend on many factors, such as the nature of the inclusion interface, elastic strain field, and chemical bond sharing with other elements at the matrix-inclusion interface. Several studies on internal boundaries serving as hydrogen traps have been reported [120,121]. Further studies on this area are still needed because hydrogen trapping in steel welding predominantly involves internal boundaries across a wide range of temperature.

Certain precipitates such as TiC have been considered as irreversible traps, whose binding energy vary with the degree of coherency of the matrix-precipitate interface [14,86,122,123]. Different experimental methods reveal conflicting results as to how the binding energy changes with the degree of Ti(C,N) interface coherency. One of the earliest observations by Berntein and Pressoyure, using hydrogen permeation techniques [14], showed that large incoherent TiC precipitates, in pure iron, act as irreversible traps with a large binding energy as high as 95 kJ/mol-H. In later investigations, a 600° C - aged microalloyed steel, contained fine (20-40 A) and possibly coherent TiC precipitates, showed very low hydrogen diffusivity [86]. Upon aging at higher temperatures, the particle coarsened and hydrogen diffusivity increased. These findings have been interpreted as indicating that the interface becomes a deeper trap as the degree of coherency increases. In addition, Takahashi et.al. [122] also observed that, after aging at 600 °C, fine coherent TiC (less than 100A) precipitates were produced, characterized by high binding energy. Finally, Valentini et.al. [121] investigated iron - titanium alloys. In these studies the number of trap sites, both reversible and irreversible, were determined as a function of heat treatments. It was shown that coherent Ti(C,N) (less than 350A) precipitates behave as irreversible traps. One disadvantage of investigating hydrogen trapping through permeation measurements of steel samples, containing inclusions with different sizes and distributions, is the difficulty in separating the effect of change in trap density from that of the binding energy. The density of trap sites will certainly reduce when the steel is heat treated at higher temperature. This effect may overshadow any

increase of binding energy due to the change of coherency of the matrix-inclusion interface.

A simple theoretical approach to explain the trapping potential of an interface has been suggested by Lee et. al. [122]. Adopting the derivation specifically made for grain boundary segregation by McLean [43], the Gibbs adsorption theorem [124] was used as the starting point;

$$\frac{d\gamma}{d\ln a} = -RT\Gamma \tag{11}$$

where γ is the specific interfacial free energy, Γ is the interfacial excess quantity, which is the excess of interfacial composition relative to the matrix due to segregation of hydrogen to the interface. The activity of hydrogen, a, at the interface expressed in terms of fraction of hydrogen occupancy, ϕ, at the interface [$a = \phi/(1-\phi)$]. Following this,

$$\frac{d\gamma}{d\ln a} = -RT\Gamma = -RT\phi N_T \tag{12}$$

On integration between the interface composition limits zero and ϕ, Equation (12) becomes :

$$\gamma^o - \gamma = -RTN_T \ln(1-\phi) \tag{13}$$

where γ^o refers to the specific interfacial free energy of the hydrogen free interface. The driving force for hydrogen trapping, hence, the magnitude of the binding energy, is associated with the lowering of interfacial energy $(\gamma^o - \gamma)$. From this standpoint, the incoherent interface would have a higher binding energy than does a coherent interface. With a hydrogen thermal desorption analysis, Lee et. al [122] reported that as TiC precipitates size coarsen and its interface character changed from semi-coherent to incoherent, the trap-hydrogen binding energy increases. Following this theoretical approach, the change of stress field around the precipitate, as the degree of coherency is altered, must also be considered for a better description of the interfacial structure dependence of binding energy.

Mixed interactions between hydrogen atoms and trap sites

The previous studies emphasize the importance of considering all interactions that may influence trap binding energies. Generally, a hydrogen trap has two or more types of interactions. Several investigators [77,85] considered that most of the traps energy arise from coupled behavior of physical and chemical interactions, since every physical distortion of the lattice is always accompanied by an electronic disturbance. A good example is that of the edge dislocation; the attractive chemical character arises through displacement of lattice atoms by the tensile stress field, and the physical character arises from interactions with the dislocation core.

In the case of attractive interactions, mixed characters have been observed in the interactions of hydrogen and oxygen at metal/oxide interfaces in palladium alloyed with aluminum, manganese, zinc, or zirconium [125]. Internally oxidized Pd-Me samples (Me is the previously mentioned alloying element) formed oxides which are superstoichiometric in oxygen. These oxides act as irreversible traps with an estimated trap energy of 90 kJ/mol-H. Upon reheating, these oxides start releasing hydrogen at about 300 °C. It is assumed that an oxygen layer surrounds the MeO_x oxide particles and this layer belongs partly to the MeO_x oxide and is partly bonded to the palladium atom in the matrix. To maintain stoichiometry of the stable oxides, the irreversible trapping of hydrogen is then described as :

$$MeO_x + xPdO + xH_2 = Me(OH)_{2x} + Pd.$$

Calculated trap energies from this reaction give values ranging from 106 to 130 kJ/molH for the various oxide forming metals (Me). These values are nearly equal in magnitude to the enthalpy of formation of water (= −119 kJ/mol H) and in good agreement with the irreversible trap energy of 90 kJ/mol experimentally determined. Therefore it is reasonable to attribute the irreversible trapping in these oxides to the formation of O-H bonds at the Pd/oxide interface. However, not all oxide-metal interfaces exhibit such strong trapping tendencies. A trap energy of approximately −10 kJ/mol-H has been observed in niobium [126,127]. Although, a difference of −20 KJ/mol H in binding energy, arising from the different reference state of the solid solution in palladium as opposed to the niobium matrix [128], should taken into consideration when comparing

these results. It was argued that the tendency of oxygen in niobium to form O-H bonds is less than the more pronounced competing reaction to form NbO. As palladium does not form a stable oxide this competing reaction is absent in palladium.

When the palladium matrix samples were subsequently annealed in vacuum, the oxygen diffused out leaving the oxide in excess of the metal (Me) surrounding the oxide outermost layer. It was then observed that the oxide becomes reversible with trap energies of approximately –30 kJ/mol, which is between measured binding energies of –20 to –60 kJ/mol H for edge dislocations in palladium [129]. The origin of this reversible trapping was assumed to be both the elastic interaction with the interface and a little contribution of chemical interaction with chemical species at the interface.

2.3. The Role of Traps in Hydrogen Embrittlement

Pressouyre [85], in his trap theory of hydrogen embrittlement, discussed the effect of employing both reversible and irreversible traps to the resistance to hydrogen embrittlement. In this theory, the interaction of two different types of traps, 1 and 2, with different H-trap binding energies is described as :

$$\frac{\phi^2}{\phi^1} = K_{12} = \exp\left(\frac{\Delta E_{12}}{RT}\right) \tag{14}$$

where $\Delta E_{12} = E_{B1} - E_{B2}$. If trap 2 is stronger than trap 1 then ΔE_{12} will be positive and K_{12} will be higher than one, which results in higher hydrogen occupation in trap 2 than that in trap 1. In the case of hydrogen transport accommodated by lattice diffusion, every type of trap site (as trap 2) interacts only with lattice sites (as trap 1). Since the interaction energy between lattice and trap, ΔE_{LT} , will always be positive, the fraction of occupation at reversible or irreversible traps (ϕ^R *or* ϕ^I) will always be greater than that in the lattice site (ϕ^L), resulting in the reduction of diffusible hydrogen concentration, c_L. Provided that the traps are fine and homogeneously distributed throughout the lattice, these traps are beneficial to the resistance to hydrogen embrittlement. To achieve this resistance, homogeneous distribution of the traps is required to decrease the probability that any

particular trap will reach saturation and/or the critical concentration that has the potential to initiate cracking.

In the situation where the hydrogen is transported by moving dislocations in a Cottrell atmosphere, as shown in Figure 19, the traps not only interact with the lattice but also with dislocations as reversible traps. The interaction energy between the reversible trap and the dislocation, $\Delta E_{DT\text{-}r}$, can now be positive or negative, depending on the strength of the trap. On moving through the lattice, a dislocation can pick up hydrogen atoms from an occupied reversible trap or deposit hydrogen atoms to an empty reversible trap. However, for irreversible traps, $\Delta E_{DT\text{-}i}$ will always be positive and ϕ^I will never be smaller than ϕ^D. As a result, a dislocation can only drop hydrogen atoms into irreversible traps and there will be a net transfer of hydrogen from the reversible traps (which act as an internal source of hydrogen) to the irreversible traps assisted by dislocation motion. In time, with a large number of interactions between dislocations and the various traps, the hydrogen content in both dislocations and reversible traps will be depleted, while that in the irreversible traps will be increased. This uneven distribution of hydrogen accelerates the rate at which irreversible traps reach the critical hydrogen concentration (c_K) potential to initiates cracking. Reversible traps then become detrimental, if the hydrogen is transported as dislocation atmospheres. For the best resistance to hydrogen embrittlement, the preferred trapping sites should be fine, uniformly distributed, and strongly irreversible.

The beneficial effect resulting from fine and uniformly distributed irreversible traps has been reported by Luppo and Ovejero-Garcia [130], who investigated ASTM A-516 G60 steel with different heat treatments. They observed that heterogeneously distributed reversible traps of the as quenched steels, such as martensite laths and prior austenitic grain boundaries, promote hydrogen localization, giving rise to high hydrogen sensitivity of the steel. When tempered at 453 K, ε carbides formed at the highly dense dislocations in martensite as fine and uniformly distributed precipitates. These fine ε carbides strongly trapped hydrogen, in addition to the reduction of dislocation density after the tempering heat treatment, was shown to increase the steel resistance to hydrogen induced cracking.

3. DESIGN ASPECTS FOR HYDROGEN CRACKING RESISTING STEEL WELD METAL

The microstructural dependence of HAC in high strength steel includes the nature of the metallic phase; defect shape, size, and distribution; grain size; degree of inclusion – metal matrix coherency; as well as the extent of segregation. These aspects have been reviewed in detail by Bernstein and Pressouyre [77] and by Yurioka and Suzuki [131]. Utilizing traps with high binding energy alone is not enough to allow one to design a weld microstructure that is highly resistant to hydrogen cracking. Assessment of the critical hydrogen concentration for HAC (c_K) of the corresponding trap site, which depends on the matrix and the trap interface structure, is also necessary.

The first goal that one has to achieve is to determine the type of metallic phase and microstructural defects that are prone to HAC. Secondly, the distributions of these susceptible microstructural features within the weld metal, (which result from the solidification process) must be understood. Hydrogen resistant steel, designed to incorporate hydrogen trapping, should contain carefully distributed deep trap sites to reduce the diffusible hydrogen associated with susceptible microstructural features. To achieve this task, one needs to assess the effect of solidification and phase transformations on the structure, size, and distribution of trap sites, which usually exist as inclusions. With this knowledge, proper trapping additions to the weld metal can be selected from several potential candidates.

3.1. Heat Affected Zone Microstructure

An observation by Hart [132] on the heat-affected zone of various steels led to a conclusion that factors for controlling hydrogen cracking fall into two conditions. For a high level of hydrogen, at around 10 ml/100 g deposit metal, the resistance to cracking was primarily controlled by weld metal hardness. At a lower level of hydrogen, less than 5 ml/100 g, resistance to cracking was determined more by microstructure than by hardness.

Hardness has been regarded as a rough index describing the susceptibility to hydrogen cracking. The value of 350 HV is often specified as the maximum allowable HAZ hardness for avoiding hydrogen cracking [133,134]. The Vickers hardness has been correlated to the carbon equivalent (CE), which is an index of hardenability, or the weldment's potential to form a martensitic structure. The HAZ and weld metal hardness for various heat treatments have bee predicted by using different carbon equivalents proposed by several authors [135,136].

Results pertaining to the effect of the HAZ microstructure on HAC have been reviewed by Suzuki and Yurioka [131]. Susceptibility to hydrogen cracking in the HAZ increases with increasing hardness, hence it increases through the series : lower bainite, quenched and tempered martensite, and martensite [137–139]. Hard microstructure promotes localized accumulation of hydrogen in the triaxial stress region, as has been observed by Phalen and Vaughan [140], who found that hydrogen accumulated at the tension side of a hydrogen-charged, bent, martensite specimen but not in the same location in a ferrite specimen. Schiapparelli [141] investigated steel samples with different microstructures which were loaded under the same hydrogen environment. He reported that martensitic or bainitic structures exhibited high susceptibility to HAC, and fractured either in a cleavage or in an intergranular fracture manner. Bainitic-pearlitic structures exhibit some susceptibility and fracture in a ductile intergranular manner. Finally, ferritic-pearlitic structures, which have the lowest susceptibility, fracture with ductile failure morphologies.

In high strength steel welding, formation of martensite should be prevented and is commonly minimized by reducing the carbon content. The resistance to hydrogen cracking of modern pipe line steel [142] and structural steel [143] weldments has been greatly improved, mainly through the reduction of carbon content. Low carbon content (0.05 wt. pct.) has been thought to be the reason for the absence of HAC in API-X65 steel, even when the steel was welded under no preheat condition with hydrogen-containing cellulosic electrodes [144]. In addition to low carbon content, most hydrogen resistant steels have been designed by careful selection of the alloying elements and their compositions, especially the elements that promote the formation of martensite such as manganese, chromium, molybdenum, vanadium, copper, nickel, and silicon [145].

3.2. Weld Metal Microstructure

Weld metal is not wrought metal in that it has a specific memory of the solidification experience with less homogenization than the wrought product commonly obtained from thermo-mechanical processing. Weld metal normally contain high oxygen and nitrogen concentration, mainly in the form of inclusions. Since hydrogen trapping is directly associated with microstructural features and their corresponding interfaces, it is important to understand the microstructural nature of steel weld metal and its evolution.

Weld metal possesses a solidification structure containing both compositional and microstructural gradients. On cooling through the two-phase (liquid-solid) field, a compositional profile in the liquid ahead of the solid/liquid interface develops. The composition of the solute in the liquid adjacent to the solid/liquid interface is given by C_o/k', where C_o is the initial liquid metal composition and k' is the solute partition coefficient. At distances further away from the solidification front, the solute concentration decreases exponentially. As solidification progresses, the solute partitions between the liquid and solid according to k'. As the solid/liquid interface advances, the solute atoms are carried with and accumulated in front of the solid/liquid interface. As neighboring dendrites thicken and approach each other, the last liquid to solidify in the interdendritic region could have a composition as high as $2C_o/k'$, as is illustrated in Figure 20. This interdendritic solute redistribution occurs numerous times across a given grain. For example, in a typical submerged arc weld, between four and six dendrites will comprise a given longitudinal cross-section of a columnar grain.

The solute partition coefficient k' can have values greater than or smaller than one. In the case that k is less than one, solute additions will lower the liquidus temperature of the alloy, and the interdendritic liquid will have a higher solute content than the bulk material. With k' greater than one, the solute addition will increase the liquidus temperature of the alloy and solute will be depleted from the interdendritic regions. For most of the alloying elements added to iron and nickel alloy systems, k' is smaller than one, resulting in positive segregation in the interdendritic regions.

The resulting weld metal compositional variations, especially oxygen, can result in inclusions which oscillate in occurrence as one transverses across the weld metal. The microsegregation influences the specific types, numbers, and size distribution of these inclusions. These inclusions produce interfaces which will serve to some degree as hydrogen traps. Also this variation of composition will cause modulation in the amount of martensite across the weld bead, which can influence the hydrogen transport in the weld deposit during cooling.

Role of weld metal solidification on inclusion formation

During cellular or dendritic solidification commonly observed in steel weldments solute elements segregate to the liquid at the solid/liquid interface, and the liquid concentration can reach high solute levels in the interdendritic spaces. For dendritic solidification, it can be assumed that diffusion in the liquid can occur throughout the interdendritic space, and that diffusion in the solid occurs only for high diffusivity solutes. Neglecting solid diffusion, the composition in the liquid at the solid/liquid interface can be modeled by the non-equilibrium lever rule or Scheil Equation [146]:

$$C_L = C_O f_L^{k'-1} \tag{15}$$

where C_o is the bulk concentration of solute in the weld pool, C_L is the concentration in the liquid at the interface, and k' is the solute partition coefficient. This equation can be modified to account for diffusion in the solid [147148] if so desired. The solute partition coefficient, k', has a strong influence on the extent of segregation. Table 2 shows some approximate values of the solute partition coefficients, k', for various solutes in low alloy steel.

Table 2. Solute Partition Coefficients

Element	C	Si	Mn	Al	Ti	B	O	S	N
k'	0.17	0.80	0.70	0.95	0.50	0.001	0.01	0.20	0.04

Consider the formation of an inclusion of the following stoichiometry [149]:

$$xM + yN + zO = M_xN_yO_z \tag{16}$$

The free energy of formation, ΔG, of $M_xN_yO_z$ can be written as:

$$\Delta G = \Delta G^o + RT \ln \frac{[M_xN_yO_z]}{[M]^x[N]^y[O]^z} \tag{17}$$

where [M], [N], and [O] are the solute activities in the liquid; and x, y, and z are the stoichiometric constants from Equation (16). $[M_xN_yO_z]$ is the activity for the specific inclusion and can be assumed to have the value of one.

Using Equation (15) to represent the extent of segregation, the solute activities ahead of the solid-liquid interface can be written as:

$$[M] = [\gamma_M][M_O] f_L^{k'_M - 1} \tag{18}$$

$$[N] = [\gamma_N][N_O] f_L^{k'_N - 1} \tag{19}$$

$$[O] = [\gamma_O][O_O] f_L^{k'_O - 1} \tag{20}$$

In these equations f_L is the volume fraction of the liquid metal, $[M_O]$, $[N_O]$, and $[O_O]$ are the bulk concentrations of M, N, and O in the melt, $[\gamma_M]$, $[\gamma_N]$, and $[\gamma_O]$ are the activity coefficients for the solutes.

Substituting Equations (18) through (20) into Equation (17) gives the free energy as a function of the fraction of liquid remaining:

$$\Delta G = \Delta G^o + RT \ln \frac{[M_xN_yO_z]}{[\gamma_M M_O]^x[\gamma_N N_O]^y[\gamma_O O_O]^z} + RT \ln f_L^{x(1-k_M)+y(1-k_N)+z(1-k_O)} \tag{21}$$

Equation (21) expresses the free energy driving force for the formation of the oxide. The first term on the right side, (ΔG^o), represents the free energy of reaction at standard state, which corresponds to the average composition of the alloying elements in the weld pool. The second term represents the departure from the standard state caused by changes in temperature or reactant concentrations, and the third term is a correction factor for the change in free energy caused by segregation during solidification. This last term is a function of the stoichiometric constants and the solute partition coefficients. Equation (21) can be used to analyze the influence of microsegregation on the formation of various types of inclusions in weld metal.

Inclusion formation in weld metal may be considered as a two step process. First, primary inclusions are formed by deoxidation reactions in the weld pool above the liquidus temperature. Second, segregation during solidification increases the reactant concentrations in the interdendritic liquid. This second stage precipitation leads to an increase in the size of existing inclusions and to the formation of new inclusions. First stage inclusion formation reactions are driven by weld pool reactant concentrations above equilibrium, and these reactions may be assumed to approach equilibrium as the weld pool cools to the liquidus temperature. This assumption is often used when dealing with deoxidation equilibria [148]. Under equilibrium conditions before the start of solidification, the free energy driving force and the final term representing solidification are zero. Conditions at the end of the first stage can then be represented by:

$$\Delta G^{o} = -RT \ln \frac{[M_x N_y O_z]}{[\gamma_M M_O]^x [\gamma_N N_O]^y [\gamma_O O_O]^z} = -RT \ln K \tag{22}$$

In this equation, K is the equilibrium coefficient for the deoxidation reaction. For the purpose of this model the deoxidation reactions which comprise the first stage of inclusion formation are assumed to reach equilibrium, so that the concentrations of dissolved alloy elements and oxygen at the beginning of the solidification process can be calculated from tabulated values of the equilibrium coefficients.

To evaluate the deoxidation sequence, it is assumed that the first stage deoxidation reactions in the weld pool, with deoxidants such as aluminum, reach equilibrium with deoxidants such as aluminum, reducing the dissolved oxygen content of the weld pool to low levels. Consider a weld produced on carbon steel plate which was aluminum-killed in the ladle. A standard aluminum deoxidation addition of 0.05 wt. pct. will reduce the soluble oxygen level to about 0.0006 wt. pct. The composition resulting from the first stage of deoxidation can be considered to be this oxygen level along with the ladle compositions for the remaining elements. This assumed condition is the starting point for the second stage of deoxidation which occurs during solidification. As microsegregation increases the concentrations of alloy elements and oxygen in the interdendritic liquid, additional deoxidation reactions will either grow oxide onto existing inclusions or form new inclusions.

Variations in the solute partition coefficient, (k'), and in ΔG will influence the size of the inclusions. Because each type of inclusion will have its own specific free energy of formation, Equation (23) also indicates that each inclusion will have its own critical radius for nucleation :

$$r_c = \frac{-2\gamma V \varphi}{\Delta G} \tag{23}$$

In this expression, γ is the solid/liquid interfacial energy, V is the molar volume, and φ is the correction factor for heterogeneous nucleation.

It is expected that the number of inclusions formed during the solidification process will have a significant effect on microstructural features which will influence the nature of hydrogen trapping. The influence of the critical radius on the rate of nucleation, I, for specific weld metal inclusion is given by :

$$I = A\exp\left(\frac{-4\pi r_c^2 \gamma}{3RT}\right) \tag{24}$$

The nucleation rate influences both the size distribution and concentration of inclusions. Equations (23) and (24) show that the nucleation rate for a particular type of inclusion is influenced by the equilibrium partition ratio through the critical radius r_c and the free energy of formation ΔG. To promote hydrogen trapping by specific alloying additions, it is important that these additions survive the primary deoxidation and participate in the secondary interdendritic deoxidation so that these elements are at the edge of primary inclusions or are the part of the makeup of the small interdendritic inclusions.

3.3. The Role of Inclusions in Reducing Hydrogen Assisted Cracking of Steel Weldments.

Inclusions have the potential to reduce HAC in high strength steel in two ways: (1) by promoting the formation of tougher microstructure, and, (2) by trapping hydrogen during the cooling cycle following the welding process. The role of sulfide and oxide inclusions in promoting tougher microstructure by decreasing hardenability of the weldment microstructure has been confirmed. Observations concerning the role of hydrogen trapping by inclusions depend strongly on the binding energy of the trapping

inclusions. Olson et. al. [10] showed that strongly, irreversible traps may prevent HAC by promoting accelerated reduction of diffusible hydrogen during the cooling cycle after the welding process. In this way, the amount of diffusible hydrogen at susceptible HAC temperatures (below 100° C) can be assured to be below the allowable limit. The performance of inclusions in preventing HAC depends not only on their binding energies but also many other factors, such as the steel martensite start temperature and the stress state at the inclusion-matrix interface.

Role of oxide inclusions

The solubility of oxygen in liquid iron is approximately 1600 ppm at the melting point [150]. During solidification, this solubility decreases to about 860 ppm at 1500°C in delta iron. Oxygen, because of its low solubility in iron, will combine with other alloying elements to form oxides. Most of the alloying elements present in liquid steel reduce oxygen solubility through deoxidation equilibria. Steelmaking processes typically yield analytical oxygen levels in the range of 70 to 100 ppm. Welds typically pick up oxygen to levels of several hundred ppm, then deoxidize to oxygen levels of around 200 to 300 ppm with the formation of oxide inclusions.

It is these oxide inclusions that affect the weld metal microstructure in low carbon and high strength steels [151–154]. Liu and Olson [154,155] suggested that for low carbon microalloyed steel weld metals, the presence of a large number of inclusions of size greater than the Zener diameter is desirable to promote large prior austenite grains. Large prior austenite grains allow for a larger portion of the austenite grain to achieve greater undercooling and thus produce a finer ferrite structure, rather than producing a large amount of allotriomorphic or grain boundary ferrite. Liu and Olson [154] also proposed that intragranular oxide inclusions, particularly those rich in titanium and aluminum, will promote the formation of high toughness acicular ferrite. The type and size distributions of the oxide inclusions have been shown to be a function of weld metal oxygen and the alloying content [154,155].

Inclusions in the size range of 0.1 to 0.5 μm play an important role in the nucleation of acicular ferrite. Inclusions less than 0.1 μm in size are instrumental in

pinning austenite grain boundaries to prevent grain growth, and thus result in excess grain boundary ferrite. This grain boundary ferrite becomes a direct crack path during weld metal fracture. Size and distribution of these inclusions are not only important for developing preferable microstucture, but also significantly affect hydrogen trapping in the weld metal since these inclusions offer interfaces that are primary hydrogen trapping sites.

A number of oxide inclusions have been identified as relatively weak but irreversible trap sites, such as Al_2O_3 (E_B = 79 kJ/mol-H) [156] and iron oxide (E_B = 50 – 70 kJ/mol-H) [157]. The performance of these weak irreversible traps in preventing hydrogen cracking strongly depends on the microstructure or, more specifically, the martensite start temperature of the steel matrix.

With longitudinal butt-tensile restraint cracking (LB-TRC) testing, several investigators [158,,160] have studied the effect of oxygen content on hydrogen cracking susceptibility in weld metal of high strength steel. LB-TRC testing was used to enable the investigators to impose mechanical tensile loading on a weld bead when the temperature reached 150° C during cooling after welding. With this testing method, Matsuda, et. al. [159] reported that, in GTA welding of HY-130 steel with the resulting diffusible hydrogen content around 9 ml/100g fused metal, the lower critical stress for fracture is just slightly decreased with increasing oxygen content. The fraction of intergranular fracture increased with increasing oxygen content, but the effect became gradual after the oxygen content exceeded 80 ppm. As a consequence of increasing oxygen level, the weld metal microstructure changed from lath martensite to acicular ferrite, which might have influenced the results. The areal density of microvoids and microcones on the intergranular fracture surface increased with higher oxygen content, suggesting that the inclusions, assisted by the diffusible hydrogen, acted as crack initiation sites. It should be noted that the diffusible hydrogen levels used in this investigation were significantly higher than the allowable level for this type of steel.

Also with LB-TRC testing, Shinozaki, et al. [160] investigated the effect of oxygen on the mechanical integrity of HY-100 and HSLA-100 steels samples, welded with hydrogen contamination to obtain 4.7 ppm hydrogen in the weld metal. As shown in Figure 21, HY-100 steel welds, which consistently revealed a martensitic microstructure

under natural welding cooling rate, experienced a reduction in the critical stress for HAC as the oxygen content was increased up to 200 ppm. With increasing oxygen content, the fracture mode was altered from quasi-cleavage to intergranular. Intergranular failure occurred via oxide-matrix decohesion at prior austenite grain boundaries. These oxide trap sites may be too weak and consequently, the rate of hydrogen trapping may not be sufficiently fast to prevent accumulation of hydrogen at grain boundary areas of high stress concentration. Similar results were obtained for HSLA-100 steel welds which were quenched immediately into iced water to get complete martensitic structures (Figure 21).

The susceptibility to hydrogen damage in steels depends on the characteristics of the matrix-inclusion interface [161].Several oxide inclusions, such as Al_2O_3 and Ca-Al_2O_3, are nondeformable. These inclusions act as a stress intensifier, and promote a localized plastic deformation in steels [162,163]. Hydrogen concentration around the inclusion can be increased locally, and the critical concentration for HAC can be reached earlier. In other inclusions, trapped hydrogen help prevent HAC by promoting decohesion, which could facilitate the formation of a blunt crack at the inclusion-matrix interface, instead of fracture of the oxide inclusions. Separation of the inclusion-matrix interface gives rise to local relaxation of the plane-strain condition at a crack tip, as proposed by Venkatasubramanian and Baker [164]. In this way, trapped hydrogen could increase the critical stress for HAC, because a stress relaxation mechanism is available without the formation of a sharp crack associated with the fracture of oxide inclusions. The relationship between inclusion-matrix decohesion, toughness, and HAC deserve further investigation.

Opposite trends were observed for HSLA-100 steel welds which experienced a natural welding cooling rate, shown in Figure 22 [160]. The role of oxide inclusions in the HSLA-100 steel weld sample was thought to be overshadowed by the increasing formation of acicular ferrite or bainite structure as the oxygen content increased. An increase of critical stress with increasing oxygen content, up to 638 ppm, was observed and thought to be a result of the formation of tougher microstructures. However, it has been widely observed that, in the absence of hydrogen, the impact toughness of weld metal does not continuously increase with increasing oxygen content, but usually reach a maximum value at an oxygen content of 250 ppm [165]. In this particular investigation, it

is highly possible that the formation of acicular ferrite in HSLA-100 steel occurred at a higher temperature than the formation of martensite in HY-100 steel. In this situation, hydrogen capturing was more effective in HSLA-100 steel and contributed to the increase of critical stress for HAC. Reduction of diffusible hydrogen was faster in HSLA-100 steel than in HY-100 steel for the same welding cooling cycle.

Role of sulfide inclusions

Suzuki and Yurioka [131] summarized numerous publications which reported the increased risk of hydrogen cracking in low sulfur steels. Increased hardenability due to ultra-low sulfur concentration is recognized as the main cause for an increased risk of hydrogen cracking [166–168]. Reduction in sulfur content results in a hard microstructure caused by the loss of intragranular ferrite nucleation sites usually promoted by sulfide inclusions, particularly MnS. Yamamoto [169] proposed that the formation of MnS around an oxide or nitride created a manganese-depleted zone which facilitated carbon diffusion and ferrite nucleation in the inclusion vicinity. It is thought that the number of sulfide inclusions, rather than the amount of sulfur, is important for the ferrite nucleation. Since MnS inclusions form around oxide or nitride inclusions, large number of sulfide inclusions can be produced by utilizing several finely formed oxides such as REM oxy-sulfide, calcium oxide, and titanium oxide [169,170], while aluminum oxide is ineffective for ferrite nucleation due to its generally large size [171].

While sulfur content in steels has been reduced to improve mechanical properties, some papers have reported that a reduction of non-metallic inclusions, mainly sulfides, could increase the risk of HAC in the HAZ. Hirose, Araki and Kikuta [172] observed that, in quenched and tempered HSLA steels containing 10 ppm hydrogen, the critical stress for HAC increased with increasing sulfur content up to 300 ppm, shown in Figure 23. The sulfur content was directly proportional to the MnS inclusion density, which was the main microstructural feature responsible for suppression of HAC. With the matrix of all the sample being martensite, these sulfides were thought not to reduce HAC by reducing the hardenability of steels. Instead, because of the fact that the apparent hydrogen diffusivity decreased with increasing MnS density, the above investigators concluded that MnS inclusions served as hydrogen trap sites, thus suppressing HAC.

These investigators suggested that the presence of hydrogen at the interface of these inclusions did not become the initiation site for HAC because MnS inclusions are deformable. Deformable inclusions, such as MnS and oxide-MnS, do not raise the local stress level and thus do not promote HAC. Manganese sulfide has been identified as a weak irreversible trap with a binding energy of 72 kJ/mol-H [173].

Role of carbide inclusions

TiC precipitates in micro-alloyed HSLA steel has been of great interest for many investigators due to the high binding energy (E_B= 95 kJ/mol-H) [14]. Stevens and Bernstein [174] had attempted to evaluate the mechanical response of TiC-containing HSLA steel. Unfortunately, they could not exclude the deleterious effect of sulfur or phosphorous segregation to grain boundaries, which occurred during annealing heat treatments that were intended to vary the density of TiC precipitates. The presence of small and finely distributed TiC precipitates were shown to improve the resistance to HAC, since they compensated for the loss of resistance to HAC caused by segregation of sulfur or phosphor. It was thought that, without the presence of such deep trap sites, the fracture toughness of the hydrogen-charged HSLA steel would decrease significantly.

VC inclusions have also been investigated as hydrogen traps to prevent disbonding of austenitic stainless steel cladding from 2 ¼ Cr –1 Mo steel base plates [175]. Disbonding usually occurs at the interface of the two steel layers when a hydrogen-containing pressure vessel is cooled down from an elevated temperature. While disbonding in ordinary steel started to occur when the specimen was cooled down from 450° C and 14.7 Mpa hydrogen pressure, disbonding in VC modified steel was not observed even after cooling from 500° C and 19.6 Mpa (and thus containing a higher level of hydrogen). The role of VC was thought to be that of a hydrogen trap, which alleviated the localization of hydrogen at the cladding interface.

Quite recently a more comprehensive evaluation of VC particles has also been done through both hydrogen measurement and notched tensile testing [176]. Two similar classes of steel, AISI 4340 and ASTM A723 steels, were modified to obtain the same vanadium and carbon content. These modifications promoted the formation of VC particles, which were shown to significantly improve the resistance to HAC relative to

the base steel compositions. The embrittlement index for AISI 4340 steel was decreased by the formation of VC particles from 61.2 percent down to 22.2 percent. A smilar case was observed for the ASTM A723 steel (from 5.8 percent down to 3.8 percent). Quantitative evaluation of the binding energy of VC particles has not been reported. Extraction studies that were performed in this investigation showed that the particles did not release the trapped hydrogen during sample reheating at 200° C, which implies that these particles are irreversible traps.

3.4. Trapping Inclusions : Type, Quantity, Geometry and Distribution.

It is believed that the shape of an inclusion can have a significant role in hydrogen cracking since it often determines the hydrogen pressure that can be reached at an interface [177]. Inclusion shape also modified the local stress state [178], and changes the net transport of hydrogen to potential crack initiation sites, including the trap itself [179]. In his trap theory of hydrogen embrittlement, Pressouyre [76,180] reported that elongated MnS inclusions initiated cracks at lower critical hydrogen concentration for HAC (c_K) than rounded ones, and that the effect was more pronounced in bainite-martensite than in ferrite-pearlite structures. Hence, small spherical second phase particles are desirable, particularly those particles having coherent interfaces. Large inclusions are detrimental because of their higher probability to intersect grain boundaries. This particular situation yields the lowest c_K zone in the microstructure, which then becomes highly susceptible to crack initiation, leading to intergranular crack propagation.

While fine inclusions can be obtained by providing a larger number of nucleation sites in the liquid melt [181], the preferred small spherical inclusions can be achieved by decreasing the metalloid content [182], including sulfur. However, there is a limit to the reduction of the sulfur content because of the increased risk of formation of martensite structure. Rare earth metal additions or calcium treatments are considered viable solutions for the sulfide inclusion problem in steel HAC. These treatments spheroidise the sulfide inclusions, keeping the size to less than one micrometer and increasing the total number of inclusions. Therefore, the rare earth treatment allows one to minimize the sulfur content but still obtain sufficient intra-granular ferrite nucleation sites. Hart

reported an apparent lower hardenability of the REM treated steel than that of the high sulfur content steel [166].

The influence of type and density of inclusions on hydrogen embrittlement of 2.25 Cr-1 Mo steel has been investigated by Valentini. The MnS inclusions, in the bainite-martensite matrix, were always associated with the critical sites for crack nucleation while carbides were not. It was observed that the maximum critical hydrogen concentration for HAC was obtained for samples which contained fine dispersions of M_7C_3 and $M_{23}C_6$ inclusions behaving as irreversible traps. It was also shown that the relationship between hardness and critical hydrogen content was only meaningful when correlated with the diffusible hydrogen content. The total hydrogen content, however, did not correlate with the hardness of the microstructure. These results demonstrated that the nature and density of hydrogen traps must be incorporated with the hardness value of the metallic phase for one to develop a more consistent HAC indicator.

3.5. Segregation to Internal Boundaries.

Some segregating impurities (metalloids) are detrimental, and known to decrease the cohesive strength of internal boundaries. This effect may be synergistic with that of interfacial hydrogen trapping [138,185]. Particularly prone to such effects are steels containing nickel, chromium, and molybdenum, and austenitic steels that exhibit temper embrittlement [77]. Nickel and chromium have been identified to promote the segregation of phosphorus, antimony, tin and arsenic to internal boundaries, while manganese promotes phosphorus segregation [182]. In addition, carbon, manganese and silicon have also been found to lower the hydrogen-environmental threshold stress intensity, K_{th} , when segregated to grain boundaries [170,186,187]. These data for carbon are surprising because carbon intrinsically strengthens steel grain boundaries [188].

In a metallographic and fractographic investigation, Lynch [189] showed that the HAC fracture appearance of tempered martensitic high strength steel depended upon the degree of metalloid segregation. Different steel sample tempering temperatures varied the degree of metalloid segregation. When tempering temperature was low (290° C), the fracture surface exhibited dimpled fractures predominantly along martensite lath

boundaries. A higher temper, 400° C, yielded a brittle intergranular fracture surface that followed prior austenite grain boundaries. Finally, after a 600° C heat treatment, dimpled intergranular fracture along prior austenite grain boundaries was observed. Without the presence of hydrogen, overload fractures of the steels with all level of tempering temperatures were transgranular and dimpled. The dimples were generally larger and deeper than those dimples after HAC.

Reduction of grain boundary fracture toughness due to segregation of both the impurity atoms and the hydrogen atoms has been proposed [190,193]. One formulation of fracture toughness as affected by segregation is given as [193]:

$$\sigma_f = \sigma'_f - \alpha_i . X_i^{1/2} - \alpha_H . c_o . \exp\left\{\frac{\sigma . V_H}{RT}\right\} . \exp\left\{\frac{-E_B}{RT}\right\} \qquad (25)$$

where σ_f and σ'_f are the environmental fracture stress and fracture stress in the absence of impurities and hydrogen, respectively. The terms X_i and $c_o.\exp\{\sigma_H.V_H/RT\}.\exp\{E_B/RT\}$ are the grain boundary concentrations of impurity and hydrogen respectively. The terms α_i and α_H are constants with units of Mpa-at.frac$^{-1/2}$, V_H and E_B are the partial molar volume for hydrogen and grain boundary trap binding energy, and σ is the operative hydrostatic stress at the grain boundary. Fracture occurs when σ is greater than σ_f.

Different results have been reported on hydrogen trapping at metalloid - segregated grain boundaries in iron alloys. Lee et al., using a hydrogen thermal desorption analysis of iron and carbon-manganese steels, reported that a reduction in the peak temperature of hydrogen evolution rate occurs as the concentration of sulfur and phosphorus at the grain boundaries increases [194,195]. It was suggested that both the trap-hydrogen binding energy and the number of trap sites decreased with increasing segregation of these metalloids to grain boundaries. On the other hand, Pyun and Lim [196], from electro-permeation measurement of nickel-chromium steel, reported that the addition of alloying elements nickel, chromium, and manganese to iron increased the trap density, while segregated phosphorus slightly increased the hydrogen - trap binding energy. Some of the above alloying elements are expected to cosegregate with phosphorus to the grain boundaries and may have some influence on hydrogen trapping at grain boundaries. In fact, the hydrogen trapping in these complex grain boundaries alone may be considered as a segregation problem. Therefore, hydrogen segregation to

grain boundaries may have to be treated simultaneously with the other alloying or impurity elements in the iron matrix.

A thermodynamic model of grain boundary segregation in multicomponent alloys has been developed by Guttman [197,198] for regular ternary solutions where the occupation of an element on a grain boundary depends on both the binary and the ternary interaction coefficients of the alloying elements. Several cases of cosegregations between alloying and metalloid elements, as well as the uphill diffusion of carbon in Fe-Si-C steel, have been successfully explained by this model. Even though segregation of hydrogen to internal boundaries usually takes place after the completion of segregation of other larger elements, such thermodynamics models that include segregation of hydrogen in multi-component system is very useful in understanding the synergistic interactions of alloying elements, metalloid impurities and hydrogen at internal boundaries.

3.6. Influence of Grain Size

There is conflicting evidence in the literature regarding the effect of grain size on hydrogen embrittlement. Conflicts may arise because of the difference in the degree of hydrogen segregation to grain boundaries in samples possessing different grain size. Another possible cause of these disagreements are the different microstructures obtained in the effort to produce varying grain sizes.

Fine grain sizes, as well as fine carbide sizes, were reported to have beneficial effects [137]. With grain boundaries being hydrogen trapping sites, grain refinement should have a beneficial effect because the hydrogen is more evenly distributed [182]. Moreover, segregating elements that lower the cohesive strength of the grain boundaries, will also be more evenly distributed. Such beneficial effects of grain refinement have been observed for ferrite as well as austenitic steels [199–202]. Investigations by Proctor and Paxton [203] on AISI 4340 steel processed by thermal cycling techniques demonstrated that grain refinement led to longer failure times (decreased *da/dt*) during stress corrosion cracking.

Opposite conclusions were reached by Carter [204], using AISI 4340 steel with added silicon, and Lessar and Gerberich [205], using a single tempered AISI 4340 steel,

who obtained a longer time to failure as grain size become coarser. Gerberich proposed that crack growth kinetics are affected mostly by a diffusion controlled process, which may either be related to the area of the grain boundary or the amount of retained austenite at the boundary. Ryder et. al. [206] also reported similar results for AISI 4340 steel and proposed that coarse austenite grain size provides interfaces that promote crack branching which improves the steel toughness.

Alloying elements commonly used for grain refinement are niobium and vanadium below 0.05 wt. pct., as well as aluminum when it form oxides. However, niobium and vanadium raised the HAZ hardness in higher heat input welding or in longer cooling time welding, through the precipitation hardening by their carbonitrides [207,208]. In the case of aluminum addition, a superhardening effect was reported in a 0.35C-1.5Mn steel [209]. Some authors reported an increasing risk of hydrogen induced cracking with an increase in aluminum [210,211], whereas Campbell [212] did not find such an effect by aluminum in the hydrogen cracking of Controlled Thermal Severity (CTS) testings.

3.7. Microalloying Elements and Impurities

Various elements have been deliberately added to HSLA steels to achieve different physical and mechanical properties. These elements may have a synergistic influence on hydrogen embrittlement. A systematic study has not been conducted; however, general trends have been drawn by Bernstein [77]. A more detailed discussion of the effect of individual alloying element has also been addressed for low carbon steel by Lunarska [213]. Among the many alloying elements, manganese appears to be generally detrimental for HAC, while additions of silicon, vanadium, niobium, cobalt, and palladium are generally beneficial. The synergistic effects of alloying elements on hydrogen induced cracking are not limited to the trapping capacity of each solute element or inclusion particle, but, are also related microstructure and complex interactions between the alloying elements. The specific role of solutes on microstructural development can vary, leading to either an increase or a decrease in matrix or interfacial

cohesive strength, or to changes in stacking fault energies and dislocation mobility. These microstructural changes can alter the resistance to crack initiation, propagation and arrest.

Quite recently, Lee [214] attempted to predict hydrogen embrittlement in binary and ternary alloys of transition metals. An empirical model for hydrogen embrittlement can resulted from a good correlation between hydrogen embrittlement index data and the electron density of states (N(E)) of the alloy. In this model the electron density of states was deduced from the heat capacity of the alloy. An example of a calculated prediction and the corresponding experimental data for hydrogen embrittlement of Fe-Ni-Cr alloys is shown in Figure 24. It is not clear, however, whether variations in hydrogen content into the alloys can be incorporated in this model or not.

A particular case study of the effect of microalloying in high strength steel welding was conducted by Watanabe [215]. He observed that both the sulphide inclusion content and the HAZ liquation susceptibility could be correlated to the HAC of two different steels, HY-80 and SM50B. The segregation bands in the cold worked structure of HY-80 steel are rich in solute element such as nickel, chromium, and molybdenum. Congruent melting in this band occurs at a relatively low temperature, and migrating austenite grain boundaries are likely to intersect with this band, and become arrested. Furthermore, MnS inclusions can dissolve and reprecipitate at these grain boundaries [216]. Transport of manganese and sulfur is enhanced by the formed liquid, so that the reprecipated MnS inclusions align at the solute-rich grain boundary intersections. In addition, the segregation band is highly hardenable, and during a cooling cycle, will produce martensite. The combination of hard matrix and a high capacity for MnS inclusions to trap hydrogen produces regions with a high susceptibility to HAC.

Unlike the segregation bands in HY80 steel, the SM50B steel segregation band only contains high manganese and moderate silicon. On heating, manganese diffuses out of the segregation band and no liquification occurs. Hence, the segregation of manganese and sulfur to austenite grain boundaries is limited. Therefore, resistance of this steel to HAC is higher than the resistance of HY-80 steel because there are no local hardened regions containing a high density of MnS inclusions.

3.8. The Role of Traps and Blocking in Reducing Hydrogen Cracking Initiation at Susceptible Defects

On many occasions, formation of defects with low critical hydrogen concentration for HAC values, c_K , can not be prevented. Therefore, it is necessary to reduce the hydrogen trapped in such defects. When uptake of hydrogen to a steel cannot be eliminated, as in the case during welding processes, introducing hydrogen traps into the steel has been considered as a possible solution. To be effective, the hydrogen traps themselves should have high c_K value. Conditions for the best resistance to hydrogen embrittlement have been discussed in the previous sections. The preferred hydrogen trapping sites should be rounded, fine, uniformly distributed, and strongly irreversible. Traps corresponding to the descriptions given above are substitutional elements such as scandium, lanthanum, calcium, tantalum, neodymium, hafnium, and yttrium or carbonitrides with elements such as vanadium, zirconium, titanium, niobium, and boron [77,182].

Addition of blocking elements to steel is also considered a possible solution, because they effectively decrease the hydrogen solid solubility and diffusivity. Elements which have been recognized as beneficial blocks include palladium, cobalt, aluminum, silicon, gold, platinum, silver and sometimes copper. Nickel, as an important alloying element in high strength steel, may not be considered as a blocking element because it exhibits a slightly negative value of the interaction coefficient ε_H^{Ni} [111]. Other blocking elements such as sulfur, phosphor, arsenic, and antimony, especially in the presence of nickel and chromium, have been recognized to be detrimental because they segregate to internal boundaries [77].

The feasibility of using blocks has been investigated by adding small concentration of alloying elements, such as palladium, to reduce the susceptibility to HAC in certain steels (e.g. AISI 4130 steel and PH-13-8 Mo martensitic stainless steel) [9,217,218]. Submonolayer coverage of palladium was found at martensite lath boundaries and manganese sulfide-ferrite interfaces [217,219]. Tritium autoradiography indicated the absence of tritium at MnS inclusions when complexed by segregated palladium [220]. The explanation suggested was that interfacial segregation of palladium

promoted the rejection of hydrogen from these otherwise strong hydrogen trapping sites [221]. Intergranular HAC was significantly reduced in PH-13-8 Mo stainless steel by additions of, up to one wt pct., palladium. Both the blocking capacity of palladium in solid solution and the trapping capacity PdAl precipitates were cited [218]. However, the role of PdAl inclusions as trap sites was not the only important factor because the addition of palladium was found to alter other metallurgical parameters (e.g. chromium and molybdenum grain boundary segregation tendencies). Moreover, the PdAl precipitates were found unable to suppress hydrogen induced quasi-cleavage fracture.

4. HYDROGEN ABSORPTION AND TRAPPING IN STEEL WELDMENT

Hydrogen absorption during the welding process occurs when the metal is in liquid state. In most cases, this absorbed hydrogen becomes supersaturated just after solidification. To prevent hydrogen cracking, this supersaturated hydrogen has to be given sufficient time to degas from the weldment so that the final content at hydrogen cracking susceptible temperature (100° C) is below the allowable value. Therefore, it is necessary to minimize the initial hydrogen absorption during welding process because effective heat treatment for hydrogen degassing is limited to maintain the formation of strong and tough microstructure. Understanding of hydrogen absorption during the welding process has been the primary concern for many investigators in their effort to reduce the amount of diffusible hydrogen in weldment.

Heat treatments to allow sufficient hydrogen degassing depend on the initial amount of absorbed hydrogen and the equilibrium hydrogen solubility in the solidified steel, the weld thickness, as well as the hydrogen diffusion coefficient in steel. Traditional predictions of these heat treatments account for only the hydrogen solubility of steel without the presence of trap sites. However, the complexity of microstructure in high strength steel requires consideration of trap site occupation by hydrogen atoms for a more useful prediction of heat treatment for this class of steel.

Solubility of hydrogen in metals containing trap sites, especially in the form of interstitial and substitutional solutes, has been studied and predicted through the use of statistical thermodynamics [222]. Experimental data compilation has also been provided by Fromm and Horz [223], such as solubility, adsorption, and absorption, as well as mechanical behavior. Additional information about hydrogen solubility in transition metals and their alloys has been contributed by Oates and Flanagan [224]. In addition to the energy solution, they also reviewed the configurational and non-configurational partition function, as well as the effect of alloying to hydrogen solubility in metals. More recently, Fukai [225,226] provides a comprehensive review of hydrogen-metal systems.

4.1. Hydrogen Absorption in Weldment during Welding Process

In arc welding, hydrogen contamination is always present to some extent as a result of decomposition of hydrogenous compounds in the welding arc. This contamination comes from absorbed water in shielded metal arc electrode coatings and submerged arc welding fluxes, lubricants on solid wires for gas metal arc and gas tungsten arc welding, contaminants on base materials, and a humid welding environment. Some water of hydration is always present and necessary in coatings and fluxes, while complete removal of lubricants from solid wires would make them nearly informable and inoperable. [227]. Absorption of water by liquid slag after completion of shielded metal arc welding process can also become the source for hydrogen in the weld metal below the slag. North et.al. [228] showed, as in Figure 25, that there is a good correlation between the amount of absorbed water and the optical basicity index. Hence, basicity index can be used as a basis for design of an optimum low hydrogen welding slag. Since the hydrogen contamination in the electrode core wire and in the base metal are small, the major source of molecular hydrogen in the gas metal arc (GMA) welding comes from high-temperature decomposition of water vapor [228] :

$$H_20\,(g) = H_2\,(g) + 1/2\,O_2\,(g)$$

Both the hydrogen and the oxygen gases are absorbed by the weld pool and commonly described according to the well known Sievert's Law

$$1/2\,H_2\,(g) = [H]$$
$$1/2\,O_2\,(g) = [O]$$

One can combine the three equations into the reaction:

$$H_2O = 2[H] + [O] \quad , \Delta G^\circ = 46{,}180 + 1.57T \text{ Joule}$$
$$K = \frac{[P_{H_2O}]}{[H]^2[O]} = \exp\left(\frac{-\Delta G^o}{RT}\right) \tag{26}$$

Savage et.al. [229] reported that water vapor adds more hydrogen to the weld pool than does an equal amount of hydrogen gas. In another investigation, Shinozaki [160] observed that during GTA welding of HY-100 and HSLA-100 steels with identical oxygen levels in the shielding gas, higher hydrogen additions yield weld metals containing less oxygen. Sorokin and Sidlin [230] also found inverse hydrogen – oxygen relationship when quantifying pore formation in SMA weld deposits. The inter-dependency between oxygen and hydrogen content suggests that these solutes follow the water dissociation reaction. Reduction of the amount of hydrogen in weld metal by using oxidizing electrode during underwater wet welding has been successfully achieved by Pope et. al. through careful addition of hematite (Fe_2O_3) to the covering of electrode flux coating [231,232]

Several studies have been conducted to verify the applicability of Sievert's law in arc melted weld pool. Even though most of these studies revealed that the hydrogen content in the weld pool follow the square root dependence of Sievert Law, it is much higher than the hydrogen solubility of the molten steels examined. Two different explanations have been proposed.

1. Salter [233] and Howden [234] examined the hydrogen absorption in a stationary GTA weld pool in a controlled arc atmosphere. According to their model, the hydrogen is rapidly absorbed into the high temperature 'active' zone, where the arc impinges on the pool where a rapid equilibrium is achieved. Electromagnetic stirring action in the pool transports the hydrogen - saturated liquid metal to cooler regions, in which the solution becomes supersaturated.

2. Gedeon and Eagar [235] reevaluate the initial diffusible hydrogen data of previous investigators. The data is corrected according to theoretical analysis by Terasaki [236] which compensates the amount of hydrogen lost before ice quenching in iced water. He found that the absorption temperatures (calculated from Sievert Law) for hydrogen in welds is in excess of 3000° C. This value is much higher than the temperature limit of 2500° C shown by Block-Bolten and Eagar [237] due to evaporative cooling of iron. In addition, Howden [234] has shown that metal evaporation also reduces weld pool

hydrogen absorption at high temperatures. A new model for weld pool hydrogen absorption was proposed, where hydrogen in the arc partly dissociates so that diatomic and monatomic hydrogen are both absorbed by the weld pool :

$1/2\ H_2\ (g)$	=	[H]	$\Delta G^o = 36{,}482 - 46.14T$ Joule
$1/2\ H_2\ (g)$	=	H(g)	$\Delta G^o_{298} = 0 + 130.6T$ Joule
H (g)	=	[H]	$\Delta G^o = -187{,}360 + 14.14T$ Joule

In contrast to the Sievert law, which assumes diatomic absorption, the monatomic absorption decreases with increasing reaction temperatures. It was assumed that due to a very large temperature gradient in the welding plasma, substantial deviations from local thermal equilibrium (LTE) present in the anode boundary layers so that the monotomic hydrogen may not completely recombine before striking the weld pool. With several assumptions, such as a radial temperature distribution on the weld pool surface; absorption and dissociation reaction temperatures of 2300° C and 2500° C respectively; and 0.01 atm hydrogen partial pressure in the shielding gas, the highest hydrogen absorption will take place around the outer edge of the weld pool, as shown in Figure 26.

Effect of solute metal oxidations on the diffusible hydrogen content

Predictions of the effect of solute metal oxidation on diffusible hydrogen content can be developed based on metal - oxygen thermodynamic equilibria assuming water vapor as the source of hydrogen and oxygen in the weld metal. Some solute metals in the weld pool consume the absorbed oxygen in order to form metal oxides [238]. For example, aluminum, which has a very negative free energy for oxide formation, will react with the absorbed oxygen earlier than does any other alloying element, as shown for isothermic reactions in Figure 27. The subsequent weld metal de-oxidation takes place successively depending on the order of decreasing reactivity for each metal oxide formation as suggested by the Ellingham diagram [239]. In the hydrogen – oxygen reaction, which is the last oxidation reaction in the weld metal, the diffusible hydrogen concentration in equilibrium with the oxygen solute then increases as long as there are

still metal atoms available for oxide formation and kinetics or cooling rates permit. On the other hand, the formed oxides themselves are prospective irreversible hydrogen trap sites which will capture some of the hydrogen and effectively reduce the diffusible hydrogen content in the weld metal. An optimum oxygen content is required to yield the lowest diffusible hydrogen concentration in the weld metal.

Effect of surface active elements on weld pool hydrogen absorption

Li and North [240] have reviewed the effects of impurity elements on surface activity. These elements are thought to alter the balance between hydrogen dissolution and evolution rates at the weld pool surface. It has also been suggested that hydrogen absorption, when a slag is present, may affect the partition of hydrogen between metal and slag and this behavior may more effectively lower the final hydrogen content than does a gas shielded welding process. However, this argument was questioned because the weld pool temperature is high (2500° C) which limits the degree of segregation. In addition, electromagnetic stirring in the weld pool will be dominant and prevent segregation of these elements.

Experimentally, Hirai [241] and Seriu [242] found that the diffusible hydrogen content in Al-killed steel SMA weld deposits increases when the sulfur content in the steel decreases. Also, Seriu [242] indicated that tellurium, selenium and sulfur additions in SMA welding electrode coating formulations markedly lowered the diffusible hydrogen content of low alloy steel weld metal. Du et. al. [243] suggested that some of rare earth elements, being surface active in the molten pool, reduce the surface tension of the liquid metal, which in turn reduces the absorption of hydrogen into the molten pool. Their experiments, using yttrium and tellurium additions to the weld metal, reduced the amount of diffusible hydrogen.

Effect of welding parameters on diffusible hydrogen content of weld metal.

Different welding processes have different sources of hydrogen contamination and absorption reactions. One needs to carefully examine diffusible hydrogen data obtained from different welding processes before drawing any conclusion or make any interpretation. Quintana [244] investigated the influence of process variables in

submerged arc (SA) welding on the amount of diffusible hydrogen in weldments. Welding voltage and current type/polarity have measurable effects on diffusible hydrogen. Increases in voltage are generally associated with larger volumes of fused flux and, therefore, larger amounts of moisture available to contaminate the arc atmosphere. Current type is believed to have a measurable effect on diffusible hydrogen because of its possible influence on decomposition of active components in the flux. The change in current type from DCRP to AC increased diffusible hydrogen by a factor of two to three. The flux may contain carbonates, which are designed to break down in the welding arc and to reduce the partial pressure of hydrogen in the arc atmosphere. This decomposition of carbonates may be retarded in the AC arc as the current passes through zero. Consequently, there would be less CO_2 to displace the hydrogen.

Study of the effect of welding parameters on diffusible hydrogen content in gas metal arc (GMA) welding using cored wires has been attempted by White at.al. [245]. Various welds were made using rutile, basic, and metal cored wires with constrained welding parameters to get 1.4 kJ/mm and 4 gram weld deposit (in 15 mm sample long) for all welds. When rutile wire is used, decrease in current or increase in standoff distance yields a considerable reduction in weld diffusible hydrogen content. On the other hand, low hydrogen levels were obtained when using basic wire, independent of welding current or standoff. As for metal cored wires, a reduction of diffusible hydrogen was observed at low currents when a change of metal transfer mode, from spray to short circuit occurred. The effect of polarity has also been investigated with a conclusion that, under spray transfer conditions, significant reduction of diffusible hydrogen values was obtained when the polarity was changed from electrode negative (DCEN) to positive (DCEP) [246]. Similarly, Pokhodnya and Suptel [247] found that the absorption of hydrogen at the electrode tip, for electrode positive, is lower than the other polarity. It was argued that lower hydrogen pick-up for electrode positive is due to the more spherical shape of the droplets, less agitation, and shorter time of flight.

Chew and Willgoss [248] studying GTA welding, found that an increase in current decreases the amount of hydrogen and thus decreases the corresponding effective reaction temperature (back calculated from diffusible hydrogen). However, it is also possible that the calculated reaction temperature does not correspond to the absorption

temperature, but rather reflects a decrease in the cooling rate, which allows more hydrogen to escape [235]. The effect of polarity in GTA welding may be thought as dominated by electrochemical effect, unlike in GMA welding where metal transfer across the arc plasma involves much more complicated reactions. Ionized hydrogen may be present in the cathode boundary layer so that there may be an electrochemical effect that will draw hydrogen toward the cathode. If the electrochemical effect is dominant, this theory predicts that DCEP welds will have more hydrogen than DCEN welds [249,250].

4.2. Hydrogen Solubility in Defect-Free Metal

A large volume of data regarding hydrogen solubility in iron has been reported [223]. The data of different investigators often show mutual discrepancies in the solubility, and especially in the hydrogen diffusivity. Quick and Johnson [251] performed permeability measurements of hydrogen for the temperature range of 282 to 910° C using zone refined Freeovac E iron with 0.026 wt. pct. carbon. Their results reported an equilibrium lattice concentration of hydrogen, θ, which varies with temperature, T, and hydrogen partial pressure, P_{H_2}, according to Sievert's law.

$$\tfrac{1}{2}H_2 \Leftrightarrow [H]$$

$$\theta = \frac{n_L}{N_L} = 0.00185\sqrt{P_{H_2}}\exp(-3440/T) \tag{27}$$

where n_L is the number of hydrogen atoms in lattice interstitial sites and N_L is the number of available interstitial sites in bcc iron. The above expression is formulated for hydrogen partial pressure P_{H2} in atmosphere and T in Kelvin.

Alternatively, McLellan and Kiuchi [252] correlated a solubility data from various sources reflecting different measurements methods and temperature ranges. They found, through exhaustive statistical analysis, that the data obtained by electrochemical methods and H_2-gas equilibration methods using UHV techniques as well as palladium-coated membranes were among the most reliable. This data was fit over the temperature range of 300 - 1750 K with a statistical-mechanical model. The model was developed using the quasi-regular model [222,253] where the chemical potential of hydrogen atoms

in the solid was assumed equal to that potential of hydrogen atoms in the gas phase. Assuming that the number of hydrogen atoms, n_L , is much less than the number of interstitial lattice sites, N_L , $(n_L << N_L)$, θ is given below according to the Maxwell-Boltzmann distribution as:

$$\theta = \frac{n_L}{N_L} = \frac{P^{1/2}{}_{H_2}\psi}{T^{7/4}} \exp\left\{-\frac{\overline{H}_H - E_o^D/2}{kT}\right\} \exp\left(\frac{\overline{S}_H^{XS}}{k}\right) \tag{28}$$

where $-E_0^D$ is the dissociation energy of H_2 molecule at 0 K per atom, ψ is a known constant [222], and $\overline{H}_H$ and $\overline{S}_H^{XS}$ are the partial enthalpy and excess entropy of dissolved interstitial atoms (hydrogen). They found that the combined data did not linearly fit this model. The simplest explanation for the non-linearity in the $ln(\theta T^{7/4})$ vs $1/T$ plot, shown in Figure 28, was argued to be due to oscillating nature of hydrogen atoms in different interstitial sites over the entire temperature range [254]. The hydrogen atoms occupy the tetrahedral sites in the BCC lattice at low temperature, but can simultaneously occupy both tetrahedral and octahedral sites at high temperatures.

4.3. Hydrogen Solubility in Metal with Trap Sites

Models for the solubility and fractional trapping occupation of hydrogen in metal containing trap sites have been reviewed by McLellan and Kircheim. [129,255,256]. For many of these models, simple nearest - neighbor (first order) statistics were used to calculate the temperature and concentration dependence of the partitioning of interstitial atoms between normal lattice sites and trapping sites. In addition, the energetically distinguishable sites are limited to only two types, i.e. normal site (lattice interstitial sites) and trapped site. An interstitial solute atom (hydrogen atom) whose site is a first neighbor to a trapping site is regarded as occupying a normal site. The situation is schematically depicted in Figure 29. In Figure 29, $\overline{G}_L$ is the free energy required to transfer a hydrogen atom from a standard state to an interstitial lattice site, while $\overline{G}_T$ is the free energy required to transfer from the standard state into a trap site. The total free energy of the defect crystal can be described as

$$G_T^{'} = G_{alloy}^{u-v} + n_L \bar{G}_L + n_T \bar{G}_T - TS_H^c \tag{29}$$

Where G_{alloy}^{u-v} is the free energy of the *u-v* alloy system, without the presence of hydrogen atoms. Here the configurational entropy is given by the Fermi-Dirac distribution, i.e.

$$S_H^c = k.\ln\left[\frac{N_L!}{(N_L - n_L)!\,n_L!}\frac{N_T!}{(N_T - n_T)!\,n_T!}\right] \tag{30}$$

where n_L is the number of hydrogen atoms in lattice site, N_L is the number of lattice interstitial sites, n_T is the number of hydrogen atoms occupying trap sites, and N_T is the number of available trap sites. Applying the constraints :

$$n_T + n_L = n \ = \text{total number of H atom}$$

and

$$\left(\frac{\partial n_L}{\partial n_T}\right)_N = -1 \qquad \text{and} \qquad \left(\partial G_T^{'} / \partial n_T\right)_n = 0.$$

The minimum of $G_T^{'}$ occurs when

$$\overline{G}_T - \overline{G}_L = kT \ln\left\{\left[\frac{N_T - n_T}{n_T}\right]\left[\frac{n_L}{N_L - n_L}\right]\right\} \tag{31}$$

From this formulation, the equilibrium distribution function for hydrogen occupying trap sites n_T can be obtained in the form :

$$\frac{n_T}{(N_T - n_T)} = \frac{n_L}{(N_L - n_L)}\exp\left(\frac{-E_B}{kT}\right) \tag{32}$$

where $E_B = \overline{G}_L - \overline{G}_T$

This formalism yields the fraction of hydrogen occupation at trap site as :

$$\phi = \frac{n_T}{N_T} = \frac{n_L \exp(-E_B / kT)}{N_L + n_L \exp(-E_B / kT)} \tag{33}$$

Graphical description of this hydrogen distribution, under common hydrogen contamination in the atmosphere (approximately 5 ppm), was calculated for selected trapping and is presented in Figure 30. A trap with a high binding energy, E_B , captures hydrogen atoms at higher temperature than traps having lower E_B (shown more clearly for 0.9 fraction of filling for various traps in Figure 31).

Bescher [257] accentuated the Fermi-Dirac form of the above distribution function by rearranging Equation (33) as follows

$$\frac{n_T}{N_T - n_T}\exp\left(\frac{\overline{G}_T}{kT}\right) = \frac{n_L}{N_L - n_L}\exp\left(\frac{\overline{G}_L}{kT}\right) = \lambda^{-1} \tag{34}$$

In turn the probability of occupying trap site *I* is given by,

$$\phi_i = \frac{n_i}{N_i} = \frac{c_i}{c_i^0} = \frac{1}{\exp[(G_i - \mu)/kT] + 1} \tag{35}$$

Here, μ is the hydrogen Fermi energy, $c_i = n_i/N$, and $c_i^0 = N_i / N$, with $N = N_T + N_L$.

The same expression has also been derived from a more general statistical-thermodynamics analysis by Canneli et. al. [258], for the case of the occupation of substitutional atom trap site not affected by the presence of any other hydrogen atom (noninteracting particles). In this statistical model, several cases of interstitial trapping by a substitutional atom has been simulated. The relative concentration of various substitutional-interstitial complexes *S-I, S-2I, ..., S-zI* has been proposed (*z* is the coordination number). For a general case where occupation of a site is affected by the presence of another interstitial atom, some types of cluster formation are prohibited. For example, a subtitutional atom, *S*, with a coordination number, *z*, can not trap more than m interstitial atoms, where $m < z$. Assuming that the energies of all trap sites around a substitutional atom are equal ($E_{sj} = E_s$), the mean occupation number of a substitutional atom, with the formation of complexes limited up to of *S-mI* was given as :

$$\bar{\phi}_s = \sum_{j=1}^{m} j\binom{z}{j}\left(\frac{\exp\left[\frac{j\mu - E_s^{(k)}}{kT}\right]}{Q_s}\right) \tag{36}$$

where $Q_s = \sum_{h=0}^{m}\binom{z}{j}\exp\left[\frac{h\mu - E_s^{(k)}}{kT}\right]$ is the grand partition function of a set of trap sites around S. The function $\binom{z}{j}$ is the number of ways in which the cluster *S-jI* can be arranged and $E_s^{(k)} = jE_s$ is the energy of a cluster *S-jI*.

By introducing the density of states function *g(E)*, such that *g(E)dE* is the number of states per metal atom with energy between E and $E+dE$, the total concentrations of interstitial (hydrogen) atoms can be written as :

$$c = \int g_T(E)\bar{\phi}_T(E)dE + \int g_L(E)\bar{\phi}_L(E)dE \tag{37}$$

where the subscripts T and L refer to the trap sites and lattice sites. The energy of a substitutional atom trap site is perturbed by the long-range interactions with the substitutionals. Following Stoneham [259] a Lorentzian distribution function for trap site was assumed, while a Gausian function was chosen for the lattice sites. The relative concentrations of various *S-jI* clusters were then calculated for different cases and the results are shown in Figure 32. as a function of temperature. For most cases the S-I cluster dominates the trap-interstitial atom cluster population.

Partitioning of hydrogen atoms between lattice and trap sites can also be formulated using the Fermi-Dirac distribution, expressed in Equation (35). For two-energy state partitioning (lattice and one type trap site), the total number of hydrogen atoms can be obtained by summing the number of hydrogen atoms over the two levels of energy , $\overline{G}_L$ and $\overline{G}_T$ [226]

$$c_L + c_T = c$$

Writing the trap free energy as $\overline{G}_T = \overline{G}_L - E_B$,

$$c = \frac{c_L^o}{1+\exp[(G_L-\mu)/kT]} + \frac{c_T^o}{1+\exp[(G_L-E_B-\mu)/kT]} \tag{38}$$

from which one obtains the hydrogen chemical potential

$$\mu = \overline{G}_L + kT\ln c - kT\ln\frac{1}{2}\left[\left(c_L^o - c + (c_T^o - c)\exp(E_B/kT)\right) + \sqrt{\left(c_L^o - c + (c_T^o - c)\exp(E_B/kT)\right)^2 - 4c(c^o - c)\exp(E_B/kT)}\ \right] \tag{39}$$

Here, as before, $c_L = n_L/N$, $c_T = n_T/N$, $c_L^o = N_L/N$, $c_T^o = N_T/N$, $N = N_L + N_T$, and $c^o = c_L^o + c_T^o$. Variation of the chemical potential with hydrogen concentration , c, is shown in Figure 33. Three cases are illustrated in this figure: blocking (E_B/kT=–10); no interaction (E_B=0); and trapping (E_B/kT=10), with $c_T^o = 0.2$. As shown, hydrogen trapping is effective in low concentrations of hydrogen, while blocking is effective in high concentrations of hydrogen.

Under conditions where the Fermi-Dirac statistics is reduced to the more commonly used Boltzmann statistics, i.e. for small hydrogen concentrations, $c << c_T^o < 1$, the following expression is obtained

$$\mu = \overline{G}_L + kT\ln\frac{c}{1-c_T^o + c_T^o\exp(E_B/kT)} \tag{40}$$

Substituting μ back into Equation (38), the concentration of hydrogen in lattice sites, the diffusible hydrogen concentration, is given as :

$$c_L = \frac{c}{1-c_T^o + c_T^o(-E_B/RT)} \tag{41}$$

For dilute alloys or low density of traps (c_T^o << 1) [260]

$$c_L = \frac{c}{1+c_T^o(-E_B/RT)} \tag{42}$$

Note that, with the Boltzmann statistics, no assumption has been made regarding the value of E_B, it may have a lower value (trap) or higher value (anti-trap) than G_L. Therefore, Equation (40) (38)–(42) are valid for repulsive interaction or blocking as well.

5. PHENOMENOLOGY OF HYDROGEN TRANSPORT IN STEEL

It is well known that hydrogen transport in steels cannot be fully described in terms of a Fourier's type equation; i.e.

$$\partial c / \partial t = \nabla.(D \nabla c) \tag{43}$$

This equation ignores trap effects, diffusion obstacle, non-uniform solubilities, and transport by dislocations. Its simplicity, however, has made it useful for prediction of heat treatment for weld joint so that sufficient hydrogen is degassed from the weld metal before the hydrogen cracking susceptible temperature (100° C) [1,136]. These predictions help prevent hydrogen cracking in mild steels. However, the complexity of microstructures and stress states in high strength steel weldments made such predictions inappropriate. Models which have been proposed to supplement the above equation can be divided into three classes [261] :

(i). Diffusion with trapping models

(ii). Transport by dislocation models

(iii). Non-uniform solubility model in which Fourier's equation is replaced by $\partial c / \partial t = \nabla.[DS\nabla(c/S)]$, (S = hydrogen solubility).

The first two models relate directly to the hydrogen - trap interactions. The third model has been applied toward the study of diffusion in bimetallic materials [262,263]. It can be applied whenever solubility is non-uniform, for instance, in the presence of a temperature gradient.

More generalized and comprehensive models have also been proposed such as that of Hashimoto and Latanision [264]. This model attempted to account for both hydrogen capture by trap sites, as well as hydrogen transport by dislocation sweeping. Their model was developed within the framework of the McNabb and Foster formalism but modified to include the accumulation or depletion of hydrogen due to moving traps as

well as the increase of stationary trap site density with time, as a result of plastic deformation.

Another general diffusion model was proposed by Leblond and Dubois [261]. They used a Boltzmann type statistical transport equation to model the random jumps of hydrogen from site to site. Except for hydrogen transport by dislocations, the other previously mentioned models are special cases of their statistical model. With a different approach, Ueda and Murakawa [265] proposed a two phase diffusion model of hydrogen in steel by developing two mass balance equations, one for diffusible and another for trapped hydrogen. Under appropriate assumptions, their model also reduced to models of the McNabb and Foster for the non-equilibrium case and the Yurioka model [266] for the situation where the equilibrium between lattice and trapped hydrogen is achieved instantaneously.

5.1. Apparent Diffusivity of Hydrogen in Steel

Published values for the diffusivity of hydrogen in steel [251,267270] are plotted in Figure 34. When the temperature falls below 200° C, the apparent diffusion rate of hydrogen in ferritic steels becomes smaller than that for the actual lattice diffusion of hydrogen in an iron matrix. This reduction in hydrogen mobility has been attributed to hydrogen trapping by reversible traps. On the basis of a hydrogen trapping theory, Oriani [260], with the assumption of local equilibrium between the mobile hydrogen and trapped hydrogen populations, proposed the following equations for the apparent diffusion coefficient:

$$J = -D_a \frac{dc}{dx} = -D_L \frac{dc_L}{dc}\frac{dc}{dx} \tag{44}$$

Using Equation (42), $c_L = \dfrac{c}{1 + c_T^o(-E_B / RT)}$ for the relationship between c_L and c, the following expression was obtained :

$$D_a = D_L \frac{dc_L}{dc} = \frac{D_L}{1 + c_T^o \exp(E_B / RT)} \tag{45}$$

Koiwa [271] also proposed an equation for hydrogen apparent diffusivity in the presence of substitutional impurities. He started with the premise that longer diffusion time is necessary due to longer residence time of hydrogen atoms in trap sites (with vibration frequency ν_T) than in the lattice (with vibration frequency ν_L). His model yields similar result as that proposed by Oriani [260] and is given as

$$D_a = \frac{D_L}{1 - c_T^o + c_T^o(\nu_L/\nu_T)\exp(E_B/RT)} \tag{46}$$

Another factor that influences the apparent diffusivity of hydrogen at low temperature is the precipitation of hydrogen gas at microcracks or voids. It has been clearly demonstrated that voids may be formed at the site of non-metallic inclusions in steel by the action of cold working. A model for hydrogen diffusivity in steel containing voids has been developed by Chew [272] by combining Fick's first law, Sievert's law, and ideal gas law. For partial pressure of hydrogen gas equal to one atmosphere,

$$D_a = D_L \frac{RTS}{RTS + 2P_{H_2}^{1/2}F} \tag{47}$$

where S is the solubility of hydrogen in iron at one atmosphere, F is the volume fraction of voids. However, ideal gas law is not valid at higher pressure and thus, Chew extended his equation for p>1atm as follows,

$$D_a = D_L \frac{XRTS}{XRTS + 2p^{1/2}F} \tag{48}$$

where $X = \exp\left(\frac{K'-1}{2}\right)K'^3$, and K′ is the ratio of actual pressure volume product to that of the ideal gas.

5.2. Diffusion of Hydrogen with Trapping Models

A large number of hydrogen trapping studies has been assessed from permeation experiments, wherein a thin membrane of metal is exposed to a high hydrogen partial pressure on one side and the hydrogen flux coming through the membrane is continuously measured, typically recorded as shown in Figure 35. To correlate the measured hydrogen flux with lattice hydrogen diffusivity and with trap binding energy

and density, McNabb and Foster developed a phenomenological model describing diffusion of hydrogen in the presence of traps [79,273,274]. This model leads to the equation,

$$\frac{\partial c_L}{\partial t} + N\frac{\partial \phi}{\partial t} = D_L \nabla^2 c_L \tag{49}$$

where $\frac{\partial \phi}{\partial t}$ is the rate of trapping and ϕ is the fraction of occupied traps ($\phi = n_T/N_T$). The physical nature for this equation is general; it assumes that the traps are isolated and of one kind, i.e. do not form an extended network, and that transport between traps is by lattice diffusion. For the presence of a reversible trap, the rate of trap filling is the net rate of capture and release with parameters κ and ρ, respectively, and is given by :

$$\frac{\partial \phi}{\partial t} = \kappa c_L (1-\phi) - \rho\phi \tag{1}$$

Intricate analytical solutions of this equation have been obtained by using dimensionless parameters for specific cases [274]. Since the introduction of the McNabb and Foster solution, a large number of mathematical models pertaining to hydrogen permeation in thin membranes have been developed to study hydrogen trapping in various metals and under various environmental conditions.

Refinements of the McNabb and Foster model have been proposed and have been solved, analytically or numerically. Caskey and Pillinger [275] treated the McNabb and Foster mathematical analysis in dimensionless form. They applied the finite difference method to solve the non-linearity of the McNabb and Foster equation. The effects of both the reversible and irreversible traps on hydrogen permeation and evolution were simulated for a wide range of boundary conditions corresponding to permeation, absorption, and evolution. An important result of their investigation was that trapping can be present to a significant degree, but may go undetected during a permeation experiment. Analysis of the experimental data by simple time-lag or inflection point techniques do not of themselves detect trapping, and may lead to substantial error in calculations of diffusivity and solubility. The presence of trapping may be detected by

conducting both permeation and evolution experiments, in succession, and comparing the two curves, as shown in Figure 36.

The kinetics of trapping at low hydrogen concentration was examined by Iino [81]. For low hydrogen concentration, a modification of the McNabb and Foster formalism was used because the a-priori assumption that the trap and lattice concentrations were in equilibrium is not satisfied. Hence, less effect will be observed in hydrogen diffusion than that when the trap is still far from equilibrium occupation. Under these conditions the steady state hydrogen distribution in a permeation slab is not linear , resulting delayed permeation characteristics as shown for various trap strengths in Figure 37.

Another analysis on irreversible traps was also investigated for a wide range of hydrogen concentrations. Figure 38 shows the calculated result reported by Iino [276] for irreversible trapping. It shows that, for low hydrogen concentrations, trap coverage remains low and irreversible trapping continues to be active. Iino's investigation with large hydrogen concentrations showed that the traps are saturated after a short time and hydrogen diffusivity is no longer dependent on the presence of traps. For intermediate hydrogen concentration, the permeation flux exhibits, in general, the first plateau when the trapped population is increasing and then transferred to a normalized flux value of one when the trapped population ceases to increase. Similar behavior has been experimentally observed by Bernstein [86], in a permeation experiment of titanium microalloyed HSLA steel.

The possibility that the traps are not uniformly distributed in the lattice has been addressed by several researchers [277,278]. It has been found that the distribution of traps may have an error function type dependency. This behavior has been observed in ion implanted specimens and through diffusion annealing. Such a distribution for reversible traps has been shown to be less effective in limiting hydrogen diffusion in metals than a uniform trap distribution with the same number of traps. As shown in Figure 39, an error function trap distribution would have the same effect on hydrogen diffusion as that caused by a uniform trap distribution with an order of magnitude fewer traps.

Some other efforts to improve the understanding of hydrogen diffusion in metals containing traps have involved the study of physical phenomena that occur at the metal

surface. Behavior at the metal surface must be understood because it is directly related to the boundary condition for the McNabb and Foster model. The metal or steel surface in common permeation technique has always been coated with palladium to fix the surface hydrogen concentration [279], otherwise the measured permeation rate can vary with metal surface conditions. Relevant to this subject, Makhlouf and Sisson [280] incorporated the hydrogen mass transfer at the metal surface as the boundary condition in their model for hydrogen permeation without palladium coating. They assessed the database for the surface limiting hydrogen mass transfer coefficient, for various metal and surface conditions, by comparing both the data obtained with and without palladium coating. Kleshnya and Krapivnyi [281] also proposed a model that improved the McNabb and Foster model by considering the fact that the trap occupation at the hydrogen entry surface varies with time until a steady state condition is achieved. Their model was developed to explain the maxima of hydrogen flux found in some permeation measurement of steels containing different sulfur content [282].

5.3. Transport of Hydrogen by Dislocation Models

Moving dislocations can act as rapid and efficient carriers or sweepers of hydrogen, as was experimentally verified by tritium release rate and penetration experiments of Donovan, Louthan, and co-workers [283,284,285], and also by permeation experiments of Kurkela and Latanision [286]. Dislocation sweeping has been thoroughly studied by Tien et. al [287,288] who also showed the close relationship between the kinetics of embrittlement, under strain loading, and the transport of hydrogen to critical failure sites within the material. Hydrogen atom can follow the motion of dislocation with a velocity which was derived through the Einstein-Stokes relationship [289] :

$$\upsilon = \left(\frac{D}{kT}\right)F \tag{50}$$

where D is the lattice diffusivity of hydrogen and F is the effective driving force per atom of hydrogen on the dislocation. A critical velocity υ_c, for hydrogen to move along with dislocation, was assumed for a critical driving force F_c , that corresponds to a gradient of

hydrogen - dislocation binding energy, E_B , assumed to be distributed over a distance of 30 Burgers vector ($F_c=E_B/30b$). Above υ_c, or at a strain rate greater than $\dot{\varepsilon}=\rho.b.\upsilon_c$ the dislocation line can be expected to break away from its hydrogen cloud and dislocation sweeping is no longer effective.

Dislocation sweeping can produce hydrogen enrichment in the matrix, which was postulated to occur through two possible mechanisms. The first mechanism is by the annihilation of hydrogen carrying mobile dislocations with each other, while the second mechanism is by the transfer of hydrogen from the dislocations to deeper traps.

The first mechanism, known as the dislocation annihilation model, was first analyzed by Johnson and Hirth [290]. They found it to be non-operative as a lattice enrichment mechanism in a trap free matrix because the arrival rate of hydrogen containing dislocations at annihilation sites is lower than the departure rate of hydrogen out to the surface of the material. However, Nair et.al. [288] included trap sites in their model and found that hydrogen accumulation at dislocation annihilation sites in the matrix is preserved by the presence of traps and the leakage rate out to the surface is insignificant.

The second mechanism, which is termed the dislocation stripping model, was derived by Tien et. al [287,291] and Nair et.al. [288]. This model is based on hydrogen accumulation at trap sites due to dislocation-barrier collisions rate, the stripping of the hydrogen from the dislocation along the encounter length, and the leakage rate of hydrogen from the traps (Figure 40). The kinetic equation of trap interface enrichment is expressed in term of hydrogen arrival flux at the trap interface

$$I_A = \left(\frac{g.L^2}{b^2 f^{1/3}}\right)\dot{\varepsilon} \tag{51}$$

where I_A is the arrival rate of hydrogen atoms to the interface, g is a geometric factor, L is the particle dimension intercepting the dislocation, f is the volume fraction of the particles, b is the burger vector and $\dot{\varepsilon}$ is the strain rate. I_A drops to zero as $\dot{\varepsilon}$ exceeds $\dot{\varepsilon}_c$. The trap site (inclusions interface) was assumed to be in local equilibrium with adjacent lattice sites. Both the Boltzmann and the Fermi-Dirac distributions were applied to determine the hydrogen concentration at the trap sites as a function hydrogen

concentration at the adjacent lattice sites. The leakage rate was approximated by lattice diffusion of hydrogen from the lattice sites adjacent to the trap sites. For a trap having a finite binding energy, the ratio of the leakage rate and the hydrogen arrival rate is :

$$\frac{I_L}{I_A} = 1 - \exp(t/\tau) erfc\left[(t/\tau)^{1/2}\right] \tag{52}$$

where $\tau = \dfrac{(\delta \exp(-E_B/kT))^2}{D_H}$ and δ is the trap interface thickness that holds hydrogen atoms. The leakage rate is inversely proportional to the time constant τ and, for an irreversible trap, was shown to be negligible.

A more recent attempt to model the variation of hydrogen concentration in the matrix was the proposed macroscopic diffusion model by Hashimoto and Latanision [292]. This model included the effect of both the stationary trap sites and the net flux mobile trap sites (dislocations). The McNabb and Foster formulation was used for the hydrogen accumulation by the stationary traps, while the other mode of hydrogen accumulation of hydrogen was assumed to be proportional to the accumulation of flux dislocations within a small elemental body. Their calculations show that dislocation transport of hydrogen becomes important when lattice hydrogen concentration is small so that the majority of hydrogen is trapped at dislocations.

6. EXPERIMENTAL METHODS TO EVALUATE HYDROGEN TRAPPING, HYDROGEN CONTENT AND DISTRIBUTION IN STEEL WELDMENT

There are several methods suitable for the experimental study of hydrogen – trap site interactions [293, 294]. These methods include :

1. Long range diffusion method, which involves measurements of hydrogen diffusivity either through a thin membrane in a permeation experiment or out of a charged sample in a thermal desorption or annealing experiments.
2. Magnetic relaxation method, developed by Kronmuller [295] , makes use of the interaction of hydrogen dissolved in a ferromagnetic material with the walls of magnetic domains.
3. Mechanical relaxation method, which applies the internal friction principles of iron containing hydrogen, including the short range Snoek relaxation at low temperature [296] and the long range Gorsky relaxation [297].

6.1. Permeation Technique

Permeation methods have been used to determine the hydrogen solubility and diffusivity in metals [78,298]. All permeation techniques involve the measurement of the time necessary for hydrogen to enter into the metal, migrate through the thickness of the specimen, and then be detected on the output side. Most permeation techniques are performed with electrochemical methods [299,300], as in the pioneering work of Devanathan and Stachurski [301], where hydrogen introduction into the metal is done in an aqueous solution by electrochemical charging, either using a galvanostatic or a potentiostatic arrangements. Limitation of this technique has been discussed [302]. Among these limitations are difficulties in determining the input hydrogen fugacity resulting from a strong dependence of permeation on the nature of electrolyte (acid or basic), whether or not it contains poisons, surface conditions, current and voltage ranges. An alternative technique, by gas phase charging [303,304], can provide easy control of inlet hydrogen fugacity but was found impractical for low temperature measurement due

to the surface impedance problem. This problem limits its application to low fluxes which are far below the level of interest in low temperature stress corrosion and hydrogen embrittlement studies [305, 306].

A gaseous permeation technique which utilizes the well-defined input fugacity of gas phase charging, coupled with the sensitive electrochemical detection method for studying hydrogen diffusion behavior at low temperatures was developed by Lin and Johnson [302]. By using the sensitive electrochemical detection technique, it is possible to measure the hydrogen fluxes which correspond to equilibrium with hydrogen gas at one atmosphere pressure and 300 K, i.e. lattice hydrogen concentration of the order of one hydrogen atom for every 108 iron atoms. A typical set-up is shown in Figure 41. Similar set-ups have also been developed by Surkein and Heidersbach [306].

The variation of diffusion data due to inconsistent hydrogen input fugacity can be minimized, if the gas-electrochemical hybrid technique is used. However, there are still two other sources of errors which arise from variations in exit surface reactions and variations in calculation technique. Palladium coating has been suggested as the best solution toward minimizing surface reactions, while the other source of error remains a matter of continuing controversy. No generally accepted means of calculating hydrogen permeation rates now exists.

Computational models of transport are dependent on the hydrogen charging method. The simplest techniques use a simple Fick's second law approach

$$\frac{\partial c}{\partial t} = D_a \frac{\partial^2 c}{\partial x^2} \tag{53}$$

where the effect of trapping is embodied in the apparent diffusion coefficient D_a. Different charging condition such as single current pulse techniques [307], potentiostatic techniques [308], and difference techniques using two materials with different diffusivities have been proposed and their distinctive solutions to the second Fick's law has been obtained. Curve fitting of the measured quantities with analytical solutions of Equation (53) for the appropriate boundary conditions can be used to extract the apparent diffusion coefficient. The shortcoming of such techniques is that the effect of the number of trap sites and hydrogen-trap binding energy to hydrogen permeation flux can not be

easily distinguished. Moreover, Oriani's description of the apparent diffusion coefficient assumes local equilibrium between trap sites and lattice sites, while most of the permeation experiments are transient in nature, starting with trapping conditions that are far from equilibrium.

Incorporating the McNabb and Foster formalism into the Fick's second law enables one to obtain solutions for various charging conditions that consider the binding energy from the number of traps as separate variables. Time lag analysis has been the preferred method for investigating the trapping phenomena in metals by potentiostatic charging. In this analysis, the transient stage of the permeation process is measured by a time lag parameter. The time lag is defined by the extrapolation of the integral of output flux against time, as shown schematically in Figure 42. With the proper initial and boundary conditions for potentiostatic charging, McNabb and Foster [79] derived the time lag solution for the phenomenological equation which is given by

$$t_T = t_L\left[1+\frac{3\alpha}{\beta}+\frac{6\alpha}{\beta^2}+\frac{6\alpha}{\beta^3}(1+\beta)\ln(1+\beta)\right] \tag{54}$$

where t_T is the time lag of a permeation measurement of metal containing traps; t_L is the time lag of the metal without the presence of traps, related to lattice diffusion by,

$$t_L = \frac{L^2}{6D_L} \tag{55}$$

where $\alpha = N_T\kappa/\rho, \beta = c_S\frac{\kappa}{\rho} = \frac{\phi}{1-\phi}$ is the hydrogen activity in traps at the input surface (input surface hydrogen concentration is c_S), and $N_L\frac{\kappa}{\rho} = \exp(E_B/RT)$.

In contrast to the simple Fick's Law analysis, the time lag analysis enables one to determine both the hydrogen-trap binding energy and the trap density. Figure 43 shows the time lag from a series of permeation experiments which is carried out under various hydrogen activity at the input surface. At low trap coverage (low hydrogen fugacity), Equation (54) becomes $\frac{t_T}{t_L} = 1+\alpha$. This equation is applicable to region (a) of

Figure 43. At high coverage Equation 44 becomes $\frac{t_T}{t_L} = 1 + 3\frac{N_T}{c_S}$, which is applicable to region (c) of the same figure.

Different analytical methods for the study of hydrogen diffusion have also been proposed. Mc Kibben et. al. [309] applied a potentiostatic double step hydrogen charging method to analyze the data for either the case of diffusion control or interface control. Another technique which allows quantitative analysis to be made of multi trap materials is that proposed by Robertson [310] where periodic changes of input concentration with a particular frequency range can activate only a specific trap site. Bockris and Subramanyan developed a simpler mathematical model than that of McNabb and Foster, assuming that equilibrium between trap and lattice sites is attained immediately after the permeation experiment has started [311]. Several other investigators deduced trapping parameters by curve-fitting permeation curves with numerical models similar to the McNabb and Foster model [312].

6.2. Hydrogen Thermal Desorption Analysis

The hydrogen thermal desorption analysis uses steel samples that have been charged with hydrogen at high temperature and subsequently quenched to subambient temperature, preventing premature evolution of hydrogen from the sample. Inside a hydrogen gas flow measuring device, usually connected to a hydrogen measurement device, such as vacuum gauge [92], gas chromatograph (with thermal conductivity detector) [313], or quadropole mass spectrometer [314], the sample is heated to degas the supersaturated hydrogen out. The nature of the hydrogen gas flow out of the sample has been shown to be sensitive to hydrogen diffusivity in the steel. This sensitivity is thought to be due to the presence of trap sites and the sample geometry. Measurement techniques using this method make use of two applied thermal cycles to detect the evolved hydrogen, first, isothermal, with a rapid heat up of the specimen to the final temperature and second, a slow heat up of the specimen to a final temperature (non-isothermal).

An analytical study regarding isothermal hydrogen evolution from cylinders of iron and steel was presented by Foster, McNabb and Payne [315]. A more practical

experimental set up for the isothermal effusion measurements, based on the method developed by Paltsevich [316] was presented by Pavlik [317]. From these measurements, it is possible to calculate the diffusion coefficient for hydrogen and the activation energy of hydrogen from the hydrogen evolution which was able to escape deep traps. The model started from Equation (1)

$$\frac{\partial\phi(t)}{\partial t} = \kappa(1-\phi(t))c_L(t) - \rho\phi(t) \tag{1}$$

where the trap occupancy $\phi(t)$ and the lattice hydrogen concentration $c_L(t)$ change with heating time due to evolution of hydrogen from the sample. During isothermal heating, the concentration $c_L(t)$ was approximated by :

$$c_L(t) = c_0 . exp[-K.D(T).t] \tag{56}$$

with c_o as the initial lattice hydrogen content, K is a geometrical factor in the fourier solution, and $D(T)$ is the lattice hydrogen diffusion coefficient. During charging, equilbrium between diffusible and trapped hydrogen is attained, so that $\frac{\partial\phi(0)}{\partial t} = 0$ and the initial trap occupancy $\phi_o = \phi(0) = \frac{\kappa c_o}{\kappa c_o + \rho}$. With the above constraints, a first order solution of Equation (1) gives the trap occupancy during hydrogen evolution as a function of time. Such solutions are plotted as line n_1 and n_2 in Figure 44 (the experimentally measured hydrogen content in the specimen is also presented). During initial measurements, the hydrogen evolution is dominated by degassing of diffusible hydrogen from the sample, but later, it is controlled by hydrogen escaping from the trap sites. The hydrogen escape rate, ρ, from the trap site can be determined from the slope of the measured rate of hydrogen evolution when the evolution is controlled by the hydrogen escaping from trap sites, as shown in Figure 45.

Lee et.al [318,319] published several interesting articles about non-isothermal evolution of hydrogen. A typical experimental set-up is shown in Figure 46, where the charged sample is heated in a chamber continuously flushed with argon. The evolved hydrogen gas is detected through either a sensitive pressure detector or by a thermal conductivity detector. With a constant heating rate, it is possible to get different peaks of

hydrogen evolution corresponding to different types of trap sites in the sample. Assuming that the hydrogen can only escape from trap site during the non-isothermal heating, the rate at which hydrogen escapes from trapping sites can be derived as,

$$\frac{dX_T}{dt} = A_c(1 - X_T)\exp\left(\frac{-E_T}{RT}\right) \tag{57}$$

where X_T is the fraction of hydrogen evolved and A_c is a constant related to the hydrogen escape rate, ρ. Correspondingly, $(1\text{-}X_T)$ is equal to ϕ in Equation (1) and dX_T/dt is the instantaneous flux of hydrogen from the specimen by one trap site. E_T is the sum of the trap binding energy, E_B , and saddle point energy, E_S (E_T=E_B+E_S). For a constant heating rate $\lambda = dT/dt$, the maximum rate at which hydrogen can escape from a trap site is obtained when

$$\frac{d(dX_T/dT)}{dt}\Big|_{\max} = \left[\frac{E_T\lambda}{RT^2} - A_c\exp\left(\frac{-E_T}{RT}\right)\right]\left(\frac{dX_T}{dt}\right) = 0 \tag{58}$$

where $T = T_0 + \lambda t$, and T_0 is the initial temperature. Solving the above equation gives

$$\frac{E_T}{RT_c^2} = A_c\exp\left(\frac{-E_T}{RT_c}\right) \tag{59}$$

where T_c is the temperature at which maximum hydrogen evolution occurs. Assuming E_S to be constant, T_c decreases with decreasing trap binding energy. By differentiating the above equation with respect to $1/T$, and taking the log of both sides,

$$\frac{\partial\ln(\lambda/T_c^2)}{\partial(1/T_c^2)} = -\frac{E_T}{R} \tag{60}$$

As λ and T_c are known, E_T can be calculated from the slope of $\ln(\phi/T_c^2)$ vs. $(1/T_c)$. Some limitation of this model may be the assumption that the hydrogen evolution out of the specimen is the same as the hydrogen detrapping rate, neglecting lattice diffusion.

With this method, identification of different types of traps coexisting in the specimen can be determined. As shown in Figure 47, experimental results for a specimen containing dislocation and microvoids exhibit two distinctive peaks corresponding to the two types of traps. Also, the influence of the traps interface characteristic to the binding energy has also been observed, such as the result for TiC particles shown in Figure 48.

A different analytical approach for non-isothermal experiment has been presented by Ono and Meshi [94]. They followed the Flynn solution [320,321] for gas evolution out of a sample, where the diffusion coefficient is time dependent (due to the change of temperature with time) and independent of the lattice space. The evolution of hydrogen from the specimen was approximated as :

$$\frac{\partial c_L}{\partial t} = -\alpha^2 D_L (c_L - c_L^e) = -\alpha^2 D_a (c - c_L^e) \tag{61}$$

where c_L is the diffusible hydrogen concentration, $c = c_L + c_T$ is the total hydrogen concentration, c_L^e is the equilibrium hydrogen concentration, and $\alpha = \pi/2d$ is the lowest order eigenvalue satisfying the boundary conditions. The apparent diffusion coefficient, D_a, is lower than the lattice diffusion coefficient, D_L, and is defined as :

$$D_a = \frac{D_L . c_L}{c_L + c_T} = \frac{D_L}{1 + \left[1 + (\kappa/\rho).c_T^o\right]} \tag{62}$$

where $D_L = D_o exp(-E_S/kT)$ and $\kappa/\rho = \gamma\, exp(E_B/kT)$. The effect of both lattice diffusion and detrapping kinetics to hydrogen evolution is included in the apparent diffusion coefficient D_a. Since both D_L and κ/ρ are functions of temperature, the evolution curves were curve-fitted by the numerical solution of Equation (62) to obtain the two trapping parameters E_B and γ, while the concentration of the trap site, c_T^o, is directly proportional to the area of the evolution curve. Larger E_B and $\gamma . c_T^o$ shift peak to higher temperature. In contrast to the Lee model, a number of combinations of E_B and $\gamma . c_T^o$ can locate the peak at the same temperature. On the other hand, the peak height and the shape of the curve are unique to a combination of these values.

Recently, Trube and Pavlik [313] developed a modified Pavlik analytical model for isothermal heating [317] to curve-fit the measured evolution curves for non-isothermal heating experiments. The diffusible hydrogen content is calculated from a modification of Equation (56) by considering the fact that the hydrogen diffusion coefficient becomes time dependent, because temperature of the specimen changes with time, giving :

$$c_L(t) = c_0 . \exp\left\{ -K \int_0^t D(T(t)).dt \right\} \tag{63}$$

The factor $\int_0^t D(T(t))dt$ is termed the thermal factor. The contribution of hydrogen detrapping to the total hydrogen evolution was modeled using an equation similar to Equation (2). The hydrogen escape from the trap sites is still based on the McNabb and Foster theory. Under the condition of small specimen dimensions (a) :

$$D/a^2 >> \rho.$$

This constraint means that evolution of hydrogen becomes independent of the geometry of the specimen. Hydrogen is assumed to depend only on detachment from the traps. Since the trap release rate also has a temperature dependency, the trap occupation by hydrogen during non-isothermal heating is described as :

$$c_T(t) = c_T^o \exp\left\{ -\int_0^t p(t)dt \right\} \tag{64}$$

The total hydrogen evolution curve from the specimen is obtained by summing up the derivative of Equation (63) and (64).

6.3. Measurement of Weld Diffusible Hydrogen Content

Diffusible hydrogen content in weldment is commonly determined by degassing the welded specimen in eudiometers filled with collecting fluids, such as glycerin or mercury. In American Welding Society (AWS) specification [322], the weld sample has to be quenched in iced water within five seconds upon completion of the welding process. Following this procedure, the weld sample has to be cleaned and stored in dry ice and acetone solution (–60° C) for a maximum time of three days or in liquid nitrogen (–196° C) for three weeks. Mercury filled eudiometers yield the more accurate results because of the high density of mercury and low solubility of hydrogen. The size of weld specimen for the AWS specification [322] is different from the International Institute of Welding (IIW) specification [323]. Due to the need for a lower detection limit for high strength steel weld specimen, the AWS specification increased the specimen size to 80 mm long from a smaller size specified in early AWS tests. Both the AWS and IIW

standards for diffusible hydrogen require mercury as the collecting fluid, while the Japan Industrial Standard (JIS) allows the use of glycerin. However, the health hazards associated with exposure to mercury limit the use of mercury. Glycerin tests are more widely used in several countries. Due to the high solubility of hydrogen in glycerin and some other collecting fluids, test results obtained from measurements using these fluids should not be considered as accurate.

Due to the health hazards and long period of time required for collection of hydrogen associated with the use of mercury, alternative methods to measure hydrogen from steel samples are used or are still being developed. Alternative methods to substitute the mercury test can be calibrated to the results of the mercury test to allow fairly accurate diffusible hydrogen content value to be reported.

1. Gas chromatography

   This method involves placing a sample in a chamber filled with argon gas at an elevated temperature, usually 150° C. In some systems, the argon gas flows through and thus directly carries the hydrogen gas to the gas chromatograph during heating of the chamber [324,325] . Other methods keep the argon gas in the chamber which will be subsequently injected into the gas chromatograph, together with the collected hydrogen gas after completion of the isothermal heating [326]. Several studies report that gas chromatography is comparably accurate to the mercury method [327,328,329]. The flexibility of gas chromatography has also been applied to measure the residual gas, such as the analysis developed by Pavlik [313].

2. Polymer Electrolyte-Based Hydrogen Sensor

   This sensor is a conducting polymer film coated with palladium on either side [330]. One side of the sensor is exposed to an argon-hydrogen gas mixture and the other side to dry air. The monotomic hydrogen absorbed by the polymer film changes its electrical conductivity; hence, the electric current flowing through the sensor is directly proportional to the hydrogen content in the gas mixture.

3. Wear enhanced method

   Another analytical method, to measure both diffusible and residual hydrogen simultaneously, has been proposed by Baek et. al [331]. Hydrogen is extracted from steel samples by a wear process and subsequently measured by potentiostatic method.

Determination of the trapped or the commonly termed residual hydrogen is traditionally done after the diffusible hydrogen completely degassed from the weld sample. This measurement is done by using the interstitial combustion analysis [332] or by vacuum extraction at 650° C [333].

All of the above mentioned hydrogen determination methods report only the bulk content of the hydrogen content, either as diffusible or as residual hydrogen. The measurement of the distribution of hydrogen in steel weldment has been attempted by various methods. These measurements are :

1. Microsectioning of different weld zones at low temperature followed by hydrogen extraction [334].
2. Bubble counting on the polished cross-section of a weld covered by a film of glycerin [335,336,337].
3. Microprinting of a polished cross-section through a neodymium film [338] or nuclear emulsion silver bromide [339].
4. Spot fusion of a weld cross-section by laser beam followed by mass spectrometric analysis of evaporated hydrogen [69,340].
5. Spot fusion of a weld cross-section by laser beam followed by emission or breakdown spectroscopy [10].
6. Spatial distribution measurement of weld metal hydrogen using tube insertion to weld metal and gas chromatography [341].

7. ROLE OF HYDROGEN TRAPPING IN PREVENTING HYDROGEN CRACKING IN HIGH STRENGTH STEEL WELDING.

The hydrogen content which is established upon the completion of the welding process reduces at a rate that depends on the thermal experience of the weldment. Hydrogen will degas from the weld metal during cooling cycle due to decrease in hydrogen solubility as the temperature drops. In the meantime, the remaining hydrogen atoms in the weld metal will also redistribute themselves to various microstrutural traps in the weld metal, as well as to regions of stress concentration in the weld joint as restraint stresses build up during the cooling cycle. The principles of thermodynamics of hydrogen solubility and hydrogen transport discussed in previous sections have been utilized in many models to calculated hydrogen content and distribution during welding thermal experience. These calculations were made to carefully determine the heat treatment necessary for the weld joint.

The presence of deep hydrogen traps in the weld metal may significantly alter hydrogen content and distribution during welding thermal experience. A reduction of the concentration of diffusible hydrogen has been demonstrated by Pokhodnya [342] through the introduction of rare earth elements into the weld metal, shown in Figure 49. Lensing et.al. [343] have found similar results through the introduction of neodymium and yttrium, as Nd-Fe and Y-Fe powders inserted into GMA welding metal cored wire. Their result for low carbon-low alloy steel is shown in Figure 50. Significant reduction of diffusible hydrogen by more than 50 percent (from 4.5 to 1.5 ml H_2/100 g-deposit metal) when 600 ppm trapping elements were incorporated into the weld metal. In their study, hydrogen thermal desorption analysis has also been conducted. In Figure 51, the hydrogen evolution from weld metal containing neodymium additions is contrasted with evolution from a weld metal free of deep traps. At high temperatures (800-900 K), a peak of hydrogen evolution in the weld sample which contains neodymium, indicative that deep irreversible traps were present.

7.1. Prediction of Hydrogen Solubility and Distribution in High Strength Steel Weldment.

Terasaki, Karpi and Satoh [344] showed that the diffusible hydrogen content of the weld metal after it reaches 100° C (called the residual diffusible hydrogen at 100° C, H_{R100}) correlates to the critical stress required for HAC better than does initial hydrogen content, H_o. Since the values of diffusible hydrogen in standard AWS measurement correspond to temperatures not far below the solidification temperature, numerous calculations to predict the hydrogen content at 100° C from diffusible hydrogen data have been performed, specific to weld thermal cycle, weld geometry, and weld microstructure [344,345,346,347]. These calculations made use of an important operand $\sum D\Delta t$ which is called the thermal factor. The ratio of the remaining diffusible hydrogen, H_R , at any temperature, to the initial diffusible hydrogen content, H_o , can be predicted by using the thermal factor. Such a prediction is considered justified, since good correlation between experimentally assessed H_R/H_o values with the thermal factor values is obtained for several welding processes, as shown in Figure 52 [345]. This data suggests the utility of the thermal factor for calculations of hydrogen evolution from the weld metal.

Further predictions for weld metal hydrogen content and safe conditions for welding led to calculations of the distribution of hydrogen in weldment using finite elements methods [348,349]. The objective of these calculations is the correlation between crack locations with hydrogen localization in the weldment. Such calculations have been correlated with actual crack data in HT-80 steels, where a stress gradient was imposed on a weld bead through tensile loading of weld samples after completion of welding process [349]. Experimentally, it was observed that the crack that initiated in the weld metal is temporarily arrested in the vicinity of the fusion line before resuming to propagate. This temporary arrest was predicted by the FEM analysis to be the time required for hydrogen atoms to accumulate at the crack tip.

Dislocation-assisted transport of hydrogen atoms contributes a major fraction of HAC in high strength steels. The high strength level of this steel causes high restraint stress, even when the weldment temperature is still high, and dislocations are very mobile. This situation leads to extensive dislocation-assisted hydrogen transport in

weldment. Theoretical study to include the role of dislocation-assisted hydrogen transport to localization of hydrogen has been attempted by Kikuta et. al. [350]. In their model, an effective hydrogen concentration, defined as a function of dislocation density $\rho_{\perp}$, was used in the formulation of the strain induced diffusion equation. To a first order of approximation, the dislocation density was assumed to be linearly related to the equivalent plastic strain, or $\rho_{\perp} = \alpha\bar{\varepsilon}_p + \beta$, which implies that only mobile dislocations contribute to this mode of hydrogen transport. In an extreme case, when plastic deformation is confined to the heat-affected zone, their calculation predicted an accumulation of hydrogen in the weld root as high as 5.25 times the concentration in the center of the weld metal.

A more extensive theoretical study has been conducted by Yurioka et.al. [351,352] who considered not only the effect of dislocation assisted hydrogen transport but also the effect of stress assisted hydrogen diffusion to hydrogen localized accumulation in weldment. They introduced a general potential μ:

$$\mu = \mu^{\circ} + RT\ln\gamma.c \tag{65}$$

where $\gamma = \gamma_m.\gamma_p$ is a generalized coefficient, which is a product of factors related to dislocation density ($\gamma_m = \gamma_m(\rho_{\perp})$) and stress gradient ($\gamma_p = exp\ (V_H.\sigma/RT)$). These coefficients may be regarded as weighting functions rather than the actual activity coefficients in thermodynamics definition because they do not correlate to the atomic bonding between hydrogen and the other elements in the solid solution. The equation for diffusion in a heterogeneous medium is given in terms of the activity $a = \gamma c$, where

$$\frac{\partial a}{\partial t} = \frac{a}{\gamma}\frac{\partial \gamma}{\partial t} + \gamma\nabla.\left(\frac{D}{\gamma}\nabla a\right) \tag{66}$$

Finite difference methods were used to solve the above equation and a non-uniform hydrogen distribution, such as that shown in Figure 53, was obtained.

The most useful application of the finite element analysis is the prediction of safe welding conditions, i.e. proper preheat treatment, for various weld joint geometries. Such a capability has been developed by Karpi et. al. [353] who introduced a stress field

parameter. This parameter was designed to include the effect of the stress concentration at a notch as a driving force for hydrogen accumulation, both by lattice diffusion and by dislocation assisted transport. A semi empirical equation has been formulated to determine the necessary conditions for HAC at the crack tip in high strength steel. This formulation utilizes the stress field parameter, combined with the remaining diffusible hydrogen at 100° C (H_{R100}) and the hardness of HAZ (from knowledge of the welding $\Delta t_{8/5}$ and the carbon equivalent (CE) of the steel). Inversely, it is also possible to carefully determine the heat treatments necessary to prevent HAC in high strength steel welding.

7.2. Role of Hydrogen Trapping for Diffusible Hydrogen Control in High Strength Steel Weldment.

In many occasions, heat treatments to prevent HAC in high strength steel require very tight temperature control because they allow only narrow windows of time and temperature ranges. While an extensive heat treatment is necessary for sufficient hydrogen degassing, limitations are necessary to maintain mechanical properties and to minimize hydrogen localization due to the stress assisted diffusion and the dislocation assisted transport of hydrogen. Localized hydrogen accumulation in high strength steel has been shown to be enhanced after post weld heat treatment is imposed upon the weld joint [354]. In this study, hydrogen distribution was measured in a welded joint without heat treatment (Figure 54.a) and with post-weld heat treatment (In Figure 54.b). In Figure 54.b, local accumulation of hydrogen in the welded joint is developed after post weld heat treatment. This localized hydrogen accumulation occurred even though the average content of hydrogen is less than that of the weld joint prior to post weld heat treatment, shown in Figure 54.a. This result implies that, for certain critical weld joints, high restraint stresses preclude recommending any acceptable heat treatment consistent with safe welding conditions.

Prevention of HAC in high strength steel would require an alternative solution to substitute the heat treatment procedure. Hydrogen trapping offers the prevention of HAC during high strength steel welding by reducing the diffusible hydrogen without an extensive heat treatment. Hence, localization of hydrogen at regions of stress

concentration can be minimized. A theoretical calculation of an accelerated reduction of hydrogen in weld metal due to the presence of hydrogen traps has been reported by Olson et.al [10]. They investigated the partitioning of hydrogen between lattice sites and trap sites during the welding cooling cycle with a diffusion model, similar to that of the McNabb and Foster model [79]. Such a model calculates the variation of diffusible (c_L) and trapped (c_T) hydrogen content (in Figure 55.a.) as a function of temperature and time during the cooling cycle (in Figure 55.c.) An abrupt change of slope can be observed in the diffusible hydrogen content right after the martensite start temperature, Ms, of the weld metal. The phase transformation from austenite to martensite is accompanied by a large increase in the hydrogen diffusion coefficient. This model also shows that the diffusible hydrogen content (c_L) of the weld metal containing traps is predicted to be lower than that of the steel without traps. The kinetics of hydrogen capture can be more clearly explained from Figure 55.b, which shows the equilibrium trap occupancy (ϕ_{eq}), the actual trap occupancy (ϕ), and the rate of hydrogen capture ($d\phi/dt$). The hydrogen capture rate depends both on hydrogen diffusivity and the driving force for hydrogen entrapment ($\phi_{eq}-\phi$). It can be seen that a sudden increase in the rate of capture always follows the occurrence of martensite phase formation, where both capture rate determining factors are maximized.

This model was developed in order to set criteria for the selection of traps to prevent HAC in high strength steel welding. Proper trap additions should reduce the amount of diffusible hydrogen rapid enough so that, during the cooling cycle, the diffusible hydrogen levels at hydrogen cracking susceptible temperatures (100-300° C) is below the critical limit. The model demonstrates that this requirement can be achieved with proper combination of several factors such as martensite start temperature of the weld metal, trap-binding energy, trap concentration, and welding cooling rate.

The effects of each of these factors to the amount of diffusible hydrogen at 100° C as well as 300° C are summarized and presented in Figure 56 to Figure 59. The first important parameter of a trap is the hydrogen-trap binding energy. In this calculation, four values of binding energies that correspond to different trap sites were used. They are 60 kJ/mole-H for dislocations, 80 kJ/mole-H for Al_2O_3 inclusions, 100 kJ/mole-H for TiC particles, and 120 kJ/mole-H for rare earth additions. As shown in Figure 56, the amount

of diffusible hydrogen content decreases with increasing hydrogen- trap binding energy. The major advantage of traps with high binding energy is that they provide a high driving force for hydrogen capture in high temperature regions. The data at 300° C provides better insight to how much faster the hydrogen is captured by high binding energy traps as opposed to those traps with low binding energy. Should the HAC start to occur at a higher temperature than 100° C (which may be possible for weld metal with low martensite start temperature) the weld metal containing high binding energy traps will have a better chance to survive.

The diffusivity of hydrogen in the austenite phase is very small, so that the hydrogen cannot be effectively captured or removed from the weld metal until the martensite temperature is reached. The lower the martensite start temperature, the longer time hydrogen has to remain in the weld metal lattice sites. This behavior also means that the available temperature range for effective hydrogen diffusivity and trapping in the ferrite phase becomes narrower and the suppression of diffusible hydrogen content by certain traps becomes less effective. The extreme situation is depicted in Figure 57 for the case of weld metal possessing martensite start temperature of 400 °C. The advantage of using a trap with higher binding energy, i.e., higher capture rate, is then obvious in this very narrow temperature range situation. However, the employment of high binding energy traps for a high martensite start temperature weld metal can lead to a situation where the trapping capacity will be wasted in high temperature regions. This behavior can occur even when the hydrogen diffusivity provides a high potential for easy hydrogen removal from the weld metal. Therefore, the selection of hydrogen traps must consider other factors than just the weld metal or consumable alloying contents.

Conventional hydrogen management usually applies proper heat treatment or sufficiently low cooling rate to provide easy hydrogen removal from the weld and to form a less susceptible microstructure to HAC. In case of weld metal containing trap sites, a certain rate of cooling is also necessary to allow sufficient hydrogen capture time before the temperature reaches 100° C. In the present calculation, the cooling rate is assumed to occur naturally and relatively fast, so that sufficient hydrogen removal by lattice diffusion alone can not be obtained. The effect of cooling rate, shown in Figure 58, appears to be similar to that of the martensite start temperature. A very fast cooling rate, such as a rate

with $\Delta t_{8/5}$ equal to one second, does not permit enough time for hydrogen to leave the weld metal or jump to trap sites. On the other hand, at a slightly slower cooling rate, the presence of traps may yield a low diffusible hydrogen content at 100° C and alleviate the tendency for weld metal HAC. This prediction shows the potential use of traps, substituting for the tight heat-treatment procedure necessary for high strength steel welding.

The concentration of trap sites translates into the capacity to hold hydrogen atoms. A higher concentration of trap sites in the weld metal will produce a lower diffusible hydrogen content, which is in agreement with the calculated result shown in Figure 59. There is also an apparent threshold number of trap sites for optimum hydrogen trapping, Figure 59. The concentration of traps used in the present calculation corresponds to a 100 to 500 ppm range of substitutional atom traps in the weld metal. In the case of inclusion traps, which is the most probable form of traps in weld metal, the trap sites on the surface are of the inclusion - matrix interface. Depending on the cooling rate, the number of trap sites used in this calculation may correspond to a relatively high inclusion volume fraction that yields weld metal with intrinsically low toughness. Obviously, the concentration of trap sites that can be used is limited to an extent in which the toughness is still maintained at an acceptable level. This issue suggests that the success of using hydrogen traps should not only be related to suppressing diffusible hydrogen in weld metal. Its main function should also be to promote a proper distribution of hydrogen, so that a high local accumulation of hydrogen at crack initiation sites can be prevented. Furthermore, in high strength steel welding, where hydrogen is highly concentrated at crack initiation sites, the presence of traps may give a higher tolerance for average hydrogen content. Normally, a low maximum acceptable level of hydrogen content in the weldment is required for conventional welding procedures.

The importance of high binding energy in minimizing release of hydrogen during multiple thermal cycles is contrasted in Figure 60 [355]. A trap site with binding energy of 60 kJ/mol-H would release an extensive amount of hydrogen during re-heating, which can easily contribute to localization of hydrogen at potential crack initiation sites, especially at the weld root. On the other hand a trap with 120 kJ/mol-H binding energy

will release a very small amount of hydrogen atoms and quickly re-trap them before these hydrogen atoms have the chance to migrate to crack initiation sites.

In summary, a trap site should have a high binding energy to allow rapid hydrogen capture, especially in cases where the martensite start temperature is low, as well as minimizing release of hydrogen from trap sites during multi-pass welding. Depending on the concentration of trap sites and their binding energies, a minimum cooling rate, which depends on traps binding energy and trap density, is still required to achieve diffusible hydrogen content below the critical limit. However, this minimum cooling rate is still predicted to be faster than those of most conventional heat treatments used to prevent HAC in weld joints.

The effect of traps on the spatial distribution of hydrogen in weld joint was investigated by Andersson [356], using finite element analysis. This analysis included hydrogen trapping as well as hydrogen transport, driven by gradient of stress and temperature, while dislocation assisted transport of hydrogen was not considered. The traps are considered to exist both as reversible traps and irreversible traps. Chew [272] void model was used for the reversible traps (which are considered to be voids) and McNabb and Foster model was used for the irreversible traps. A comparison between calculated values of the time dependent mean diffusible hydrogen content and the trapped hydrogen content with those values measured directly are shown in Figure 61. The corresponding prediction of hydrogen distribution, presented in Figure 62, shows an accumulation of total hydrogen near the fusion line. Unfortunately, this study was not intended to evaluate the performance of hydrogen trapping for hydrogen management in steel. Therefore, no comparison between different trapping conditions, especially with an absence of traps, is reported to describe the effect of hydrogen trapping on hydrogen distribution in weldment. A similar effort to calculate hydrogen distribution, which depends on hydrogen trapping and stress assisted diffusion, has also been presented by Thomas and Chopin [357], using a commercial finite element code.

8. CLOSURE

Prevention of HAC in high strength steel welding has been done by managing the four interconnecting factors that promote hydrogen cracking. These four factors are the susceptibility of the steel to HAC (hardness), the concentration of hydrogen, the stress intensity factor (due to the weld joint restraint stress), and the temperatures range (between 100° C and –100° C) [1]. In weld joints, all of these factors vary as a function of time during the thermal experience. Pre and/or post-weld heat treatment has been used to manage the four HAC factors during the welding cooling cycle. This procedure successfully prevents HAC in welding of moderate strength steel. It provides optimum cooling rates, slow enough for maximum hydrogen degassing while also maintaining slow restraint stress build up, but still fast enough to acquire an acceptable microstructure. Several practical methods have been used to predict the appropriate heat treatments to control the cooling rate in order to prevent HAC. Most of these techniques may include several variables in their empirical equations, such as carbon equivalent (CE), initial diffusible hydrogen content, plate thickness, and cooling rate from 800° C to 500° C ($\Delta t_{8/5}$) [353].

Recent efforts to understand HAC in the welding of ever higher strength steels involve investigations on distributions of hydrogen, restrain stress, hardness, and temperature in the weld joint, in addition to the effect of weld thermal history. The high strength level of these steels promotes early restraint stress build up, so that regions of stress-concentration can quickly accumulate hydrogen, even before hydrogen degassing comes to completion. Such a local accumulation of hydrogen has been proven to cause HAC, even though the nominal diffusible hydrogen concentration is below the critical value.

Introduction of hydrogen traps into the weld metal has two potential advantages which would help reduce the susceptibility of weld joints to hydrogen cracking. The first is the capability to minimize the content of diffusible hydrogen more rapidly than does hydrogen degassing. The second is the ability of these traps to help prevent localization of hydrogen during thermal cycles because reduction of diffusible hydrogen can be done

without an extensive heat treatment. The addition of trapping elements to the weld pool may have other effects, such as, the thermo-chemical reactions in the arc plasma, surface activity of the weld pool, and phase transformations during welding thermal cycles. Complex interactions between trap elements and other alloying elements are inevitable. Understanding of the various effects that influence hydrogen content and mechanical properties in the weldment has to be assessed to carefully evaluate the role of traps for hydrogen management in high strength steel welding.

9. ACKNOWLEDGMENT

The authors aknowledge and appreciate the research support of the US Army Research Office.

10. FIGURES

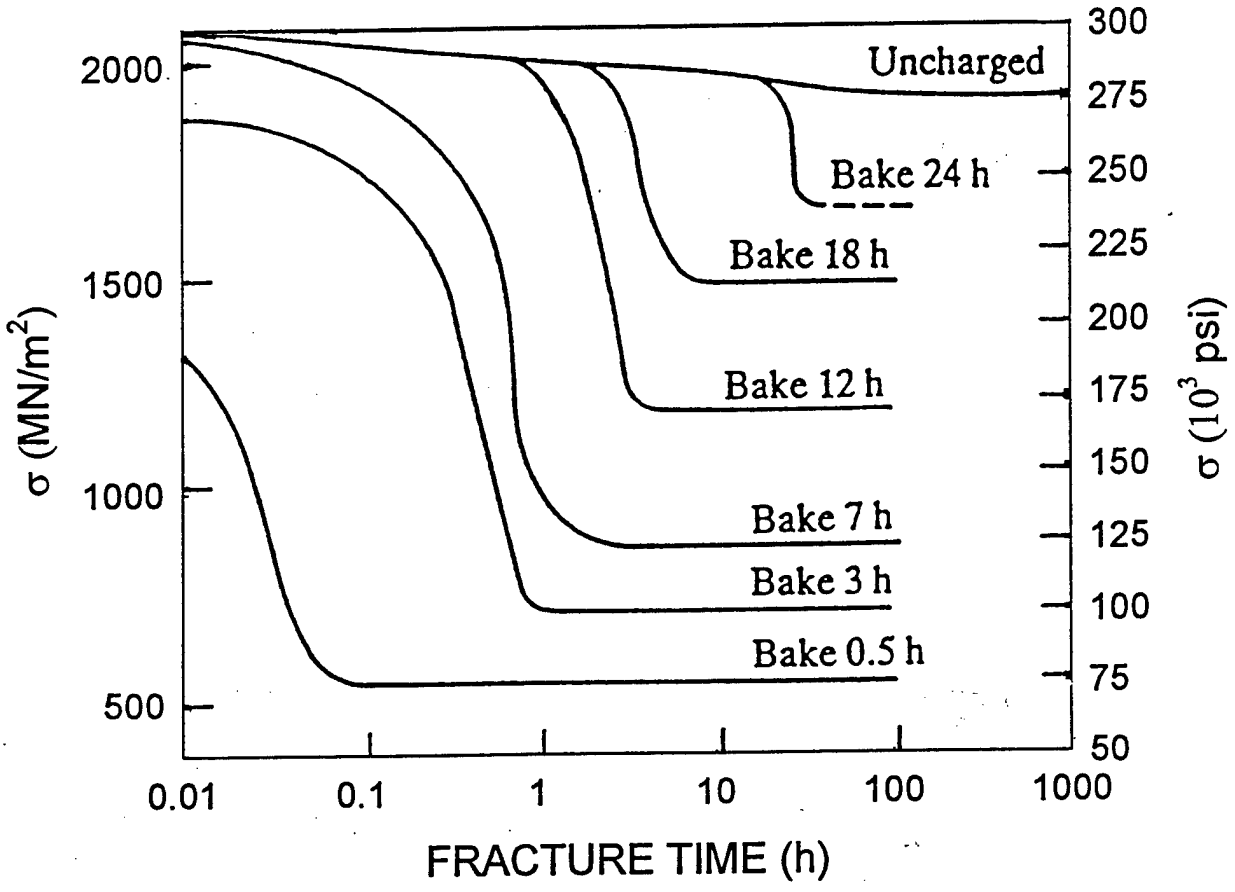

Figure 1. Delayed failure of hydrogenated high strength steel. Various hydrogen concentrations were obtained by baking at different times at 300° C. Sharp-notch specimens. 1600 Mpa strength level [13].

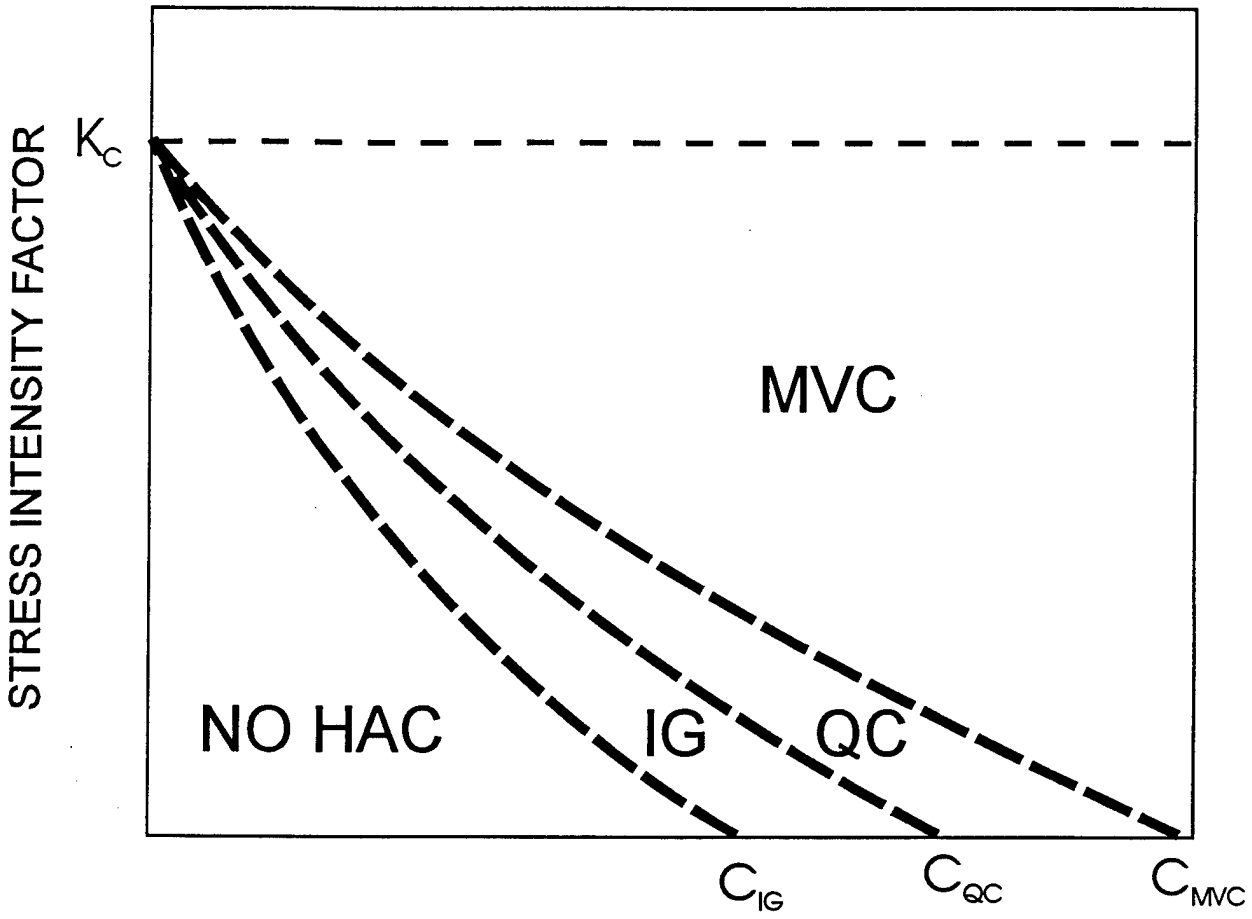

Figure 2. Suggested interrelationship between stress intensity factor, hydrogen content, and HAC deformation mode in microscopically small volumes of crack-tip material. In a constant load fracture, a crack growths with increasing stress intensity factor where the mode of fracture changes from intergranular (IG), to quasi-cleavage (QC), and finally microvoid coalescence (MVC) [16].

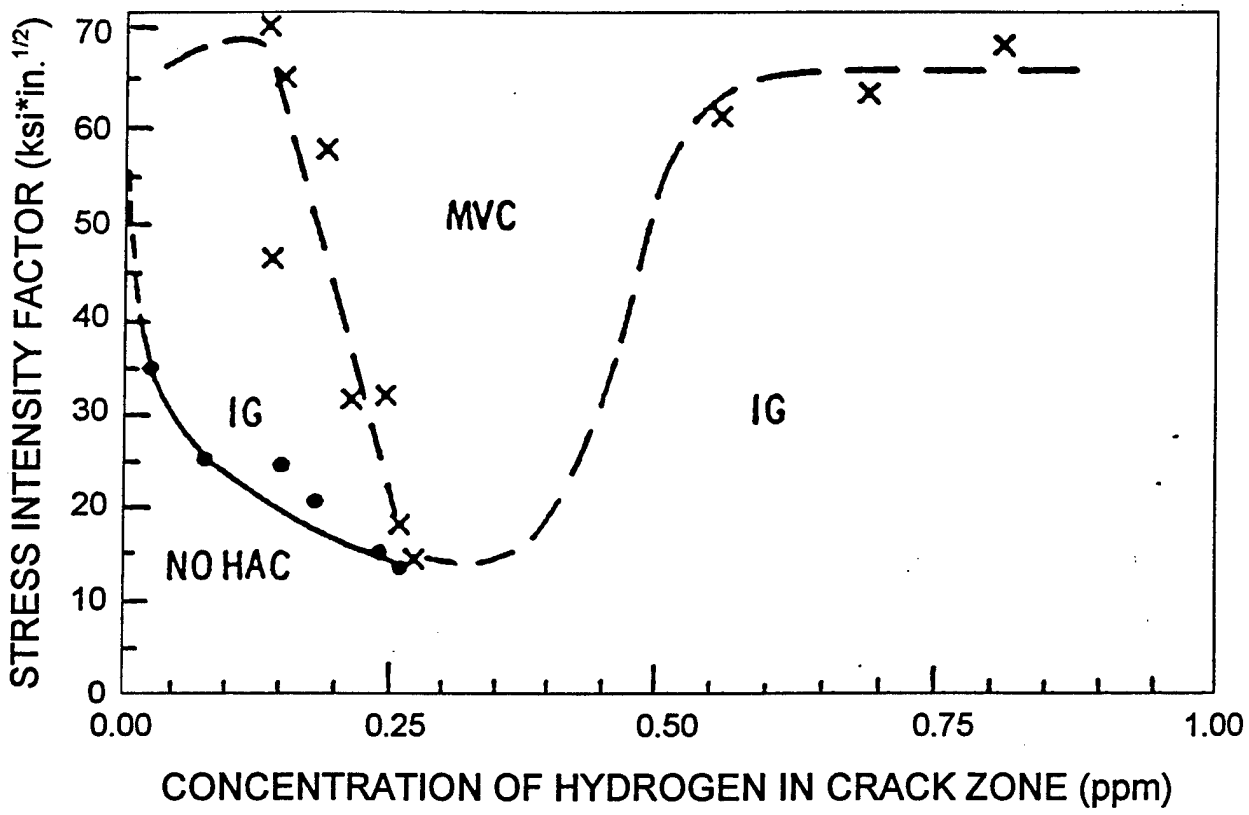

Figure 3. Interrelationship between the stress intensity factor, hydrogen content, and mode of fracture in high strength steel weld, including a hypothesized no cracking region. Observed fracture modes in weld joints were intergranular (IG) and microvoid coalescence (MVC) [7].

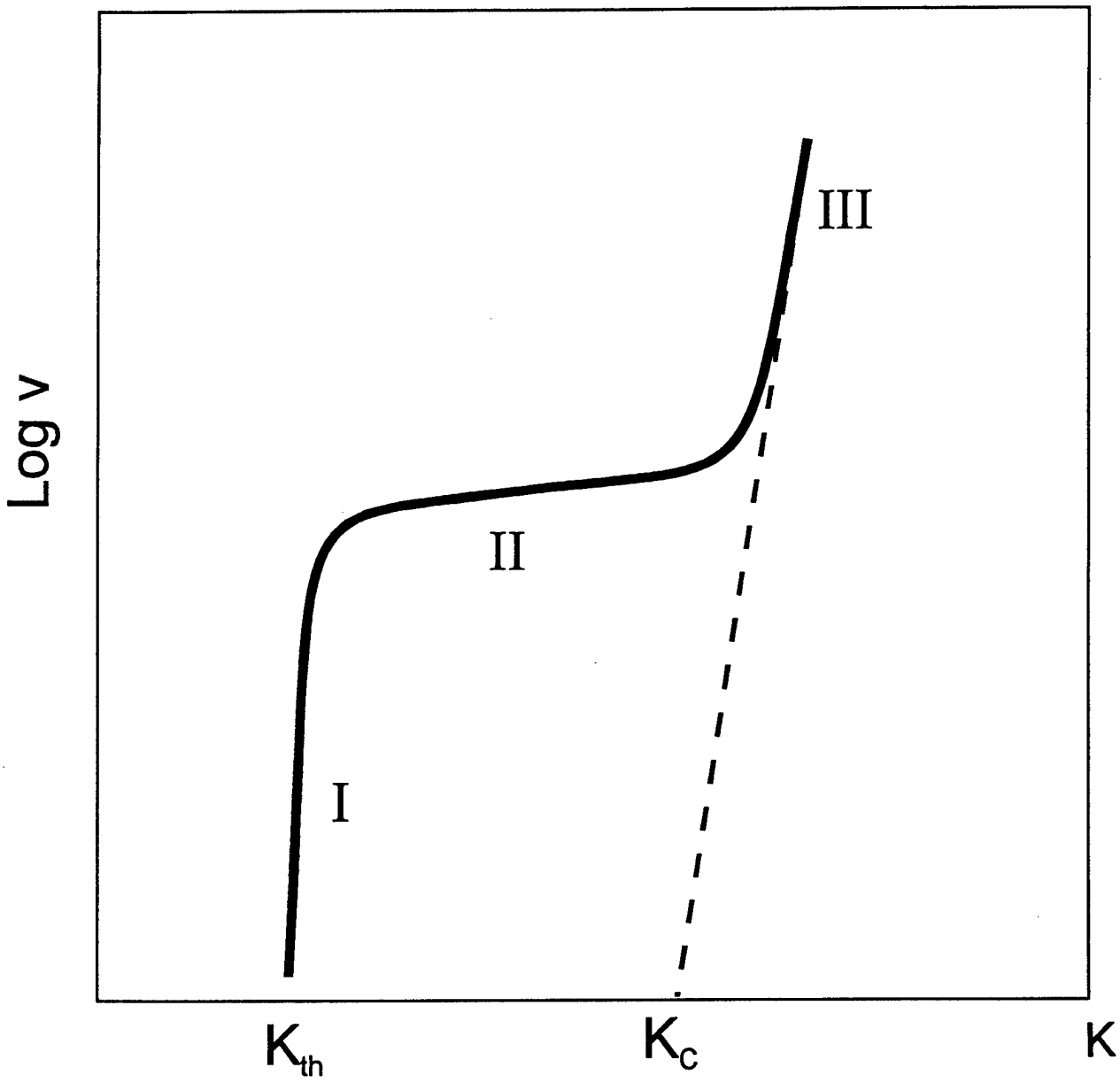

Figure 4. Schematic representation of the crack velocity - mode I stress intensity plot for crack growth under sustained load [17,19]. Th onset of stage I cracking is K_{th}, which is the threshold stress intensity in the presence of hydrogen. Stage II is the stable rate crack growth, which is strongly dependent upon the hydrogen-assisted cracking mechanism. Finally, K_C (the onset of stage III) is the critical stress intensity factor for initiation of crack propagation in air.

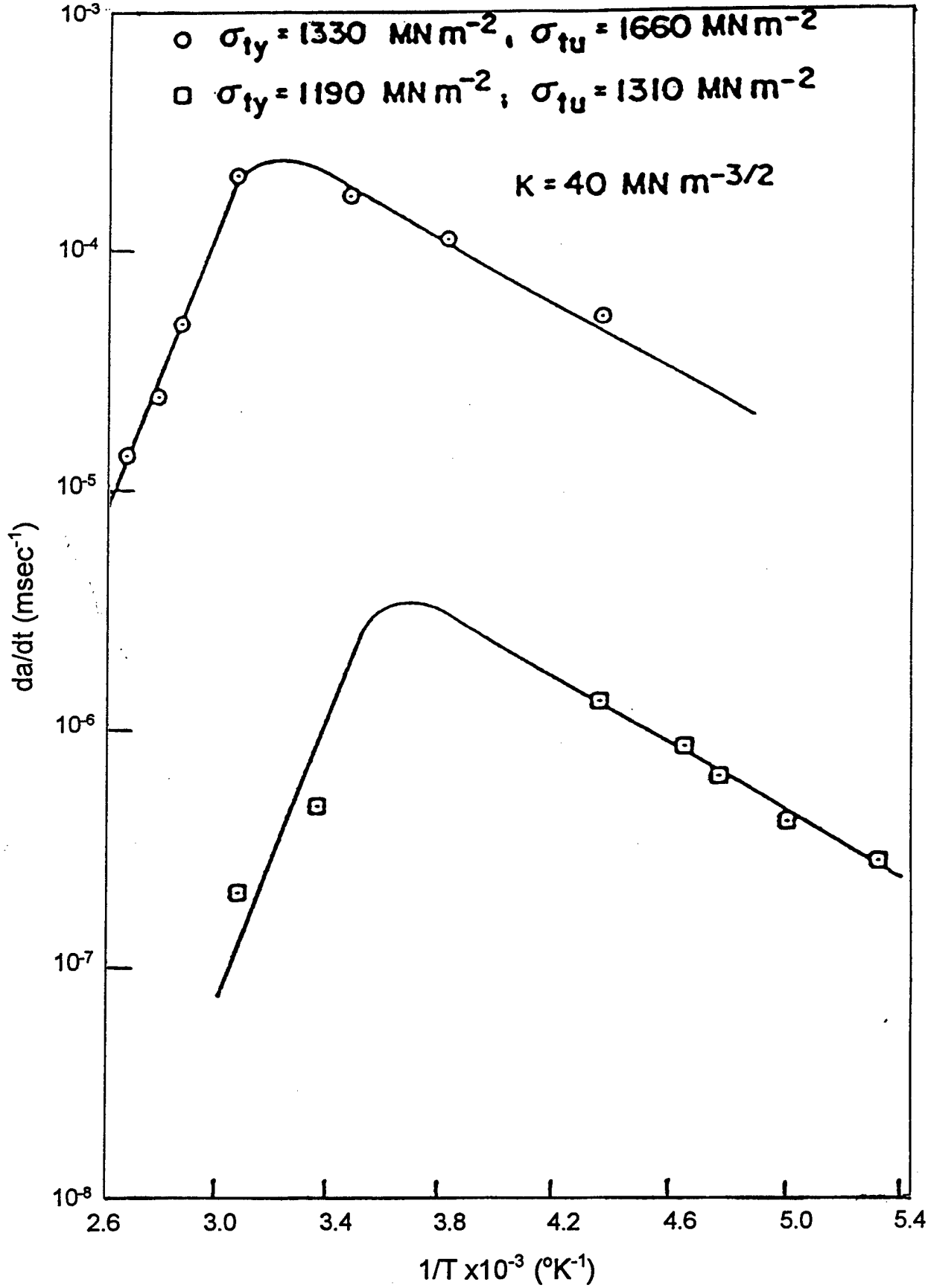

Figure 5. Crack growth rate – temperature relationship, in stage II of Figure 4 for stable crack propagation in hydrogen gas for AISI 4130 steel [13,17].

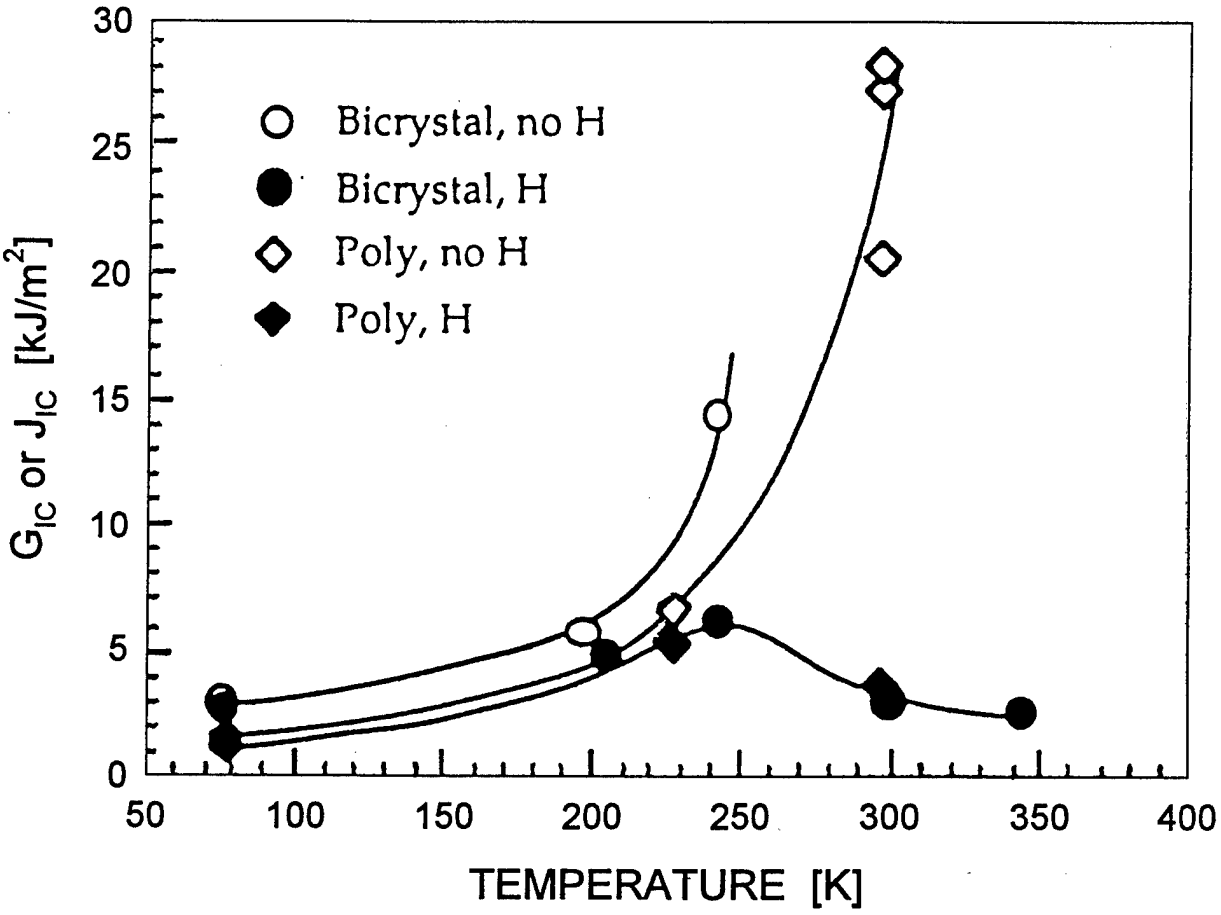

Figure 6. Temperature dependence of toughness for Fe-Si alloys with and without hydrogen [41].

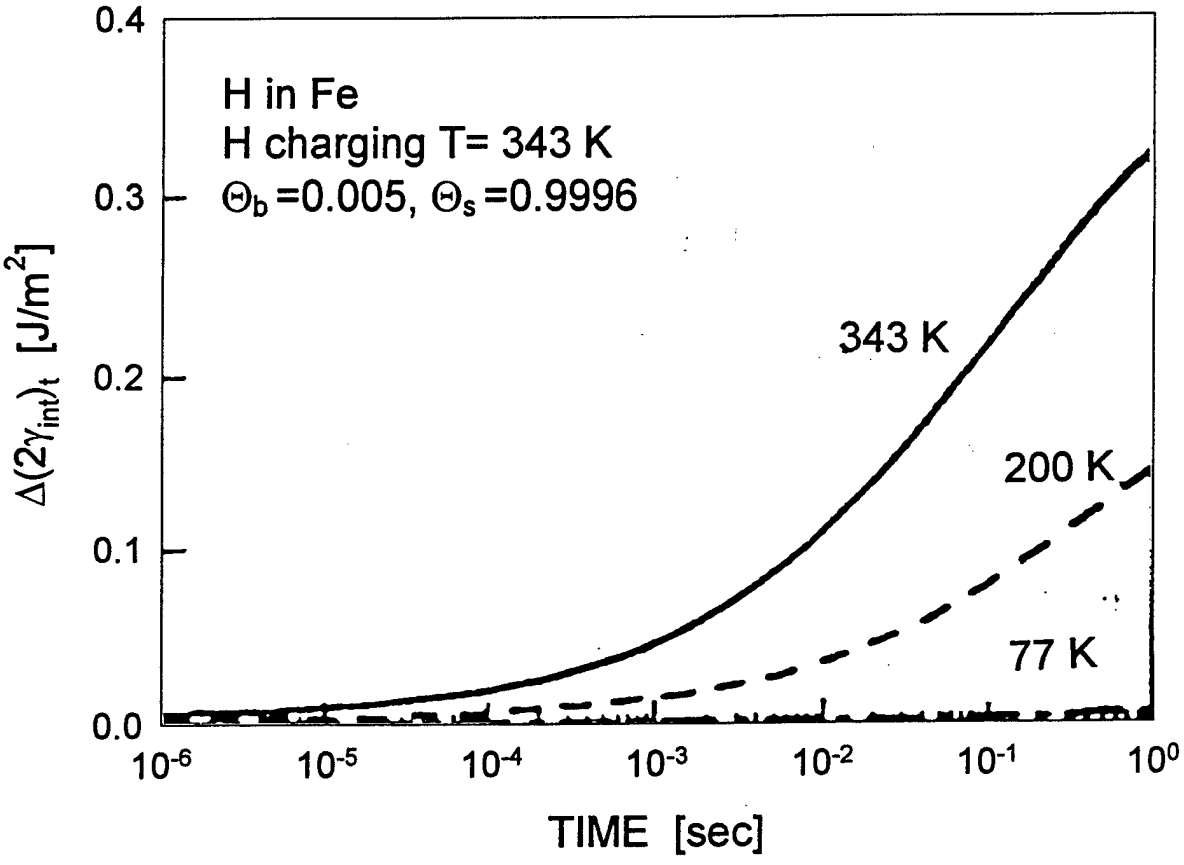

Figure 7 Transient reduction of the interfacial cohesion at 343, 200, and 77 K. The specimen is pre-charged at 343 K [41].

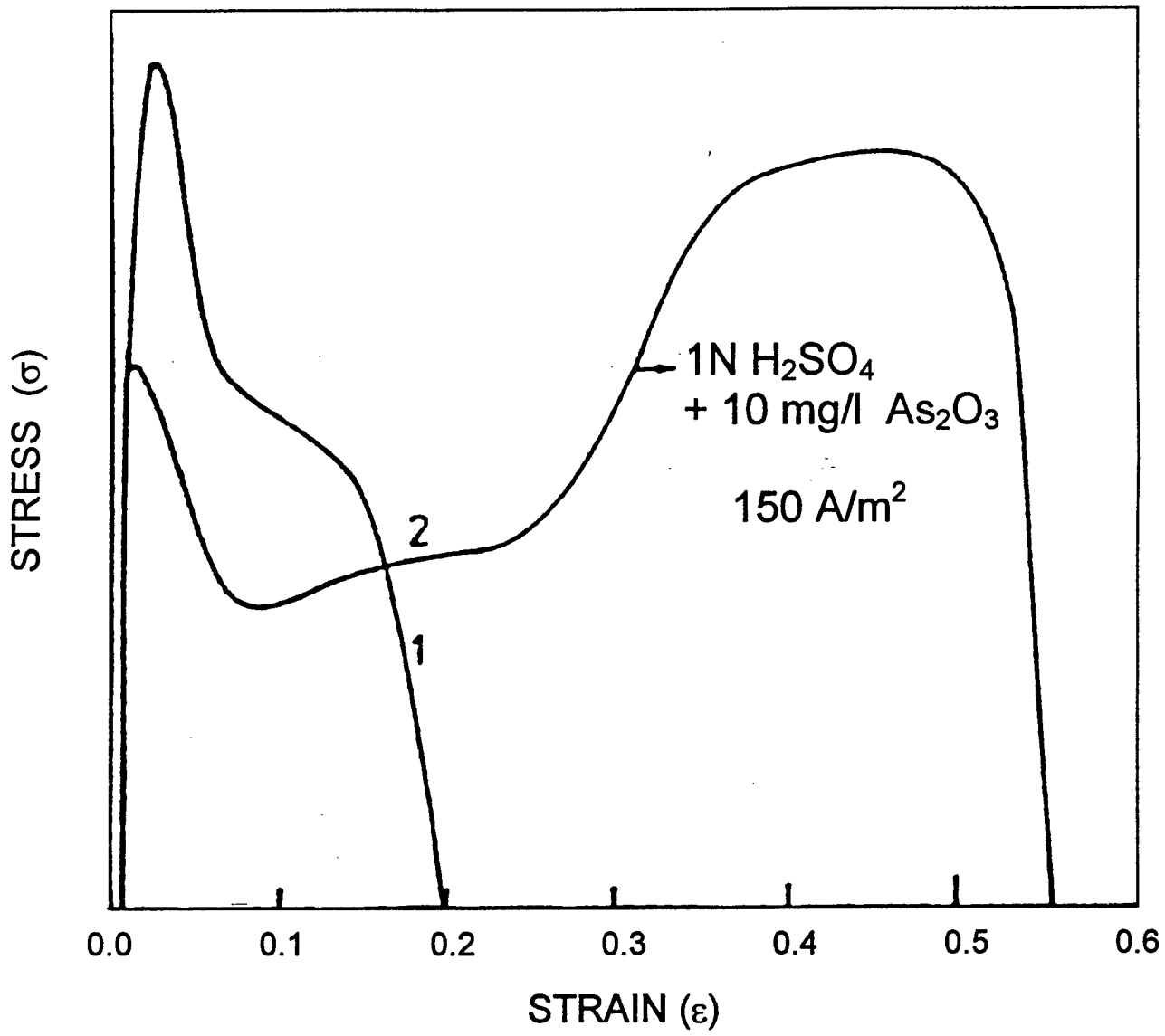

Figure 8 Stress – strain curves for hydrogen free (1) and hydrogen charged (2) iron whiskers of <111> growth direction [49].

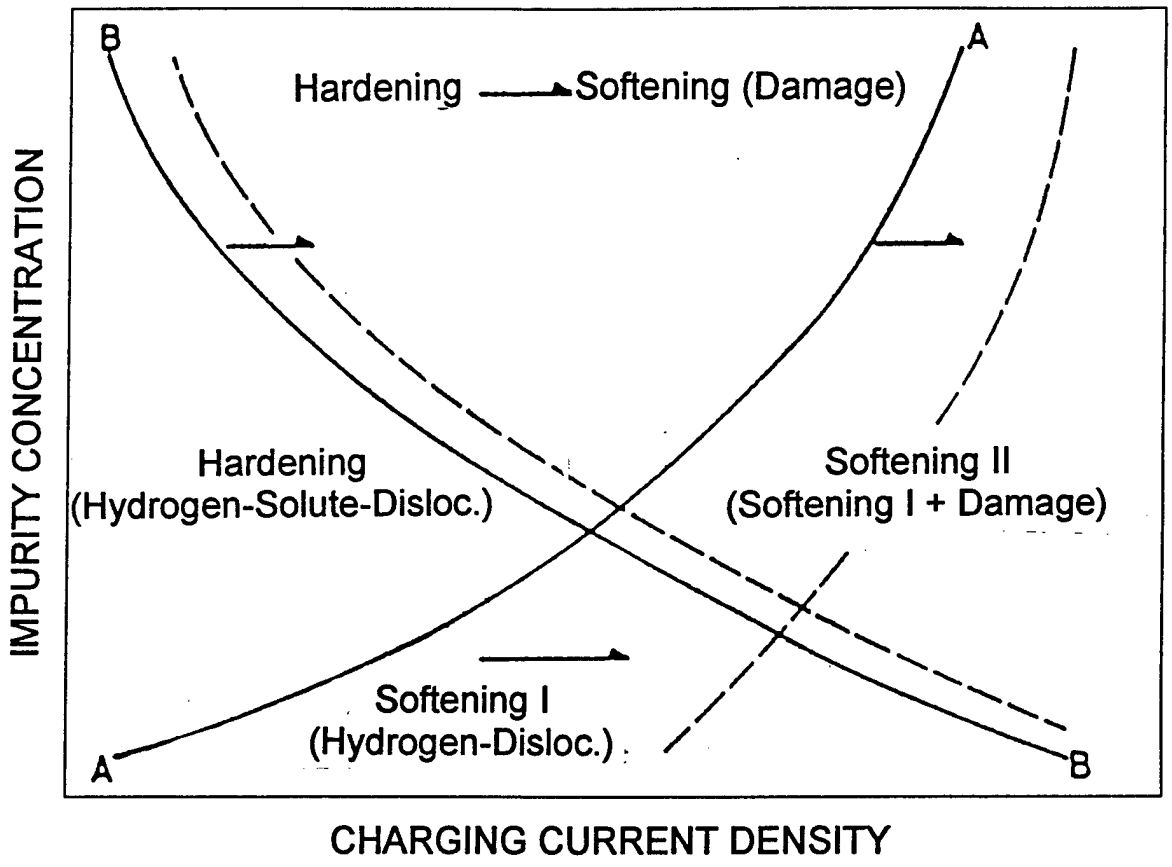

Figure 9. A schematic representation of the effect of hydrogen on the flow stress of iron, the amount of impurity and the charging current density being taken as variables. As the temperature increases, curve A and B shift to the right as shown by broken lines [62].

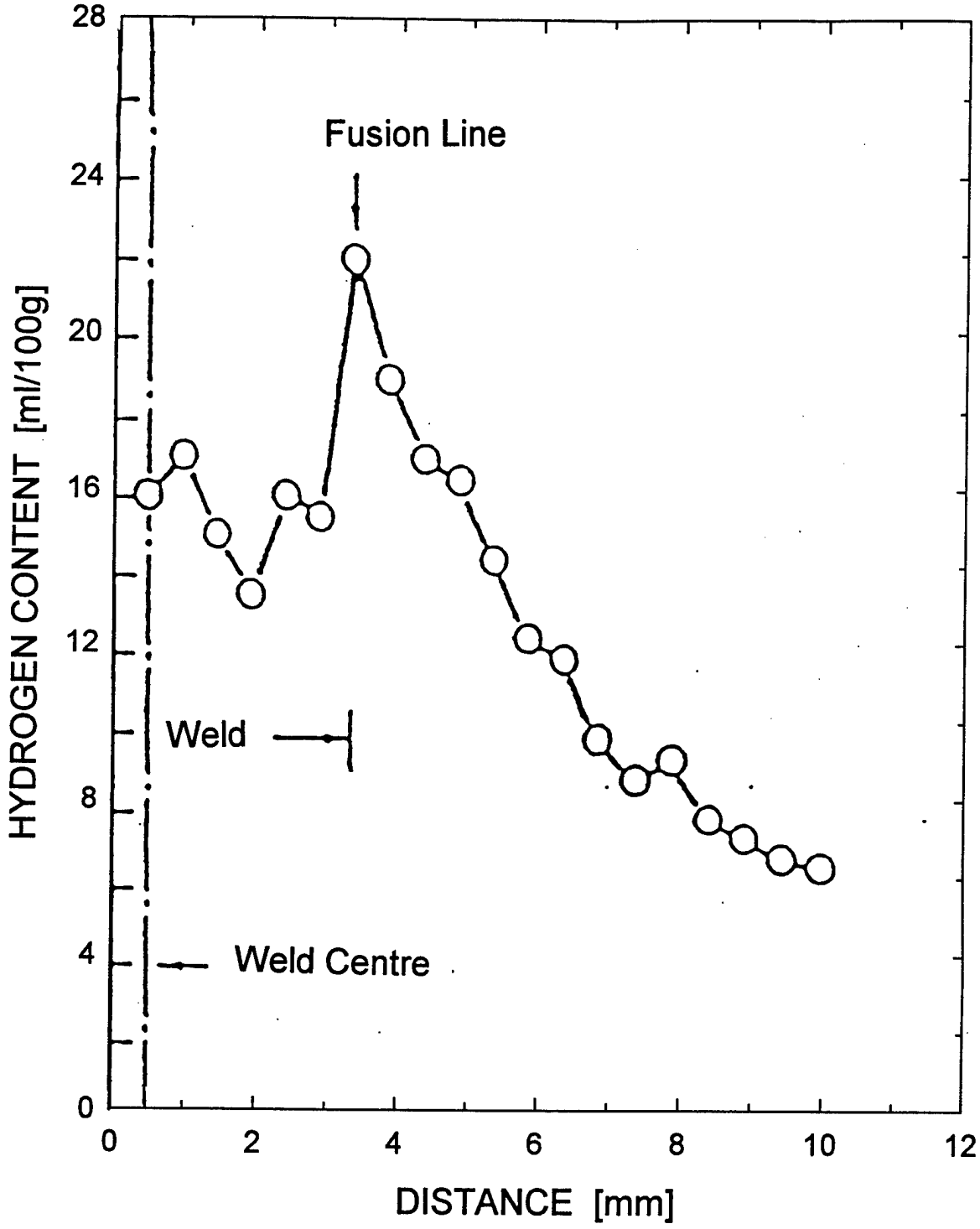

Figure 10. Hydrogen distribution across the weld fusion line [69].

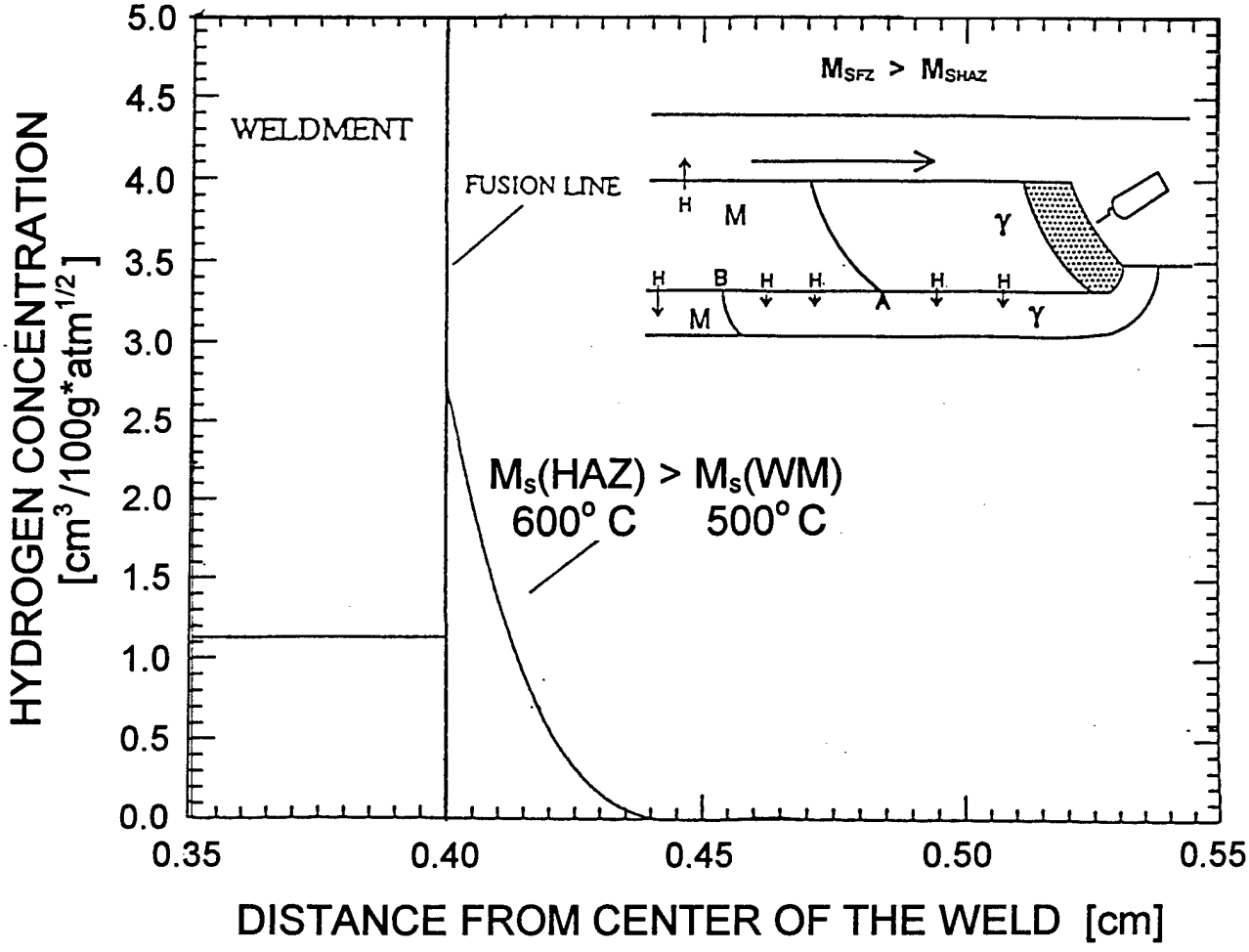

Figure 11. Calculated hydrogen distribution across the fusion line of a steel weldment for $Ms_{WM} > Ms_{HAZ}$ [73].

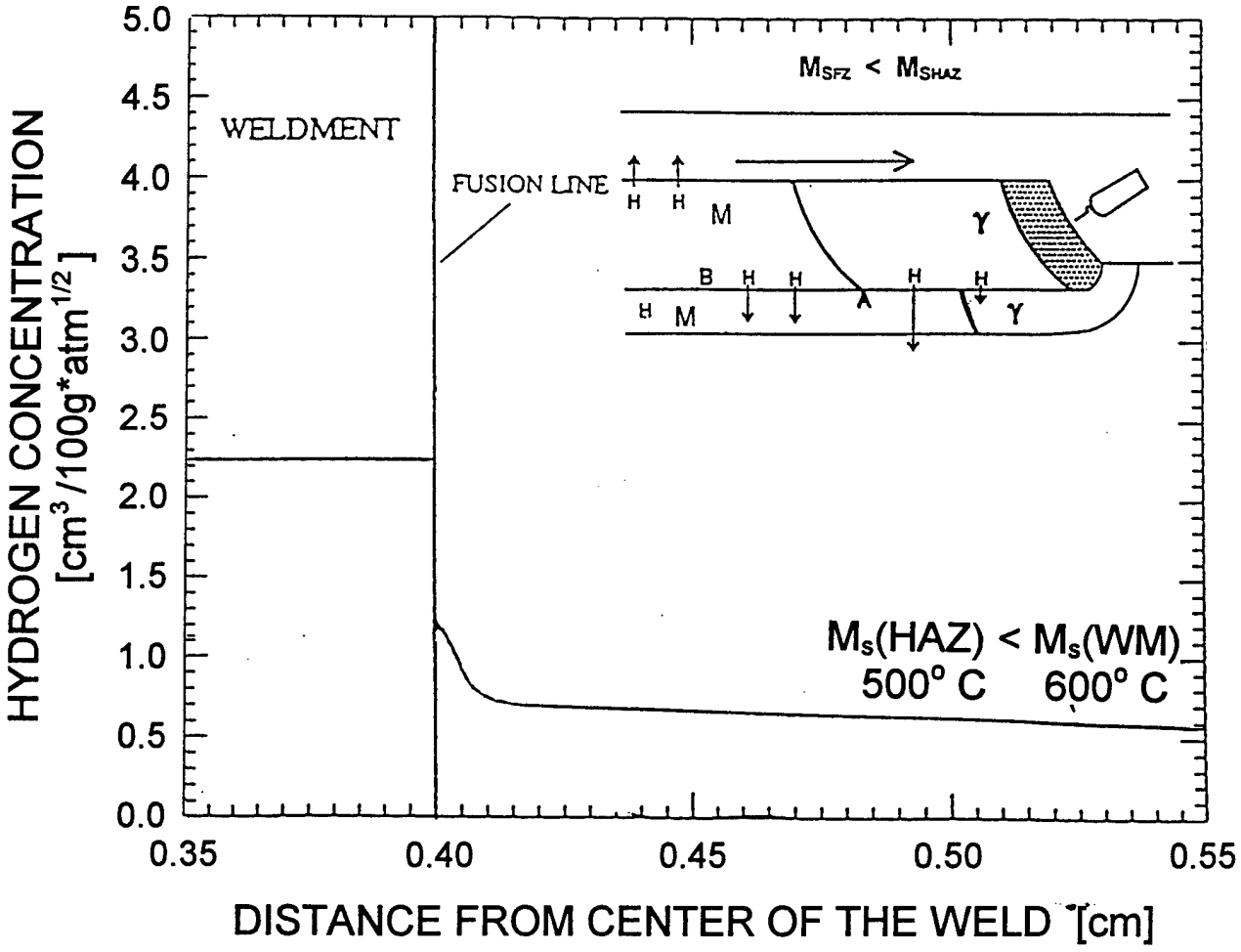

Figure 12. Calculated hydrogen distribution across the fusion line of a steel weldment for $Ms_{WM} < Ms_{HAZ}$ [73].

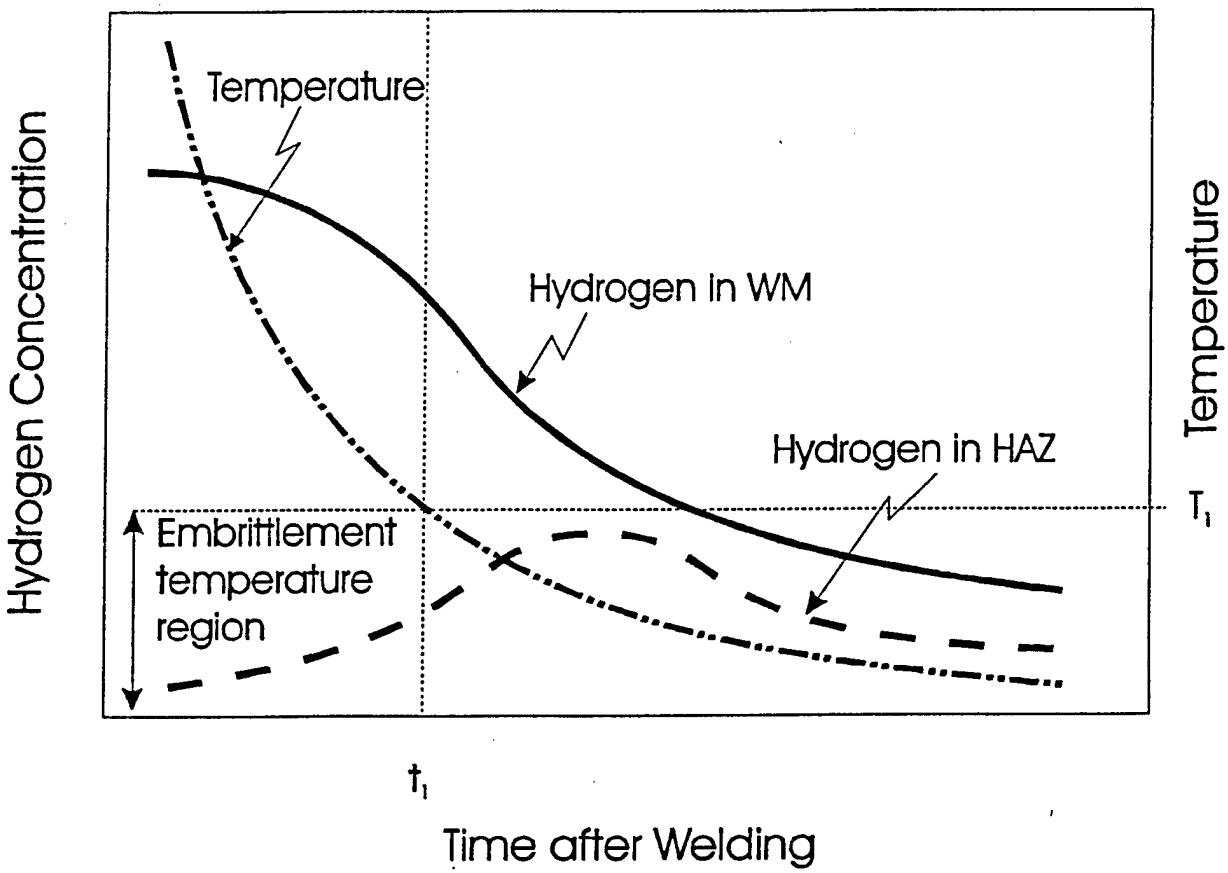

Figure 13. Variation of hydrogen concentration in weld center and in HAZ after completion of welding process [74].

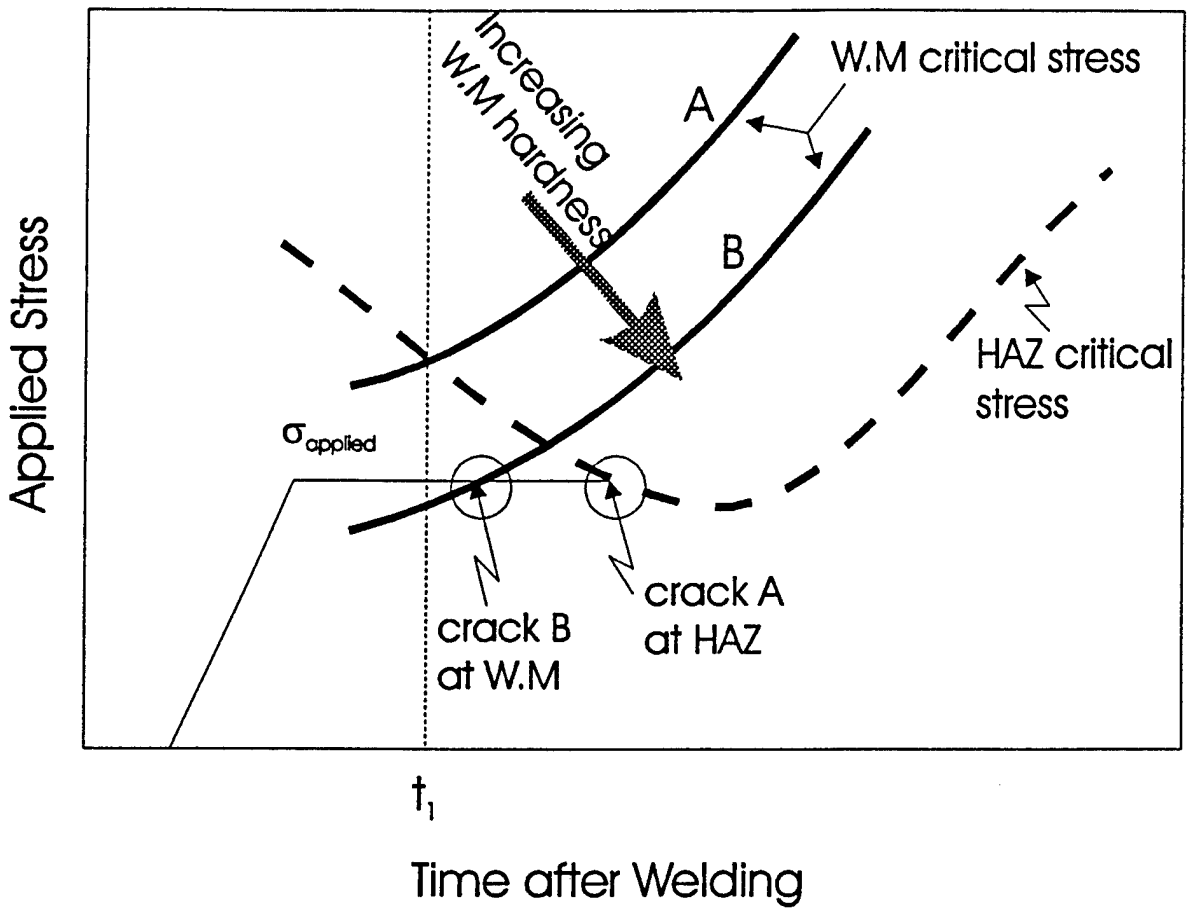

Figure 14. Variation in critical stress for HAC in weld metal (WM) and HAZ during cooling cycle. Condition (A): low W.M. hardness, crack location is in HAZ. Condition (B): high W.M. hardness, crack location is in the weld metal (W.M.) [74].

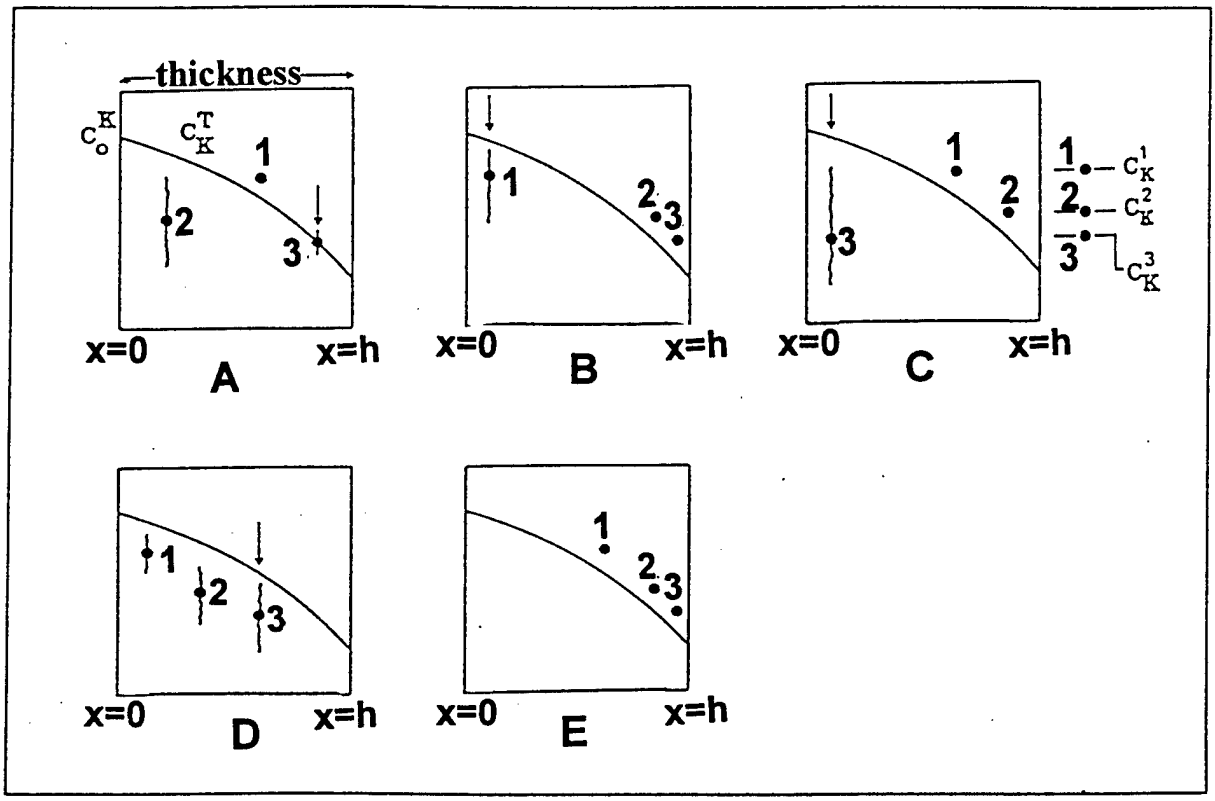

Figure 15. Different cracking situations with a given total hydrogen concentration (c=c_T + c_L) profile and three defects with $c_{K1} > c_{K2} > c_{K3}$ [75].

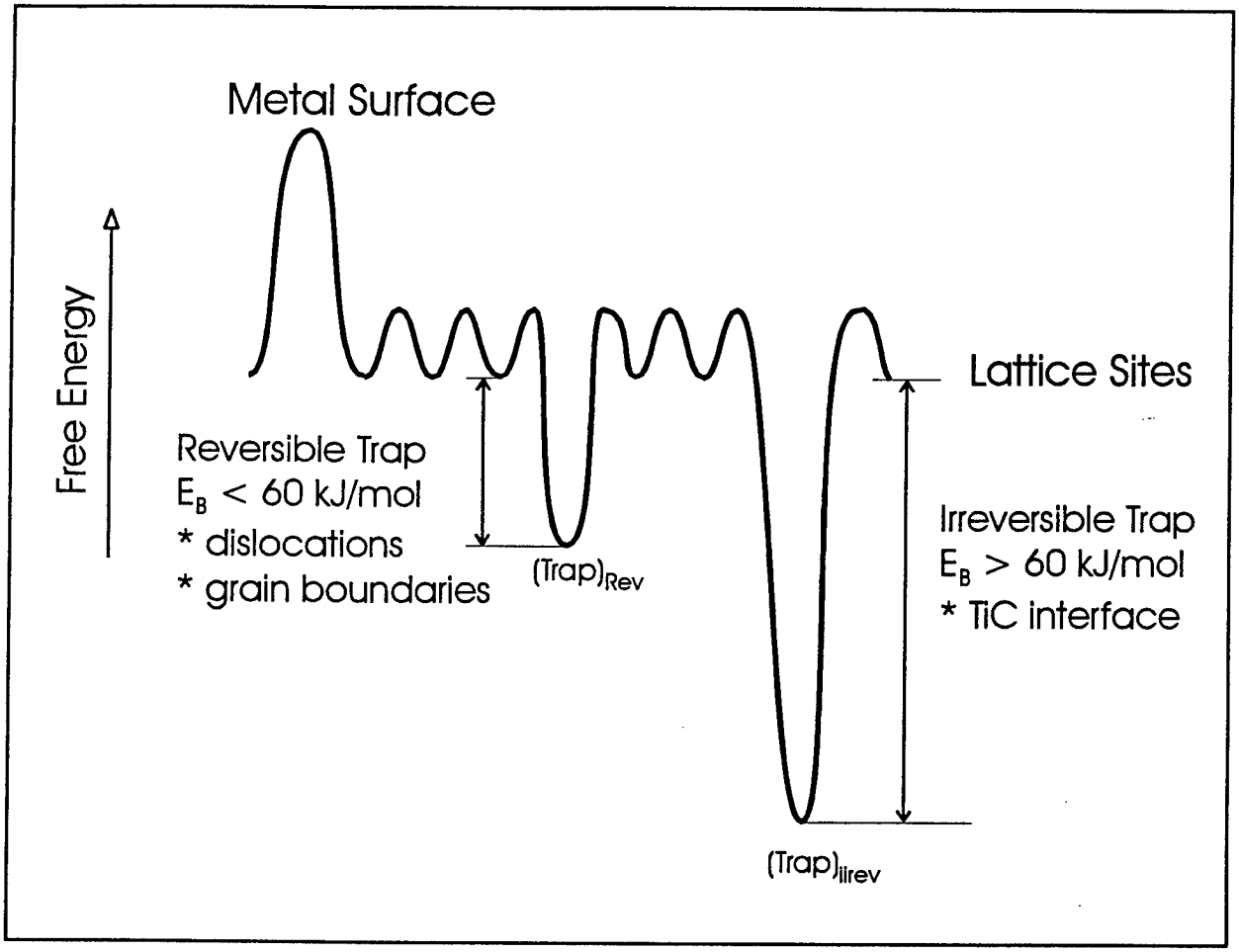

Figure 16. Schematic of general traps with the corresponding trapping energies. "Rev" stands for reversible trap and "Irev" for irreversible trap [76].

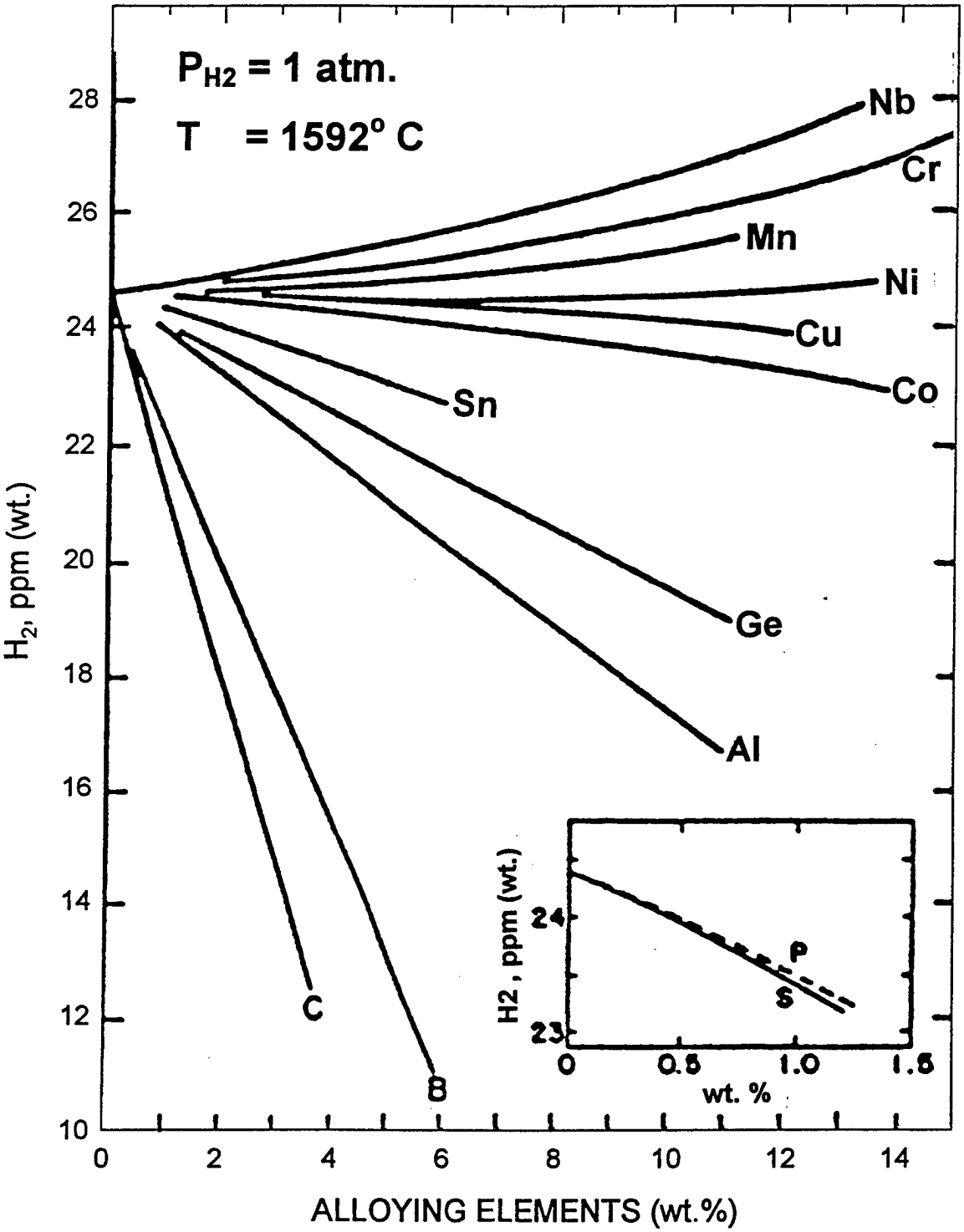

Figure 17. The effect of various solute elements on the hydrogen solubility in molten iron [106].

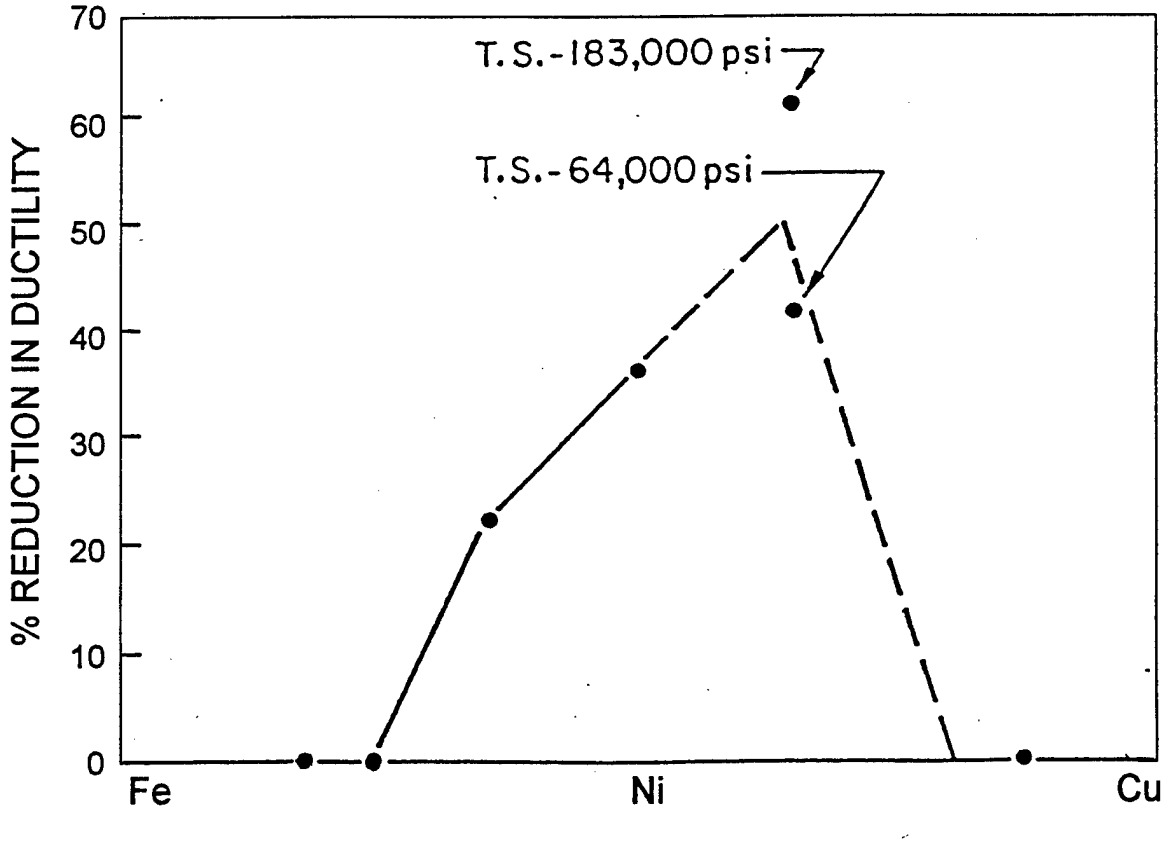

Figure 18. Hydrogen embrittlement of Fe-Ni and Ni-Cu alloys [15].

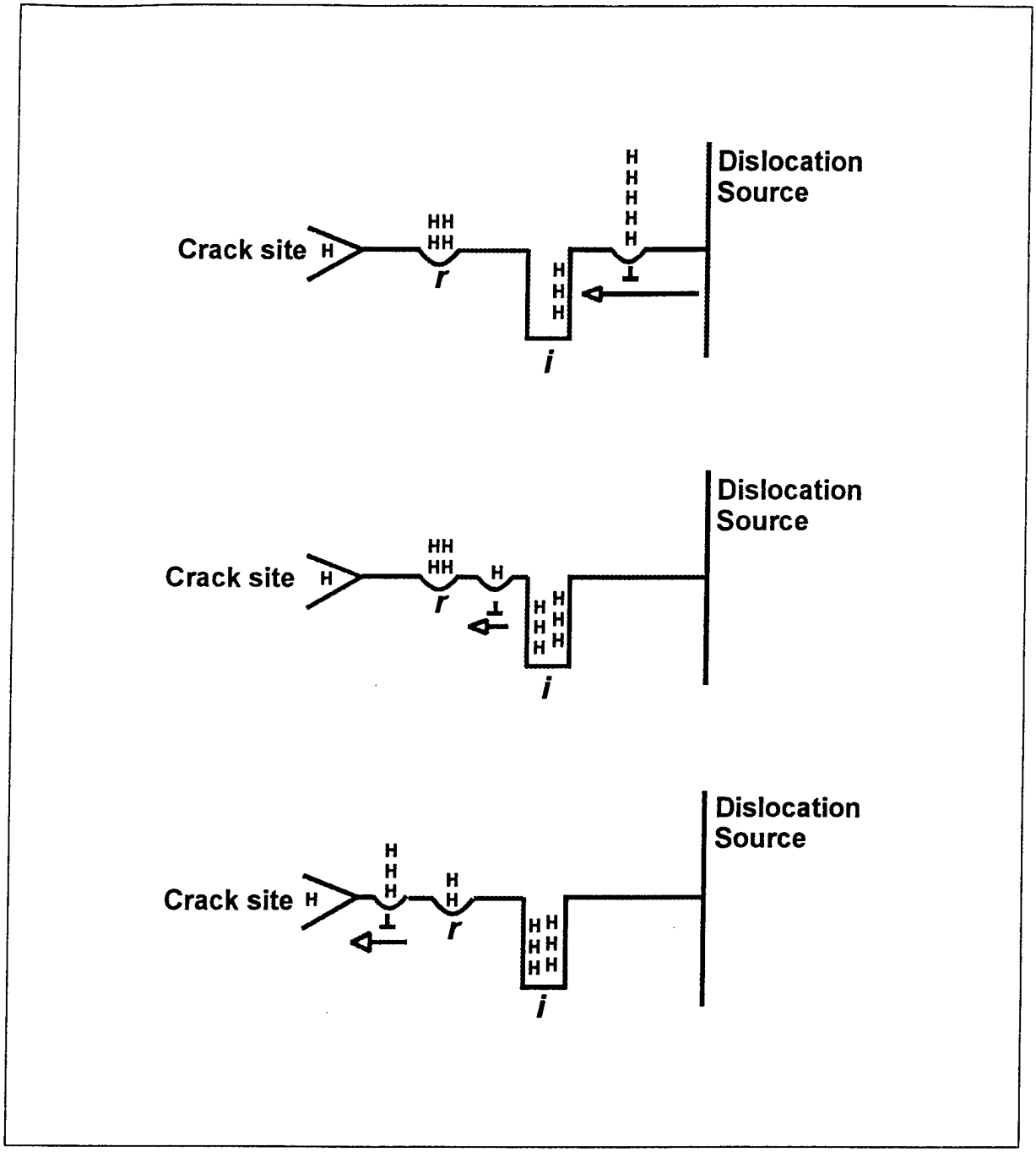

Figure 19. Exchange of hydrogen between dislocation and trap sites. (a). Hydrogen is distributed on all traps when the dislocation begins to move. (b). On passing over an irreversible (***i***) trap, some hydrogen is deposited on the ***i*** trap by the dislocations. (c). Because of the preceding loss, the dislocation recharges itself on the reversible (***r***) traps. The flaw will see more hydrogen coming in than if there had been no ***i***-trap [85].

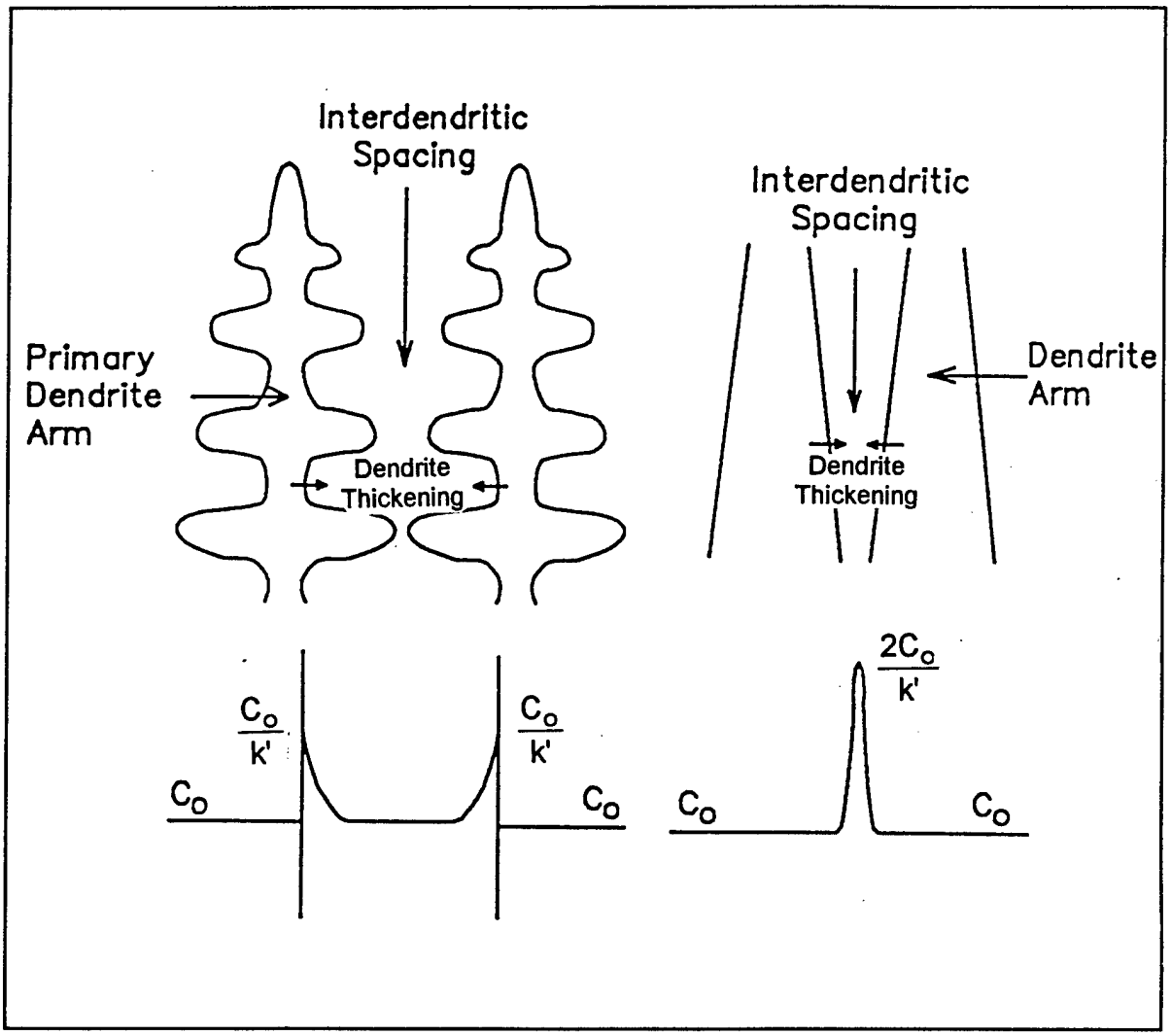

Figure 20 Schematic diagram showing the composition gradient ahead of the solid/liquid interface in the liquid. As the dendrites thicken, the last interdendritic alloy will have high solute content and high tendency to form inclusions [149].

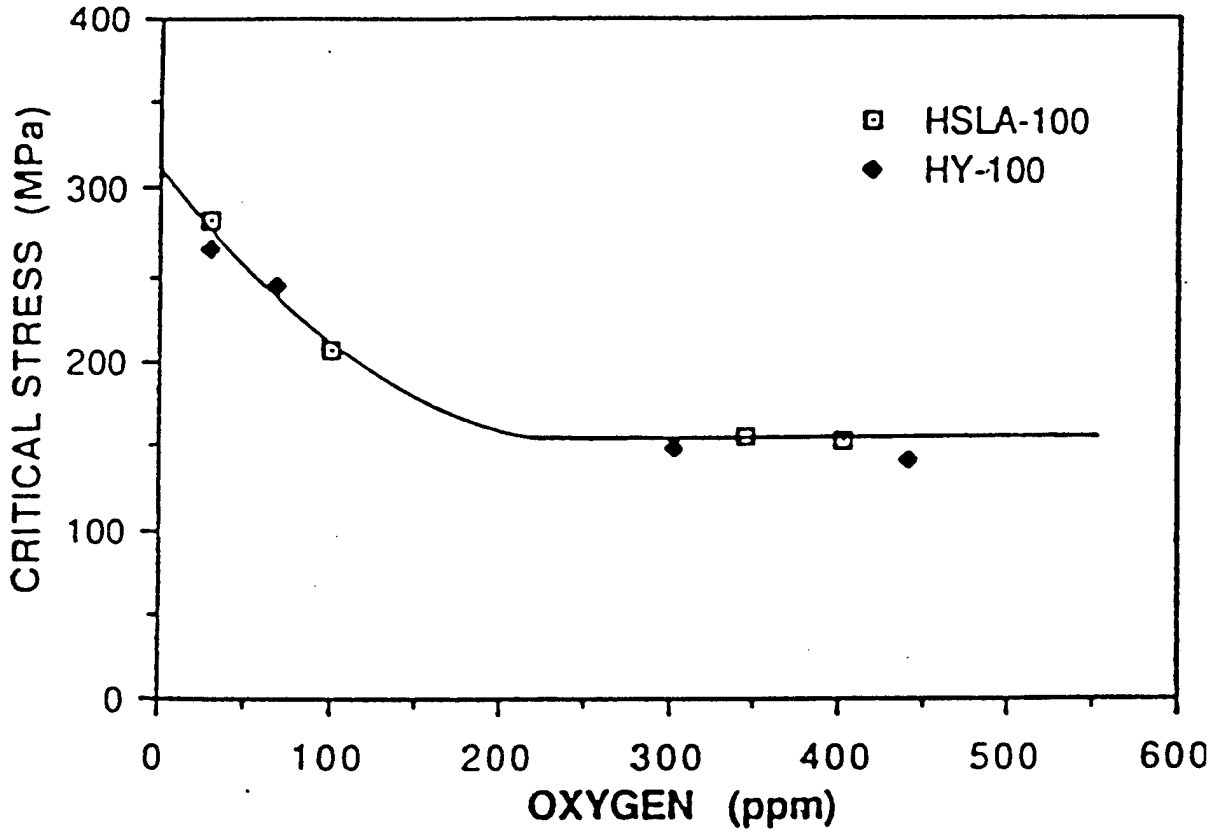

Figure 21. Effect of oxygen content on the critical stress for hydrogen cracking in high strength steel weld metal containing 4.7 ppm hydrogen. The HY-100 steel welds were let to experience natural welding cooling rate, while the HSLA-100 steel welds were quenched in iced water [160].

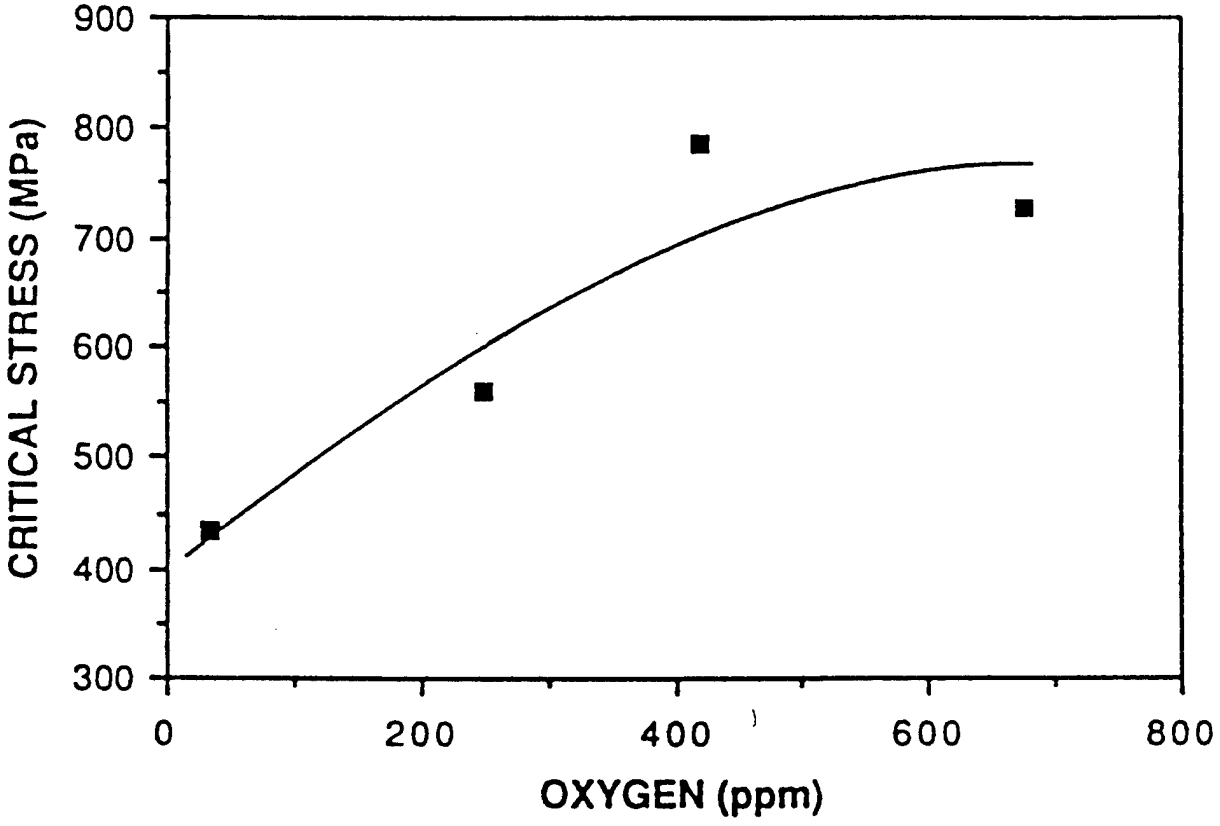

Figure 22. Effect of oxygen content on the critical stress for hydrogen cracking in high strength steel weld metal containing 4.7 ppm hydrogen. The HSLA-100 steel welds were let to experience natural welding cooling rate [160].

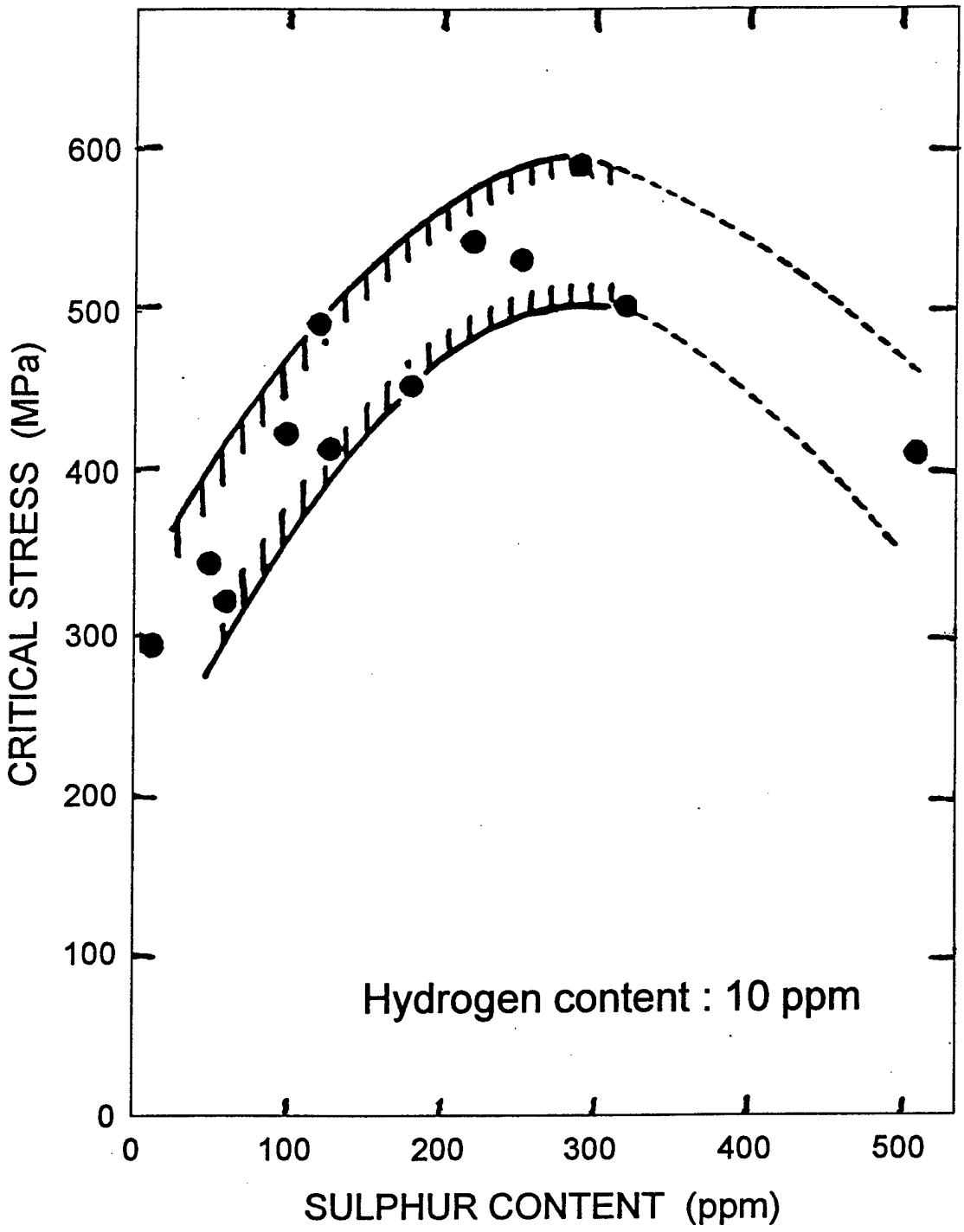

Figure 23 Dependence of critical stress for initiation of hydrogen assisted cracking (HAC) on sulfur content of steel weldment [172].

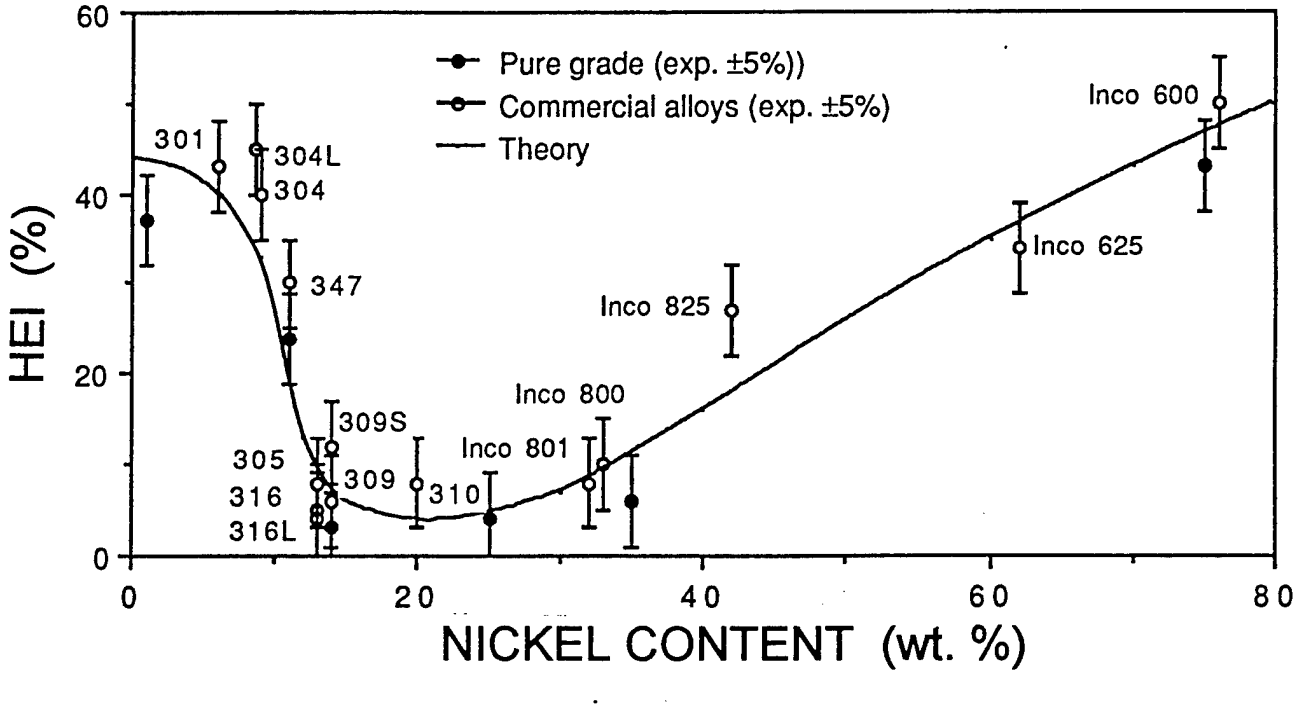

Figure 24 Hydrogen embrittlement index for many Fe-Ni-Cr alloys as a function of Ni (wt.pct) with Cr concentration mostly from 16 to 20 wt.pct [214].

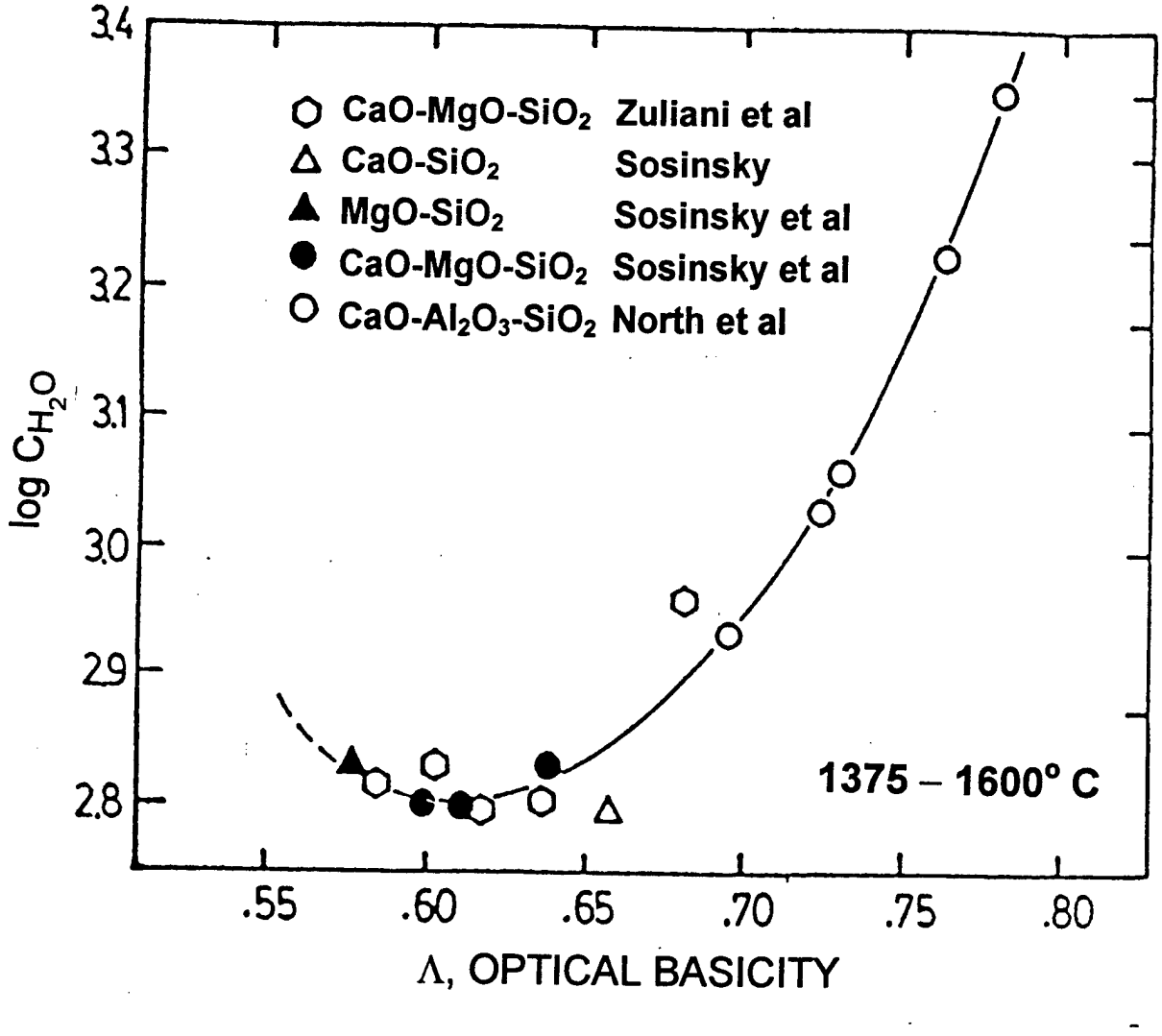

Figure 25 Relation between the optical basicity of steelmaking slags and their water capacity at temperatures between 1375 and 1600° C [228].

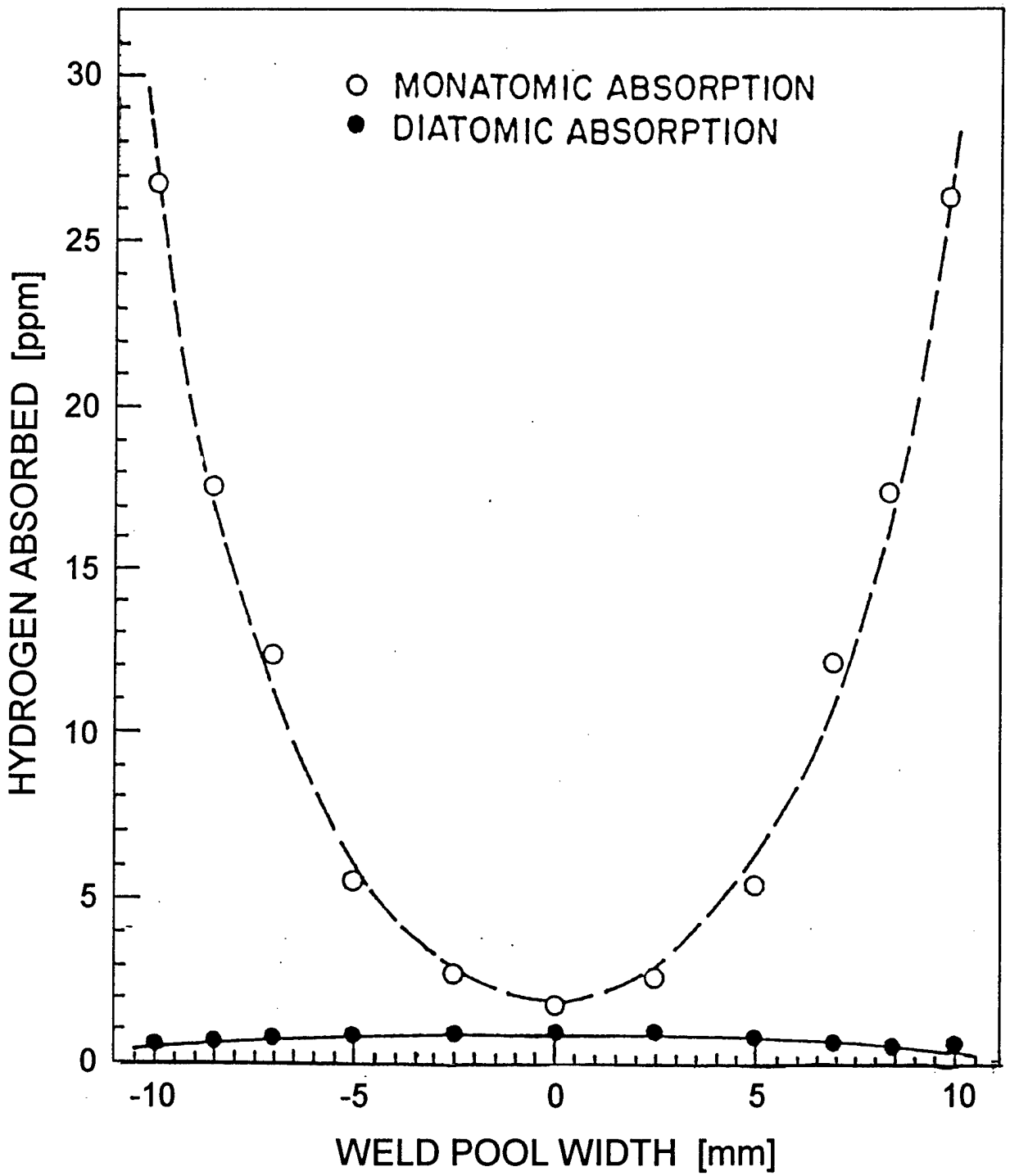

Figure 26. Hydrogen absorption due to monotomic and diatomic hydrogen absorption as a function of weld pool location. The calculated points assume a dissociation temperature of 2500 °C, 0.01 atm. hydrogen added to the argon shielding gas [235].

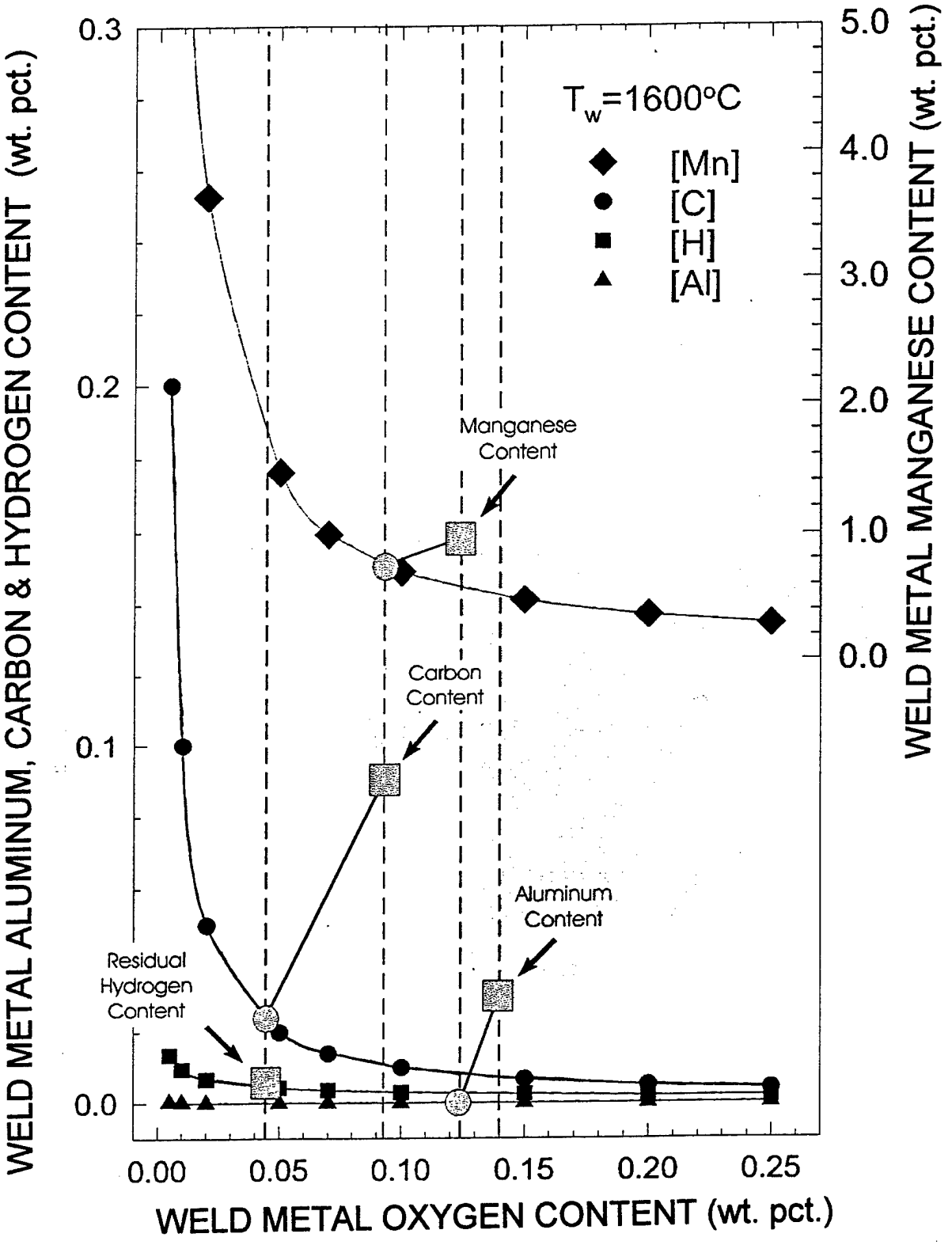

Figure 27. De-oxidation sequence in weld metal due to various alloying elements [238].

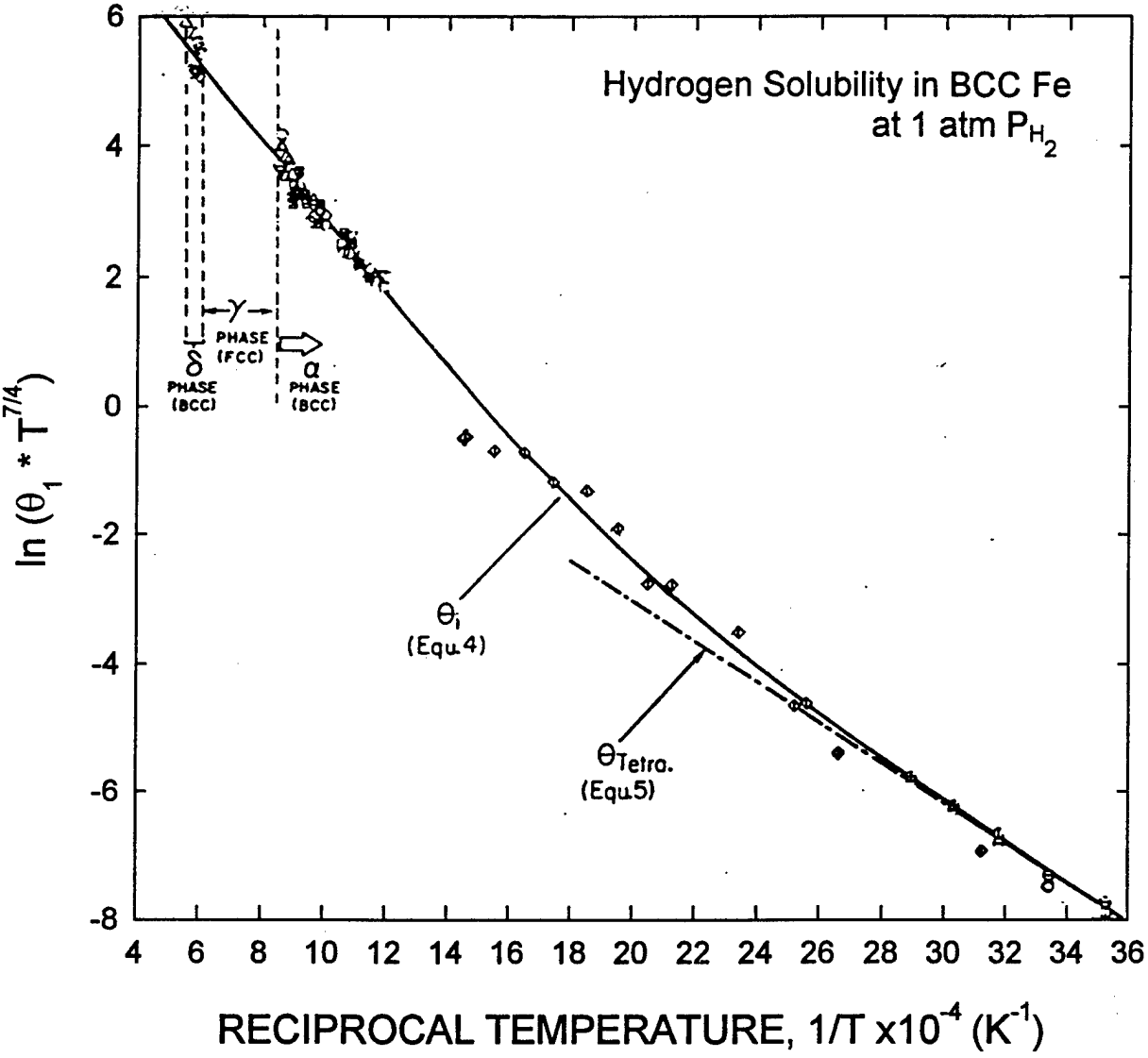

Figure 28. Plot of $\ln(\theta T^{7/4})$ vs $1/T$ for hydrogen in bcc iron. The notation θ is the hydrogen solubility (ratio of the number of hydrogen atom to the number of interstitial sites) in perfect iron matrix [252,254]

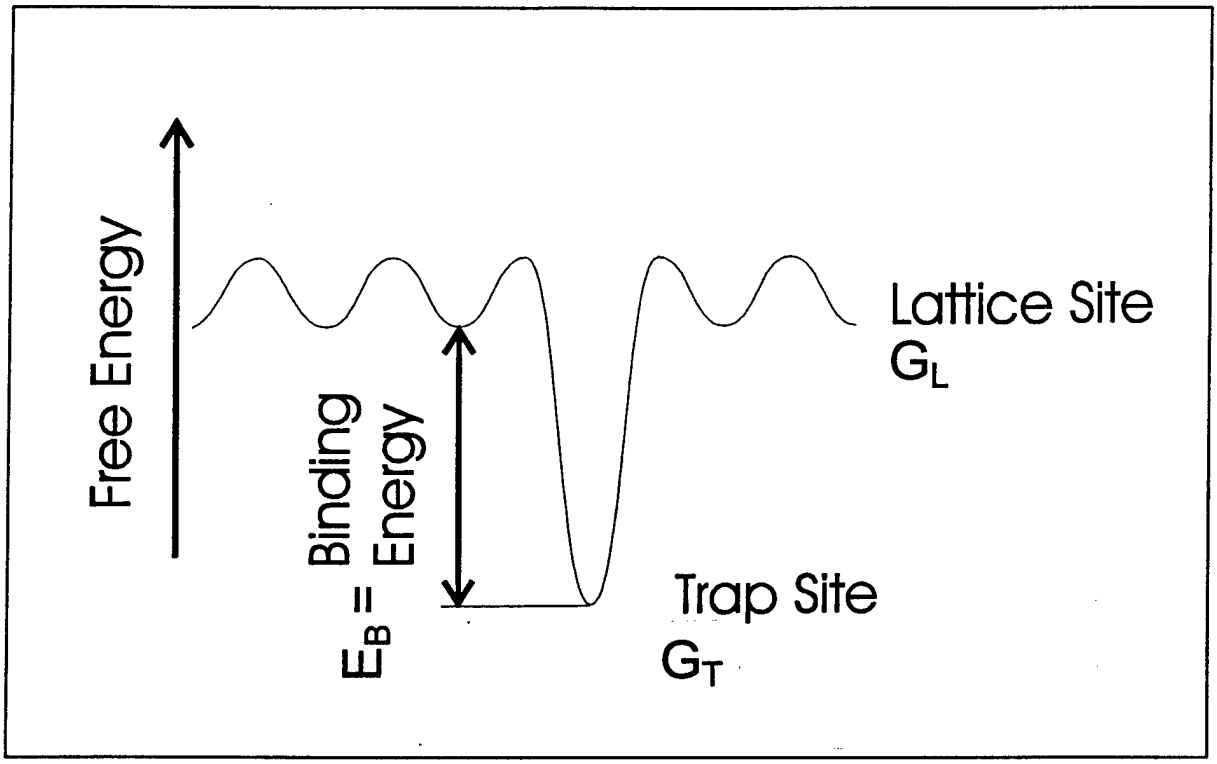

Figure 29. Energy levels of normal (lattice) sites Y and trapping sites X [255].

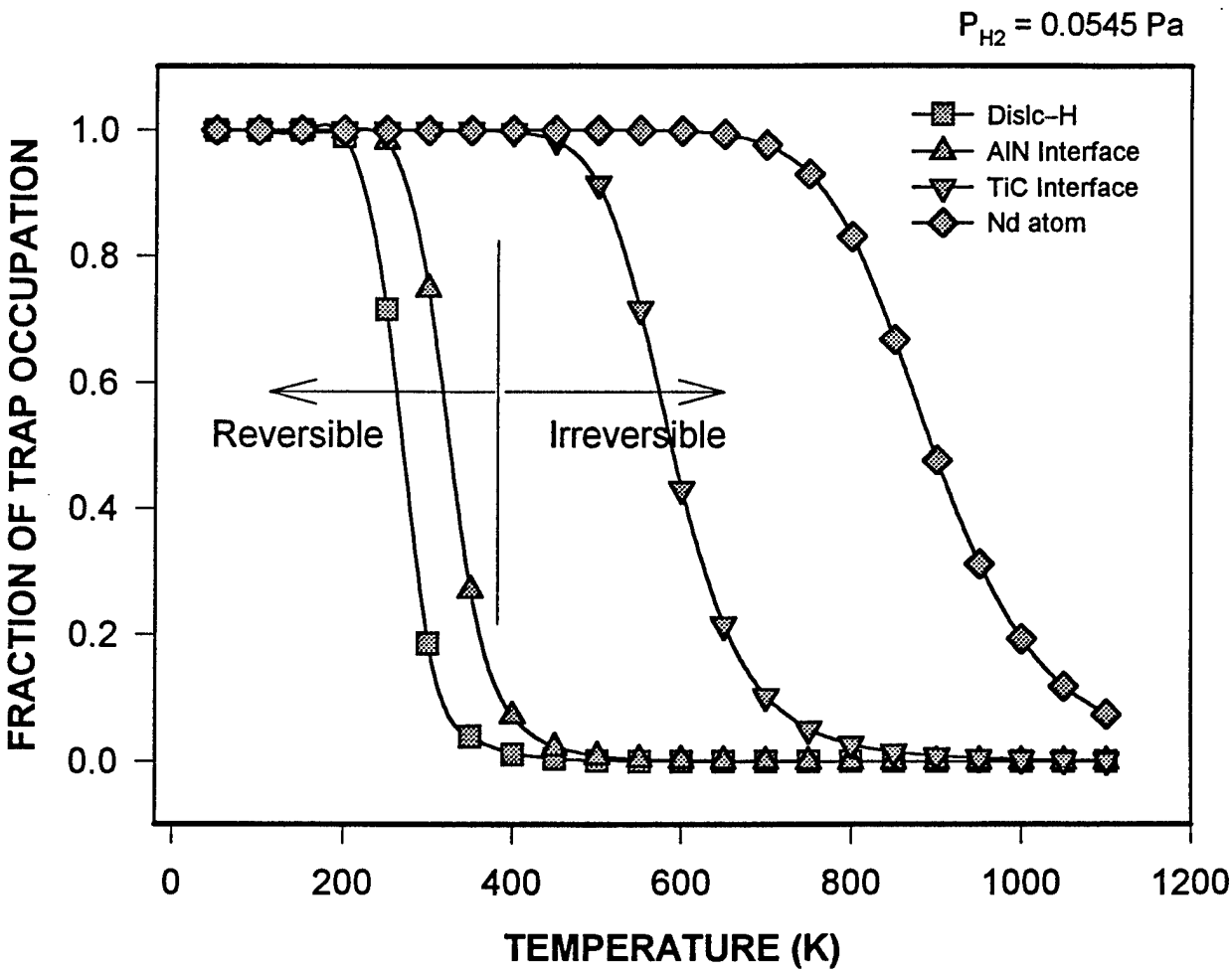

Figure 30. Fraction of filling by hydrogen at trap sites as a function of temperature for various hydrogen-trap binding energies. The calculation was done by assuming $P_{H2} = 0.0545$ Pa [10].

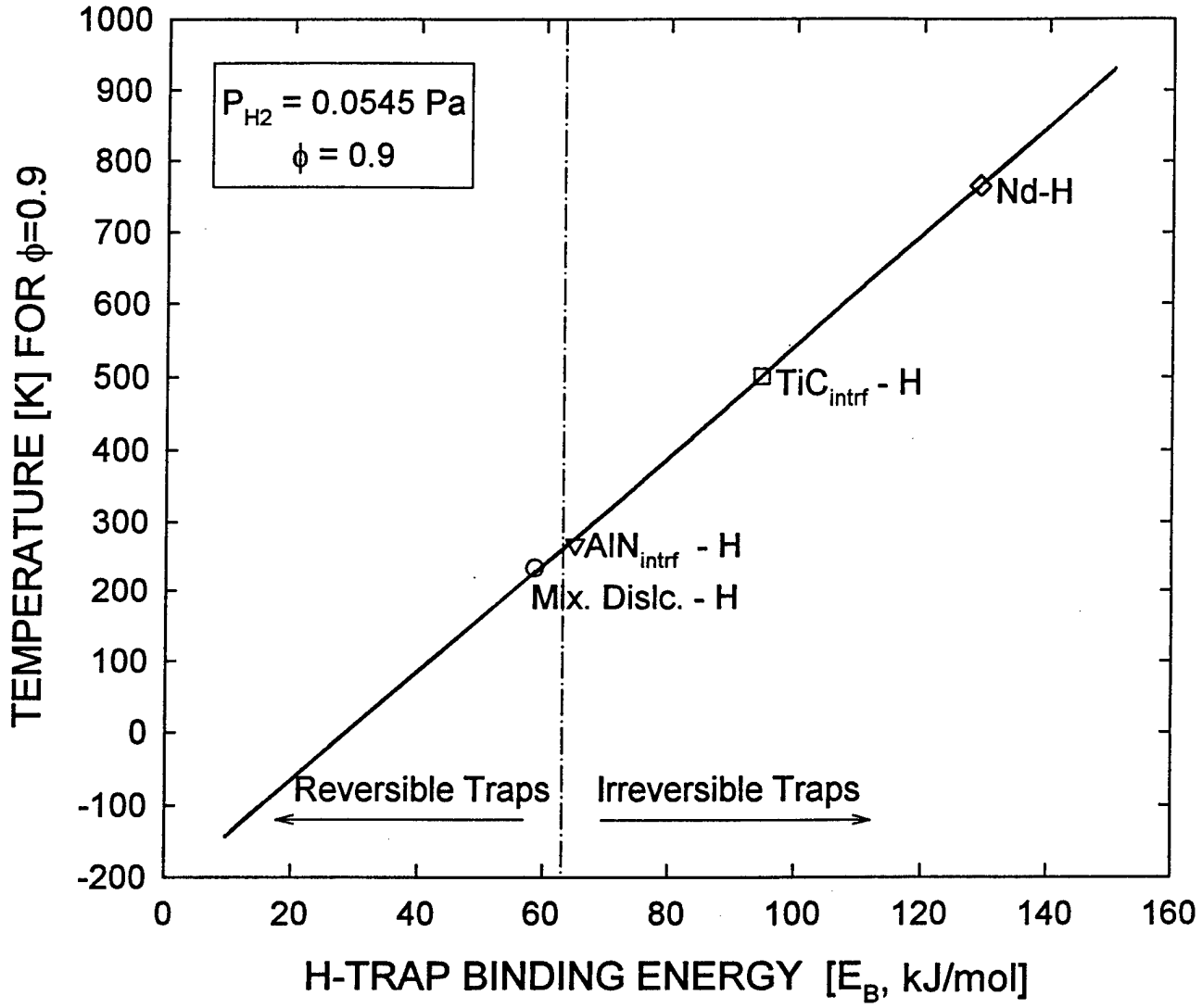

Figure 31. Temperature of ninety percent filling at various trap by hydrogen as a function of binding energy [10].

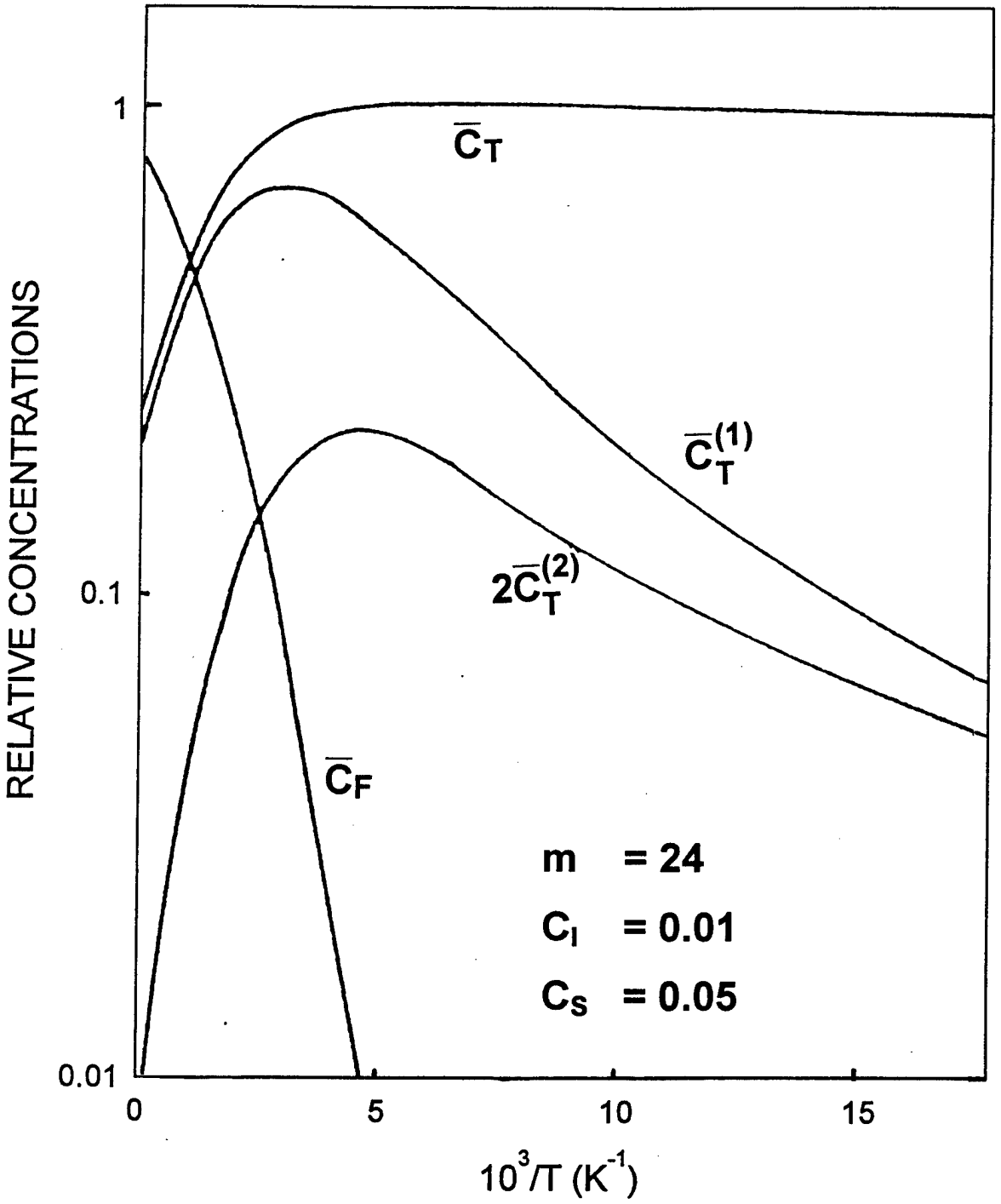

Figure 32. Relative concentration of free c_L and trapped c_T interstitials, $c_T = c_T^{(1)} + 2c_T^{(2)} + \ldots$, where $c_T^{(1)}$ and $c_T^{(2)}$ are the relative concentration of *S-I* and *S-2I* complexes with geometrical restriction that the interstitials have to be in opposite position if it forms the *S-2I* cluster, as a function of *1/T* [258].

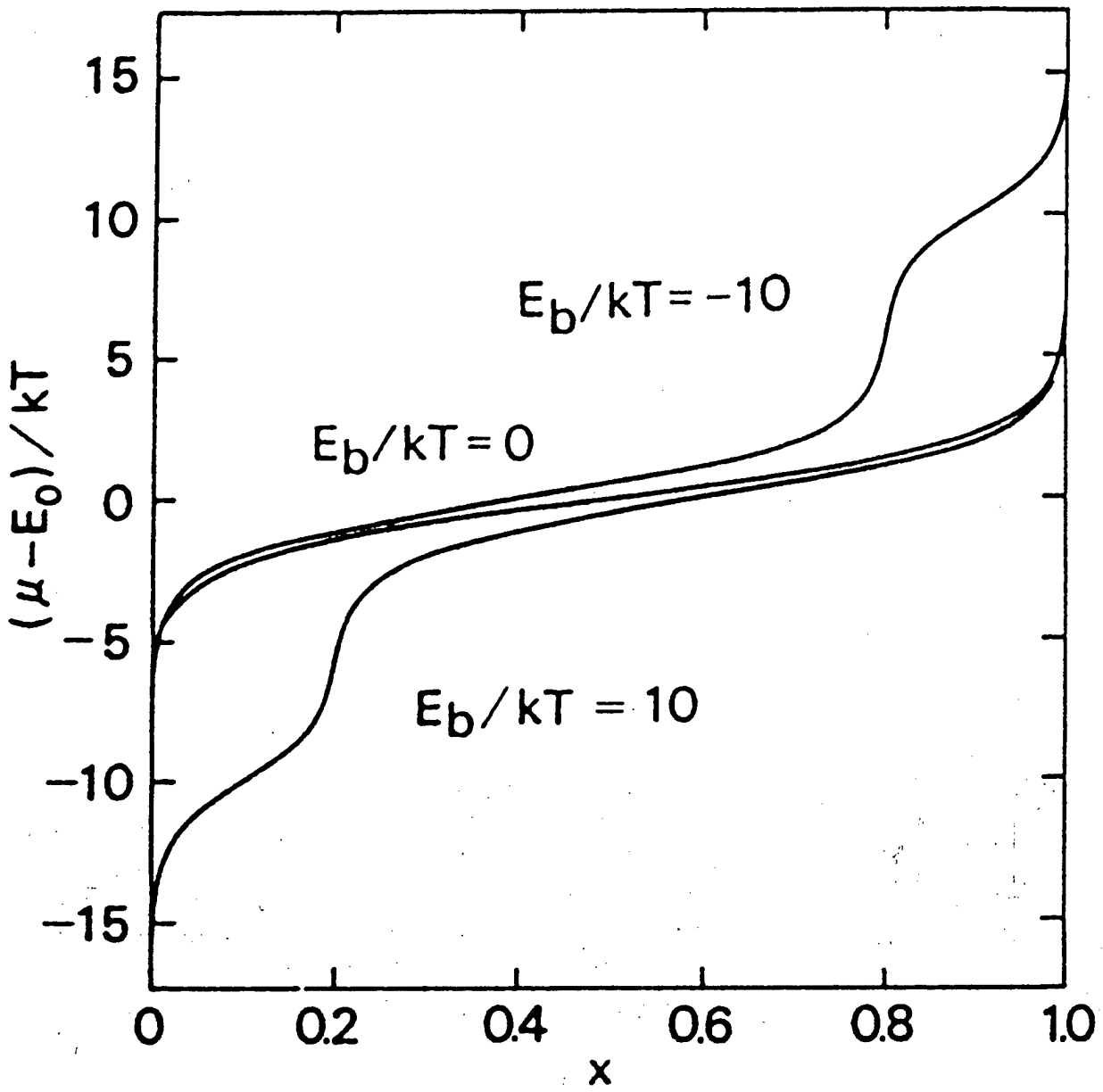

Figure 33 Chemical potential of hydrogen as a function of hydrogen concentration, $x = n/N_L$, in the presence of trapping or blocking with concentration of trap site $c_T^o = 0.2$ [226].

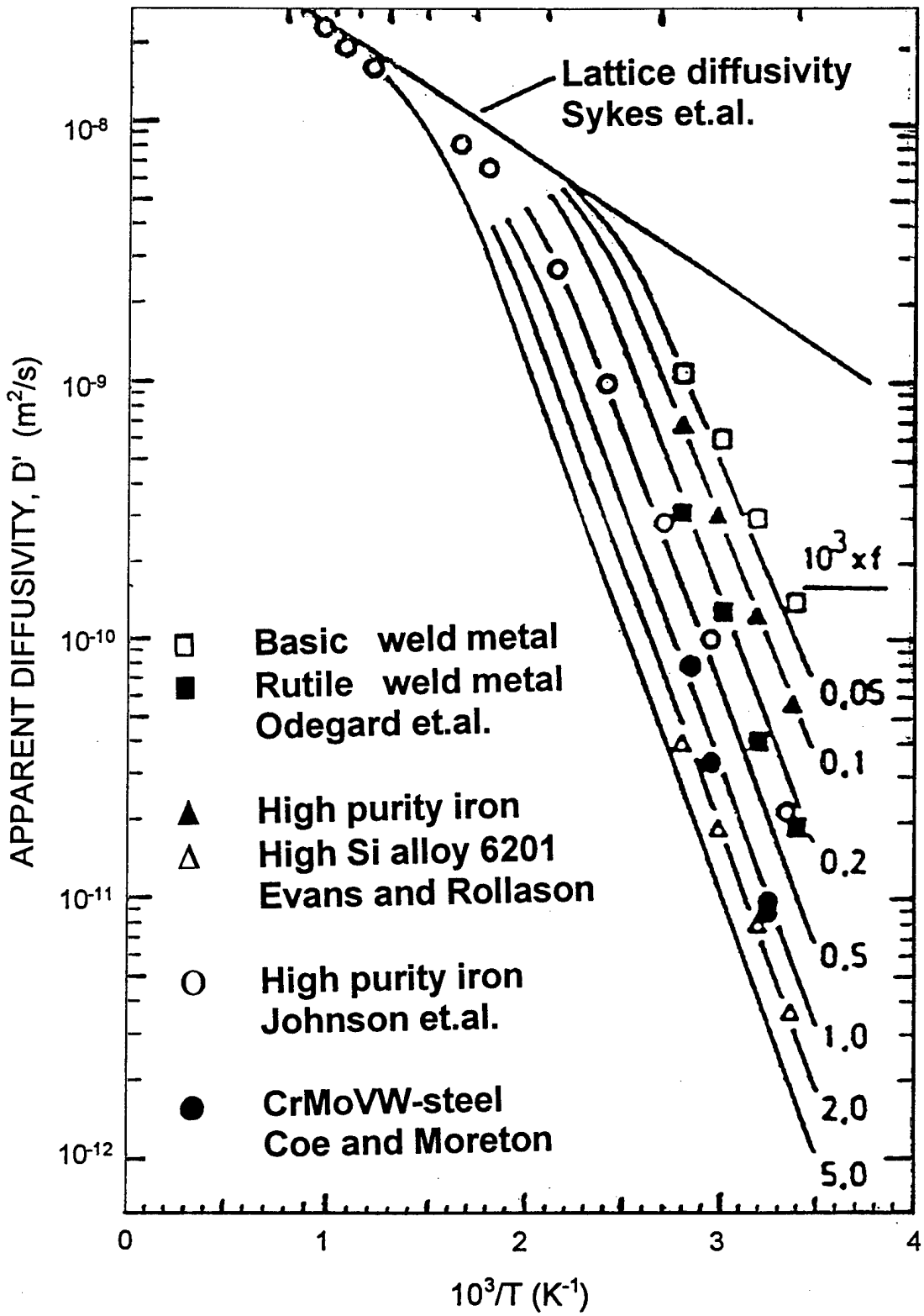

Figure 34. Hydrogen diffusivity for lattice diffusion in steel [251,267] and the apparent diffusion coefficients as function of temperature T and relative void volume f [268,269]

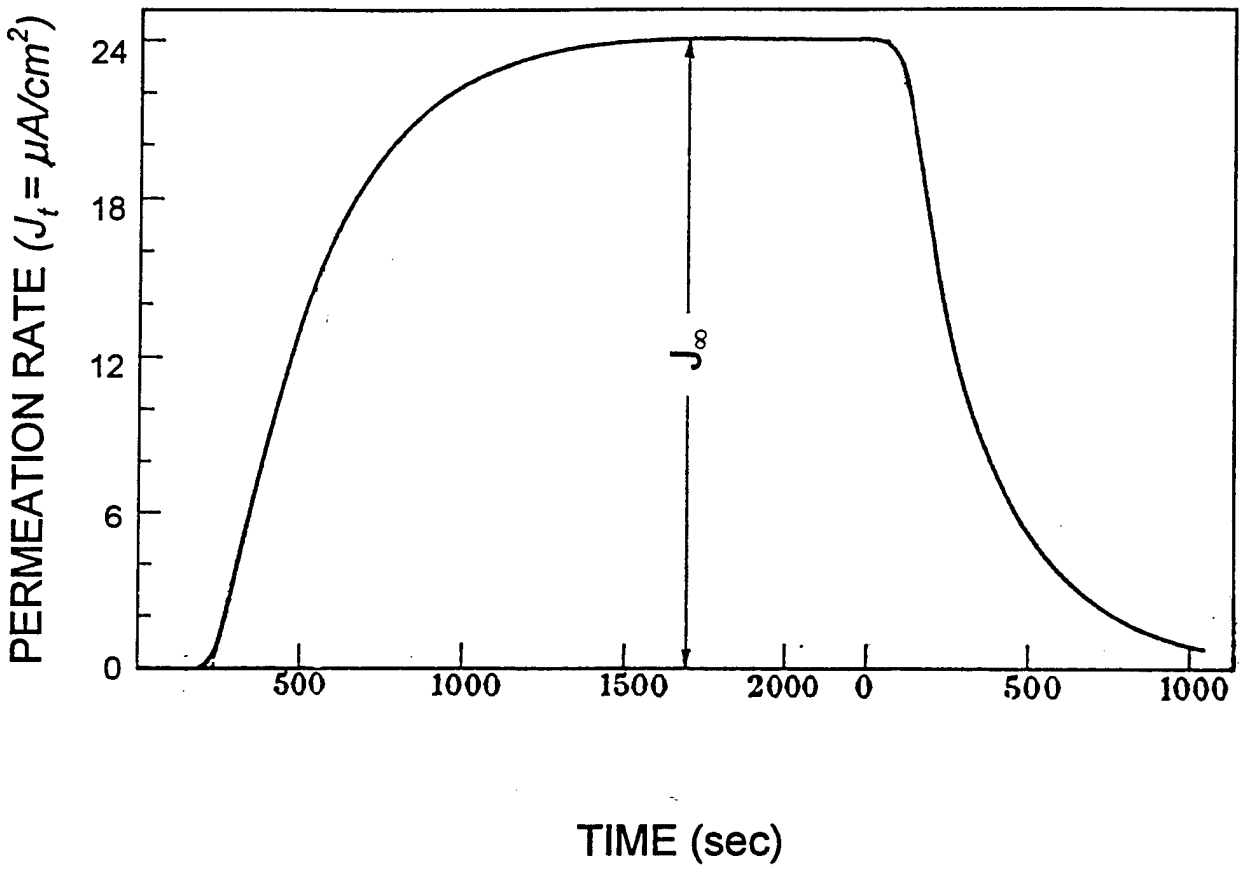

Figure 35. Typical transient record of a hydrogen permeation flux on contracted time scale. J_∞ is the steady state permeation rate [301].

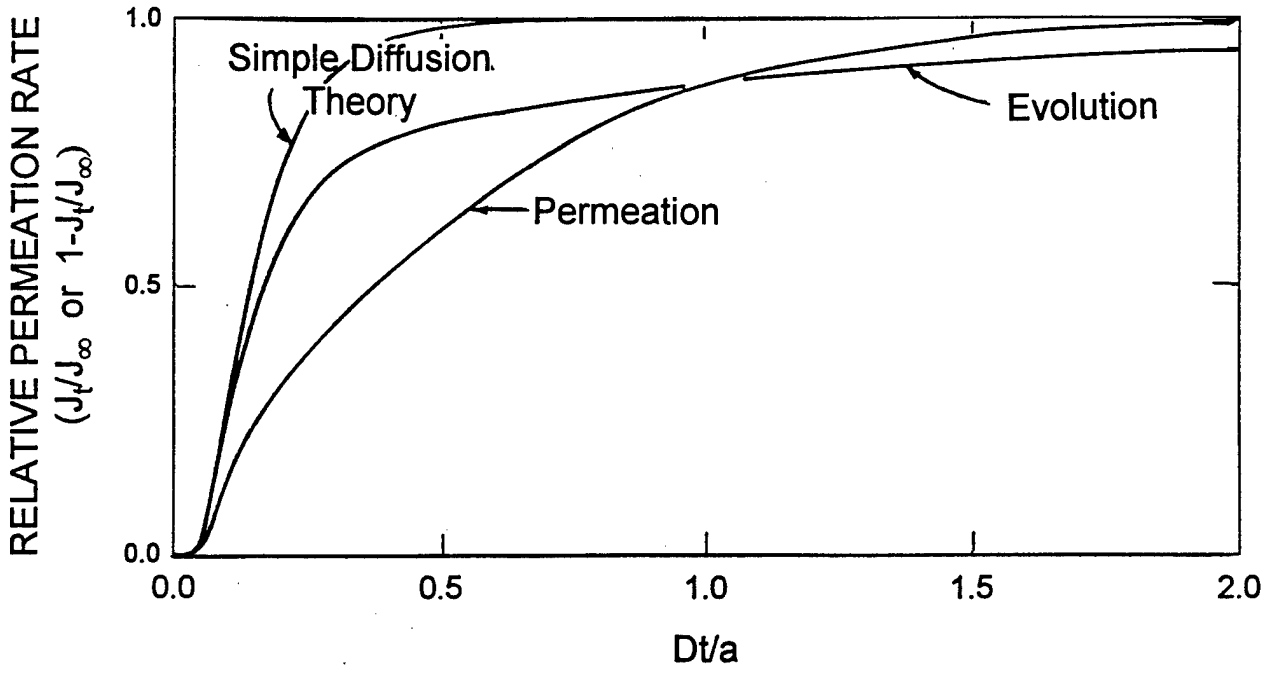

Figure 36. Permeation and evolution curves for reversible trapping. The notation D,t,and a are the diffusivity, time and sample thickness respectively. The relative flux is expressed in terms of transient flux, J_t, and steady state flux J_∞. The calculation was made for density of trap sites N=co, where co is the surface hydrogen concentration. Also, the ratio of $N\kappa/\rho$ is equal to 10, where κ and ρ are the capture and the release rate constant, respectively [275].

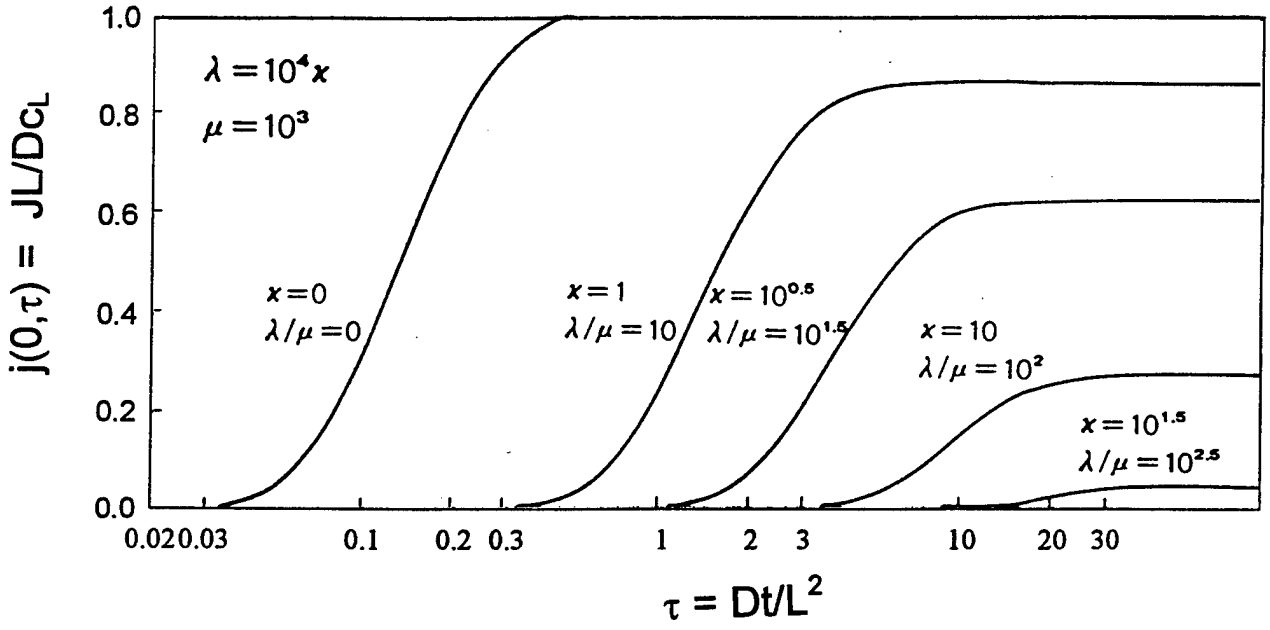

Figure 37. Influence of irreversible trap strength χ, which is proportional to $exp(E_B/RT)$, on permeation characteristics for low hydrogen concentration. Permeation rate is plotted as a function of reduced time τ, which is expressed as $\tau = Dt/L^2$ where D, t, and L are the diffusion coefficient, time, and sample thickness respectively. The non-dimensional form of permeation rate, $j=JL/Dc_L$, is expressed in terms of flux (J), thickness (L), diffusivity (D), and lattice hydrogen concentration (c_L). The dimensionless parameters λ and μ are non-dimensional form of the hydrogen capture rate (κ) and release rate (ρ), respectively [81].

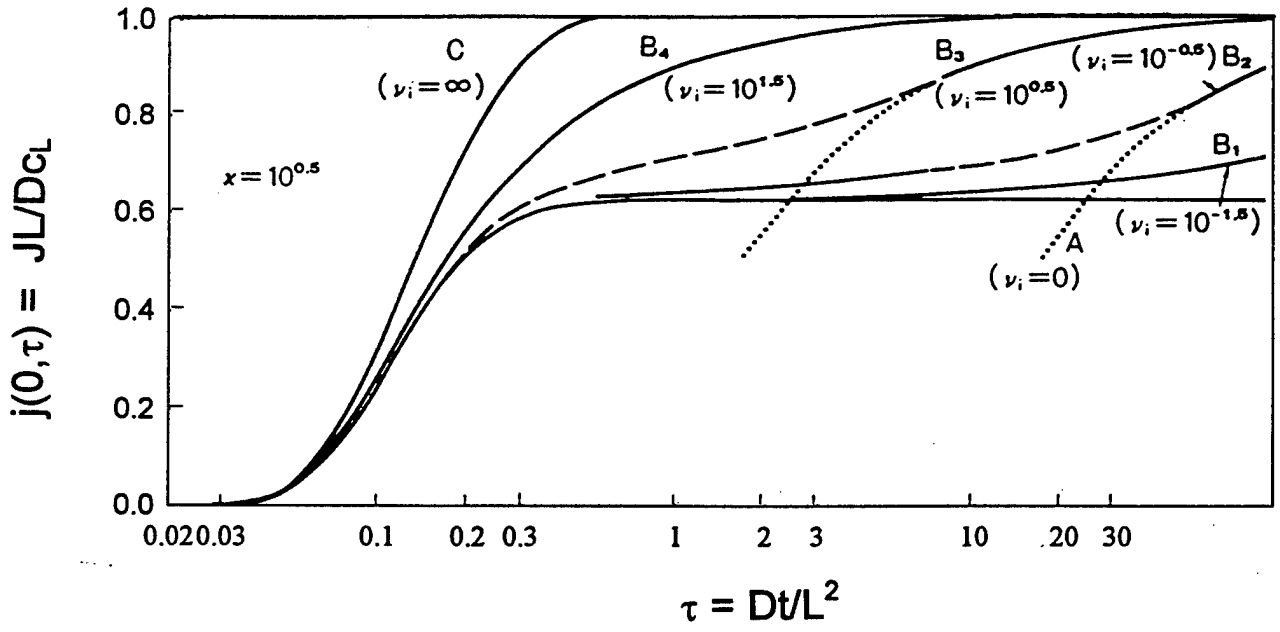

Figure 38. Diffusive permeation characteristics as a function of reduced time in a system with irreversible traps of various ν_i , which is proportional to $exp(E_{Bi}/RT)$. The permeation rate is a function of reduced time τ, which is expressed as $\tau = Dt/L^2$, where D, t, and L are the diffusion coefficient, time and sample thickness respectively. The non-dimensional form of permeation rate, $j=JL/Dc_L$, is expressed in terms of flux (J), thickness (L), diffusivity (D), and lattice hydrogen concentration (c_L) [276].

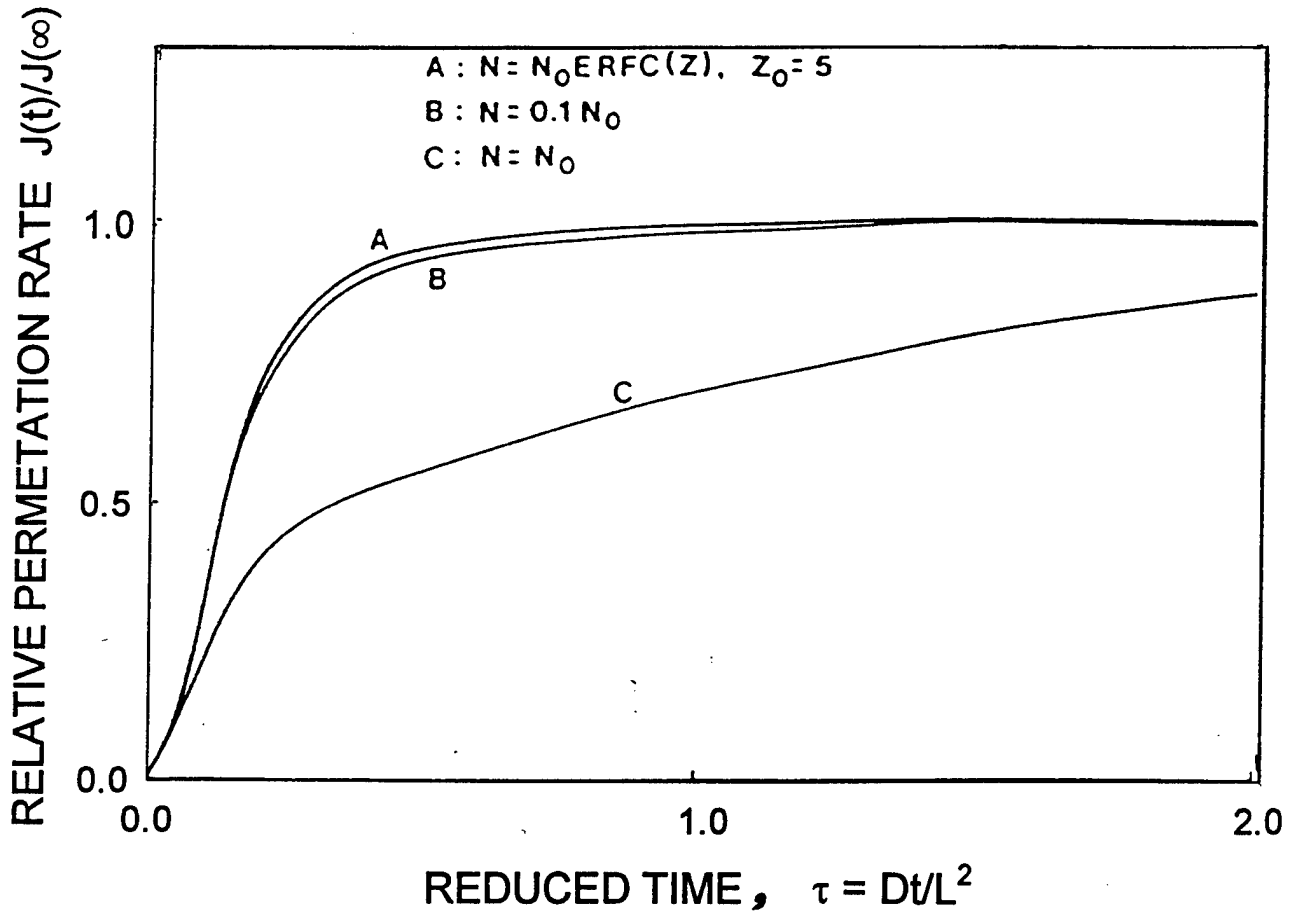

Figure 39. Comparison of relative permeation rates (a) complementary error function distribution, (b) uniform distribution, N = 0.1No, (C) uniform distribution N = No, where N_o is a uniform concentration of trap sites. The reduced time is expressed as $\tau=Dt/L^2$, where D is the diffusion coefficient, t is time, and L is the sample thickness [278]

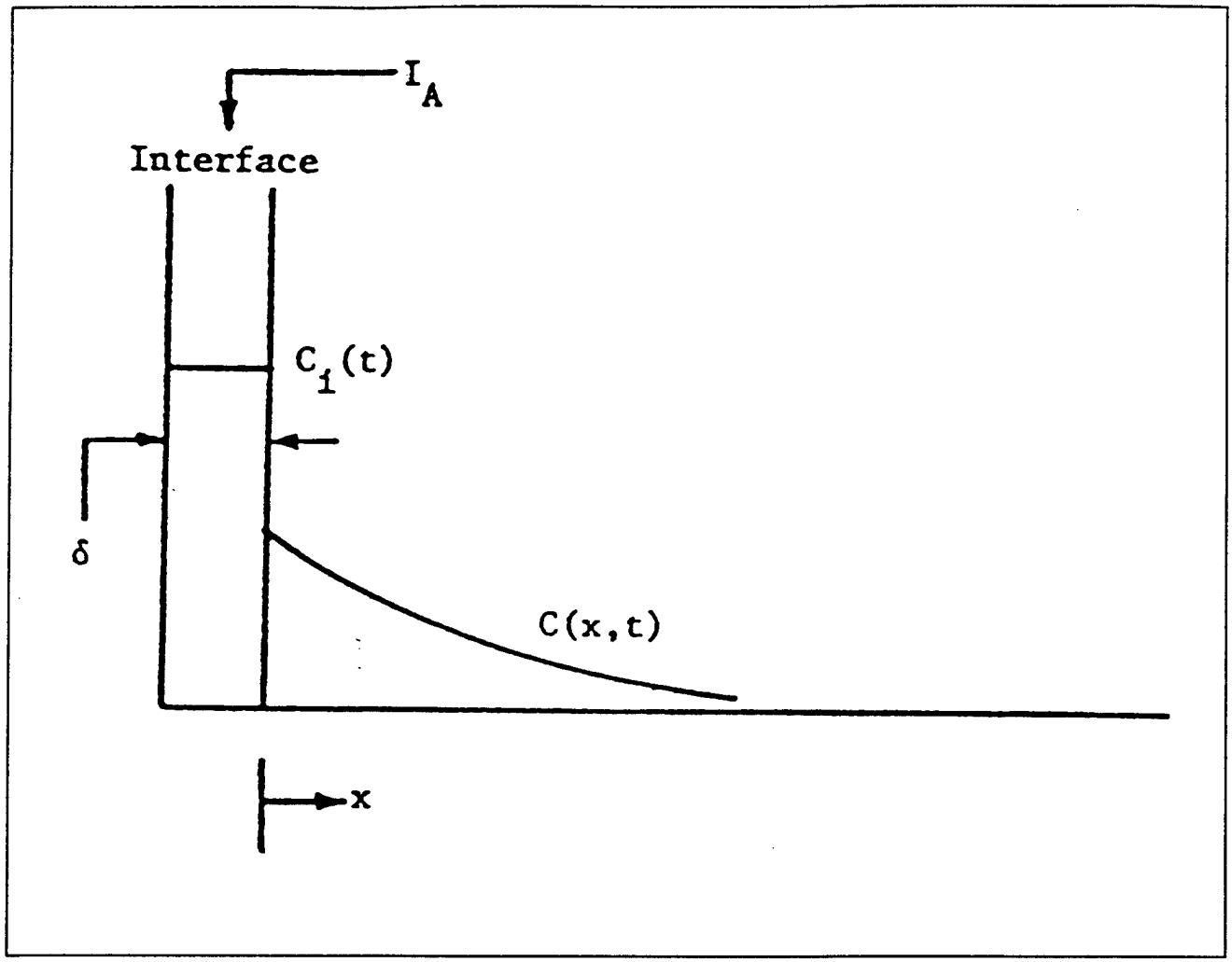

Figure 40. Schematic representation of hydrogen stripping at a trap interface of thickness δ, receiving an arriving flux I_A, which results in build-up of the interface concentration $C_i(t)$, and releasing hydrogen into matrix through flux down the concentration C(x,t) [288].

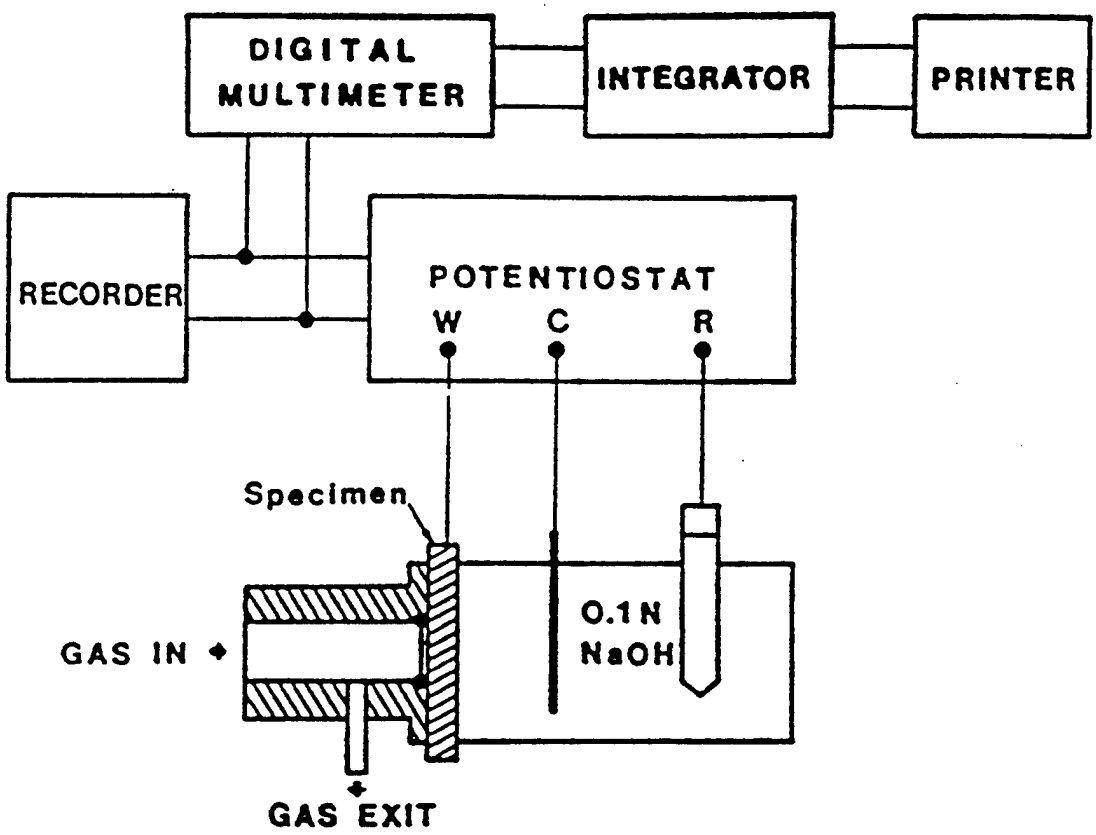

Figure 41. Schematic representation of gas-electrochemical hybrid permeation cell and flux detection system [302].

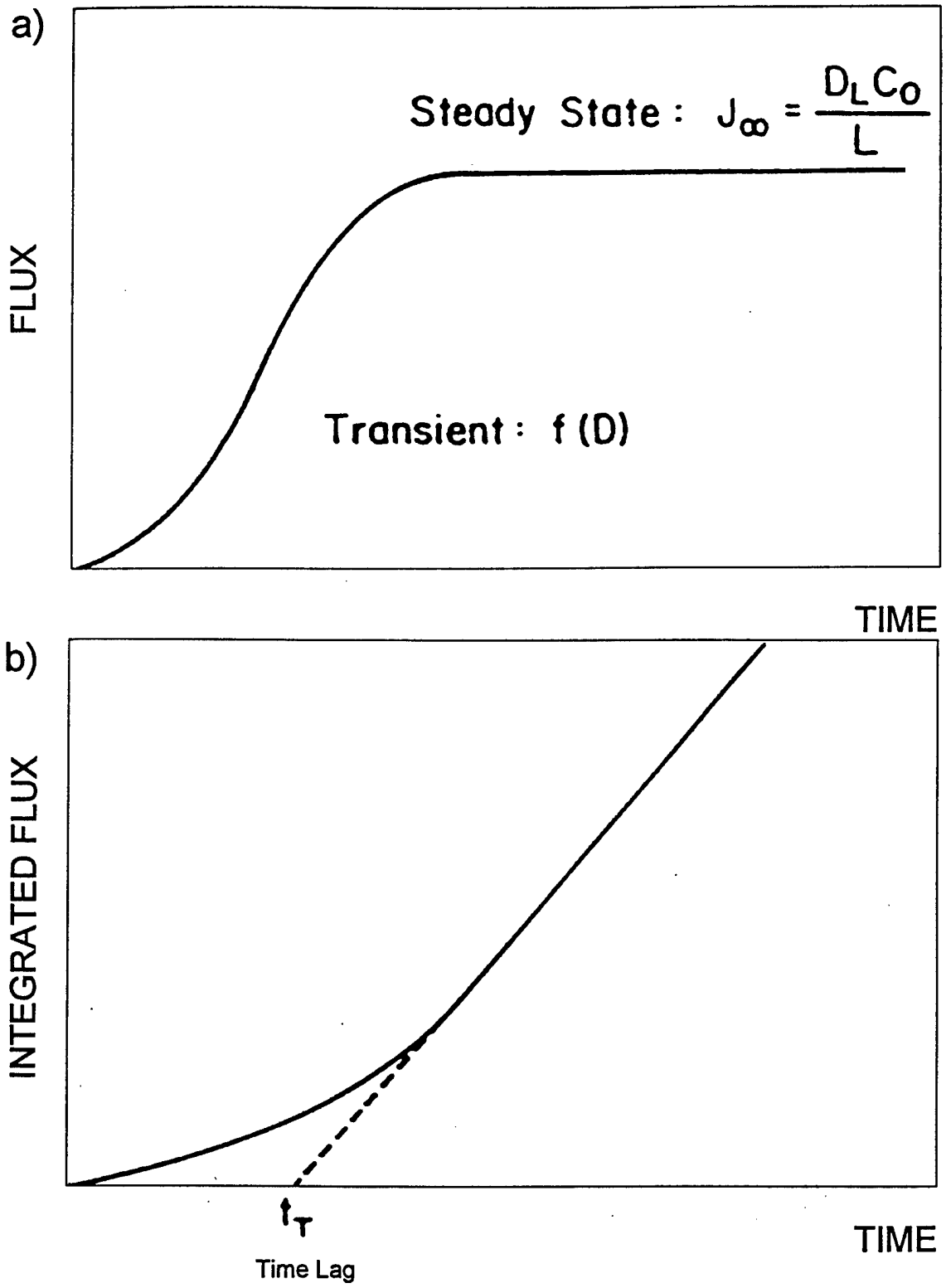

Figure 42. Schematic representation of (a). permeation curve, and (b). time lag. The term D_L is the lattice diffusion coefficient, c_o is the lattice hydrogen concentration at input surface, and L is the sample thickness [78].

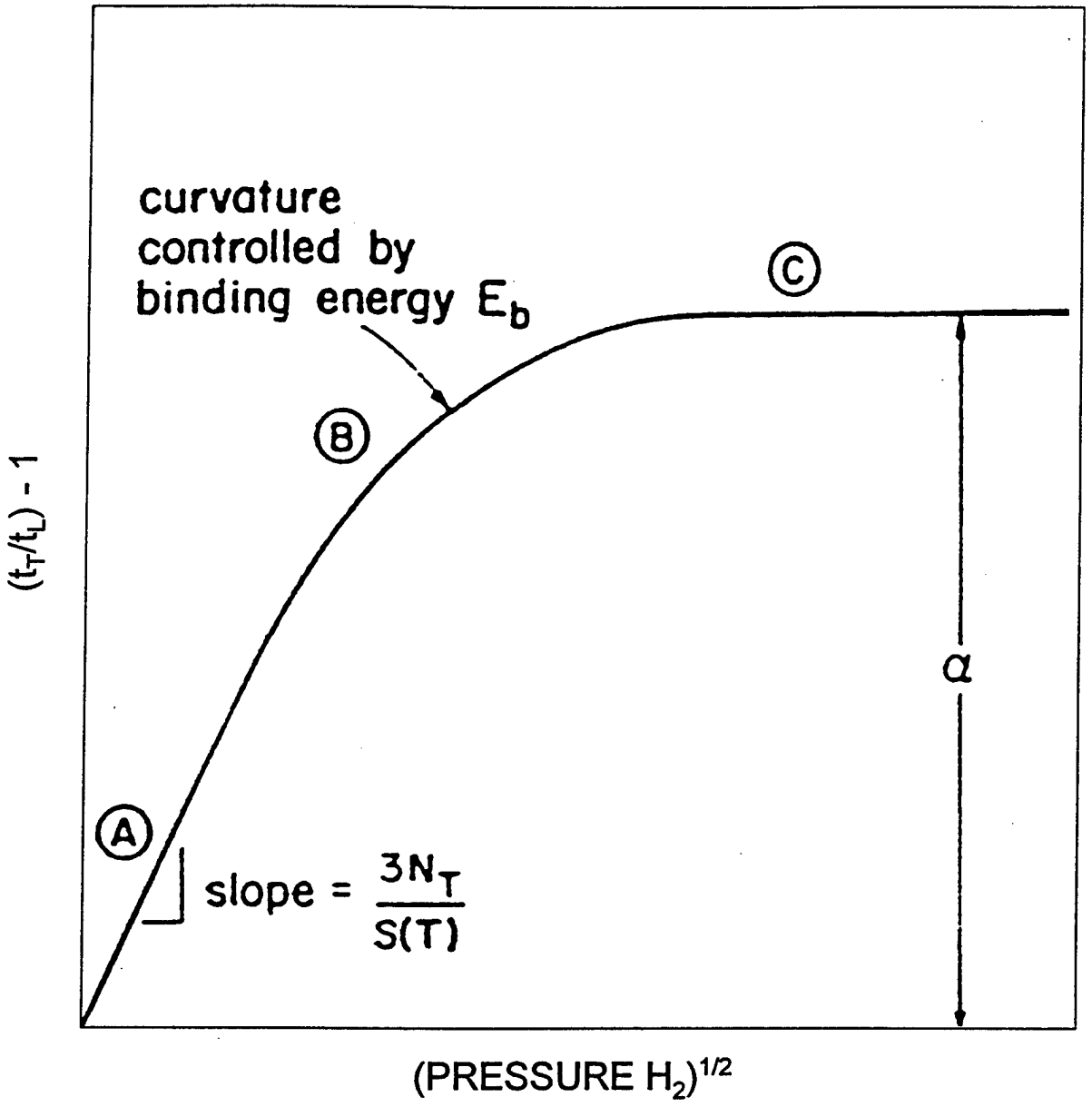

Figure 43. Schematic representation of time lag as a function of hydrogen pressure, when hydrogen traps are present. The terms t_T and t_L is are the lag time of hydrogen permeation with the presence of traps and the absence of traps, respectively. Nt is the density of trap sites and S(T) is the temperature dependent coefficient of Sieverts' law $S(T)=S_o \exp(-E_s/RT)$. The parameter α is expressed as $\alpha = N_T \kappa / \rho$, where κ and ρ are the rate for hydrogen capture and release respectively [78].

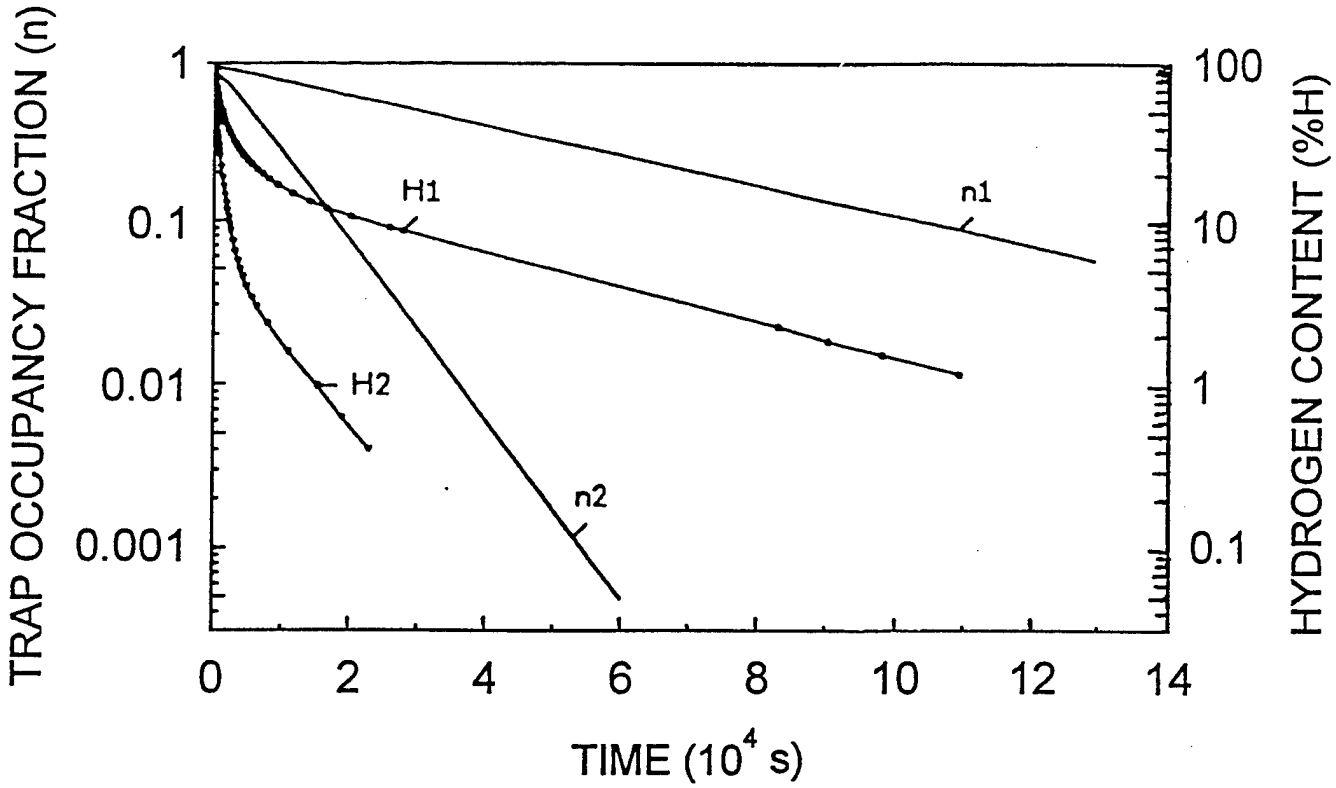

Figure 44. Time dependence of the trap occupancy fraction. Calculated and experimentally measured hydrogen content in the specimens. Rutile coated electrode ANO-4, Indices n_1, H_1 correspond to temperature 60° C; n_2, H_2 -100° C [317].

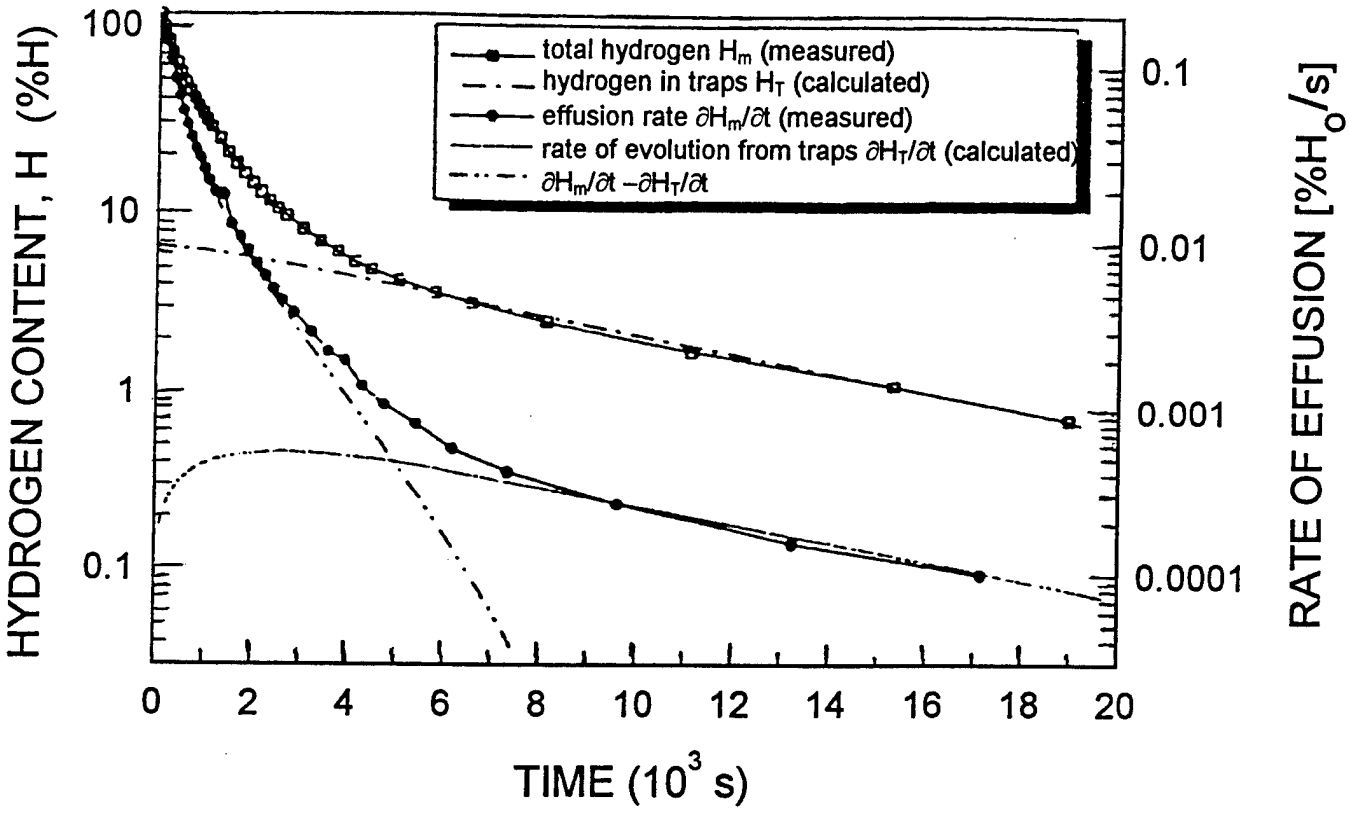

Figure 45. Hydrogen evolution from traps. The comparison of calculations with experiment [317].

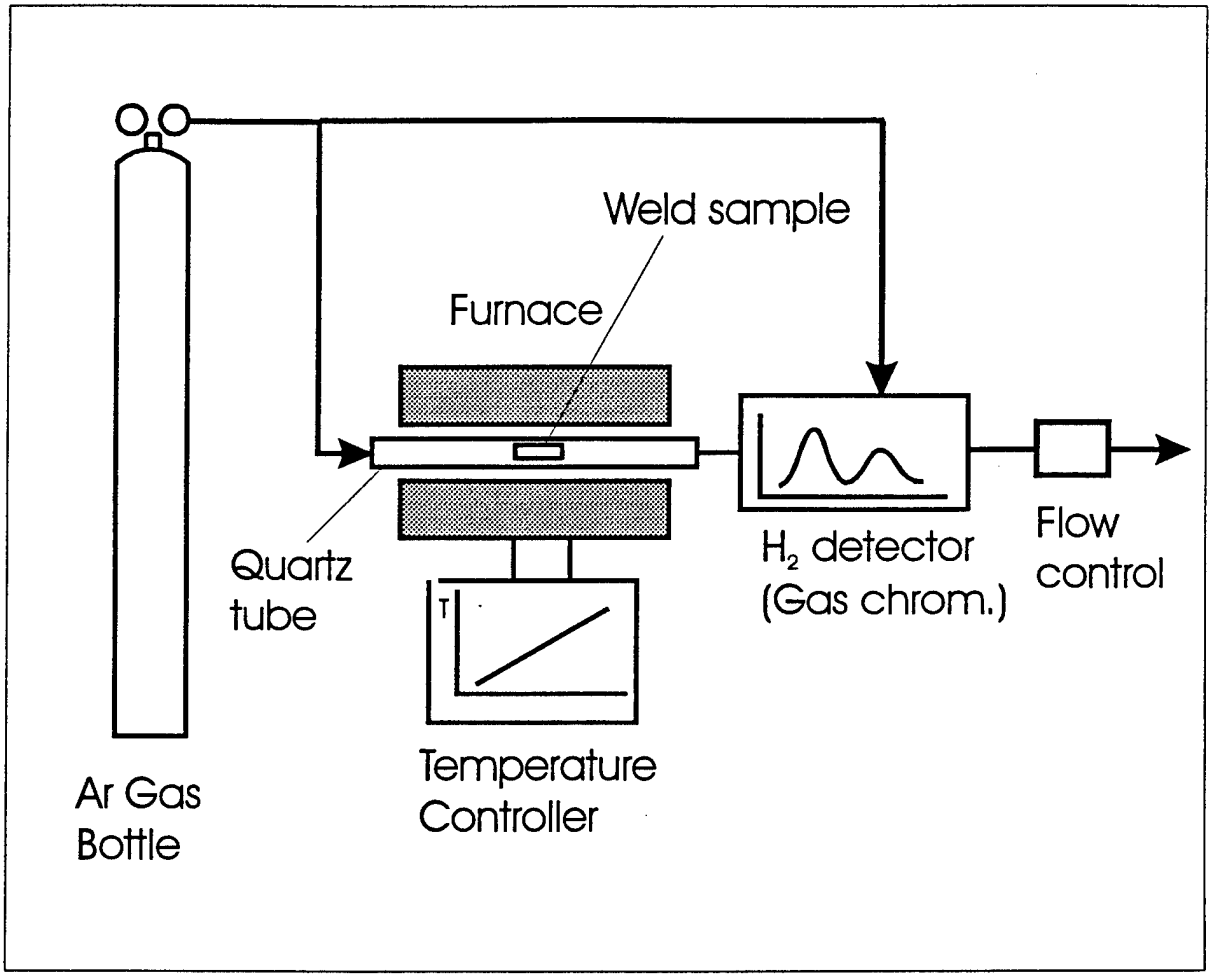

Figure 46. Typical set-up for non-isothermal hydrogen evolution measurement

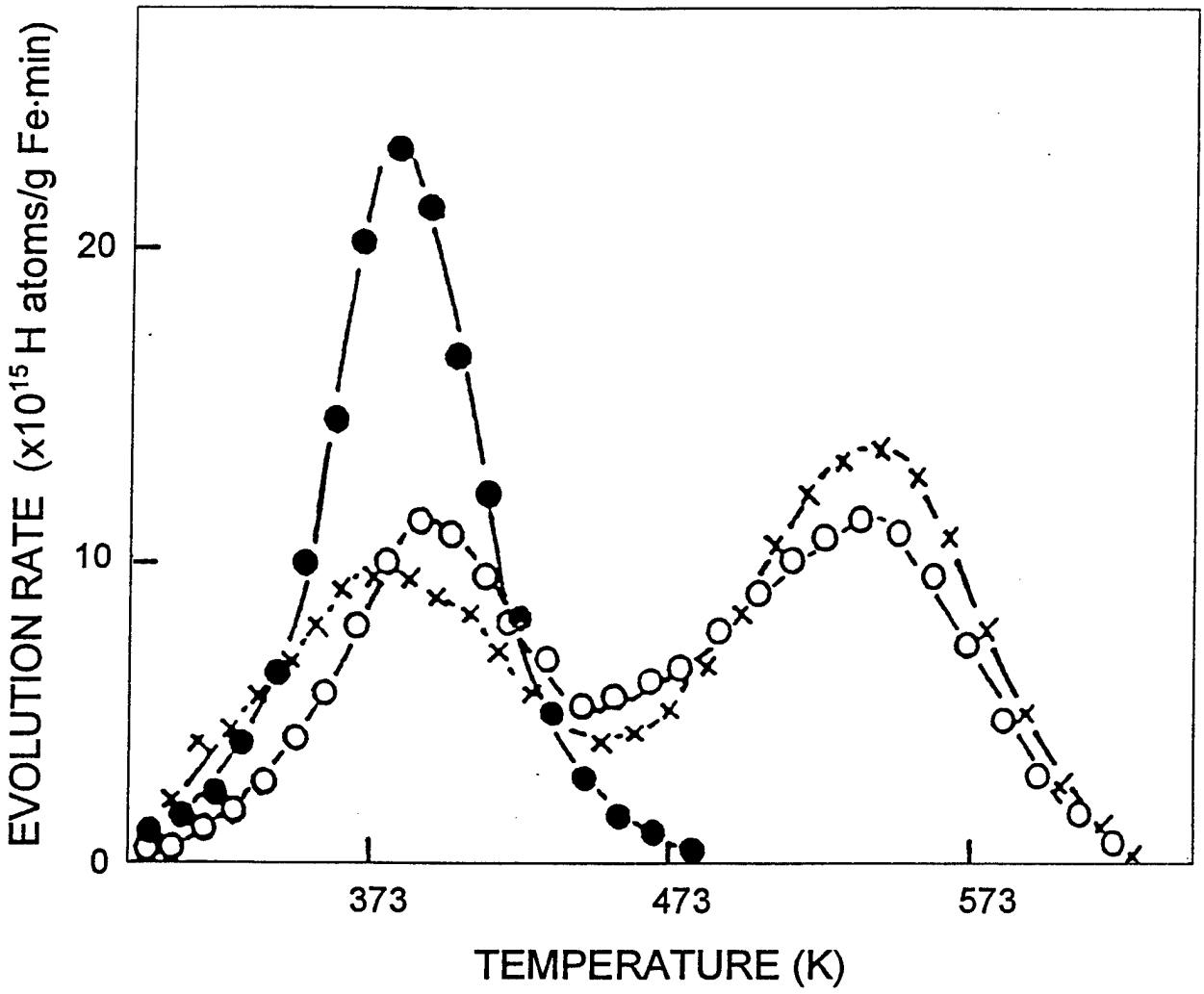

Figure 47. Variation of heights of peaks corresponding to dislocations and microvoids in a single crystal of iron. The 388K peak is related to hydrogen released from the dislocation and grain boundary and 538K peak from the microvoid, respectively [318].

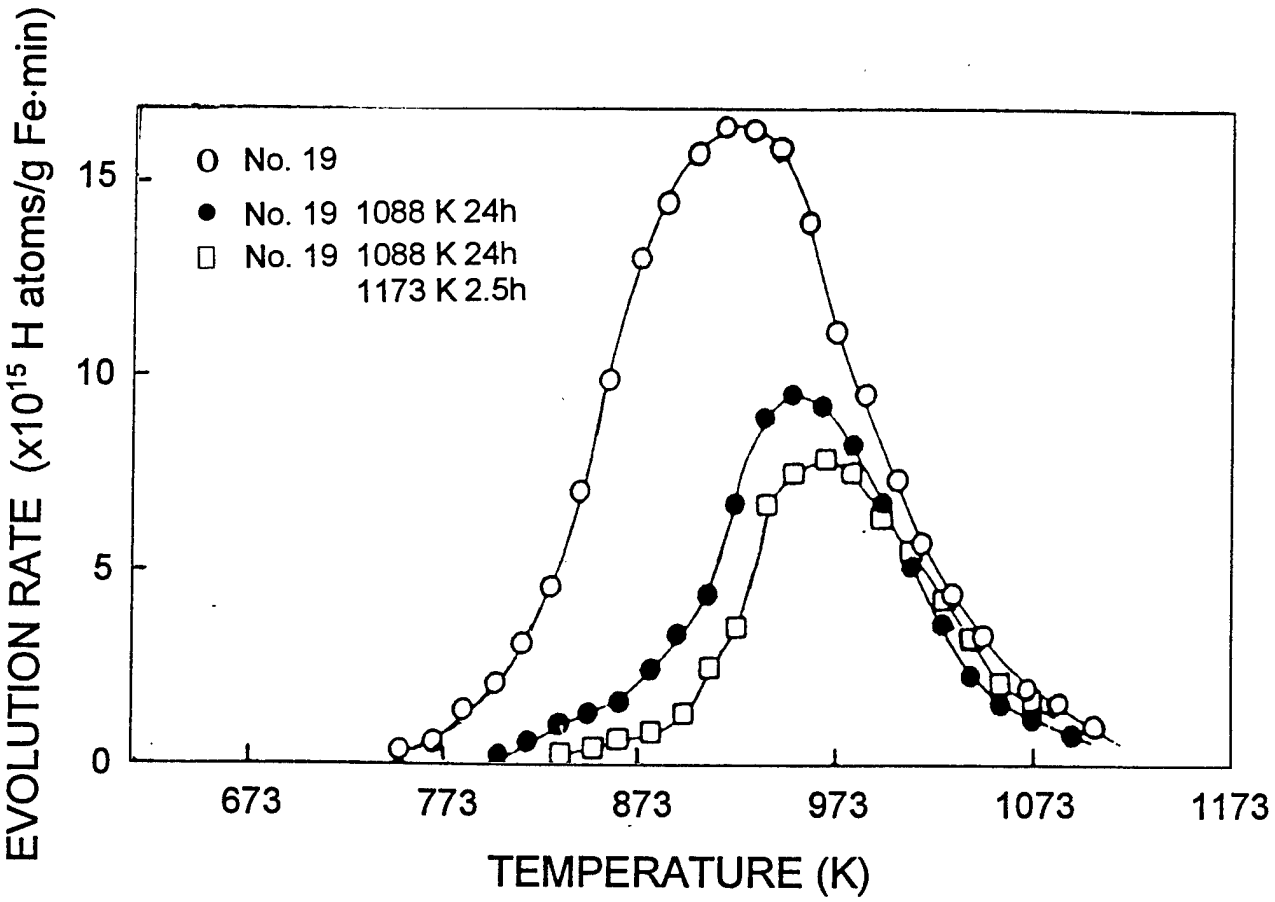

Figure 48. Dependence of hydrogen evolution rate peak on the precipitated particle size. The interface structure changes from coherent at small size to incoherent at larger size. Sample No. 19 (o) was annealed at 1311 K for 2 hrs, sample No. 19 (•) had additional annealing at 1088 K for 24 hrs, sample No. 19 (□) is sample (•) which was further annealed at 1173 K for 2.5 hrs [122].

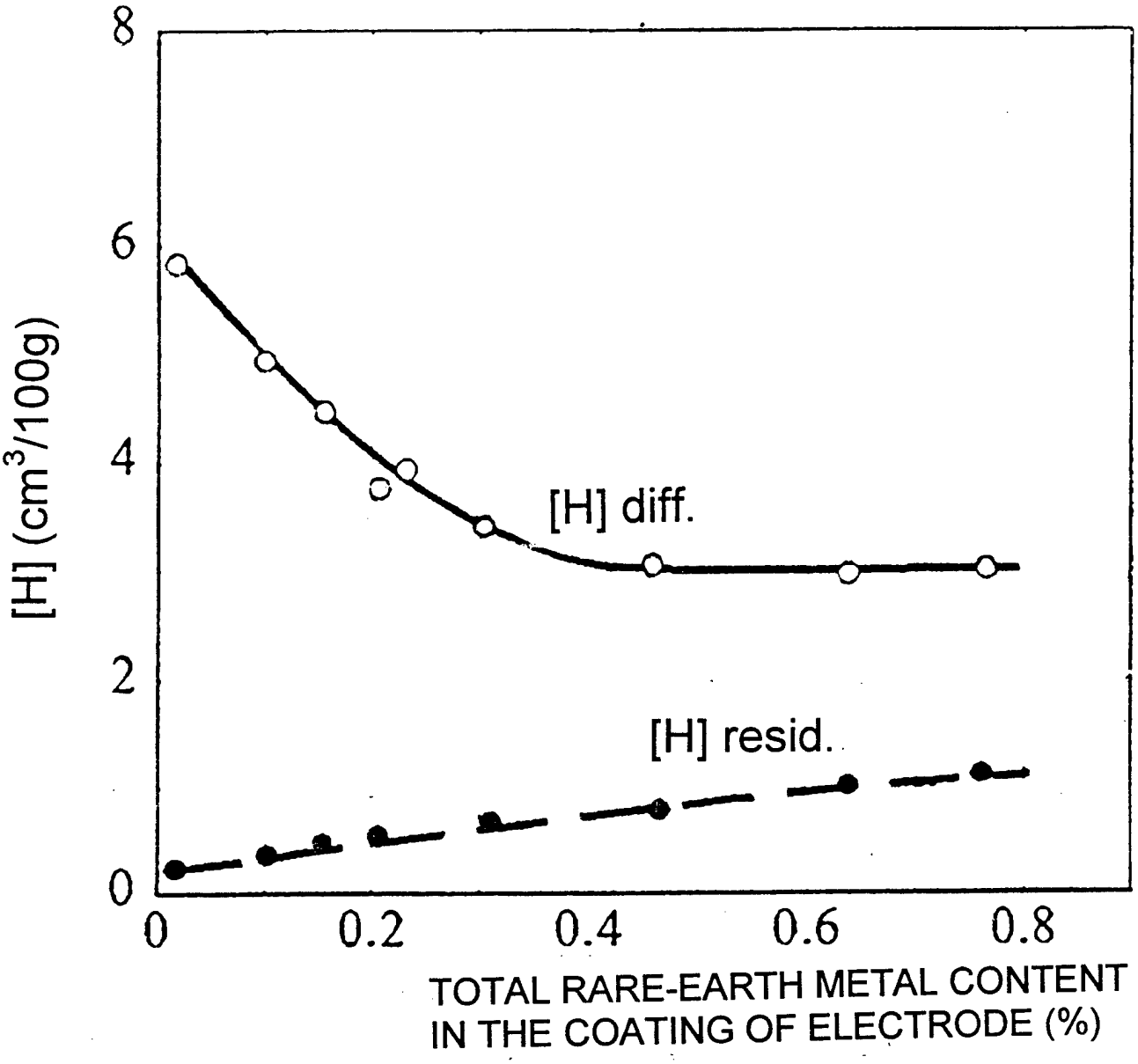

Figure 49. Influence of rare-earth metal content in electrode coating as weld metal trap additions on diffusible and residual hydrogen [342].

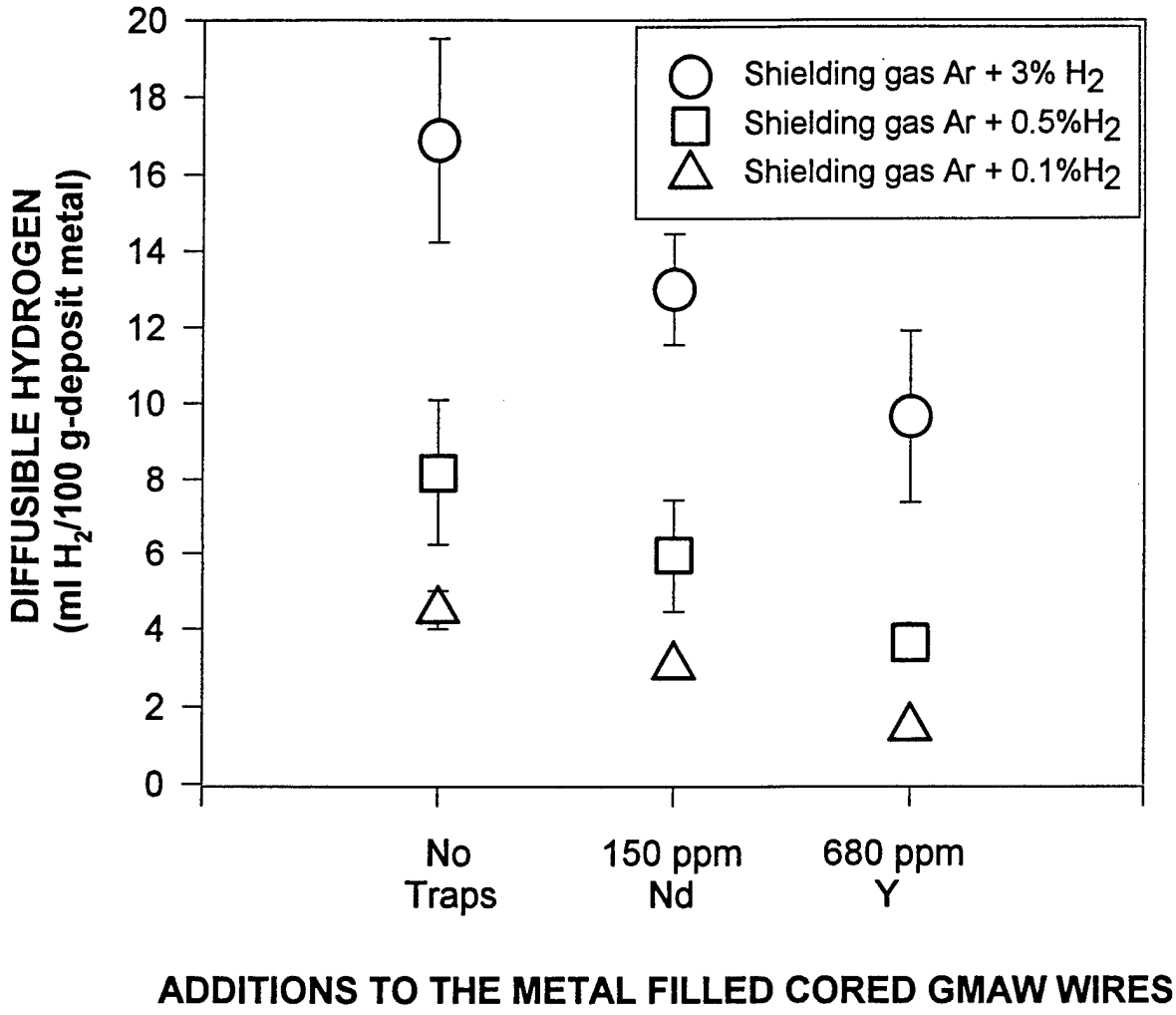

Figure 50. Effect of trap additions to the amount of diffusible hydrogen of weld samples welded with GMAW process at nominal heat input 1.5 kJ/mm [343].

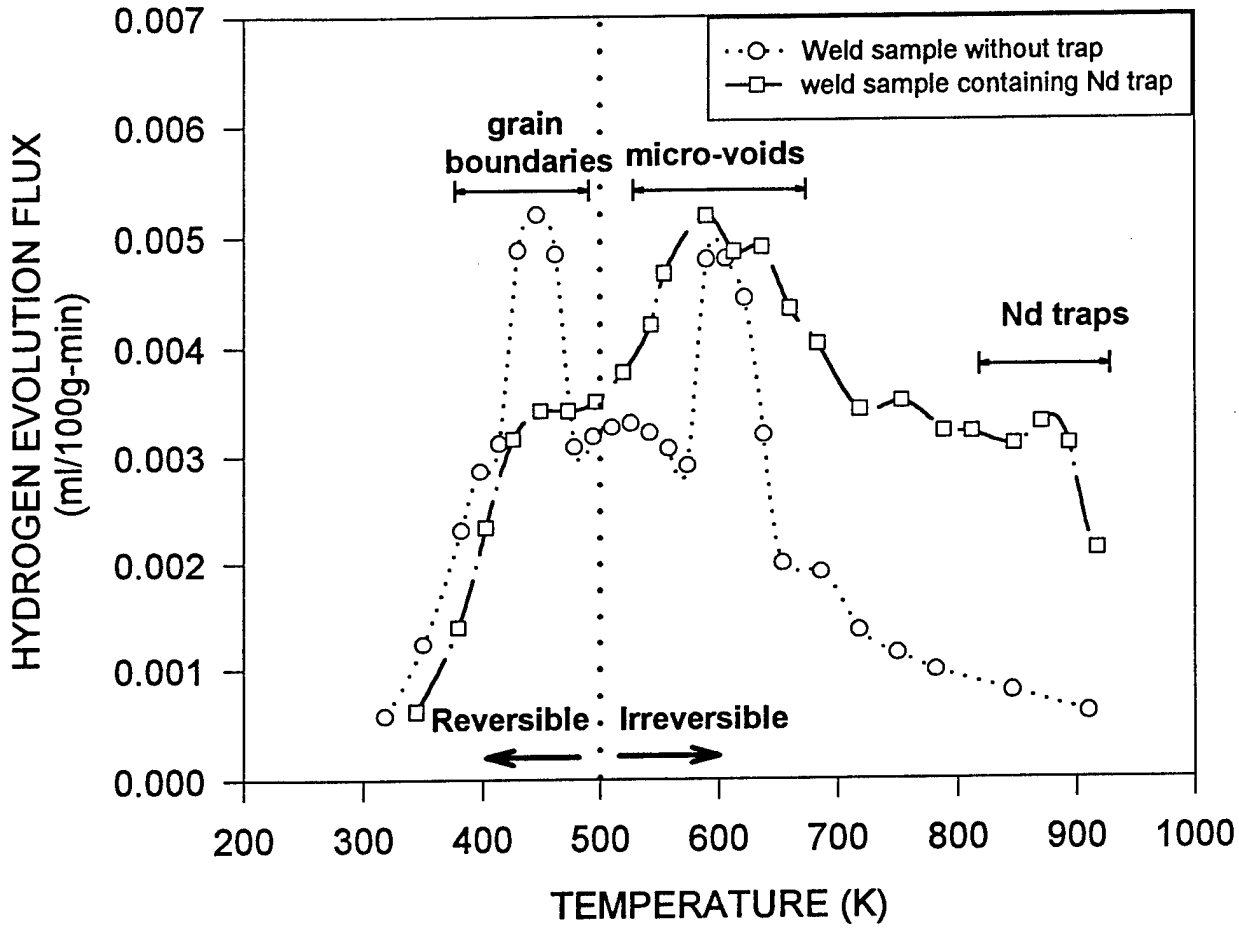

Figure 51. Hydrogen evolution curves from non-isothermal analysis (4° C/min) of weld sample free of deep traps and weld sample containing deep traps (Neodymium additions). The peak at 450 K is the hydrogen released from grain boundaries, at 620 K from micro-voids and at 875 K from Neodymium associated trap sites [343].

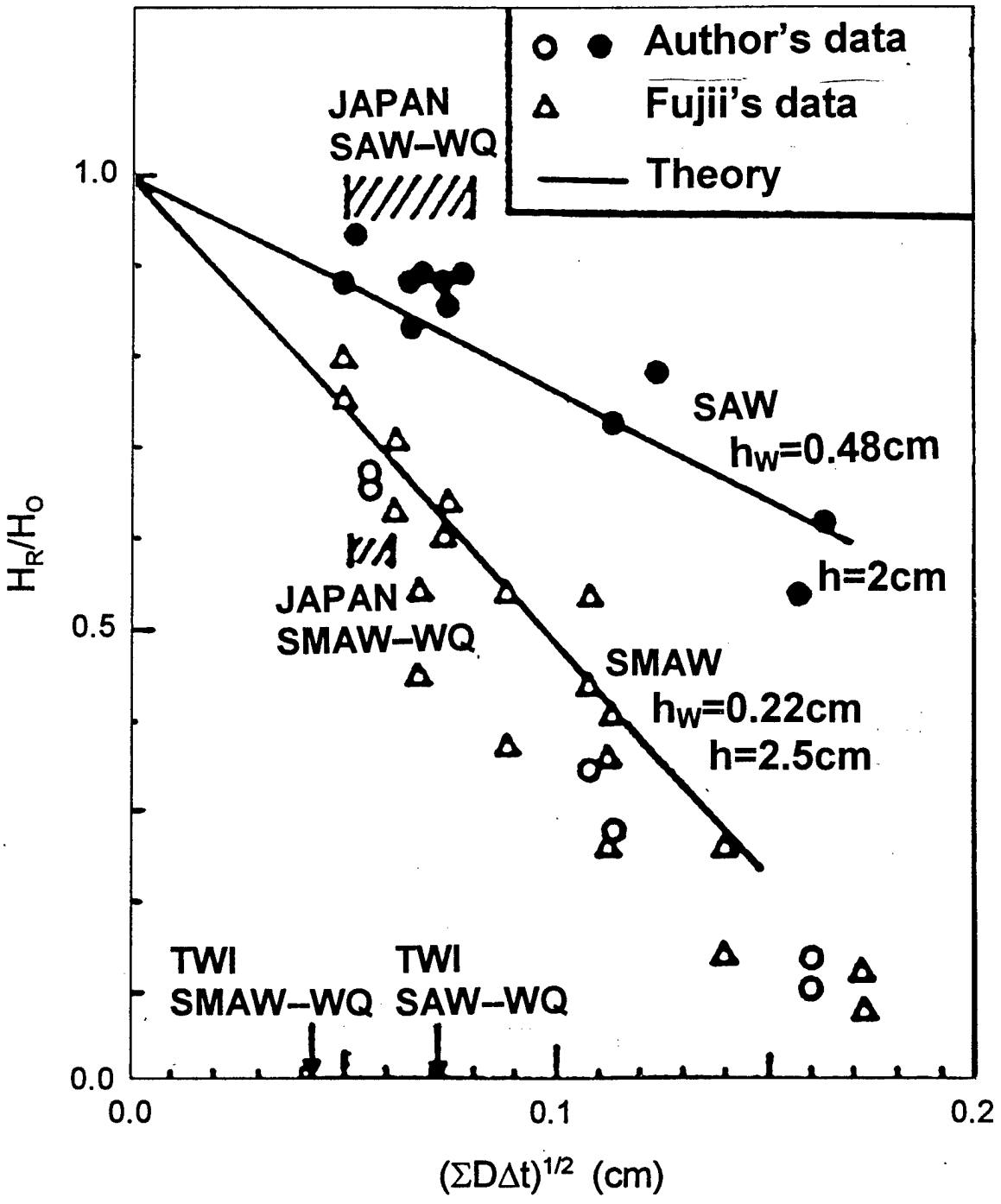

Figure 52. Comparison between experimental and theoretical results of the ratio of retained diffusible hydrogen content (H_R) to initial hydrogen content (H_O), as a function of the thermal factor $\Sigma D\Delta t$ [345].

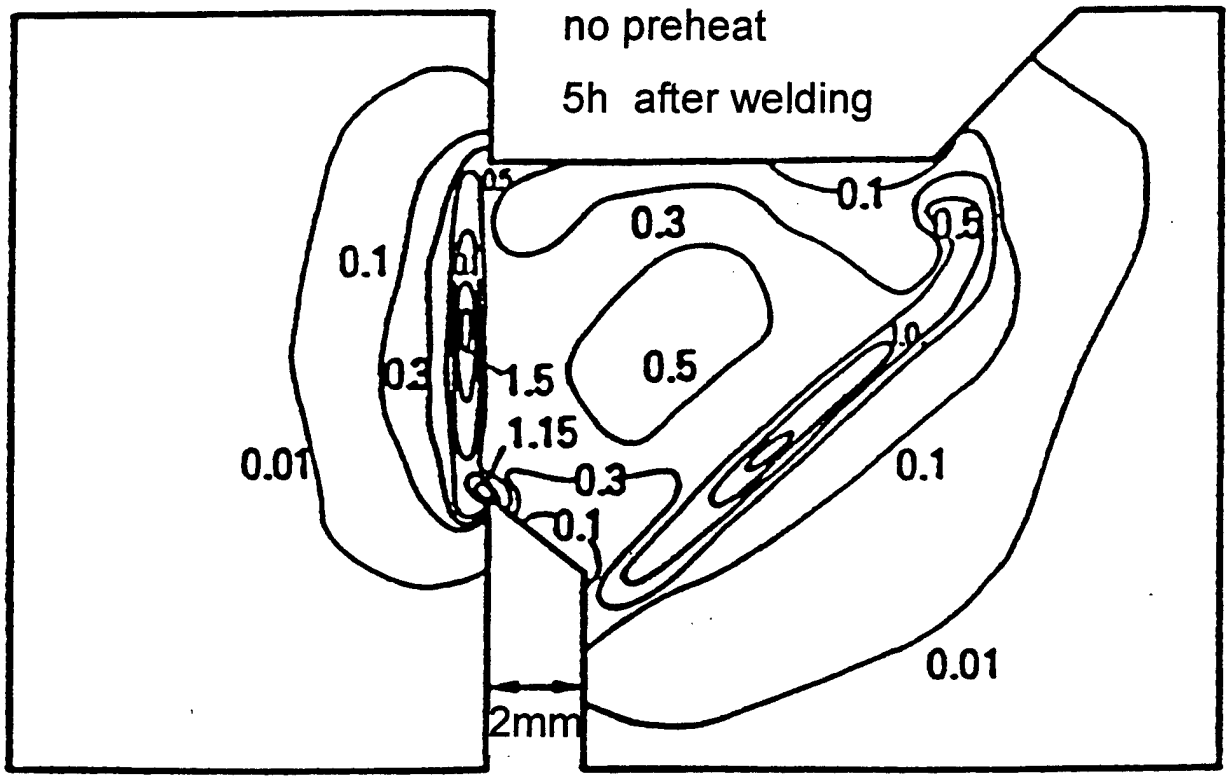

Figure 53. Distribution of hydrogen concentration (non-dimensional with respect to initial concentration in weld metal) in single bevel groove weld 5 h after welding, calculated by finite difference method. The distribution is calculated result of hydrogen transport due to stress gradient [351,352].

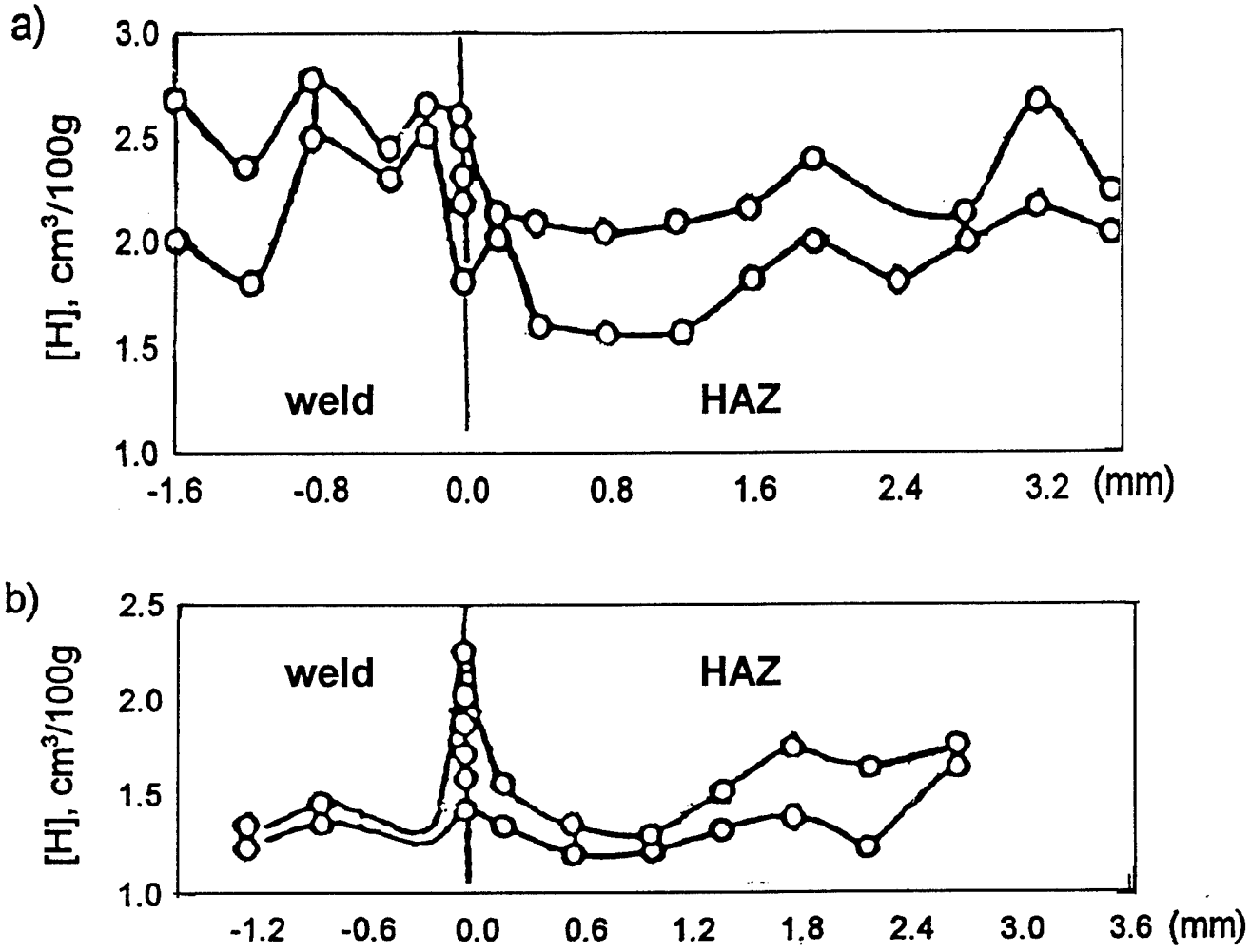

Figure 54. Distribution of hydrogen in a welded joint in 15Kh1M1F steel : (a). not heat treated after welding; (b). tempered at a high temperature (730° C) after welding [354].

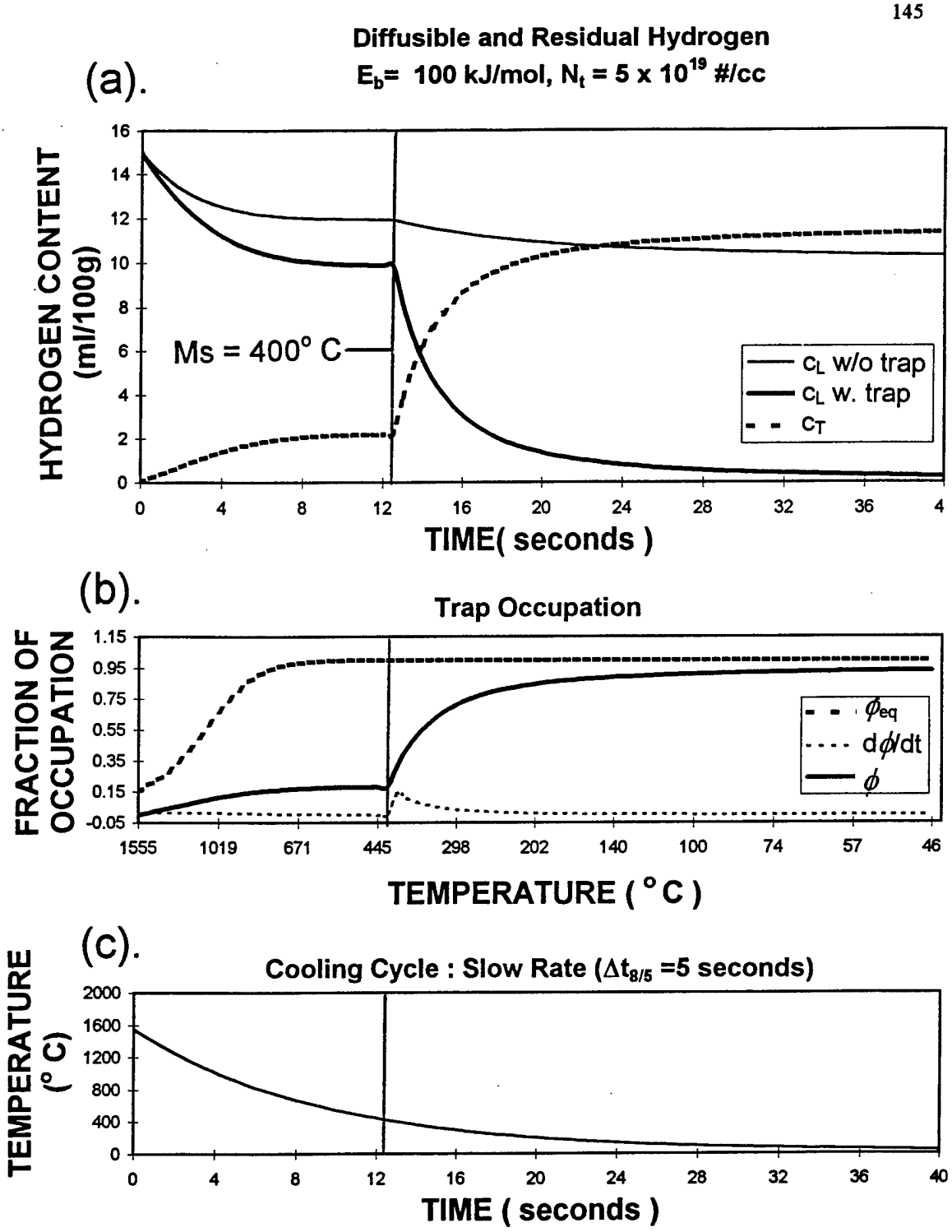

Figure 55. Hydrogen trapping during welding cooling cycle. Initial diffusible hydrogen in weld metal is 15 ml/100g. In (a).,the notation c_L stand for diffusible hydrogen, c_T is the trapped hydrogen. In (b), ϕ is the fraction of trap occupation by hydrogen and ϕ_{eq} is the equilibrium fraction of occupation determined by the Fermi-Dirac distribution [10].

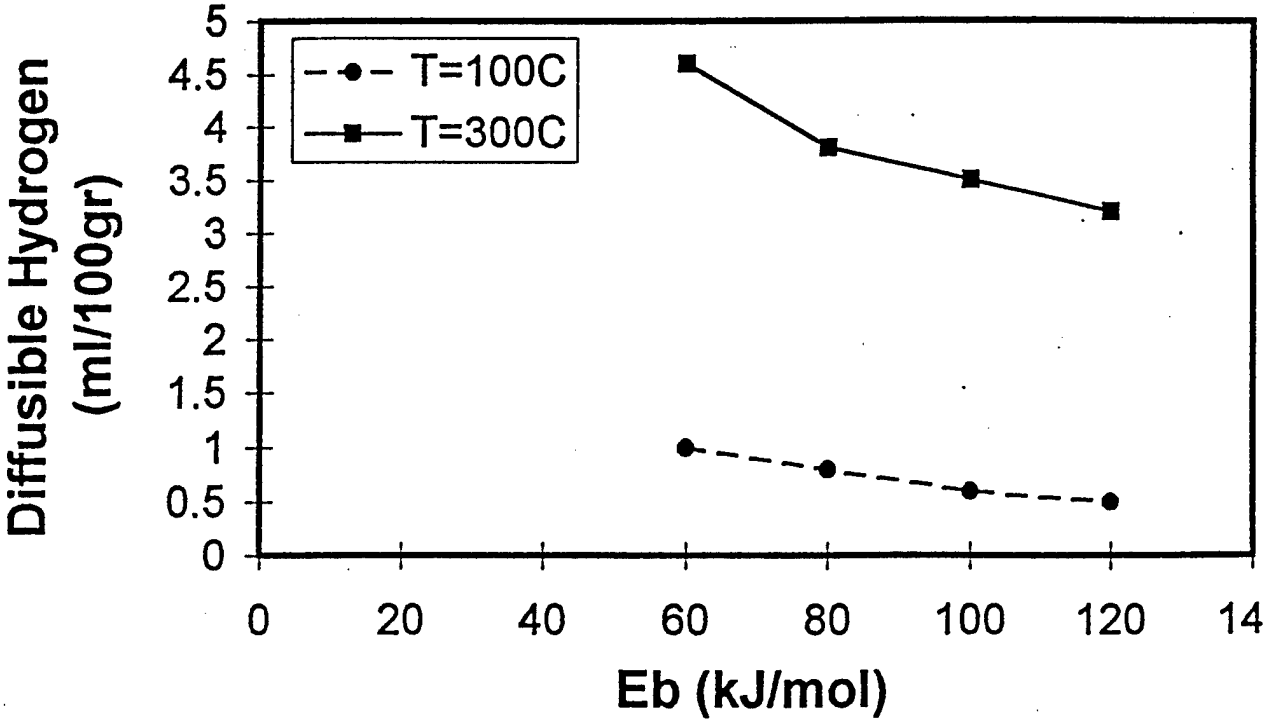

Figure 56. Summary of diffusible hydrogen content at 100 and 300° C during cooling cycle, as a function of hydrogen-trap binding energy. Initial diffusible hydrogen content is 15 ml/100g-metal. Ms = 400° C, $\Delta_{t8/5}$ is 5 seconds, trap density N_t=5 × 10^{19} # of trap sites/cc. [10].

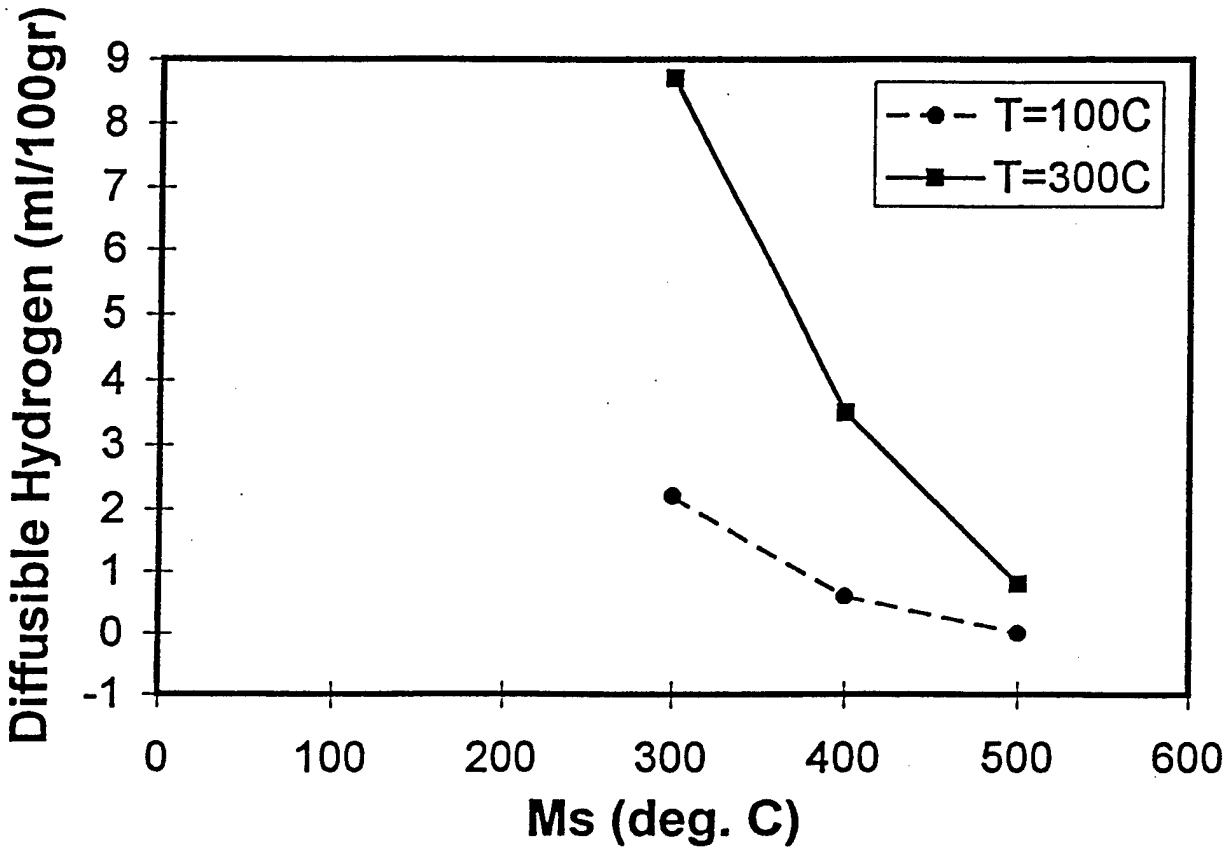

Figure 57. Summary of diffusible hydrogen content at 100 and 300° C during cooling cycle, as a function of martensite start temperature. Initial diffusible hydrogen content is 15 ml/100g-metal. E_B = 100 kJ/mol-H, $\Delta_{t8/5}$ is 5 seconds, trap density $N_t=5 \times 10^{19}$ # of trap sites/cc. [10].

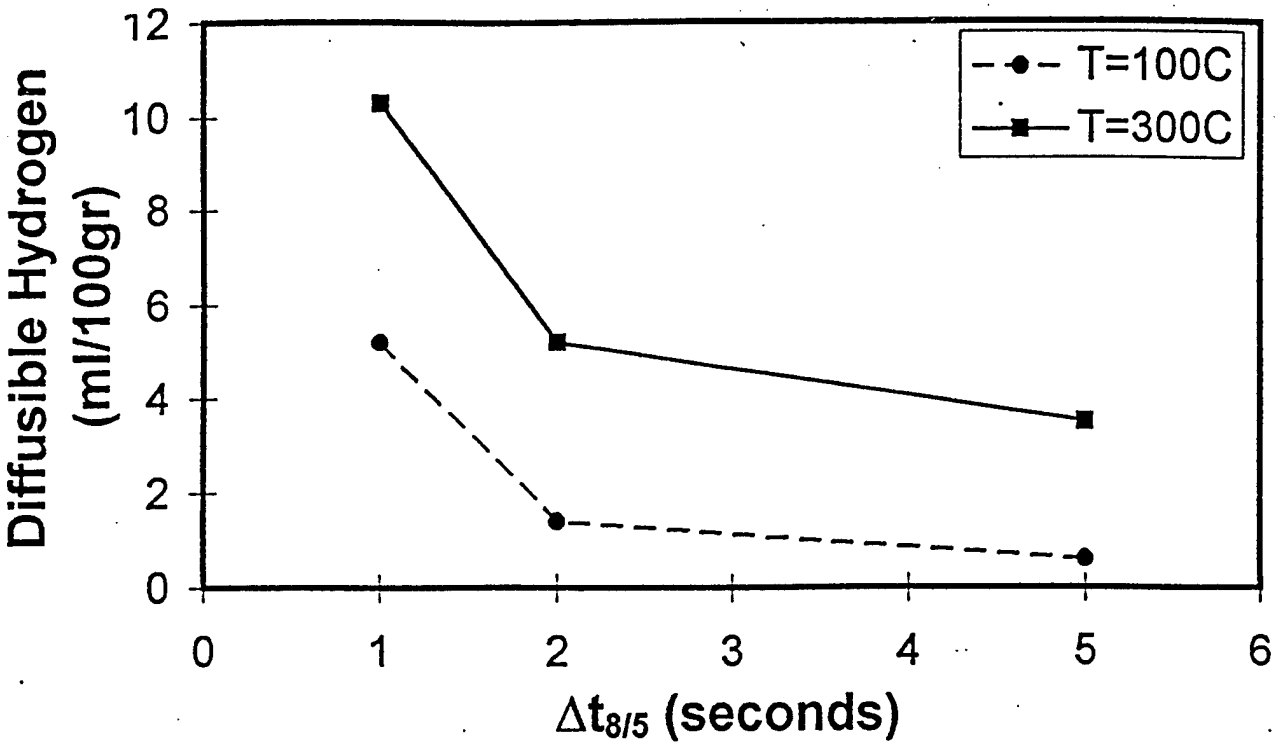

Figure 58. Summary of diffusible hydrogen content at 100 and 300° C during cooling cycle, as a function of cooling rate ($\Delta t_{8/5}$). Initial diffusible hydrogen content is 15 ml/100g-metal. Ms = 400° C, E_B = 100 kJ/mol-H, trap density $N_t = 5 \times 10^{19}$ # of trap sites/cc. [10].

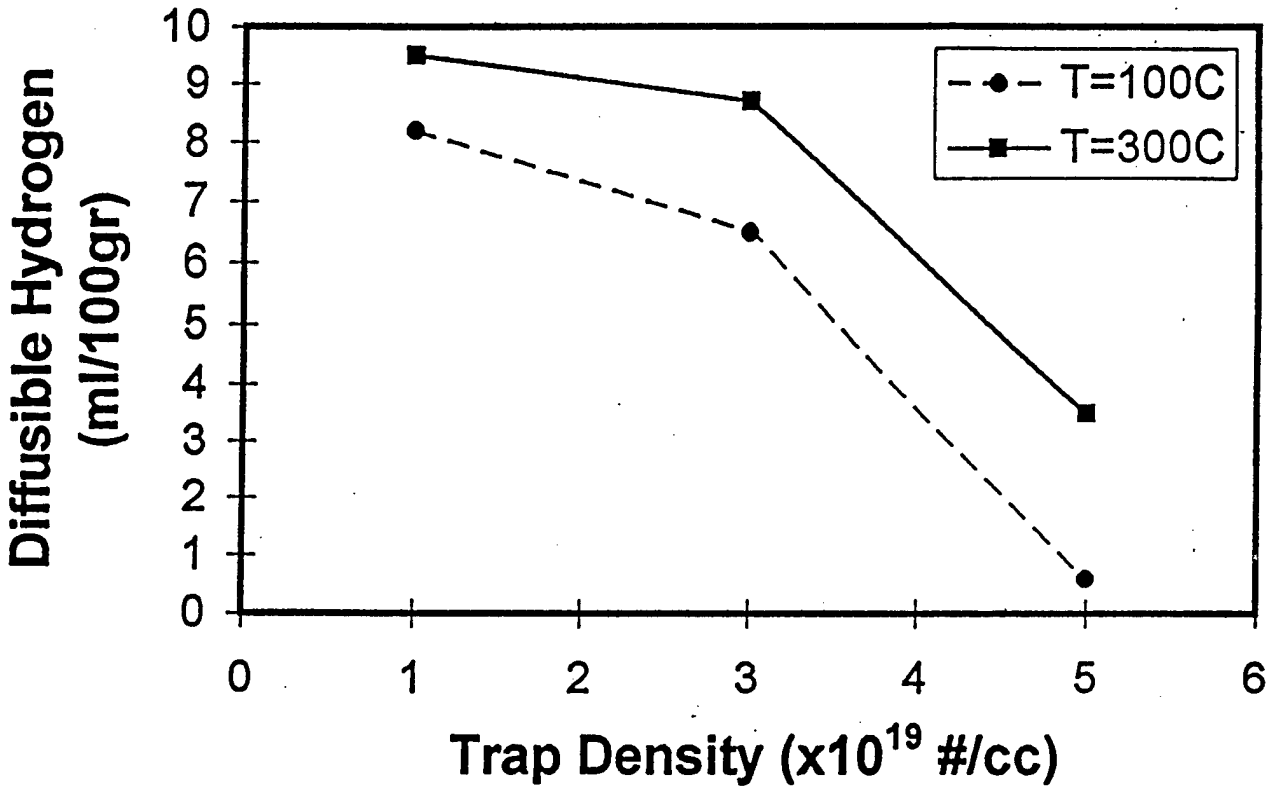

Figure 59. Summary of diffusible hydrogen content at 100 and 300° C during cooling cycle, as a function of trap density. Initial diffusible hydrogen content is 15 ml/100g-metal. Ms = 400° C, E_B = 100 kJ/mol-H, $\Delta_{t8/5}$ is 5 seconds [10].

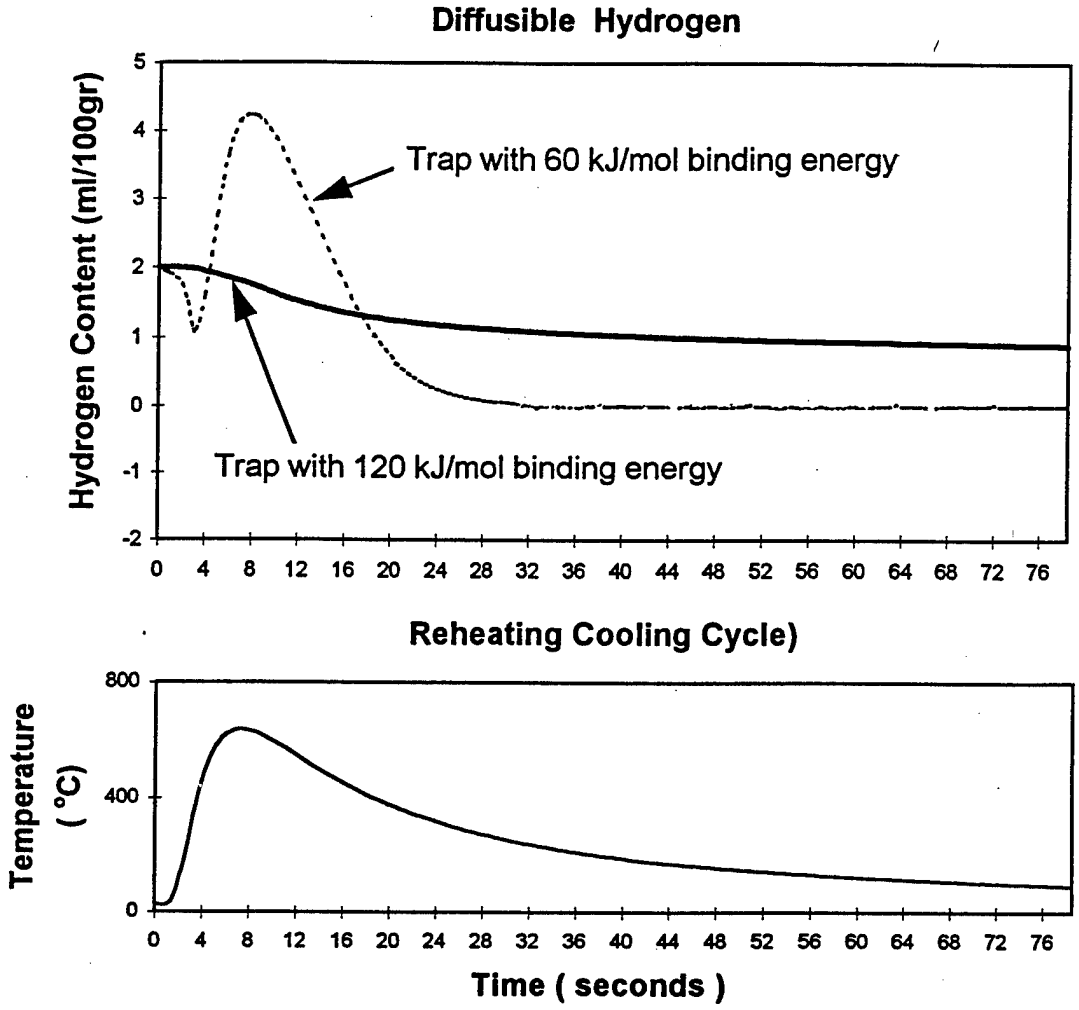

Figure 60. Theoritical evaluation on the performance of hydrogen trap during multipass welding. (a). Diffusible hydrogen (HD) of weld metal containing trap with E_B = 100 kJ/mol and E_B=60 kJ/mol (b). Thermal cycle during multipass welding [355].

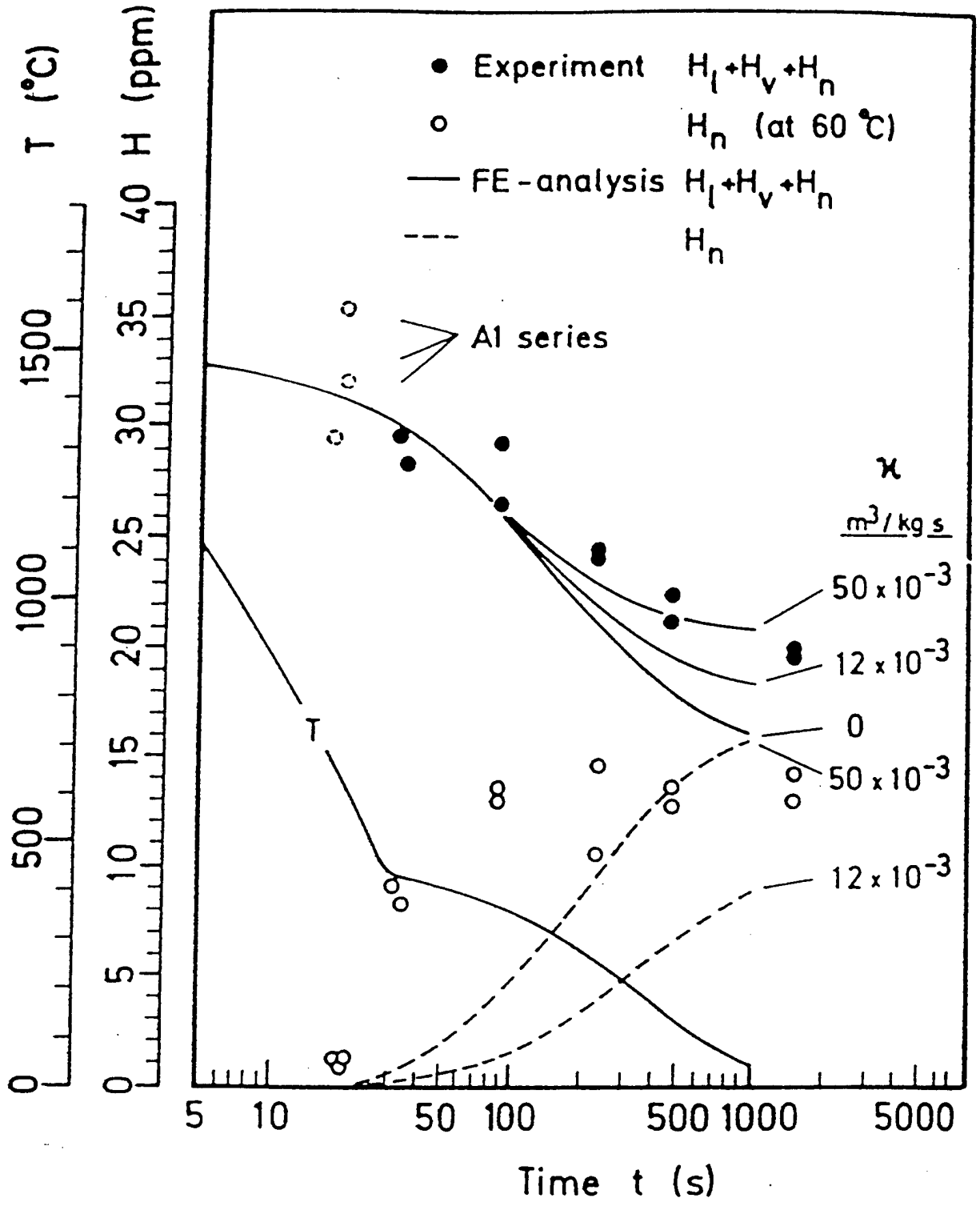

Figure 61. Calculated and measured mean concentration (ppm fused metal) of diffusible and residual hydrogen as a function of time and hydrogen capturing rate by trap sites (κ). The total hydrogen is the sum of diffusible hydrogen (H_l), hydrogen trapped in voids (H_v), and hydrogen trapped at irreversibel trap sites (H_n) [356].

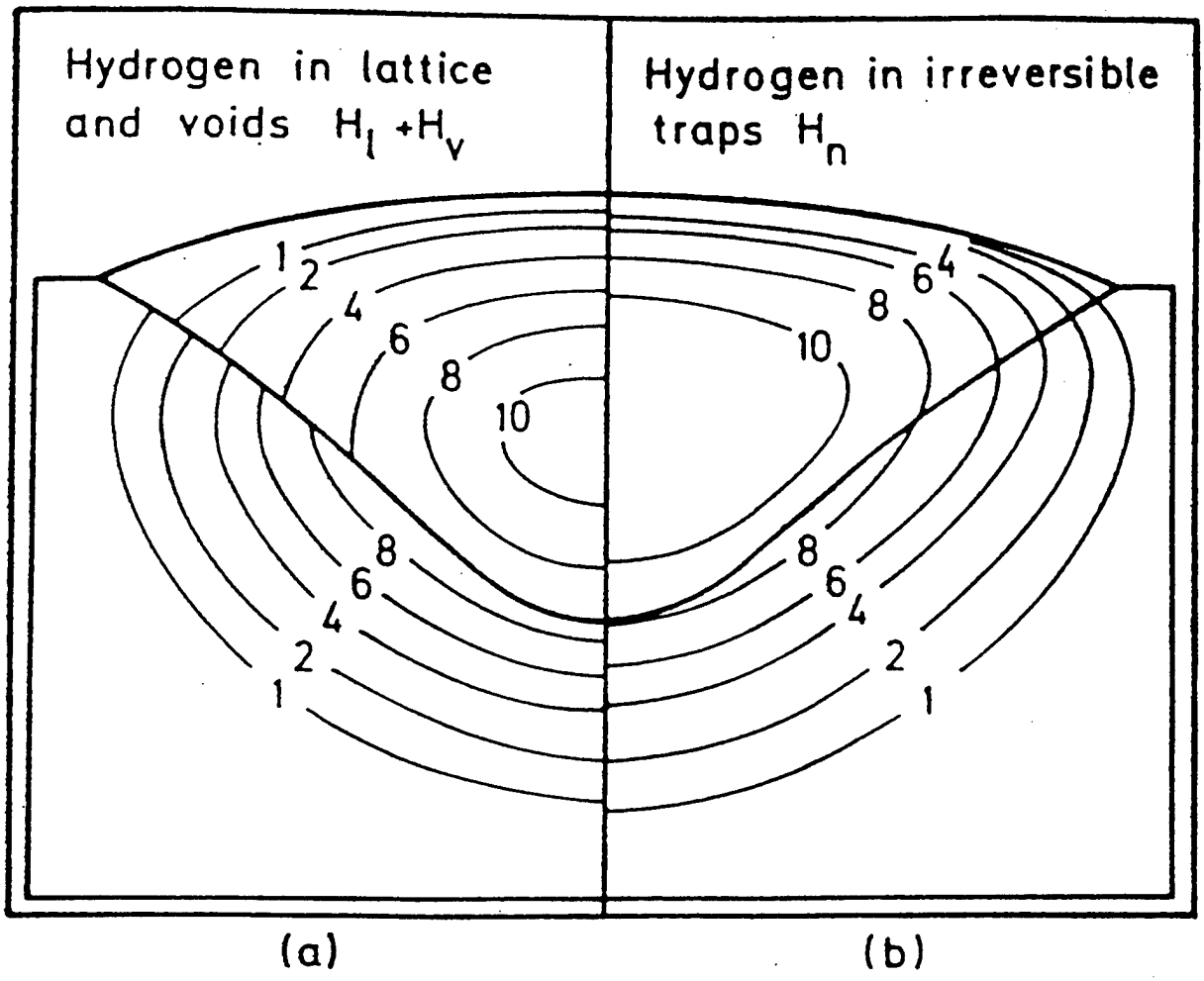

Figure 62. (a). Calculated distribution of hydrogen in voids and latice after 350 s. Curve parameter is concentration (ppm), (b). in irreversible traps [356].

11. REFERENCES

1 N. Bailey, F.R. Coe, T.G. Gooch, P.M. Hart, N. Jenkins, and R.J. Pargeter: 'Welding Steel without Hydrogen Cracking', 2nd edn, 1993, Materials Park, Ohio, ASM Int.

2 R. Wong, J. Blackburn, J. DeLoach, and R. DeNale: in 'Hydrogen Management in Steel Weldments', (ed. J.L. Davidson and D.L. Olson), 35-48, 1996, Melbourne, Australia, DSTO and WTIA.

3 V.F. Musiyachenko and S.B. Kasatkin: *Automatic Welding*, 1985, **38** (9), 22-26.

4. W.Wang, S. Liu, and D.L. Olson: in Proc. Intl. Conf. 'Offshore Mechanics and Arctic Engineering - Materials Engineering', Vol. III, Florence, Italy, 1996, ASME, 403-409.

5 . N. Yurioka and H. Suzuki: *Int. Mater. Rev.*, 1990, **35** (4), 217-249.

6. J.P. Hirth: *Metal. Trans.*, 1980, **11A**, 861-890.

7 . S.A. Gedeon and T. Eagar: *Welding Journal*, 1990, **69**, 213-220s.

8 . T. Boellinghaus, H. Hoffmeister, and C. Schubert: in Proc 4th Intl Conf. 'Trends in Welding Research', Gatlinburg, TN, June 1995, ASM Int., 25-30.

9 . J.R. Scully, J.A., Van Den Avyle, M.J. Cieslak, A.D. Romig,Jr., and C.R. Hills: *Met.Trans* .,1991, **22A**, 2429-2445.

10 . D.L. Olson, I.Maroef, C.Lensing, D. Smith, T. Wildeman, and M. Eberhart: in 'Hydrogen Management in Steel Weldments', (ed. J.L. Davidson and D.L. Olson), 1-19, 1996, Melbourne, Australia, DSTO and WTIA.

11 . R.A. Oriani: *Corrosion - NACE*, 1987, **43** (7), 390-397.

12. H.H. Johnson: in 'Hydrogen Embrittlement and Stress Corrosion Cracking', (ed. R.Gibala and R.F. Hehemann), 3-27, 1984, Metals Park, Ohio, ASM.

13 . H.H. Johnson, J.G. Morlet, and A.R. Troiano: *Trans. TMS-AIME*, 1958, **212**, 526-536.

14. G.M. Pressouyre and I.M. Bernstein: *Metall. Trans.*, 1978, **9A**, 1571-1580.

15 A.R. Troiano: *Trans. ASM*, 1960, **52**, 151-177.

16. C.D. Beacham: *Metall. Trans.*, 1972, **3A**, 437-451.

17. D.P. Williams and H.G. Nelson: *Metall. Trans.*, 1970, **1**, 63-68.

18. H.G. Nelson and D.P. Williams: in 'Stress Corrosion Cracking and Embrittlement of Iron Base Alloys', (ed by R.W. Staehle), 390-404, 1977, Houston, NACE.

19. G.E. Kerns and R.W. Staehle: *Scripta Met.*, 1972, **6**, 631-634.

20. S.M. Wiederhorn: in 'Materials Science Research', Vol.3, (ed. W.W. Kriegel and H. Palmour, III), 503-528, 1966, New York, NY, Plenum Press.

21. R.A. Oriani and P.H. Josephic: *Acta Metall.*, 1977, **25**, 979-988.

22. H.P. Van Leeuwen: *Corrosion*, 1975, **31**, 42-50.

23. H.H. Johnson: in 'Stress Corrosion Cracking and Embrittlement of Iron Base Alloys', (ed. R.W. Staehle), 382-389, 1977, Houston, NACE.

24. P. Gangloff and R.P. Wei: *Metall. Trans.*, 1977, **8A**, 1043-1053.

25. R.N. Iyer and H.W. Pickering: *Annual Review of Materials Science*, 1990, **20**, 299-338.

26. D.G. Westlake: *Trans. TMS-AIME*, 1969, **221**, 1000-1006.

27. S. Gahr, M.L. Grossbeck, and H.K. Birnbaum: *Acta Metall.*, 1977, **25**, 125-133.

28. H.K. Birnbaum: in 'Hydrogen Embrittlement and Stress Corrosion Cracking', (ed. by R. Gibala and R.F. Hehemann), 29-41, 1984, Materials Park, ASM.
29. J.P. Hirth: in 'Hydrogen Embrittlement and Stress Corrosion Cracking'. (ed. R.Gibala and R.F. Hehemann), 29-41, 1984, Materials Park, Ohio, ASM.
30. J.P. Hirth and H.H. Johnson: *Corrosion*, 1976, **32**, 3-22.
31. C. Zapffe and C.Sims: *Trans. TMS-AIME*, 1941, **145**, 225-237.
32. A.S. Tetelman and W.D. Robertson: *Trans. TMS-AIME*, 1962, **224**, 178-184.
33. G.G. Hancock and H.H. Johnson: *Trans. Metall. Soc. AIME*, 1966, **235**, 13-516.
34. H.G. Nelson, in 'Treatise on Materials Science and Technology Vol.25 : Embrittlement of Engineering Alloys' (ed. C.L. Briant, S.K. Barneji), 275-359, 1983, New York, NY, Academic Press.
35. N.J. Petch: *Phi. Mag.*, 1956, **1**, 331-337.
36. J.R. Rice: in 'Volume on Effect of Hydrogen on Behavior of Materials', (ed. A.W. Thompson and I.M. Bernstein), 455-466, 1976, Warrendale,PA, TMS.
37. J.R. Rice and J.S.Wang: *Mat Sci. Eng.*, 1989, **A107**, 23-40.
38. P.M. Anderson, J.S. Wang and J.R. Rice: in'Innovations in Ultrahigh-Strength Steel Technology' (ed. G.B.`Olson, M. Azrin, and E.S. Wright), Sagamore Army Materials Research Conf. Proc. Vol. 34, Sept. 1987, Lake George, NY.
39. J.S. Wang and H. Vehoff: *Scripta Met.*, 1991, 25, 1339-1344.
40 J.R.Rice and J.S. Wang: *Mat. Sci. Eng.*, 1989, **107A**, 23-40.
41 J.S. Wang: in 'Hydrogen Effects in Materials' (ed A.W. Thompson and N.R. Moody), 61-74, 1996, Warrendale, PA, TMS.
42 J.P. Hirth and J.R. Rice: *Metall. Trans.*, 1980, **11A**, 1501-1511.
43 D. McLean: 'Grain Boundaries in Metals', 1957, Oxford, Oxford Univ. Press.
44. J.R. Rice and R. Thomson: *Phil. Mag.*, 1974, **29**, 73-97.
45. R.P. Frohmberg, W.J. Barnett, and A.R. Troiano: *Trans. ASM*, 1955, **47**, 892-925.
46. T. Matsumoto, J. Eastman, and H.K. Birnbaum: *Scripta. Metall.*, 1981, **15**, 1033-1037.
47. J. Eastman, F. Heubeaun, T. Matsumoto , and, H.K. Birnbaum: *Acta Metall.*, 1982, **30**, 1579-1586.
48. S.X. Xie and J.P. Hirth: *Mater. Sci. Eng.*, 1983, **60**, 207-212.
49 E. Lunarska: in 'Hydrogen Degradation of Ferrous Alloys' (ed. R.A. Oriani, J.P. Hirth, and M. Smialowski), 320-352, 1985, Park Ridge, NJ, Noyes Publication.
50. T. Tabata and H.K. Birmbaun: *Scripta Metall.*, 1984, **18**, 231-236.
51 J.P. Hirth: in 'Hydrogen Degradation of Ferrous Alloys', (ed. R.A. Oriani, J.P. Hirth, and M. Smialowski), 131-139, 1985, Park Ridge, NJ, Noyes Publication.
52 A. Seeger: *Phys. Stat. Solidi*, 1979, **55A**, 457-468.
53 V. Hivert, P. Groh, W. Frank, I. Ritchie, and P. Moser: *Phys. Stat. Sol.*, 1978, **46A**, 89-98.
54 J.P. Hirth, T. Ke, G. Schoeck, A. Seeger, and I.G. Ritchie: *Scripta Metall.*, 1982, **16**, 16.
55 H.K. Birnbaum and P. Sofronis: in 'Hydrogen Effects in Materials (ed. A.W. Thomson and N.R. Moody), 15-32, 1996, Warrendale PA, TMS.
56 Y.N. Jagodzinski, L.N. Larikov, and A.Y. Smouk, in 'Hydrogen Effects in Materials', (ed. A.W. Thomson and N.R. Moody), 375-384, 1996, Warrendale, PA, TMS.

57 G. Bond, I.M. Robertson, and H.K. Birnbaum, Acta Metall., 1987, 35, 2289.

58 A. Gourmelon: *Revue de Metallurgie*, 1975, **72**, 475-489.

59 H. Matsui, A. Kimura, and H. Kimura: in 'Strength of Metals and Alloys', (ed. P.Haasen, V. Gerold, and G. Kostorz), 977-982; 1979, Oxford, Pergamon Press.

60 E. Lunarska: *Scripta Metall.*, 1981, **15**, 1149-1152.

61 C.L. Formby: *Phil. Mag.*, 1966, **14**, 745-757.

62. H. Kimura, H. Matsui, A. Kimura, T. Kimura and K. Oguri: in 'Hydrogen Effect in Metals', (ed. I.M. Bernstein and A.W. Thompson), 191-208, 1981, Warrendale, PA, TMS.

63 . R. Wu, A.J. Freeman, and G.B. Olson: *J. Mater. Res.*, 1992, 7, 2403-2411.

64 . M.E. Eberhart, M.M. Donovan, J.M. MacLaren and D.P. Clougherty*: Prog. Surf. Sci.*,1991, **36** (1), 1-34.

65 . M.E. Eberhart, R.M. Latanision, and K.H. Johnson: *Acta Metall.*, 1985, **33**, 1769-1783.

66 . M.E. Eberhart and D.D. Vvedensky: *Scripta Metall.*, 1988, **22**, 1183-1188.

67. R. Thomson, in 'Hydrogen Degradation of Ferrous Alloys', (ed. R.A. Oriani, J.P. Hirth, M. Smialowski), 454-513, 1985, Park Ridge, NJ, Noyes Publications.

68. J. Vuik: Welding in the World, 1993, 31 (5), 23-32.

69 V.D. Tarlinski: *Automatic Welding*, 1974, **27** (6), 16-20.

70. Th. Bollinghaus, H. Hoffmeister, and A. Dangeleit: *Welding in the World*, 1995, 35 (2), 83-96.

71. H. Granjon: in Proc. Conf. Intl. Symposium on 'Cracking and Fracture in Welds', 1971, Japan Welding Society, IB, 1.1.

72. B. Graville: in Proc. Conf. 'The Metallurgy, Welding and Qualifications of Microalloyed (HSLA) Steel Weldments', (ed. J.T. Hickey, D.G. Howden, and M.D. Randall), Houston, TX, Nov. 1990, Microalloying Int. Inc. and AWS, 127-150.

73 W.W. Wang, R. Wong, S. Liu, and D.L. Olson: in ' Welding and Weld Automation in Shipbuilding', Oct 29- Nov. 2 1995, (ed. R.DeNale), 17-31, 1996, Warrendale, PA, TMS.

74. F. Matsuda, H. Nakagawa, K. Shinozaki, H. Morimoto, and Y. Sanematsu: *Trans. of JWRI*, 1983, **12** (2), 75-85.

75 . G.M. Pressouyre and F.M. Faure, in 'Hydrogen Embrittlement: Prevention and Control, ASTM STP 962, (ed. L. Raymond), 353-371, 1988, Philadelphia, PA, ASTM.

76. G.M Pressouyre and I.M. Bernstein: *Metall.Trans.*, 1981, **12A**, 835-844.

77. I.M. Bernstein and G.M. Pressouyre: in 'Hydrogen Degradation of Ferrous Alloys', (ed. R.A. Oriani, J.P. Hirth and M. Smialowski), 641-685, 1985, Park Ridge, NJ, Noyes Publication.

78. H.H. Johnson: *Met. Trans.*, 1988, **19B**, 691-707.

79. A. McNabb and P.K. Foster: *Trans. TMS-AIME*, 1963, **227**, 618-627.

80 . R.A. Oriani: in Proc. Conf. 'Fundamental Aspects of Stress Corrosion Cracking', Houston, TX, Sept. 1967, NACE, 32-50.

81. M. Iino: *Acta Metall.*, 1982, **30**, 367-375.

82 . C. Zener: in 'Imperfections in Nearly Perfect Crystals', (ed. W. Shockely et. al.), 289-314, 1952, New York, NY, Wiley.

83 T.R. Waite: *Phys. Rev.*, 1957, **107**, 463-470.

84 G.M. Pressouyre and I.M. Bernstein: *Acta. Metall.*, 1979, **27**, 89-100.
85. G.M. Pressouyre: *Acta. Metall.*, 1980, **28**, 895-911.
86. M.F. Stevens and I.M. Bernstein: *Metall. Trans.*, 1989, **20A**, 909-919.
87. J.P. Hirth: in 'Hydrogen Degradation of Ferrous Alloys' (ed. R.A. Oriani, J.P. Hirth and M. Smialowski), 131-139, 1985, Park Ridge, NJ, Noyes Publication.
88. P. Kedzierzawski: in 'Hydrogen Degradation of Ferrous Alloys', (ed. R.A. Oriani, J.P. Hirth and M. Smialowski), 271-288, 1985, Park Ridge, NJ, Noyes Publication.
89. R. Gibala and A.J. Kumnick: in 'Hydrogen Embrittlement and Stress Corrosion Cracking', 61-77, 1984, Metals Park, Ohio, ASM.
90 . R. Gibala: in 'Stress Corrosion Cracking and Hydrogen Embrittlement of Iron Base Alloys', NACE-5, (ed. R.W. Staehle, J. Hochmannn, R.D. McCright, and J.E. Slater), 244-268, 1977, Houston, TX, NACE.
91 . J.P. Hirth: *Metall. Trans.*, 1980, **11A**, 861-890.
92 . W.Y. Choo and J.Y. Lee: *Metall. Trans.*, 1982, **13A**, 135-140.
93 . A.J. Kumnick and H.H. Johnson: *Acta. Metall.*, 1980, **28**, 33-40.
94. K. Ono and M. Meshi: *Acta Metall.*, 1992, **40**, 1357-1364.
95 . T. Asaoka, C. Dagbert, M. Aucouturier, and J. Galland: *Scripta Metall.*, 1977, **11**, 467-472.
96 . E. Chornet and R.W. Coughlin: *J. Catal.*, 1972, **72**, 246-265.
97. D.O. Hayward and B.M.W. Trapnell: in 'Chemisorption', (ed. B.M.W. Trapnell), 203- , 1964, London, Butterworths.
98. K.Y. Lee, J.Y. Lee, and D.R. Kim: *Mater. Sci. Eng.*, 1984, **67**, 213-220.
99. H.H. Podgurski and R.A. Oriani: *Metall. Trans.*, 1972, **3**, 2055-2063.
100. J.L. Lee and J.Y. Lee: *Metal Sci.*, 1983, **17**, 426-432.
101. J.L. Lee and J.Y. Lee: *Metall. Trans.*, 1986, **17A**, 2183-2186.
102. P. Lacombe, M. Aucouturier, J.P. Laurent, and G. La Passet: in 'Stress Corrosion Cracking and Hydrogen Embrittlement of Iron Base Alloys', NACE-5, (ed. R.W. Staehle, J. Hochmannn, R.D. McCright, and J.E. Slater), 423-430, 1977, Houston, TX, NACE.
103. H.G. Lee and J.Y. Lee: *Acta Metall.*, 1984, **32**, 131-136.
104. G.M.Pressouyre: *Metall. Trans. A*, 1979, **10A**, 1571-1573
105. T. Asaoka, G. Lapasset, M. Aucouturier, and P. Lacombe: *Corrosion*, 1979, **34**, 39-47.
106. M.Weistein and J.F. Elliot: *Trans. TMS - AIME*, 1963, **227**, 382-
107. A.I. Shirley and C.K. Hall: *Scripta Metall.*, 1983, **17**, 1003-1008.
108. W. Schwarz and H. Zitter: *Arch. Eisenhuttenw*, 1965, **36**, 343-349
109. F.E. Fujita: in 'Hydrogen Degradation of Ferrous Alloys', (ed. by R.A. Oriani, J.P. Hirth and M. Smialowski), 1-15, 1985, Park Ridge, NJ, Noyes Publication.
110. C.H.P. Lupis and J.F. Elliot: *Acta Metall.*, 1967, **15**, 265-276.
111. G.K. Sigworth and J.F. Elliot: *Met. Sci. J*, 1974, **8**, 1974, 298-310.
112. H. Mabuchi and H. Nakao: *Trans. ISIJ*, 1983, **23**, 504-512.
113. W.A. Oates and T.B. Flanagan: *Prog. Solid St. Chem*, 1981, **13**, 193-283.
114 Y. Itsumi and D.E. Ellis: *J. Mater. Res.*, 11(9),1996, pp. 2206-2213.
115 Y. Itsumi and D.E. Ellis: *J. Mater. Res*, 11(9), 1996, pp. 2214-2219.
116. M.P. Puls: in 'Hydrogen Degradation of Ferrous Alloys' (ed. R.A. Oriani, J.P. Hirth and M. Smialowski), 114-130, 1985, Park Ridge, NJ, Noyes Publication.

117. N.F. Fiore and C.L. Bauer: *Prog. Mater. Sci.*, 1967, **13**, 87-134.
118. J.P. Hirth and B. Carnahan: *Acta Metall.*, 1978, **26**, 1795-1803.
119. W.G. Wolfer and M.I. Baskes: *Acta Metall.*, 1985, **33**, 2005-2011.
120 J. Gegner, G. Horz, and R. Kirchheim: in 'Hydrogen Effects in Materials', (ed. A.W. Thompson and N.R. Moody), 35-45, 1996, Warrendale PA, TMS.
121. R. Valentini, A. Solina, S. Matera, and P. De Gregorio: Metall. Trans., 1996, **27A**, 3773-3780.
122. I. Takahashi, Y. Matsumoto and T. Tanada: in Proc. Conf. 'JIMIS-2', Minakami, Japan, 1979, 285-289.
123. S.M. Lee and J.Y. Lee: *Acta Metall.*, 1987, **35**, 2695-2700.
124. D.R. Gaskell: in 'Physical Metallurgy', 4th edn, (ed. by R.W Cahn and P. Haasen), 413-469, 1996, Amsterdam, North-Holland.
125. X.Y. Huang, W. Mader and R. Kircheim: *Acta Metall.*, 1991, **39**, 893-907.
126. G. Pfeifer and H. Wipf: *J. Phys. F :Metal Phys.*, 1976, **6**, 167-179.
127. R.B. McLellan: *Acta Metall.*, 1979, **27**, 1655-1663.
128. E. Fromm and E. Gebhart: 'Gase und Kohlenstoff in Metallen', 1976, Berlin, Springer Verlag.
129. R. Kircheim: *Progress in Materials Science*, 1988, **32**, 261-325.
130. M.I. Luppo and J.Ovejero-Garcia: *Corrosion Science*, 1991, 32, 1125-1136.
131. N. Yurioka and H. Suzuki: *Intl. Materials Review*, 1990, **35** (4), 217-249.
132 P.M. Hart: *Welding Journal*, 1986, **65**, 14-22s.
133. L. Reeve: *Trans. Inst. Weld.*, 1938, **1**, 7-34.
134. J. Dearden and H. O' Neill: *Trans. Inst. Weld.*, 1940, **3**, 203 - 214.
135. K. Lorenz and C. Duren: *IIW Doc. IX-B-11-82*, 1982, Amer. Council, AWS, Miami, Florida.
136. N. Yurioka: *IIW Doc. II-A-914-94*, 1994, Amer. Council, AWS, Miami, Florida.
137. A.W. Thompson and I.M. Bernstein: *Adv. Corros. Sci. Technol.*, 1979, **7**, 53-175.
138. T. Fujita and Y. Yamaa: in 'Stress Corrosion Cracking and Hydrogen Embrittlement of Iron Base Alloys', (ed.R.W. Staehle, J. Hochman, R.D. McCright, and J.E. Slater), 736-746, 1976, New York, NY, TMS-AIME.
139. G.E. Kerns, M.T. Wang, and R.W. Staehle: in 'Stress Corrosion Cracking and Hydrogen Embrittlement of Iron Base Alloys', (ed. R.W. Staehle, J. Hochman, R.D. McCright, and J.E. Slater), 700-733, 1976, New York, NY, TMS-AIME.
140. D.I. Phalen and D.A. Vaughan: *Corrosion*, 1968, **24** (8), 243-251.
141. E. Schiapparelli, S. Prado, J.J. Tiebas and J. Garibaldi: *J. Mater. Sci.*, 1992, **27**, 2053-2060.
142. N. Yurioka , H. Suzuki, and S. Oshita: *Welding Journal*, 1983, **62**, 147s-153s.
143. A.D. Wilson and W.G. Taylor: in Proc. Conf. 'Offshore Technol.', OTC 5071, Houston, TX, 1985, 459-468.
144. T. Hirokawa, H. H. Okumura, Y. Kawada, and H. Tamehiro: *Seitetsu Kenkyu*, 1988, **328**, 459-468.
145 K. Easterling: 'Introduction to the Physical Metallurgy of Welding', 2nd edn, 1992, Oxford, Butterworth-Heinemann.
146 M.C. Flemings:'Solidification Processing', 1974, New York, NY, McGraw Hill.
147 H.D. Brody and M.A. Flemings: *Trans. TMS-AIME*, 1966, **236**, 615-624.
148 T.W. Clyne and W. Kurz: *Metall. Trans.*, 1981, 12A, 965-971.

149. R.H. Frost, D.L. Olson, and S. Liu: in Proc. Conf. 'International Trends in Welding Science and Technology', Gatlinburg, TN, June 1992, ASM Int., 205-209.
150 S.Liu and D.L. Olson: in Proc. 3rd Int. Conf. on Trends of Welding Research, 1992, ASM, Materials Park
151. J.M. Dowling, J.M. Corbett, and H.W. Kerr: Metall. Trans., 1986, 17A, 1611-1623.
152. P.L. Harrison and R.A. Farrar: 'J. Mater. Sci.',1981, 16, 2218-2226.
153 C.W. Ramsay, D.K. Matlock, and D.L. Olson: in 'Recent Trends in Weld. Sci and Tech. TWR'89', 1990, 763-767, ASM Int., Materials Park, OH.
154. S. Liu and D.L. Olson: Welding Journal, 1986, 65, 134s-149s.
155. R.H. Frost, D.L. Olson, and S.Liu:'Influence of Solidification on Inclusion Formation in Welds', Proc 3rd Intern. Conf. on Trends of Welding Research, 1992, ASM, Materials Park,
156. K.Y. Lee, J.Y. Lee, and D.R. Kim, *Mat. Sci. Eng.*, Vol. 67, 1984, pp. 213-220.
157. J.L. Lee and J.Y. Lee, *Met. Trans.*, 1986, **17A**, 2183-2186.
158. F. Matsuda, H. Nakagawa, K. Shinozaki, H. Kitana et.al.: *Trans. JWRI*, 1977, **6** (2), 59-73.
159. F. Matsuda, H. Nakagawa, K. Shinozaki, and T. Matsumoto: *Trans. JWRI*, 1985, **14** (2), 135-142.
160. K. Shinozaki, X. Wang and T.H. North: *Met. Trans.*, 1990, **21A**, 1287-1298.
161. E. Schiapparelli, S. Prado, J.J. Tiebas and J. Garibaldi: *J. Mat. Sci.*, 1992, **27**, 2053-2060.
162. E. Pickering: *JISI*, 1958, **189**, 148-159.
163. S. Rudnik: *JISI*, 1966, **204**, 374-376.
164. T.V. Venkatasubramanian and T.J. Baker: *Metal Science*, 1982, **16**, 543-554.
165. D.J. Abson and R.J. Pargeter: *Int. Mater. Rev.*, 1986, **31**, 141-194.
166. P.H.M. Hart: in Proc. Int. Conf. 'Trends in Steels and Consumables for Welding', London, Nov. 1978, TWI, Abington Publication, 21-53.
167. P.H.M. Hart: IIW Doc. IX-1308-84, 1984, American Council, AWS, Miami, FL.
168. C.L.M. Cottrell: *Met. Constr.*, 1984, **16** (12), 740-744.
169. K. Yamamoto, S. Matsuda, T. Haze, and R. Chijiwa: in Proc. Symp. 'Residual and Unspecified Elements in Steel', Miami, FL, Nov. 1987, ASTM.
170. M. Nakanishi, Y. Komizo, and I. Seta: *J. Jpn, Weld. Soc.*, 1974, **43** (7), 117-124.
171. Y. Hirai, S. Minakawa, and J. Tsuboi: 'Effects of Sulphur on Hydrogen- Assisted Cracking in Al Killed Steel Plates', IIW Doc. IX-1160-80, 1980, Miami,FL, American Council, AWS.
172. Y. Kikuta, T. Araki, and A. Hirose, *Trans. Japan Welding Society*, 1988, **19** (1), 60-65.
173. S.M. Lee and J.Y. Lee, Acta Metall., 1987, **35**, 2695-2700.
174. M.F. Stevens and I.M. Bernstein, *Metall. Trans*, 1989, **20A**, 909-919.
175. J. Shimomura, Y. Nakano, S. Nakano, and S. Ueda, *ISIJ Int.*, Vol. 31(4), 1991, pp. 379-386.
176. G.L. Spencer and D.J. Duquette: PhD. Thesis 'The Role of Vanadium Carbide Traps in Reducing the Susceptibility to Hydrogen Embrittlement of High Strength Alloy Steels', May 1997, RPI, Troy, NY.
177. H.Y. Yu and J.C.M. Li: *J. Nucl. Met.*, 1976, **20**, 872.
178. M. Iino: *Metall. Trans.*, 1978, **9A**, 1581-1590.

179. J.C.M. Li: *Metall. Trans.*, 1978, **9A**, 1353-1380.
180. G.M. Pressouyre: in 'Hydrogen Degradation of Ferrous Alloys', (ed. R.A. Oriani, J.P. Hirth, and M. Smialowski), 27-38, 1985, Park Ridge, NJ, Noyes Publication.
181. M. Iino, N. Nomura, H. Takesawa, ansd T. Takeda: in 'Current Solutions to Hydrogen Problems in Steels', (ed. C.G. Interrante and G.M. Pressouyre), 159-167, 1982, Metals Park, Ohio, ASM.
182. G.M Pressouyre: in 'Current Solutions to Hydrogen Problems in Steels', (ed. C.G. Interrante and G.M. Pressouyre), 18-34, 1982, Metals Park, Ohio, ASM.
183. E. Snape: *Corrosion*, 1970, **24**, 396-397.
184. S.K. Barneji, C.J.Mc. Mahon, and H.C. Feng: *Metall. Trans.*, 1978, **9A**, 237-247.
185. G. Sandoz: *Metall. Trans.*, 1972, **3**, 1055-1063.
186. C.J. McMahon, Jr., J. Kameda, and N. Bandyopadhayay: in 2nd Japanese Institute of Metals Symposium 'Hydrogen in Metals', Tokyo, Nov. 1979.
187. G. Sandoz: *Metall. Trans.*, 1972, **3**, 1169-1176.
188. A.H. Cottrell: *Materials Science and Technology*, 1990, **6**, 121-123.
189 S.P. Lynch: *Acta Metall.*, 1988, **36**, 2639-2661.
190. R.O. Ritchie, J.F. Nott and J. Rice: *J. Mech. Phys. Solids*, 1973, **21**, 395-410.
191. R.A. Oriani and D.H. Josephic: *Acta Metall.*, 1974, **22**, 1065-1074.
192. H.P. Van Leeuwen: *Corrosion*, 1976, **32**, 34-37.
193. W.W. Geberich and A.G. Wright: in 'Environmental Degradation of Engineering Materials in Hydrogen', (ed. M.R. Louthan, R.P. McNitt, and R.D. Sisson), 183-205, 1981, Blacksburg, VA, VPI.
194. J.Y. Lee , U.I. Chung and D.S Ahn: *Mater. Sci. Eng.*, 1987, **95**, 273-280.
195. D.W. Kweon and J.Y. Lee: *J. Mater. Sci.*, 1989, **24**, 1629-1633.
196. S.I. Pyun and C Lim: *Corrosion Science*, 1993, **35** (1-4), 531-539.
197. M. Guttman: *Surface Science*, 1975, **53**, 213-.
198. C.J. McMahon, Jr and L. Marchut: *J. Vac. Sci. Tech.*, 1978, **15** (2), 450-466.
199. R.P.M. Proctor and H.W. Paxton: *Trans. ASM*, 1969, **62**, 989-.
200. B.B. Rath and I.M. Bernstein: *Metall. Trans.*, 1971, **2**, 2845-2851.
201. M.R. Louthan, J.A. Donovan, D.E. Rawl, Jr.: *Corrosion*, 1973, **29**, 108-111.
202. J. Chene: in 'Current Solutions to Hydrogen Problems in Steels', (ed. C.G. Interrante and G.M. Pressouyre), 263-271, 1982, Metals Park, Ohio, ASM.
203. R.P.M. Proctor and H.W. Paxton: *Trans. ASM*, 1962, **1**, 989.
204. C.S. Carter: *Corrosion*, 1969, **25** (10), 423-431.
205. J.F. Lessar and W.W. Gerberich: *Metall. Trans.*, 1976, **7A**, 953-960.
206. D.A. Ryder, T. Grundy, and T.J. Davies: in 'Current Solutions to Hydrogen Problems in Steels', (ed. C.G. Interrante and G.M. Pressouyre), 272-274, 1982, Metals Park, Ohio, ASM.
207. N. Yurioka, M. Okumura, T Kasuya, and H.J.U. Cotton: *Met. Constr.*, 1987, **19** (4), 217R-223R.
208. B.A. Graville: in Proc. Conf. 'Welding of HSLA Structural Steels', Rome, Italy, Nov. 1976, ASM and Associazione di Metallurgia, 85-101.
209. G.T. Brown and B.A James: *Met. Technol.*, 1980, 7 (7), 261-268.
210. C.E. Sims and H.M. Banta: *Welding. Journal*, 1949, **28**, 182-192s.
211. S. Hasebe: 'Effect of Aluminum on Weldability of Structural Steel', IIW Doc. IX-689-70, 1970.

212. W.P. Campbell: *Welding Journal*, 1975, **54**, 154s-161s.
213 E. Lunarska: in 'Hydrogen Degradation of Ferrous Alloys', (ed. R.A. Oriani, J.P. Hirth, and M. Smialowski), 712-736, 1985, Park Ridge, NJ, Noyes Publications.
214 J.A. Lee: in 'Hydrogen Effects in Materials', (ed. A.W. Thompson and N.R. Moody), 569-580, 1996, Warrendale, PA, TMS.
215. T.Watanabe: *Trans. Japan Welding Society*, 1988, **19** (1), 34-39.
216. T.J. Baker: *JISI*, 1972, **211** (11), 783.
217. J.B. Lumsden, B.E. Wilde, and P.J. Stocker: *Scripta Metall.*, 1983, **17**, 971-974.
218. B.E. Wilde, I. Chattoraj, and T.A. Mozhi: *Scripta Metall.*, 1987, **21**, 1369-1373.
219. M.K. Miller, S.S. Brenner, and M.G. Burke: *Metall. Trans.*, 1987, **18A**, 519-523.
220. T.D. Le and B.E. Wilde: in 'Current Solutions to Hydrogen Problems in Steels', (ed. C.G. Interrante and G.M. Pressouyre), 423-427, 1982, Metals Park, OH, ASM.
221. M. Zamazadeh, A. Allam, and H.W. Pickering: *J. Electrochem. Soc.*, 1980, **127**, 1688 - 1693.
222. R.B. McLellan: in 'Phase Stability in Metals and Alloys', (ed. P.S. Rudman, J. Stringer, and R.I. Jaffee), 1-43, 1969, New York, McGraw-Hill.
223. E. Fromm and G. Horz: *Int. Metals. Review*, 1980, **25**, 269-311
224. W.A. Oates and T.B. Flanagan: *Prog. Solid St. Chem.*, 1981, **13**, 193-283.
225. Y. Fukai: *J. of the Less-Common Metals*, 1991, **172-174**, 8-19.
226. Y. Fukai: 'The Metal-Hydrogen System', 1993, Berlin, Springer-Verlag.
227. M.A. Quintana: *Key Engineering Materials*, 1992, **69-70**, 113-128.
228 T.H. North, I.D. Sommerville, H. Li, and C.D'Souza: in 'The Metal Science of Joining', (ed. M.J. Cieslak, J.H. Peperezko, S. Kang, and M.E. Glicksman), 157-164, 1992, Warrendale, PA, TMS.
229. W.F. Savage, E.F. Nippes and E.I. Husa: 'Hydrogen Assisted Cracking in HY-130 Weldments', Final report to the Office of Naval Research, Contract No. 00014-75-C-0944 NR 031-780, Jan 1981, RPI, Troy,OH.
230. L.I. Sorokin and Z.A. Sidlin:'The Effect of Alloying Elements and of Marble in an Electrode Coating on the Susceptibility of a Deposited Nickel Chrome Metal to Pore Formation', Svar. Proiz, 1974, 11, 7-9.
231. A.M. Pope, S. Liu, and D.L. Olson: in Proc. 13th Int. Conf. "Offshore Mechanics and Arctic Eng.' (ed. M.M. Salama, M. Toyoda, S. Liu, J.F. Dos Santos, M. Kocak, E.A. Patterson, and S Berge), 1994, 361-368, Book No. H00898, ASME
232. A.M. Pope, J.C.G. Teixeira, V.R. ds Santos, M.T.P. Paes, and S. Liu: J. Offshore Mechanics and Artic Eng., 1996 118, 165-168.
233. G.R. Salter: *British Welding Journal*, 1963, **10**, 316-.
234. D.G. Howden and D.R. Milner: *British Welding Journal*, 1963, **10**, 1963, 53-.
235. S.A. Gedeon and T.W. Eagar: *Welding Journal*, 1990, **69**, 265s - 271s.
236. T. Terasaki, T. Akiyama, T. Hamashima and K. Kishikawa: *Trans. Japan Welding Society*, 1986, **17** (1), 93-101.
237. A. Block-Bolten and T.W. Eagar: *Metall. Trans.*, 1984, **15B**, 461-469.
238 S. Liu and D.L. Olson: in 'Trends in Welding Research', (ed. S. Davis), 347-352, 1996, Materials Park, OH, ASM.
239 T. Rosenqvist: 'Principles of Extractive Metallurgy', 2nd edn., 1983, New York, NY, McGraw-Hill.
240. Li and T. North: *Key Engineering Materials*, 1992, **69-70**, 95-112.

241. Y.Hirai, S. Minakawa and K. Shinozaki: *IIW Doc. IX-1160-80*, 1980, American Council, AWS, Miami, FL.
242. N. Seriu, S. Kanazawa, H. Gondo, K. Yamato, and T. Otsubo: 'The Prevention of Weld Cracking by Addition of Special Elements', 61th AWS Annual Meeting, April 1980, paper 3D, published Abstracts, AWS, Miami, Florida.
243. Z. Du. et. al: *China Welding*, 1996, **5** (2), 125-131.
244. M.A. Quintana and N.D. Fichtelberg: in 'Recent Trends in Welding Science & Tech.', (ed. S.A. David and J.M Vitek), 437-441, 1989, Metals Park, OH, ASM.
245 D. White, G. Pollard, and R. Gee: *Welding and Metal Fab.*, 1992, **60**, 209-216.
246 D. White, G. Pollard, and R. Gee, IIW Doc. II-A-867-92, 1992, Amer. Council, AWS, Miami, Florida.
247 I.K. Pokhodnya and A.M. Suptel: *Automatic Welding*, 1967, **20**, 1967, 14-20.
248. B. Chew and R.A. Wilgoss: *Proc. Int. Conf. 'Weld Pool Chemistry and Metallurgy'*, London, England, 1980, TWI and Abington Publishing, 155-165.
249. S. Ibara, D.L. Olson, and C.E. Grubbs:'Underwater Wet Welding of Higher Strength Steels', Offshore Tech. Conf., paper # 5889, pp. 67-75, Houston TX (1989)
250 S. Ibara and D.L. Olson:'Underwater Welding of Steel', in 'Ferrous Alloy Weldments' (ed. D.L. Olson and T.H. North), 1992, 350-354, Trans. Tech. Publ., Zurich, Switzerland.
251. N.R. Quick and H.H. Johnson: *Acta Metall.*, 1978, **26**, 903-907.
252. K.Kiuchi and R.B.McLellan: *Acta Metall.*, 1983, **31**, 961-984.
253. W.J. Arnoult and R.B. McLellan: *Acta Metall.*, 1973, **21**, 1397-1403.
254. R.G. da Silva, S.W. Stafford, and R.B. McLellan: *J. Less-Common Metals*, 1976, **49**, 407-420.
255. R.B. McLellan: *Acta Metall.*, 1979, **27**, 1655-1663.
256. R. Kircheim: *Acta Metall.*, 1982, **30**, 1069 - 1078.
257. D.N. Beshers: *Acta Metall.*, 1958, **6**, 521-523.
258. G. Caneli, R. Cantelli, F. Cordero: *Phys. Rev.*, 1985, **32B**, 3573-3579.
259. A.M. Stoneham: *Rev. Mod. Phys.*, 1969, **41**, 82-108.
260. R.A. Oriani: *Acta Metall*, 1970, **18**, 147-157.
261. J.B. Leblond and D. Dubois: *Acta Metall.*, 1983, **31**, 1459-1469.
262 T. Sakai, K. Asami, M. Katsumata, H. Takada, and O. Tanaka: in 'Current Solutions to Hydrogen Problems in Steels', 340-348, 1982, Metals Park, OH, ASM.
263 J.C. Devaux, D. Dubois, and J.B. Leblond: in 'Current Solutions to Hydrogen Problems in Steels', 45-52, 1982, Metals Park, OH, ASM.
264. M. Hashimoto and R.M. Latanision: *Metall. Trans.*, 1988, **19A**, 1988, 2789-2798.
265. Y. Ueda and H. Murakawa: *Trans. JWRI*, 1987, **16** (1), 51-57.
266. N. Yurioka and H. Nakamura: *J. Japan Welding Society*, 1979, **46** (9), 726-730.
267. H.G. Nelson and J.E. Stein: *NASA Report*, TND-7265, NASA Ames Research Center, Moffett Field, CA, 1973.
268. F.R Coe: *Weld. World*, 1976, **14** (1-2), 1-10.
269. J. Volk and G. Alefeld: in 'Topics in Applied Physics Vol. 28: Hydrogen in Metals I',, (ed. G Alefeld and J. Volk), 321-348, 1978, Berlin. Springer-Verlag.
270. T. Bollinghaus, H. Hoffmeister, and C. Middel: 'IIW Document IX-1812-95', 1995, Amer. Council, AWS, Miami, Florida..

271. M. Koiwa: *Acta Metall.*, 1974, **22**, 1259-1268.
272 B. Chew: *Metal Science Journal*, 1971, **5**, 195-200.
273. J. Crank: 'Mathematics of Diffusion', 2nd edn., 1975, Oxford U., England, Clarendon Press.
274. H.L. Frisch: *J. Phys. Chem.*, 1957, **61**, 93-.
275. G.R. Caskey,Jr. and W.L. Pilinger: *Met. Trans.*, 1975, **6A**, 1975, 467-476.
276. M. Iino: *Acta Metall.*, 1982, **30**, 377-383.
277. R.C. Frank, C.W. Wert, and H.K. Birnbaum: *Metall. Trans.*, 1979, **10A**, 1979, 1627-1630.
278. R.W. Lin and H.H. Johnson: *Acta Metall.*, 1982, **30**, 1819-1828.
279. N.R. Quick and H.H. Johnson: *Acta Metall.*, 1978, **26**, 903-907.
280. M.M. Makhlouf and R.D. Sisson,Jr.: *Metall. Trans.*, , 1991, **22A**, 1001-1006.
281. V.B. Kleshnya and N.G. Krapivnyi: *Soviet Mater. Sci.e*, 1993, **26** (5), 410-413.
282. M. Iino: *Metall. Trans.*, 1985, **16A**, 1985, 401-410.
283. J.A. Donovan: *Metall. Trans.*, 1976, **7A**, 1976, 1677-
284. J.A. Donovan, *Metall. Trans.*, 1976, **7A**, 1976, 145-149.
285. M.R. Louthan, Jr., G.R. Caskey, Jr., J.A. Donovan, and D.E. Rawl, Jr.: *Mat. Sci. and Eng.*, 1972, **10**, 357-368.
286. M. Kurkela and R.M. Latanision: *Scripta Metall.*, 1979, **13**, 927-932.
287. J.K. Tien, S.V. Nair and R.R., Jensen: in 'Hydrogen Effects in Metals', (ed. I.M Bernstein and A.W. Thompson), 37-56, 1981, Pittsburgh, PA, TMS-AIME.
288. S.V. Nair, R.R. Jensen, and J.K. Tien: *Metall. Trans.*, 1983, **14A**, 385-393.
289. J.K. Tien, A.W. Thompson, I.M. Bernstein and R.J. Richards: *Metall. Trans.*, 1976, **7A**, 821-829.
290. H.H. Johnson and J.P. Hirth: *Metall. Trans.*, 1976, **7A**, 1543-1548.
291. J.K. Tien: in 'Effect of Hydrogen on Behavior of Materials', (ed. A.W. Thompson and I.M. Bernstein), 309-326, 1976, NY, TMS-AIME.
292. M. Hashimoto and R.M. Latanision: *Metall. Trans.*, 1988, **19A**, 2789-2798.
293. E. Lunarska and A. Zielinski: in 'Hydrogen Degradation of Ferrous Alloys', (ed. R.A. Oriani, J.P. Hirth, and M. Smialowski), 289-320, 1985, Park Ridge, NJ, Noyes Publication.
294. P. Kedzierzawski, in 'Hydrogen Degradation of Ferrous Alloys', (ed. R.A. Oriani, J.P. Hirth, and M. Smialowski), 251-270, 1985, Park Ridge, NJ, Noyes Publication.
295. H. Kronmuller: in 'Topics in Applied Physics Vol. 28: Hydrogen in Metals I',, (ed. G. Alefeld and J. Volk), 289-320, 1978, Berlin. Springer-Verlag.
296 R. Gibala: *Trans. TMS-AIME*, 1967, 239, 1574.
297 C.A. Wert, in 'Topics in Applied Physics Vol. 29: Hydrogen in Metals II', (ed. G. Alefeld and J. Volk), 305-330, 1978, Berlin. Springer-Verlag.
298. R. Lin and H.H. Johnson: *Acta Metall.*, 1982, **30**, 1819-1828.
299. I.M. Bernstein and A.W. Thompson, in 'Advanced Techniques for Characterizing Hydrogen in Metals', (ed. N.F. Fiore and B.J. Berkowitz), 89-104, 1981, Kentucky, TMS-AIME.
300. R. Kircheim and R.B. McLellan: *J. Electrochem. Soc : Solid State Sci. and Tech.*, 1980, **127** (11), 2419-2425.
301. M.A. Devanathan and Z.O.J. Stachursky: *Proc. Roy. Soc.*, 1962, **A270**, 90-102.

302. R.W. Lin and H.H. Johnson: in 'Advanced Techniques for Characterizing Hydrogen in Metals', (ed. N.F. Fiore and B.J. Berkowitz), 105-118, 1981, Kentucky, TMS-AIME.
303. P.L. Chang and W.D.G. Bennett: *JISI*, 1952, 205-213.
304. E.W. Johnson and M.L. Hill: *Trans. TMS- AIME*, 1960, **218**, 1104-1112.
305. C. Wert and C. Zener, *Phys. Rev.*, 1949, **76**, 1169-1175.
306. M. Surkein and R. Heidersbach: in 'Advanced Techniques for Characterizing Hydrogen in Metals', (ed. N.F. Fiore and B.J. Berkowitz), 119-132, 1981, Kentucky, TMS-AIME.
307. H. Zuchner: *Z. Naturforsch*, 1970, **25A**, 1490-.
308. R. Kircheim et.al.: *Scripta Metall*, 1977, **11**, 651.
309. B.G. Pound, G.A. Wright and R.M. Sharp: *Acta Metall.*, 1987, **35** (1), 263-270.
310. W.M. Robertson: in 'Environmental Degradation of Engineering Materials in Hydrogen', (ed. M.R. Louthan, Jr., R.P. McNitt, R.D. Sisson, Jr.), 69-81, 1981, Blackburg, VA, VPI.
311. J.O'M Bockris and P.K. Subramanyan: *J. Electrochem. Soc.*, 1971, **118** (7), 1114-1119.
312. A. Turnbull, M.W. Carrol and D.H. Ferriss: *Acta Metall.*, 1989, **37** (7), 1989, 2039-2046.
313. S.Trube and V. Pavlik: 'Hydrogen Effusion under Isothermal and Non-isothermal Conditions from Mild Steel Welds' *IIW Document II-A-964-95*, Amer. Council, AWS, Miami, Florida
314 E. Abramov and D. Eliezer: in 'Hydrogen Effects in Materials', (ed. A.W. Thompson and N.R. Moody), 293-299, Warrendale, PA, TMS.
315. P.K. Foster, A. McNabb, and C.M. Payne: *Trans. TMS-AIME*, 1965, **233**, 1022-1031.
316. A.P. Paltsevich: 'The Method for the Analysis of Diffusible Hydrogen and Influence of Welding Conditions on its Content in Weld Metal', IIW-Doc. II-A-749-88, 1988, Amer. Council, AWS, Miami, Florida.
317. V.A. Pavlik: in 'Mathematical Modelling of Weld Phenomena', 2nd edn., (ed.H. Cerjak), 187-203, 1995, The Institute of Materials.
318. J.Y. Lee and J.L. Lee: *Phil. Mag.*, 1987, **56A** (3), 293-309.
319. J.L. Lee and J.Y. Lee: *Metall. Trans.* 1989, **20A**, 1989, 1793-1802.
320. C.P. Flynn: *Phys. Rev.*, 1964, **113A**, A587-A595.
321. C.P. Flynn, J. Bass and D. Lazarus: *Phil. Mag.*, 1965, **11**, 521-538.
322. ANSI/AWS A4.3-93: 'Standard Methods for Determination of Diffusible Hydrogen Content of Martensitic, Bainitic, and Ferritic Weld Metal Produced by Arc Welding', 1993, Miami, Florida, AWS.
323 IIW Doc No. II-1055-91, 1995, Paris, IIW, Amer. Council, AWS, Miami, Florida.
324. N. Jenkins and F.R. Coe: 'Hydrogen Analysis at BWRA Part 3', 1996, BWRA Bulletin.
325. K. Kpokhodnya and A.P. Paltsevich: *Automatic Welding*, 1980, **1**, 37-39.
326. M.A. Quintana and J.R. Dannecker: in 'Hydrogen Embrittlement : Prevention and Control', ASTM STP 962, (ed. L. Raymond), 247-268, Philadelphia, PA, ASTM.

327. L.C. de Abreu, P.J. Modenesi, and P.V. Marques: 'A Comparative Study of Techniques to Measure Diffusible Hydrogen Content of Welds', *IIW Doc No. II-A-908-94*, Amer. Council, AWS, Miami, Florida.
328. JIS Z3118-1986: 'Method of Measurement for Hydrogen Evolved from Steel Welds', 1986, Tokyo, Japanese Standards Association.
329. N. Jenkins, P.H.M. Hart and D.H. Parker: Welding Journal, 1997, **76**, 1s-10s.
330. S.K. Albert, C. Remash, N. Murugesan, T.P.S. Gill, G. Periaswami, and S. Kulkarni: *Welding Journal*, 1997, **76**, 251s-263s.
331. K.K. Baek, S.I. Pyun, and J.S. Kim: *Metall. Trans.*, 1988, **19A**, 1721-1726.
332. D. White, R. Gee, and R. Tongue, IIW Doc. IIA-877-93, 1993, Amer. Council, AWS, Miami, Florida.
333. O. Odegard, G.M. Evans, and N. Christensen: *Met. Constr. Br. Weld. J.*, 1971, **3** (2), 47-49.
334. N. Christensen: *Welding Journal*, 1961, **40**, 145s-154s.
335. G.L. Petrov and A. Million: *Weld. Prod.*, 1964, **11** (10), 1-8.
336. H. Shimoda, H. Ishizuka, and R. Chiba: *J. Jpn. Weld. Soc.*, 1966, **35** (12), 1966, 1195-1203.
337. R. Hopia: *IIW Doc. IX-608-68*, 1968, Amer. Council, AWS, Miami, Florida.
338. S. Toy and A. Philips: *Corrosion*, 1974, **26** (7), 16-20.
339. T.E. Perex and J.O Garun: *Scr. Metall.*, 1982, **16** (2), 161-164.
340. O.I. Sleptsov, V.E. Mikhailov, and O.V. Smijan: *IIW-Doc. IX-B-179-89*, 1989, Amer. Council, AWS, Miami, Florida.
341. N. Christensen, I. Gjermundsen, and R. Rose: *Brit. Weld. J.*, 1958, **37**, 272-281.
342. I.K. Pokhodnya: in 'Hydrogen Management in Steel Weldments', (eds. J.L. Davidson and D.L. Olson), 145-181, 1996, Melbourne, Australia, DSTO and WTIA.
343. C.A. Lensing, I. Maroef, and D.L. Olson: 'Hydrogen Trapping in Ferrous Weld Metal', 78th AWS Annual Meeting, April 1997, Los Angelos, paper 24A, published Abstract, AWS, Miami, Florida.
344. T. Terasaki, R. Karppi, and K. Satoh: *Trans. Japan Welding Society*, 1979, **10** (1), 53-57.
345. T. Terasaki, T. Akiyama, S. Hamashima, and K. Kishikawa: *Trans. Japan Welding Society*, 1986, **17** (1), 93-101.
346. T. Terasaki, G.T. Hall, and R.J. Pargeter: *Trans. Japan Welding Society*, 1991, **22** (1), 52-56.
347. N. Stenbacka: *Scandinavian Journal of Metallurgy*, 1983, **12**, 112-116.
348. G. Dickehut and J. Ruge: *Welding and Cutting*, 1988, **6**, 39-42.
349. H. Shimomura, T. Shinoda, K. Hoshino, and R. Yamashita: *Trans. Japan Welding Society*, 1990, **21** (2), 44-50.
350. Y. Kikuta: in 'Hydrogen Effects in Metals', (ed. I.M. bernstein and A.W. Thompson), 755-765, 1981, Pittsburgh, PA, TMS-AIME.
351. N. Yurioka and K. Kohira: 'A Numerical Analysis of the Diffusion and Trapping of Hydrogen in Steel Welds', IIW Doc. IX-951-76, 1976, Amer. Council, AWS, Miami, Florida.

352. N. Yurioka and S. Oshita: 'An Analysis of Effect of Microstructure, Strain and Stress on the Hydrogen Accumulation in HAZ', IIW Doc. IX-1161-80, 1980, Amer. Council, AWS, Miami, Florida.
353. R.A.J. Karppi, J. Ruusila, M. Toyoda, K. Satoh and K. Vartiainen: *Scan. J. Metall.*, 1984, **13**, 1984, 66-74.
354. I. Grivnyak, in 'Scientific Problems in Welding and Special Electrometallurgy Part 3', 38-48, 1970, Kiev, Naukova Dumka.
355. D.L. Olson, I. Maroef, and C. Lensing: in 'Proc. Indian National Welding Seminar 97', 9-24, Banglore, India, Dec. 1997, Indian Institute of Welding.
356. B.A.B. Andersson: *J. Eng. Mater. and Tech.*, 1980, **102**, 64-72.
357 J.P. Thomas and C.E. Chopin, in 'Hydrogen Effects in Materials', (ed. A.W. Thompson and N.R. Moody), 233-242, 1996, Warrendale, PA, TMS.

Appendix II

Published Manuscript

in

Proc. of the Joint Seminar on Hydrogen Management in Steel Weldments, October 1996, Melbourne, Australia

"Hydrogen Management in High Strength Steel Weldments"

Hydrogen Management in High Strength Steel Weldments

D.L. Olson, I. Maroef, C. Lensing, R.D. Smith, W.W. Wang,
S. Liu, T. Wildeman and M. Eberhart

Center for Welding, Joining and Coating Research
Colorado School of Mines
Golden, Colorado 80401-1887
USA

1. INTRODUCTION

Common practice to reduce cold cracking in high strength steel welding is the pre- or post-weld heat treatment. Heat treatment is performed to control the cooling rate and to ensure sufficient removal of hydrogen from the weld metal. Recent scientific approaches supported by FEM calculation have made it possible to determine the heat treatment that provides an appropriate combination of microstructure (hardness), stress intensity factor and diffusible hydrogen content that does not allow susceptibility to hydrogen cracking (1). More often an acceptable selection of welding parameters to avoid hydrogen cracking is achieved by a costly testing program. However, such methodologies that require tight monitoring and control of the temperature as well as welding parameters are frequently found to be impractical and complicated. Therefore, new approaches to hydrogen management in steel welding, based on more fundamental metallurgical understanding and predictions, are being investigated. The CSM approach is to develop consumables based on three independent proposed practices to hydrogen management. They are described here as three steps.

2. STEP 1: PROPER SELECTION OF WELD METAL MARTENSITE START TEMPERATURE.

The hydrogen content in a weldment is dependent on both the hydrogen source and the ability of the weldment to transport hydrogen from the weld metal to the heat affected zone. The transport aspect becomes important because of the higher hydrogen solubility but lower hydrogen diffusion rate in austenite (FCC crystal structure), in contrast to ferrite and martensite that have orders of magnitude higher hydrogen diffusion coefficients than austenite (2). As a result of the different hydrogen diffusivitiy in austenite compared to martensite/ferrite and the different thermal experience, a non-uniform distribution of hydrogen may result across the weldment according to the austenite decomposition behavior of the alloys (3,4). Evidence of this resulting localized hydrogen distribution can be seen in the laser induced breakdown spectroscopy data (5) for hydrogen spectral emission scans across a weldment as shown in Figure 1. The effect of hydrogen damage is magnified when the location of the susceptible microstructures (martensite) overlaps the localized, high hydrogen content.

Proper alloying elements and their contents in the consumable are being determined to insure maximum hydrogen transport away from the weldment (weld metal and HAZ) during the welding thermal cycle. The martensite start temperature is used as an indicator for effective transport of hydrogen. A large difference between the M_s (weld metal) and M_s (base metal) will indicate difficulties in hydrogen transport in the weldment and the tendency for high localization in hydrogen contents. Thus the martensite start temperature is a measure of the microstructure evolution and the ability to have a phase (ferrite/martensite) available for rapid hydrogen transport (3,4).

Granjon (3) introduced a conceptual model that describes how the austenite-ferrite (or austenite-martensite) phase transformation in steel weldments affects the resulting hydrogen distribution. Two cases are illustrated in Figure 2. When the austenite-martensite

transformation in the fusion zone (weld metal) occurs at a higher temperature than the heat affected zone diffusible hydrogen will segregate in the heat affected zone just under the fusion line. This HAZ region is often the location of underbead cracking in high strength steel weldments. On the other hand, when the martensite transformation in the heat affected zone occurs at a higher temperature than in the fusion zone, it is possible that excess hydrogen may accumulate in the weld metal. This situation could promote weld metal hydrogen cracking or micro-fissuring.

CASE 1: WELD METAL WITH LOWER M_S TEMPERATURE THAN THE HAZ.

This case can be described as a situation where the weld metal is overmatched with respect to the base metal with higher alloying content. The weld metal exhibits a higher strength than the base metal and its martensite start temperature is depressed to below that of the base metal. While the austenite in the HAZ has begun transforming, the austenite in the weld metal remains unchanged. After a period of time, the HAZ immediately adjacent to the fusion zone will transport hydrogen at a higher rate than that in the weld metal. If the HAZ martensite start temperature (M_s) is sufficiently high, the hydrogen will be able to transport a significant distance into the parent metal. Especially if the transformation occurs at a moderately elevated temperature, the situation described can potentially reduce the localized hydrogen content in the hard microstructure adjacent to the fusion line, thus reducing the hydrogen cracking susceptibility. However, the hydrogen transport cannot proceed extensively until the weld metal transforms because austenite has the ability of storing high hydrogen contents but can not move it fast enough to the fusion line. If the weld metal M_s temperature is too low, then the hydrogen transport from the weld metal is limited. Very little hydrogen can reach the heat affected zone adjacent to the fusion line that may eventually lead to weld metal cracking.

To demonstrate the effect of martensite start temperature on hydrogen transport, the diffusion process was modeled considering incremental time periods and temperature which decreases according to the welding heat input and cooling rate. The martensite start was allowed to occur in the HAZ and weld metal, but at different times. Simple but reasonable boundary conditions were established for the solution of Fick's 2nd law. Several hydrogen profiles were determined (6) and the dotted traced line in Figure 3 illustrates the diffusible hydrogen distribution. This profile is the case where the HAZ M_s temperature is greater than the weld metal M_s temperature, and for a location indicated in Figure 3. This situation is prone to hydrogen cracking in the weld deposit which also has been observed for some high strength weldments.

CASE 2: HAZ WITH LOWER M_S TEMPERATURE THAN THE WELD METAL.

This case can be described as a situation where the weld metal is undermatched with respect to the base metal. Since the heat affected zone transforms from austenite to ferrite at lower temperatures and at a later time than the weld metal, the HAZ becomes an austenite diffusion barrier for hydrogen transport. A high hydrogen accumulation in the heat affected zone adjacent to the fusion line results. This situation promotes underbead

hydrogen cracking. Figure 3 also plots the hydrogen profile (solid line) obtained in calculations following the procedure outlined in Case 1. Instead of having a high hydrogen concentration in the weld metal, hydrogen peaks are observed in the heat affected zone as shown in Figure 1. This profile supports the hydrogen distribution model as proposed and suggest that the hydrogen cracking being limited to a few grains (austenite) adjacent to the fusion line. Thus, a HAZ with lower M_s temperature may result in underbead hydrogen cracking and localized weld metal cracking along the fusion line.

To evaluate the ability of using the martensite start temperature as a hydrogen cracking index, the diffusible hydrogen content was plotted as a function of the calculated weld metal martensite start temperature for welds made on the same base metal (7). Figure 4 illustrates a demarcation line between the cracked and the uncracked weldments.

From the application of the M_s temperature, it is possible to obtain a ΔM_s expression, and the sign and magnitude of this ΔM_s expression will better describe the hydrogen diffusion behavior:

$$\Delta M_s = M_{s(WM)} - M_{s(BM)}$$

If $\Delta M_s < 0$, hydrogen accumulation will be in the weld metal. If $\Delta M_s > 0$, hydrogen accumulation in the HAZ is possible and underbead cracking may occur.

Some preliminary hydrogen cracking data is plotted with ΔM_s as a function of M_s HAZ in Figure 5. This data indicates some ability to establish a demarcation line between cracking and non-cracking. Further work is necessary to evaluate the correlation between cracking and ΔM_s.

Selection of the alloy additions has to be determined to achieve only a slightly higher martensite start temperature of the weld metal than that of the HAZ, for maximum hydrogen transport to the base metal. In addition, the absolute martensite start temperatures of the weld metal and the HAZ should be high enough to facilitate rapid hydrogen transport in the martensite phase.

3. STEP 2: HYDROGEN ABSORPTION CONTROL BY THERMO-CHEMICAL REACTIONS IN ARC PLASMA

Selected oxides or fluorides are being used as the consumable flux ingredient to minimize hydrogen absorption to the weld pool during arc melting. Hydrogen absorption can be minimized through the formation of water vapor or hydrogen fluoride in a thermo-chemical reaction with oxygen or fluorine gas in the welding plasma. Please notice on attached figures (Fig.6 and Fig. 7) that increasing either oxygen or fluorine will decrease the amount of hydrogen available to enter the weld deposit. These gases shall be generated from the selected fluxes that easily decompose during arc heating. The detrimental effects of excessive amounts of oxygen to the weldment toughness and those effects of fluorine to the working

environment will be considered in the determination of the types and amounts of the flux additions.

Increasing the weld pool oxygen content has been found to reduce the resulting weld metal hydrogen content by perturbing the water reaction (8). A thermodynamic analysis that sequentially follows the oxide (inclusions) formation from solidification to room temperature was performed. This methodology allows for the prediction of total weld metal hydrogen content and has been found to correlate reasonably well with experimental data. The major drawback of using oxygen to control weld metal hydrogen is the resulting oxygen pick up, primarily as inclusions. In excessive amounts, these oxides can alter the mechanical properties detrimentally. This concern requires new research into other weld pool reactions that can also significantly alter the weld metal hydrogen content.

The use of fluorine at small concentration levels to alter the HF reaction, associated with the weld pool and thus reduced the weld metal hydrogen content, is being investigated. Preliminary thermochemical calculations were made and the results illustrated that the use of fluorine holds reasonable promise. Figure 8 illustrates some of the preliminary results where fluorides in the welding flux are used to control hydrogen pick-up during welding of steel with a primer coating (9). It is also known that Teflon® additions have been made by some SMA electrode manufacturers to assist in hydrogen management.

4. STEP 3: DIFFUSIBLE HYDROGEN CONTROL BY HYDROGEN TRAPS

Final suppression of diffusible hydrogen will be achieved by introduction of selected rare earth metal and transition metal additions to the weld metal to serve as hydrogen traps. These traps, in the form of oxides or carbo-nitrides have high binding energies with hydrogen. They are capable of immobilizing hydrogen at temperature ranges much higher than 100 °C, before the risk of cold cracking emerges. With proper trap morphology, number and distribution, it is possible to have a large portion of hydrogen being trapped uniformly throughout the weld metal and leave the remaining diffusible hydrogen in a much smaller content. In this way, transport to and accumulation of hydrogen at potential cracking initiation sites will be kept below the critical value for cold cracking initiation.

In steel, hydrogen is not homogeneously distributed as it would be in a perfect iron crystal. Hydrogen will be found not only in the host lattice, but also segregated to atomic and microstructural imperfections such as vacancies, solute atoms, dislocations, grain boundaries, voids, and second phase particles. In these localized regions, the mean residence time of hydrogen atoms is considerably longer than in normal interstitial lattice sites. In the extreme case, these regions are sinks into which hydrogen atoms fall and remain even during loading. Therefore, the generic term for this behavior is hydrogen trapping.

A prominent effect of trapping is to decrease the apparent hydrogen diffusivity (10). The ability of a trap site to hold hydrogen atoms is associated with the hydrogen-trap binding energy. Consequently, a trapped hydrogen atom must acquire an energy substantially greater than the lattice migration energy to escape the trap and contribute to the measured diffusivity.

Numerous studies on different traps have been reviewed by several authors (11-14). From various reported data, values of hydrogen-trap binding energies in iron were identified and are listed in Table 1. In addition, an electronic structure calculation was also applied in searching for other forms of potential traps that can be introduced in steel welding (15). Several inclusions in steel were investigated and, among them, Ce_2O_3 oxide was found to have the highest binding energy followed by TiC, Y_2O_3, VC, NbC and finally Mo_2C, in the order of decreasing energy. The binding energy of 60 kJ/mol H for a dislocation or a grain boundary is generally regarded as the typical limiting value of a reversible trap. With this energy level, a reversible trap becomes effective in capturing hydrogen around 400 °K but does not reach saturation at room temperature, as shown in Figure 9. A graphical description of this hydrogen distribution was calculated for selected hydrogen traps and is presented in terms of the saturation temperature in Figure 10. The saturation temperature was approximated for 0.9 fraction of trap occupation and was predicted to increase with increasing binding energy. A reversible trap whose binding energy is lower than 60 kJ/mol will not be able to prevent hydrogen cracking. The trapped hydrogen will be picked up by moving dislocations and eventually be delivered to crack initiation sites (16). The preferred traps are then those having binding energies higher than 60 kJ/mol and are termed irreversible traps (17).

A preliminary numerical study of hydrogen trapping during the welding cooling cycle has been conducted as a basis for criteria of trap selection. This study involved the prediction of diffusible hydrogen content, which changes with time due to both the hydrogen removal out of the weld metal and the hydrogen capture by trap sites in the weld metal. A diffusion model of hydrogen in steel containing trap sites, similar to the McNabb and Foster model (18), has been applied. The calculation was done numerically to take account the variation of both the hydrogen diffusion coefficient and the hydrogen capturing rate by trap sites with temperature and the associated microstructure of the diffusing medium. An example of the calculated result is shown in Figure 11a, where the diffusible hydrogen content (HD) of the weld metal containing traps is predicted to be lower than that of the steel without traps.Also shown in Figure 11a is the trapped hydrogen (HT) whose amount increases with time.

An abrupt change of slope can be observed in the diffusible hydrogen content right at the martensite start temperature of the weld metal. Phase transformation from austenite to martensite is accompanied by a large increase in the hydrogen diffusion coefficient which in turn accelerates both the hydrogen capture and the hydrogen removal out of the weld metal. The kinetics of hydrogen capturing can be more clearly explained in Figure 11b which shows the equilibrium trap occupancy (neq), the actual trap occupancy (n) and the rate of hydrogen capture (dn/dt). The hydrogen capture rate depends both on hydrogen diffusivity and the driving force for hydrogen entrapment (neq-n). It can be seen that a sudden increase in the rate of capture always follows the occurrence of martensite phase formation where both capture determining factors are maximized.

The criteria for the use of traps to reduce the susceptibility of HAC should include a proper combination of several factors. These factors are the hydrogen-trap binding energy, the trap density, the martensite start temperature and the cooling rate ($\Delta t_{8/5}$). In this preliminary

investigation, each of the above mentioned variables was varied independently and the resulting amount of diffusible hydrogen at 100 °C as well as at 300 °C are summarized in Figures 12 to 15. The temperature 100 °C has been considered as the temperature where the potential for HAC starts to become a problem.

The first important parameter of a trap is the hydrogen-trap binding energy. In this calculation, four values of binding energies that correspond to different trap sites were used. They are 60 kJ/mol for dislocations, 80 kJ/mol for Al_2O_3 inclusions, 100 kJ/mol for TiC particles, and 120 kJ/mol for rare earth additions. As shown in Figure 12, the amount of diffusible hydrogen content decreases with increasing hydrogen-trap binding energy. The major advantage of traps with high binding energy is that they provide a high driving force for hydrogen capture within high temperature regions. The data at 300 °C shows a better insight to how much faster the hydrogen is captured by high binding energy traps as opposed to those with low binding energy. Should the HAC start to occur at a higher temperature than 100 °C (which may be possible for weld metal with low martensite start temperature) the weld metal containing high binding energy traps may have a better chance to survive.

The diffusivity of hydrogen in the austenite phase is very low, so that the hydrogen cannot be effectively captured or removed out of the weld metal until the martensite temperature is reached. The lower the martensite start temperature is, the longer time hydrogen has to remain in the weld metal lattice sites. It also means that the available temperature range for effective hydrogen diffusivity and trapping in the ferrite phase becomes narrower and the suppression of diffusible hydrogen content by certain traps becomes less effective. The extreme situation is depicted in Figure 13 for the case of weld metal possessing martensite start temperature of 400 °C. The advantage of using a trap with higher binding energy, i.e., higher capture rate, is then obvious in this very narrow temperature range situation. However, the employment of high binding energy traps for a high martensite start temperature weld metal can lead to a situation where the trapping capacity will be wasted at high temperature regions. This behavior can occur even when the hydrogen diffusivity provides a high potential for easy hydrogen removal out of the weld metal. Therefore, the selection of hydrogen traps must consider other factors than just the weld metal or consumable alloying contents.

Conventional hydrogen management usually applies proper heat treatment or sufficiently low cooling rate to provide easy hydrogen removal out of the weld and to form a less susceptible microstructure to HAC. In case of weld metal containing trap sites, a certain rate of cooling is also necessary to allow for enough hydrogen capture time before the temperature reaches 100 °C. In the present calculation, the cooling rate is assumed to occur naturally and relatively fast, so that sufficient hydrogen removal by lattice diffusion alone can not be obtained. The effect of cooling rate, shown in Figure 14, appears to be similar to that of the martensite start temperature. A very fast cooling rate, such as those with $\Delta t_{8/5}$ equal to one second, does not permit enough time for hydrogen to leave the weld metal or jump into the trap sites. On the other hand, in a slightly slower cooling rate, the presence of traps may yield a low diffusible hydrogen content at 100°C and alleviate the tendency for weld metal HAC. This prediction shows the potential usage of traps to substitute for the tight heat-treatment procedure necessary for high strength steel welding.

The number of trap sites translates into the capacity to hold hydrogen atoms. A higher number of trap sites in the weld metal will produce a lower diffusible hydrogen content, which is in agreement with the calculated result shown in Figure 15. There is also an apparent threshold number of trap sites for optimum hydrogen trapping that can be observed in Figure 15. The number of traps used in the present calculation corresponds to a 100 to 500 ppm range of substitutional atom traps in the weld metal. In the case of inclusion traps, which is the most probable form of traps in weld metal, the trap sites on the surface are of the inclusion - matrix interface. Depending on the cooling rate, the number of trap sites used in this calculation may correspond to a relatively high inclusion volume fraction that yields weld metal with intrinsically low toughness. Obviously, the number of trap sites that can be used is limited to an extent in which the toughness is still maintained at an acceptable level. This issue suggests that the success of using hydrogen traps should not be related to significant diffusible hydrogen suppression in the weld metal. Its main function should be to promote a proper distribution of hydrogen in weld metal so that a high local accumulation of hydrogen at crack initiation sites can be prevented. Furthermore, in high strength steel welding, where hydrogen is highly accumulated at crack initiation sites, the presence of trap sites may give a higher tolerance for diffusible hydrogen content. Normally, a low maximum acceptable level of hydrogen content in the weldment is usually required for conventional welding procedures.

5. PROSPECTIVES

Use of these three steps for hydrogen management will reduce susceptibility to hydrogen cracking in welds. With further quantification and correlations, analytical procedures can be developed for designing welding consumables and practices for high strength steel that require a very low diffusible hydrogen content.

6. ACKNOWLEDGMENT

The authors acknowledge and appreciate the research support of the US Army Research Office.

7. REFERENCES :

1 . R.A.J. Karppi, J. Ruusila, M. Toyoda, K. Satoh, and K. Vartiainen, Scandinavian Journal of Metallurgy, Vol. 13, (1984), pp. 66-74.
2. Th. Bollinghaus, H. Hoffmeister, and A. Dangeleit, "A scatter Band for Hydrogen Diffusion Coefficients in Microalloyed and Low Carbon Structural Steels". (IIW Document IX-1767-94, 1994).
3. H. Granjon, "Cold Cracking in Welding of Steels", Intl. Symposium on Cracking and Fracture in Welds, Conf. Proc. Japan Welding Society, (1971), IB, 1.1.
4. B. Gravile, "Hydrogen Cracking Sensitivity of HSLA Steels", The Metallurgy, Welding and Qualification of Microalloyed (HSLA) Steel Weldments, (1990), 127
5. R.D. Smith, Private Communication, Colorado School of Mines, (1996).
6. W. Wang, S. Liu and D.L. Olson, "Consequences of Weld Undermatching and Overmatching: Non-Uniform Hydrogen Distribution", in Intl. Conf. on Offshore Mechanics and Artic Engineering - Materials Enginnering', ASME, Vol. III, , Florence, Italy, (1996), pp. 403-409
7. D.L. Olson, S. Liu, W. Wang, R. Pieters, and S. Ibarra, "Martensite Start Temperature as a Weldability Index", in Conf. Proc. on 'Research Trends in Welding Science and Technology', pp. 615-620, Gatlinburg, Tennessee, (1995), ASM Intl., 1996.
8. S. Liu, D.L. Olson & S. Ibara, "Electrode Formulation to Reduce Weld Metal Hydrogen and Porosity", Intl. Conf. on Offshore Mechanics and Arctic Engineering, ASME-OMAE, (1994), pp. 291-298
9. K. Johnson, Private Communication, Colorado School of Mines, (1996).
10. H.H. Johnson, Metall. Trans., Vol. 19B, (1988), pp. 691-707.
11. J.P. Hirth, Metall. Trans., Vol.11A, (1980), pp. 861-890.
12. I.M. Bernstein and G.M. Pressouyre, in Hydrogen Degradation of Ferrous Alloys, ed. by R.A. Oriani, J.P. Hirth and M. Smialowski, Noyes Pub., (1985), pp 641-685.
13. P. Kedzierzawski, in Hydrogen Degradation of Ferrous Alloys, ed. by R.A. Oriani, J.P. Hirth and M. Smialowski, Noyes Pub., (1985), pp. 271 - 288.
14. R. Gibala and A.J. Kumnick, in Hydrogen Embrittlement and Stress Corrosion Cracking, ed. by R. Gibala and R.F. Hehemann, ASM, Metals Park, Ohio, (1984), pp. 61 - 77.
15. M. Eberhart, Private communication, Colorado Schoool of Mines, (1995).
16. J.K. Tien, A.W. Thompson, I.M. Bernstein, and R.J. Richards, Metall. Trans., Vol.7A, (1976), pp. 821-829.
17. G.M. Pressouyre and I.M. Bernstein, Metall. Trans., Vol. 12A, 1981, pp. 835-844.
18. A. McNabb and P.K. Foster, Trans. of the Metall. Soc. of AIME, Vol. 227, (1963), pp. 618-627.
19. W.Y. Choo and J.Y. Lee, Metall. Trans., Vol. 13A, (1982), p. 135.
20. A.J. Kummick and H.H. Johnson, Acta Metall., Vol. 28, (1980), pp. 33-40.
21. K. Ono and M. Meshi, Acta Metall., Vol. 40 (6), (1992), pp. 1357-1364
22. T. Asaoka, C. Dagbert, M. Aucouturier, and J. Galland, Scripta Metall., Vol.11, (1977), pp. 467-472.
23. E. Chornet and R.W. Coughlin, J. Catal., Vol.72, (1972), pp. 246-265.

24. D.O. Hayward and B.M.W. Trapnell, in Chemisorption, Butterworths, London, (1964), p.203.
25. J.R. Scully, J.A. Van den Avyle, M.J. Cieslak, A.D. Romig,Jr., and C.R. Hills, Metall. Trans., Vol.22A, (1991), pp. 2429-2445.
26. K.Y. Lee, J.Y. Lee and D.R. Kim, Mater. Sci. Eng., Vol. 67, (1984), p. 213
27. H.H. Podgurski and R.A. Oriani, Metall. Trans., Vol.3, (1972), pp. 2055-2063.
28. J.L. Lee and J.Y. Lee, Metal Sci., Vol. 17, (1983), p. 462.
29. J.L. Lee and J.Y. Lee, Metall. Trans., Vol. 35A, (1987), pp. 2695-2700
30. P. Lacombe, M. Aucouturier, J.P. Laurent, and G. La Passet, in Stress Corrosion Cracking and Hydrogen Embrittlement of Iron Base Alloys, ed. by R.W. Staehle, J. Hochmannn, R.D. McCright, and J.E. Slater, NACE-5, NACE, Houston, TX, (1977), pp. 423-430.
31. H.G. Lee and J.Y. Lee, Acta Metall., Vol.32, (1984), p. 131
32. G.M. Pressouyre and I.M. Bernstein, Metall. Trans., Vol. 9A, (1978), pp. 1571-1580.
33. G.M.Pressouyre, Metall. Trans., Vol. 10A, (1979), pp.1571-1573

Table 1. Hydrogen trapping in Iron. Reference state : H in perfect lattice

Trap Site	Binding Energy (kJ/mol)	Matrix	Assessment Method	Ref.
H-dislocation	26	Iron	thermal analysis	19
H-dislocation core (mixed)	59	Iron	permeation	20
H-grain boundary	18 - 20	C-Mn Steel	thermal analysis	19
H-grain boundary	60	Iron	thermal analysis	21
H-grain boundary	59	Iron	permeation	20,22
H-Free surface	70	Iron	permeation	23
H-Free surface	95	Iron	permeation	24
β-NiAl	27	Steel *	permeation	25
H-PdAl interface	34	Steel *	permeation	24
H-Fe-oxide interface	47	C-Mn Steel	thermal analysis	26
H-AlN interface	65	Iron	permeation	27
H-MnS interface	72	C-Mn Steel	thermal analysis	28
H-Al_2O_3 interface	79	C-Mn Steel	thermal analysis	29
H-Fe_3C interface	84	C-Mn Steel	permeation	22,30
H-TiC interface	87	Iron	thermal analysis	31
H-TiC interface	95	C-Mn Steel	permeation	32
H-Nd	129	Iron	calculated	33

* Matrix element is precipitation hardened martensitic stainless steel.

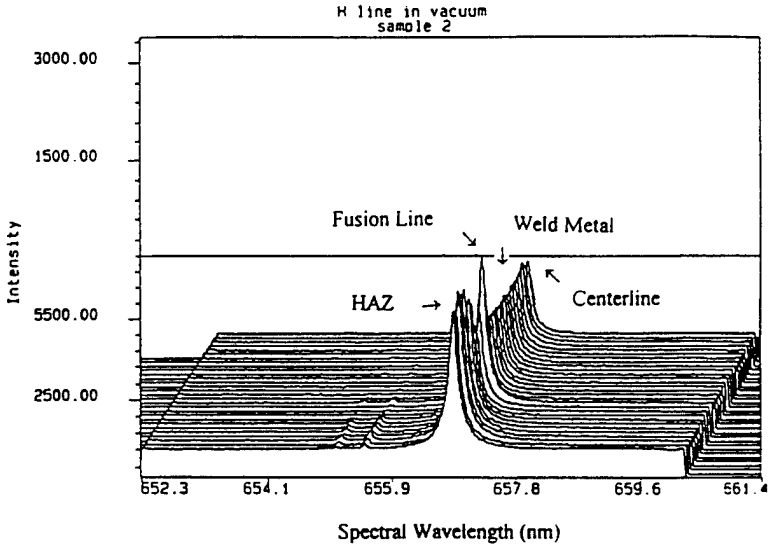

Figure 1. Non-uniform distribution of hydrogen across the center line of a weldment. Intensities of the hydrogen spectral emission are proportional to the hydrogen concentration.

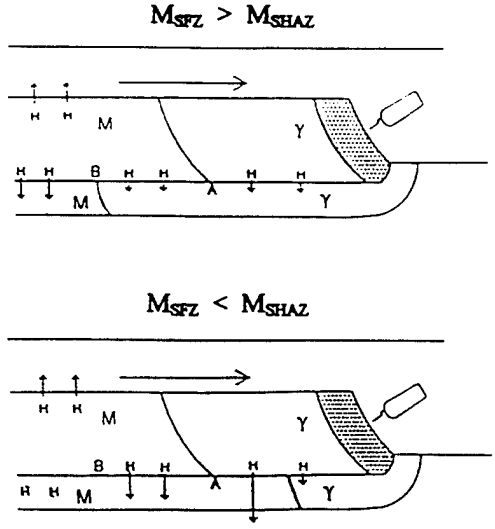

Figure 2. Illustration of hydrogen diffusion at different martensite start temperature for weldment and base metal (3)

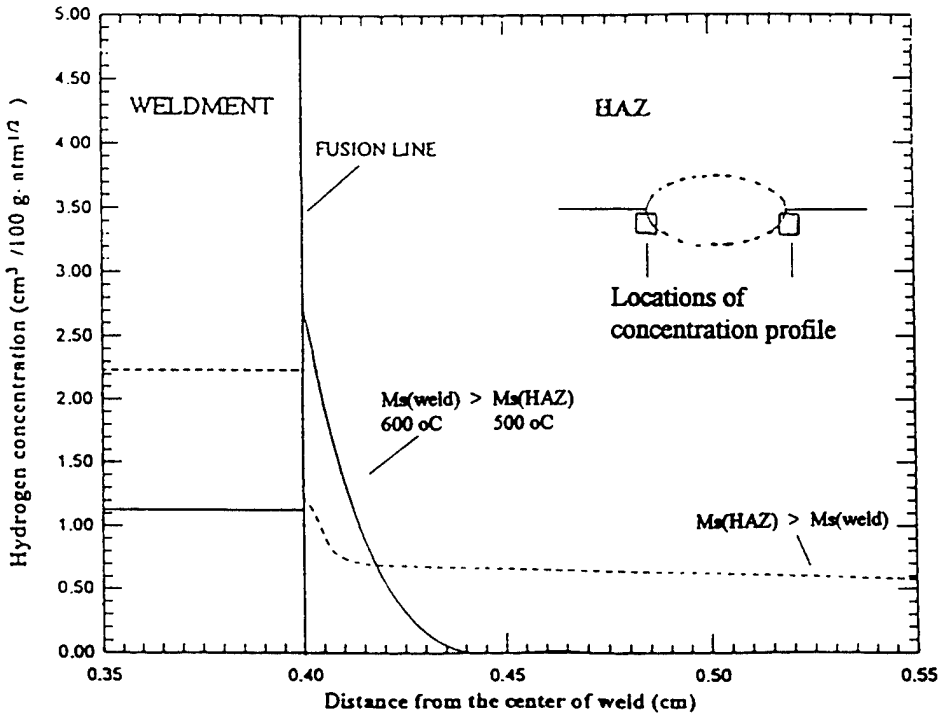

Figure 3. Hydrogen distribution across the fusion line of a steel weldment for $M_{s\ weld} > M_{s\ HAZ}$ and $M_{s\ weld} < M_{s\ HAZ}$.

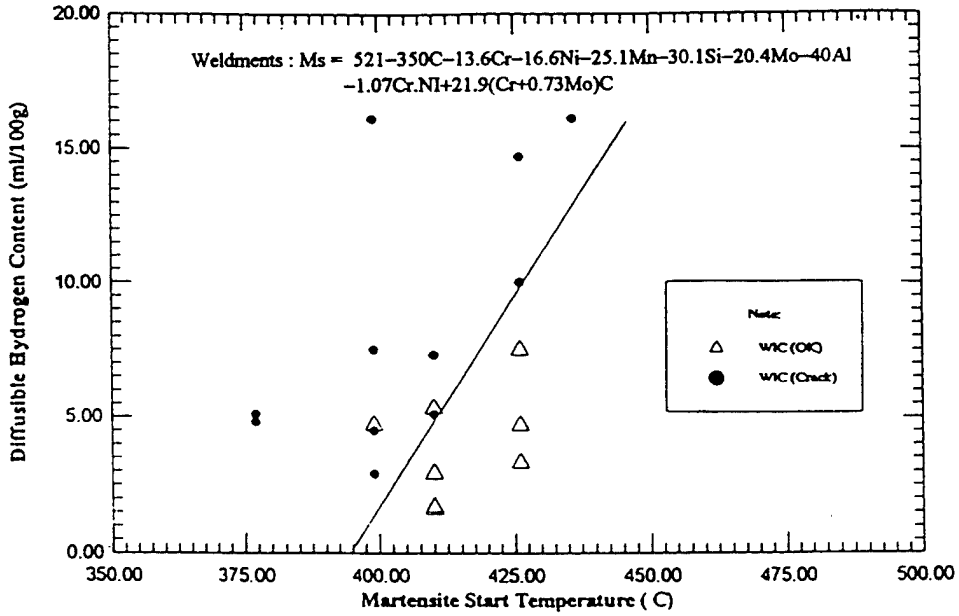

Figure 4. Conceptual illustration of cracking prediction.

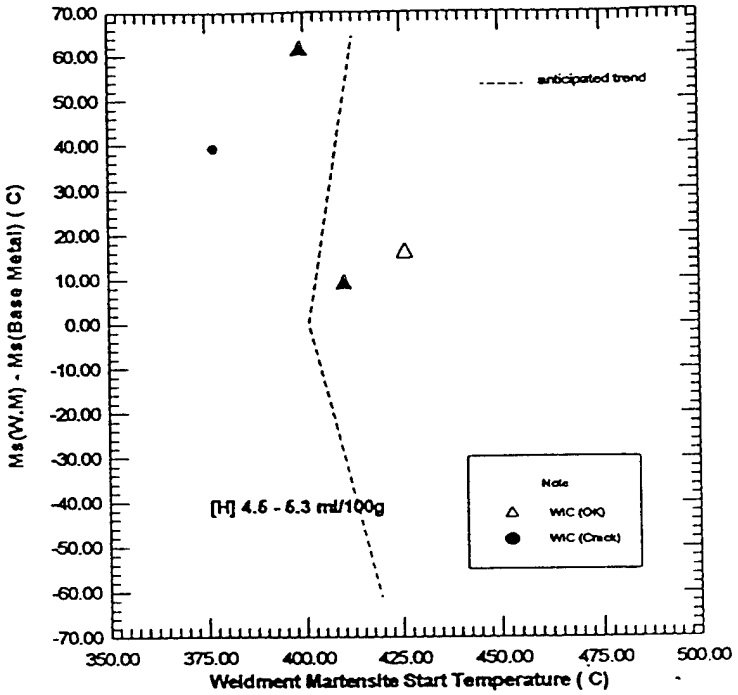

Figure 5. Illustration of hydrogen cracking/uncracking zones by hydrogen content and martensite start temperature.

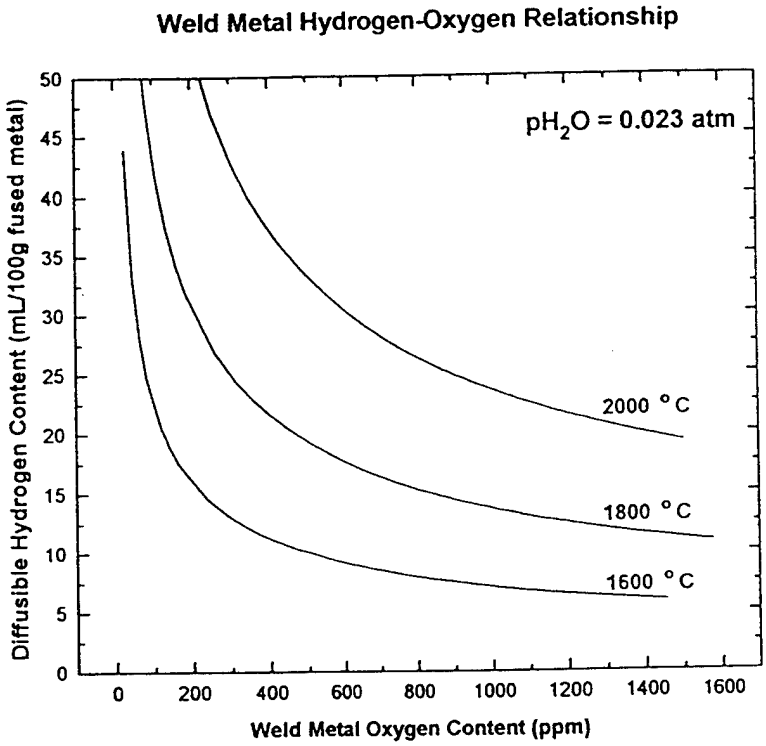

Figure 6. Thermo-chemical reaction between oxygen and hydrogen in the welding plasma.

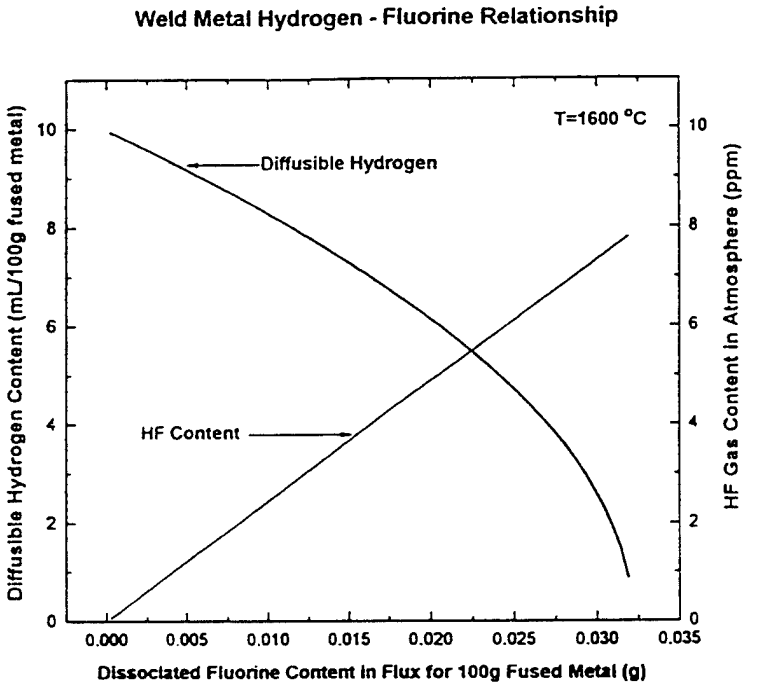

Figure 7. Thermo-chemical reaction between fluorine and hydrogen in the welding plasma.

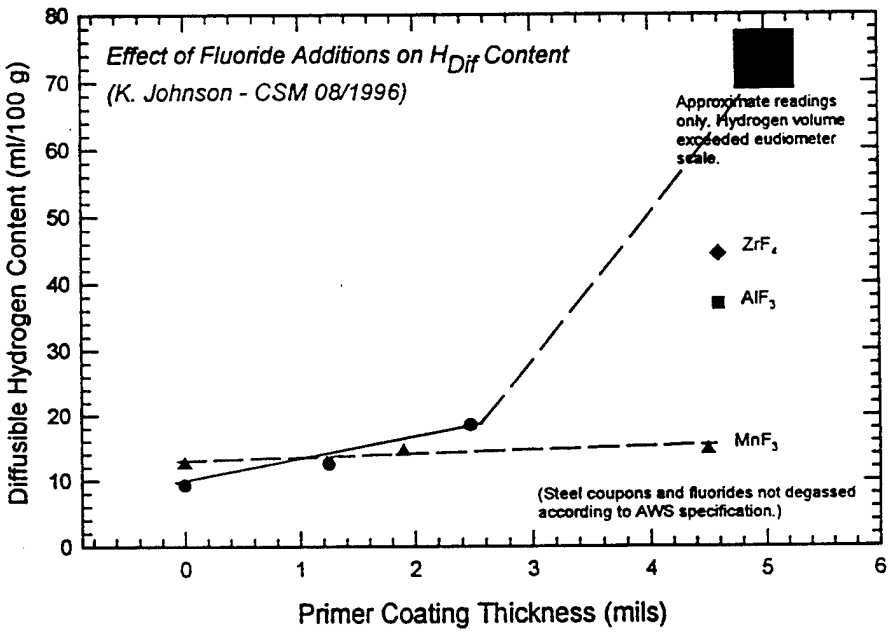

Figure 8. Effect of fluoride additions on H_{diff} content.

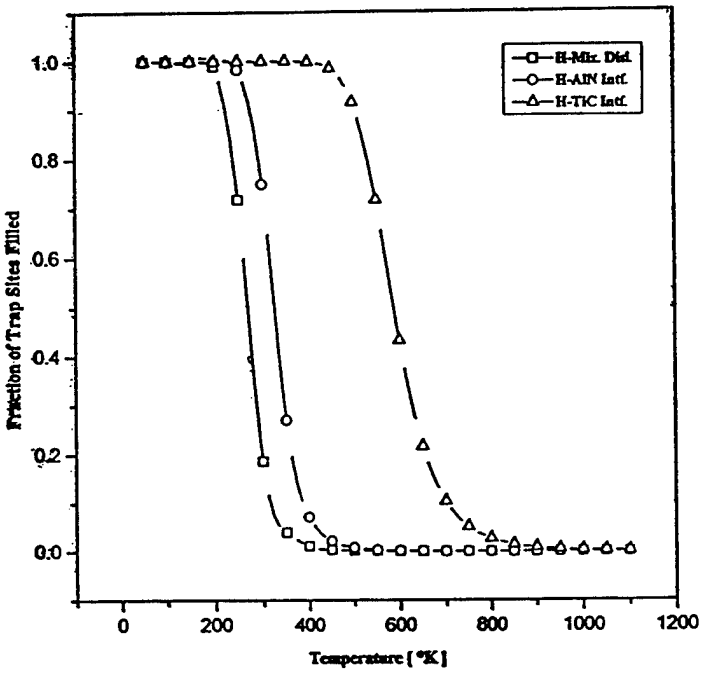

Figure 9. Fraction of trap occupation by hydrogen at trap sites as a function of temperature for various hydrogen-trap binding energies. Partial pressure of hydrogen is 0.0545 Pa.

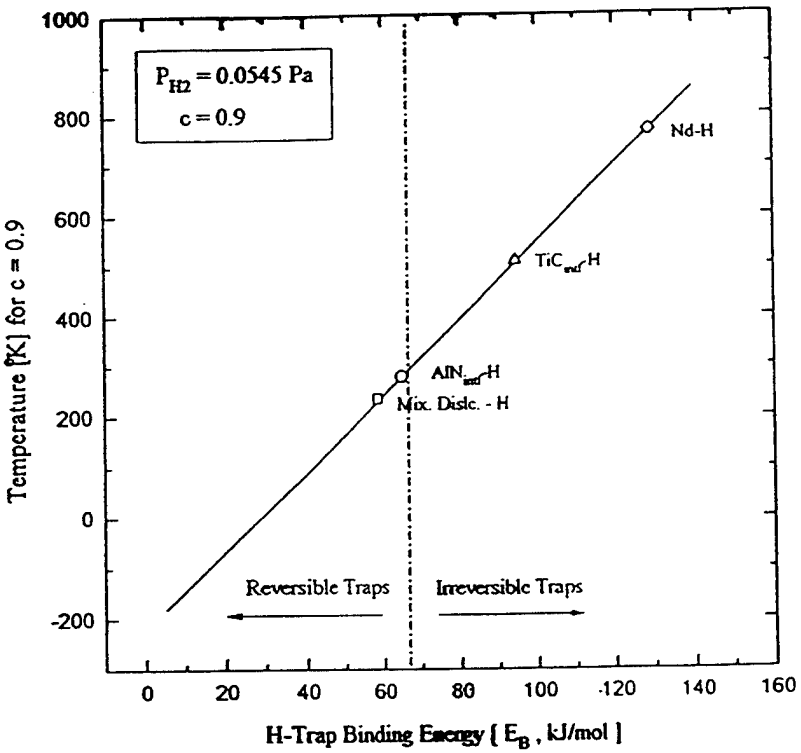

Figure 10. Temperature for ninety percent occupation at various hydrogen trap sites.

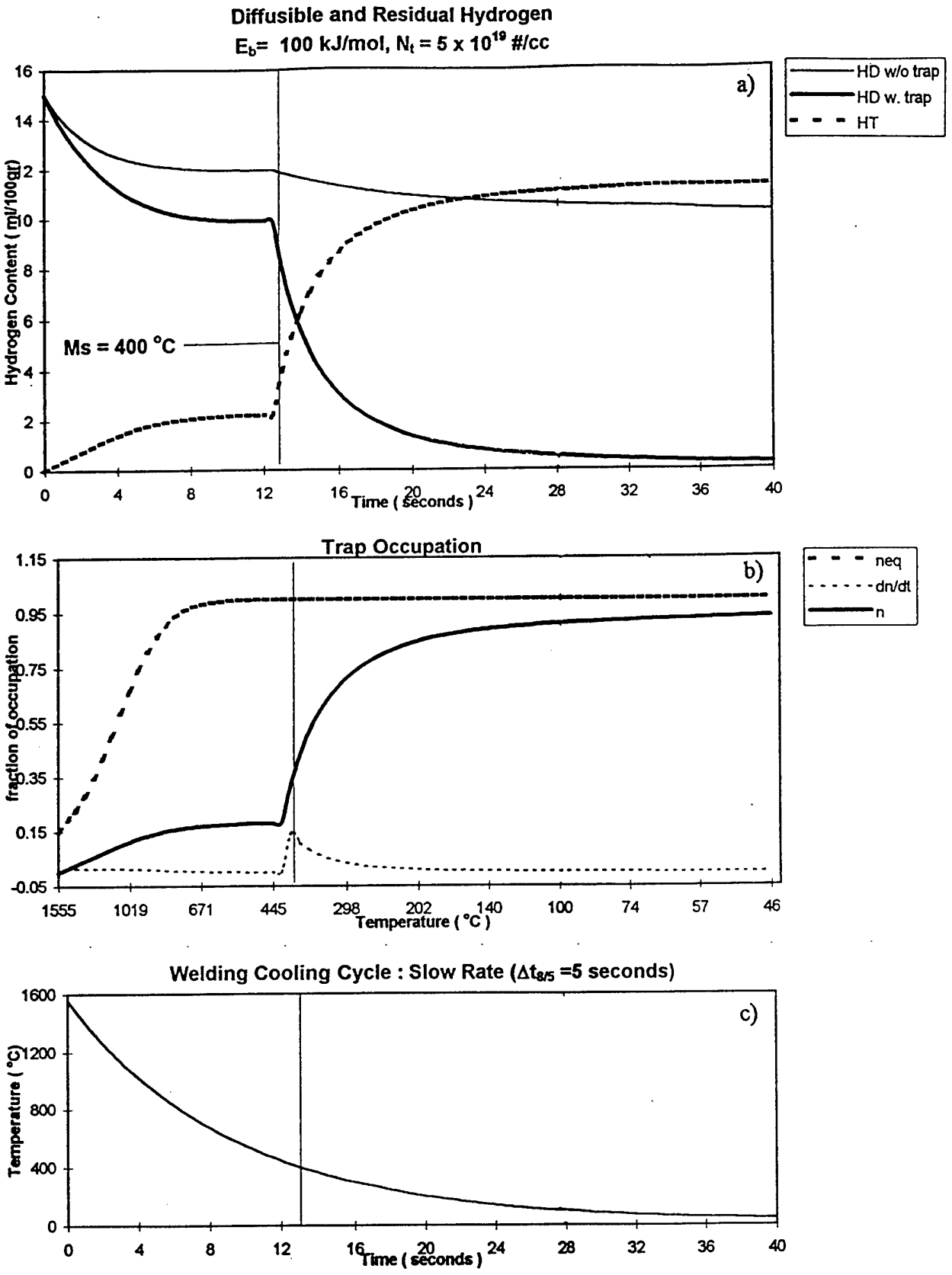

Figure 11. Hydrogen trapping during welding cooling cycle. Initial diffusible hydrogen in weld metal is 15 ml/100g. In (a).,the notation HD stand for diffusible hydrogen, HT is the trapped hydrogen. In (b)., n is the fraction of trap occupation by hydrogen and neq is the equilibrium fraction of occupation determined by the Fermi-Dirac distribution.

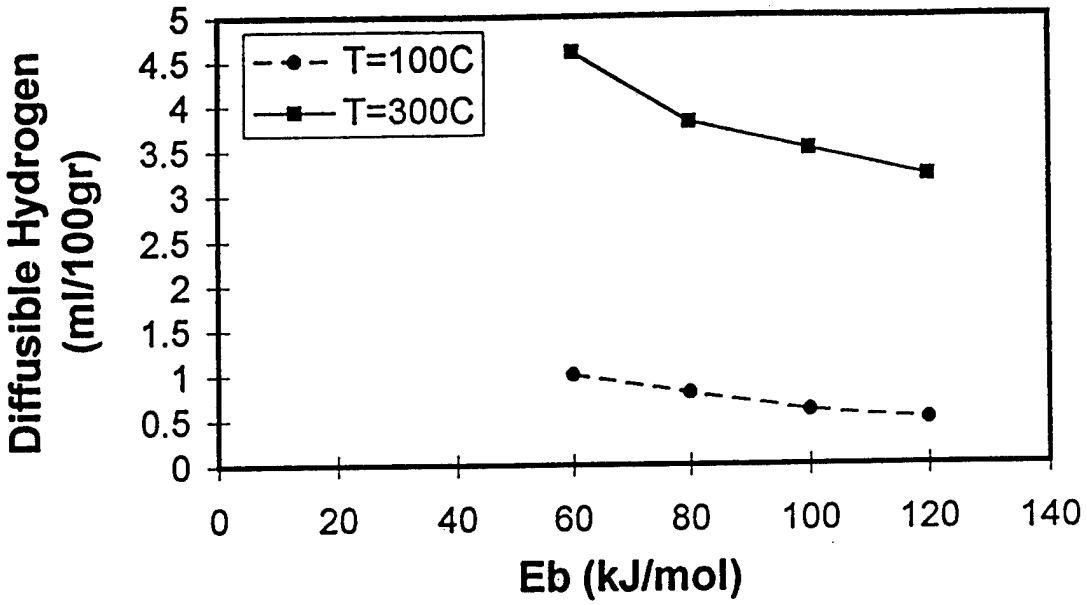

Figure 12. Effect of trap binding energy on the diffusible hydrogen content. Initial diffusible hydrogen content is 15 ml/100g. M_s =400C, $\Delta t_{8/5}$ is 5 seconds, trap density, $N_t = 5 \times 10^{19}$ #/cc.

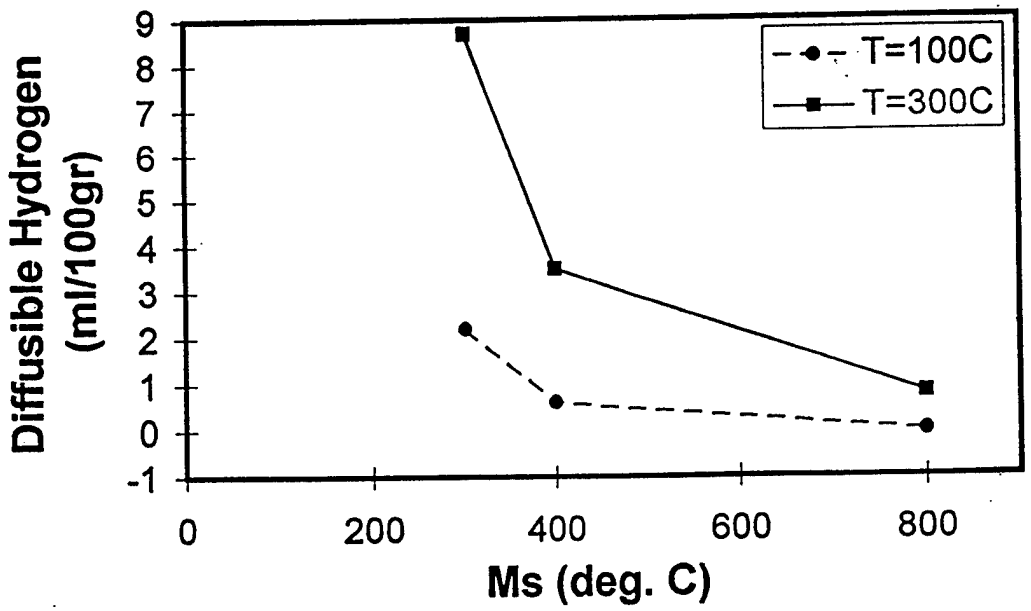

Figure 13. Effect of M_s temperature on the diffusible hydrogen content. Initial diffusible hydrogen content is 15 ml/100g. Eb is 100 kJ/mol, $\Delta t_{8/5}$ is 5 seconds, trap density, $N_t = 5 \times 10^{19}$ #/cc.

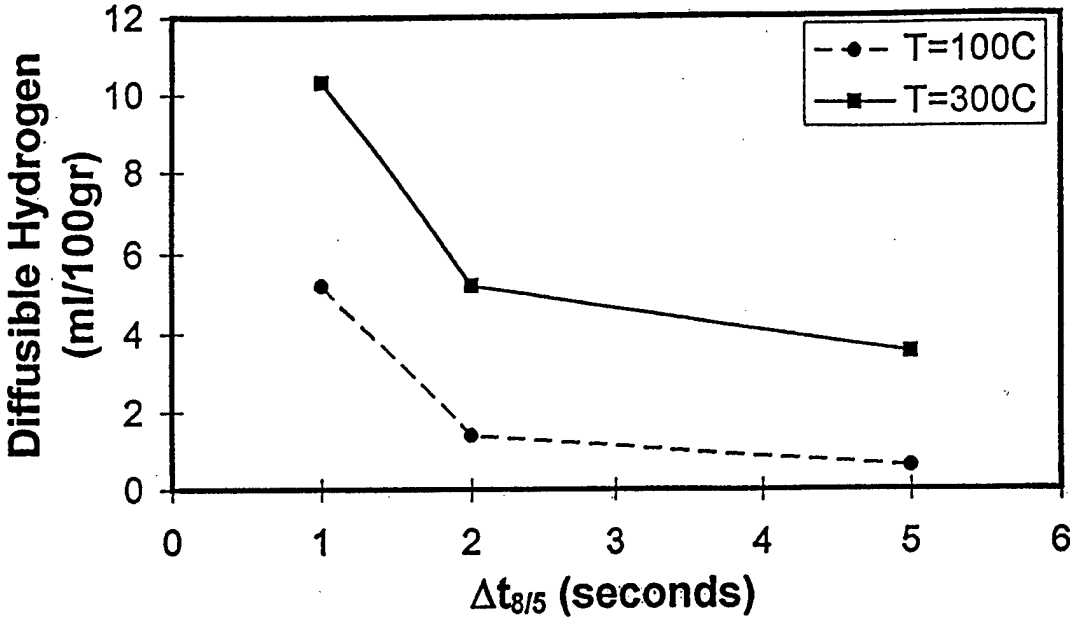

Figure 14. Effect of cooling rate on the diffusible hydrogen content. Initial diffusible hydrogen content is 15 ml/100g. M_s =400C, Eb is 100 kJ/mol, trap density, N_t =5x10^{19} #/cc.

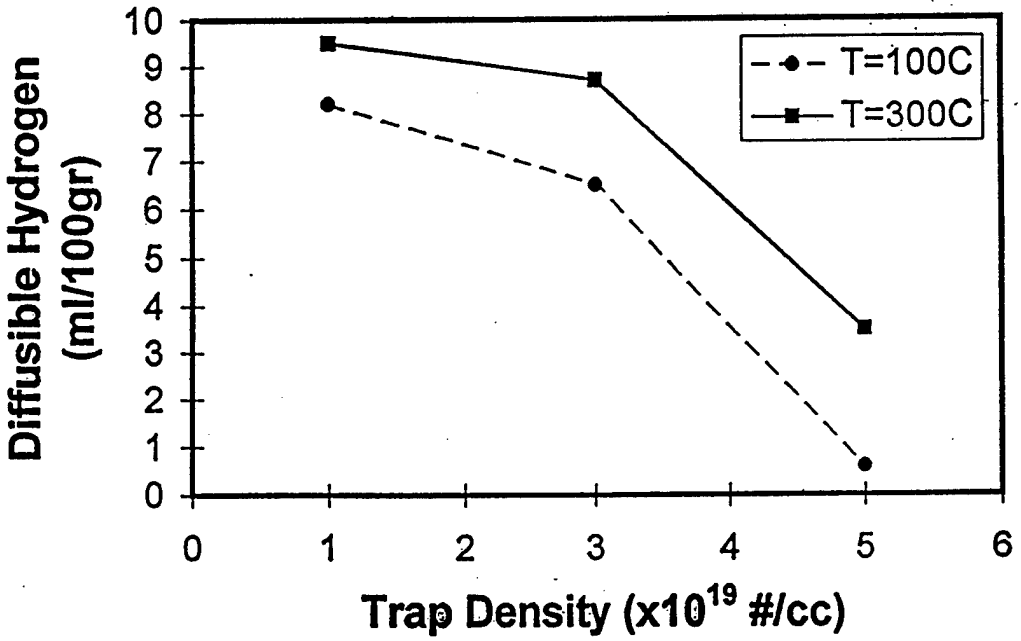

Figure 15. Effect of trap density on the diffusible hydrogen content. Initial diffusible hydrogen content is 15 ml/100g. M_s =400C, $\Delta t_{8/5}$ is 5 seconds, Eb is 100 kJ/mol.

Appendix III

Manuscript Submitted for Publication

in

Int. Conf. Proc. of Welding and Related Technologies for the XXIth Century, November 1998, Kiev, Ukraine

"Hydrogen Assisted Cracking in High Strength Steel Weldments".

HYDROGEN ASSISTED CRACKING IN HIGH STRENGTH STEEL WELDMENTS

I. Maroef, D.L. Olson, and G.R. Edwards

Center for Welding, Joining, and Coating Research

Colorado School of Mines

Golden, CO 80401

USA

Several issues on hydrogen assisted cracking (HAC) in high strength steel welding are reviewed. The concept of correlating martensite start temperature to hydrogen transport and distribution in a weld will be discussed. The model of utilizing hydrogen traps to reduce localization of hydrogen at regions of high stress concentration will be discussed. The role of carbide, oxide, and sulfide inclusions, as well as retained austenite as hydrogen traps is reviewed.

1. Introduction

Traditionally, hydrogen assisted cracking (HAC) in steel welding is considered to occur when all the necessary conditions for cracking are fulfilled simultaneously. These conditions encompass the combination of diffusible hydrogen content, restraint stress, hardness or susceptible microstructure, and temperature range between –100 and 100° C [1]. An observation by Hart [2], on the heat-affected zone of various steels, led to a conclusion that controlling factors for hydrogen cracking fall into two conditions. For high concentrations of hydrogen (approximately 10 ml H_2/100 g deposit metal), the resistance to cracking was primarily controlled by weld deposit hardness. The value of 350 HV is often specified as the maximum allowable HAZ hardness to avoid hydrogen cracking [3]. At lower levels of hydrogen, less than 5 ml H_2/100 g, resistance to cracking was determined more by microstructure than by hardness. In high strength steel welding, formation of martensite should be prevented and is commonly minimized by reducing the carbon content. The presence of oxides and sulfides, in optimal size and amount, also reduce hardenability of steel by facilitating the formation of tough acicular ferrite microstructures.

Common practices to prevent hydrogen cracking in high strength steel weldments are the pre- or post-weld heat treatment, the use of non-cellulosic electrodes with proper baking, and edge preparation. Heat treatment has been necessary to control the cooling rate after welding to allow for sufficient hydrogen removal, as well as to control the heat-affected zone (HAZ) hardness. The higher the strength of the steel, the lower the acceptable weld hydrogen content, even to levels as low as one to two ml H_2/100 g deposit metal [1,4]. With proper selection and use of welding consumables, a minimal hydrogen content can be introduced to the weld pool. However, considerations for hydrogen cracking in high strength steel welding involve further aspects. The high strength level of this class of steel results in high restraint stresses, which are non-uniformly distributed within the weld joint. High stresses are often accompanied by non-uniform hydrogen distribution in the weld joint, a condition which require very low nominal hydrogen content [5]. Evidence of non-uniformity of hydrogen distribution has been shown by Olson et.al [6], using a laser induced breakdown spectroscopy, as shown in Figure 1. Non-uniform hydrogen

distribution will become more critical issue with the welding of even higher strength steels.

The concomitant effect of localized hydrogen concentration and high restraint stress gives rise to crack initiation at stress concentrations within the weld joint. Stress concentrations are located at inclusion interfaces and grain boundaries, and at the weld fusion line. These locations may be either in the heat-affected zone (HAZ) or in the fusion zone (FZ), depending upon how hydrogen, stress, and hardness are distributed within the weldment.

Non-uniform hydrogen distribution across the weldment can result from poorly matched welding consumables and base metal compositions [7]. Stress-induced hydrogen diffusion and hydrogen transport by dislocation sweeping are also factors generally considered to be responsible for localized accumulation of hydrogen at regions of stress concentration [3,5]. Dislocation sweeping in weld joints will be operative if the hydrogen cracking mechanism is dominated by localized plasticity [8]. Through implant tests of high strength steel, micro-void coalescence, which is a result of localized plasticity, has been shown to occur by Gedeon and Eagar [9]. Microstructural heterogeneities, can function as hydrogen traps. The type and distribution of hydrogen traps are also determining factors to the short range distribution of hydrogen, through partitioning of hydrogen atoms between lattice sites and various trap sites in the weldment. Such a partitioning of hydrogen atoms may significantly improve the resistance to HAC.

2. Hydrogen Distribution and Hydrogen Cracking in Weldments with Unmatched Fusion Zone and HAZ Chemical Composition.

Commonly, hydrogen cracking occurs in the heat-affected zone (HAZ). The crack initiates near the fusion zone, at the regions with the highest stress intensity factor. However, in recent years, the development of cleaner HSLA steels (with ultra-low carbon content) led to HAC in the weld metal rather than in the HAZ [10]. To explain this situation, the locations of HAC in the weld joint have been related to the non-

uniformity of both hydrogen and stress distributions, developed during the cooling cycle after welding.

One common case of non-uniform hydrogen distribution across the weldment is the result of unmatching compositions between the weld metal (WM) and the heat-affected zone (HAZ). During the cooling cycle of the welding process, austenite-martensite phase transformations in the weld metal and in the HAZ do not take place at the same temperature. Hence, within a certain temperature range, hydrogen transport across the weldment proceeds across two different phases. As a result of much slower hydrogen diffusivity in austenite compared to diffusivity in martensite/ferrite [11], a non-uniform distribution of hydrogen across the weldment may result [12,13]. Another cause for such a non-uniform distribution is a big difference in thermal history for the weld metal as compared to the heat-affected zone.

Wang et.al [14] calculated the hydrogen concentrations across the weldment to substantiate a conceptual model, introduced by Granjon [12], that describes how the austenite-ferrite (or austenite-martensite) phase transformation in steel weldments affects the resulting hydrogen distribution. In this study, the location with the highest calculated hydrogen content was compared to the locations of crack sites obtained from hydrogen cracking tests. Two cases were illustrated. First, as shown in Figure 2, the austenite-martensite transformation in the weld metal occurred at a higher temperature than the transformation in the heat-affected zone. In this situation, diffusible hydrogen accumulated in the heat-affected zone just under the fusion line, and, as verified by experimental data, under-bead cracking occurred in the heat affected zone. In the alternate situation, shown in Figure 3, the martensite transformation in the heat-affected zone occurred at a higher temperature than in the weld metal. It is possible, in this case, that the major fraction of the initial diffusible hydrogen was retained in the weld metal, and thus promoted crack initiation in the weld metal. To minimize the susceptibility to HAC, alloying additions to welding consumables must be selected to achieve a martensite start temperature which is slightly higher in the weld metal as compared to that temperature in the HAZ. Satisfying this condition is expected to alleviate the non-uniformity of hydrogen distribution in weldments as well as to facilitate maximum rate of hydrogen transport away from the weld metal to the base plate.

Alternate hydrogen cracking location within weldments have also been illustrated by Matsuda et. al [15]. In their illustration, the variation of hydrogen concentration with time in the weld metal was assumed to be different than that variation in the HAZ, as shown in Figure 4. This difference may be caused by the difference in the thermal history of the weld metal as compared to the heat-affected zone. The corresponding time dependent critical stresses for HAC in both regions are shown in Figure 5. Figure 5 illustrated that, low weld metal hardness will cause crack to occur in the HAZ, since the critical stress for HAC in the weld metal will always be higher than the value of stress being applied to the weld joint. On the other hand, for high weld metal hardness, the crack will initiate in the weld metal, since the critical condition for HAC in the weld metal is satisfied before that condition is met in the HAZ.

3. Hydrogen Distribution in Weldment as a Result of Stress Assisted Diffusion and Dislocation Assisted Transport of Hydrogen Atoms

Moving dislocations can acts as rapid and efficient carriers or sweepers of hydrogen, as was experimentally verified by tritium release rate and penetration experiments of Donovan, Louthan, and co-workers [16,17,18], and also by permeation experiments of Kurkela and Latanision [19]. Dislocation sweeping has been thoroughly studied by Tien et. al [20,21], who also showed the close relationship between the kinetics of embrittlement, under strain loading, and the transport of hydrogen to critical failure sites within the material. Hydrogen atoms can follow the motion of dislocations with a velocity which was derived through the Einstein-Stokes relationship [22] :

$$v = \left(\frac{D_H}{kT}\right)F \qquad (1)$$

where D_H is the effective diffusivity of hydrogen in the matrix and F is the effective driving force per atom of hydrogen carried by the dislocation. A critical velocity, v_c, for hydrogen to move along with a dislocation, was assumed for a critical driving force F_c , that correspond to a gradient of hydrogen-dislocation binding energy, E_B , assumed to be distributed over a distance of 30 b, where b is the dislocation's Burgers vector ($F_c=E_B/30b$). Above v_c, or at a strain rate greater than $\dot{\varepsilon}=\rho.b.v_c$, the

dislocation line can be expected to break away from its hydrogen cloud, so that dislocation sweeping is no longer effective.

Dislocation-assisted transport of hydrogen atoms contributes a major fraction of the HAC in high strength steels. The high strength level of this steel causes high restraint stresses, even when the weldment temperature is still high, and dislocations are very mobile. This situation leads to extensive dislocation-assisted hydrogen transport in the weldment. Theoretical study on role of dislocation-assisted hydrogen transport to localized hydrogen has been investigated by Kikuta et al [23, 24], using finite element analysis. Similar study has also been conducted by Yurioka et.al. [25,26] who considered not only the effect of dislocation assisted hydrogen transport but also the effect of stress assisted hydrogen diffusion due to triaxial stress. A finite difference method was used in theoretical study and a non-uniform hydrogen distribution, such as that shown in Figure 6, was obtained.

In many occasions, heat treatments to prevent HAC require very tight temperature control because they allow only narrow windows of time and temperature. While an extensive heat treatment is necessary for sufficient hydrogen degassing, limitations are necessary to maintain mechanical properties and to minimize hydrogen localization. Localized hydrogen accumulation in high strength steel has been shown to be enhanced after post weld heat treatment is imposed upon the weld joint [27]. Hydrogen distribution was measured in a welded joint without heat treatment (Figure 7.a) and with post-weld heat treatment (Figure 7.b). In Figure 7.b, local accumulation of hydrogen in a welded joint is developed after post weld heat treatment. This localized hydrogen accumulation occurred even though the average content of hydrogen is less than that of the weld joint prior to post weld heat treatment, as shown in Figure 7.a. This result implies that, for certain critical weld joints, high restraint stresses preclude recommending any acceptable heat treatment consistent with safe welding conditions. Prevention of hydrogen cracking in this situation would require an alternative solution to substitute the heat treatment procedure.

4. Effect of Hydrogen Traps on the Hydrogen Partitioning within Weldments

In steel, hydrogen will be found not only in the host lattice, but also segregated to atomic and microstructural imperfections such as vacancies, solute atoms, dislocations, grain boundaries, voids, and second phase particles. In these localized regions, the mean residence time of a hydrogen atom is considerably longer than in a normal interstitial lattice site. In the extreme case, these regions are sinks, which retain the atom even during mechanical loading. The generic term for this phenomenon is trapping and these localized regions are hydrogen trap sites [28,29,30].

The strength of a trap site; i.e., the fraction of time a hydrogen atom resides in that trap site, depends upon the binding energy, E_B, of the hydrogen atom to the trap. The binding energy of 60 kJ/mol-H for a dislocation or a grain boundary is generally regarded as the limiting value for a reversible trap. With this energy level, a reversible trap becomes effective in capturing hydrogen around 400 K. A reversible trap with binding energy lower than 60 kJ/mol-H will not be able to prevent hydrogen cracking. The trapped hydrogen will be picked up by moving dislocations, and will eventually be delivered to crack initiation sites [31]. With regard to HAC, the preferred traps are consequently those traps having binding energies in excess of 60 kJ/mol-H. These traps are termed irreversible traps [32].

The presence of deep hydrogen traps in the weld metal may significantly alter hydrogen content and distribution during welding. A reduction of the concentration of diffusible hydrogen has been demonstrated by Pokhodnya [33] through the introduction of rare earth elements into the weld metal. Lensing et.al [34] have found similar results through the introduction of neodymium and yttrium. Their result for low carbon-low alloy steel welds is shown in Figure 8. Significant reduction of diffusible hydrogen by more than 50 percent (down from 4.5 to 1.5 ml H2/100g) when 600 parts per million of trapping elements were incorporated into the weld metal. In their study, hydrogen thermal desorption analysis has also been conducted. In this analysis, weld samples were heated with constant heating rate so that trapped hydrogen atoms were released at different temperature regimes, depending upon the

strength of the trap sites. In Figure 9, hydrogen release from weld metal containing neodymium additions is contrasted with hydrogen release from a weld metal free of deep traps. At high temperatures (800-900 K), a peak of hydrogen evolution was observed in the weld sample which contain neodymium, indicating that irreversible traps were present.

Hydrogen trapping offers the prevention of HAC during high strength steel welding by reducing the diffusible hydrogen without an extensive heat treatment. Hence, localization of hydrogen at stress concentration regions by dislocation-assisted transport can be minimized. A theoretical calculation of an accelerated reduction of hydrogen in weld metal due to the presence of hydrogen traps is shown in Figure 10. It was found through these calculations that any weld metal with low martensite start temperature requires trap sites with high binding energy to ensure rapid hydrogen capturing. On the other hand, decohesion at inclusions due to trapped hydrogen is also possible, depending upon the electronic bonding change which occur at the inclusion interfaces in the presence of hydrogen. While hydrogen trapping can prevent hydrogen cracking cause by localization of diffusible hydrogen, optimal trapping inclusions must be determined, based upon evaluation of both hydrogen capturing capabilities and mechanical properties.

Various inclusions which are effective as hydrogen traps in high strength steel have been reported. The results reported vary from advantageous effect (especially for strong irreversible traps), to detrimental effects (for weak traps), relative to weld joint mechanical integrity. Some of these reports may not accurately represent the performance of these traps in the real welding situation. To accurately evaluate trap sites, a comprehensive investigation that closely simulates both the actual steel welding and the weld joint function is required. Adequate simulations requires a meaningful level of hydrogen contamination, an actual welding cooling rate, measurement of hydrogen at critical temperatures (100° C –300° C), and an extensive mechanical testing.

Oxide Inclusions as Hydrogen Traps

A number of oxide inclusions have been identified as relatively weak but irreversible trap sites, such as Al_2O_3 (E_B = 79 kJ/mol-H) [35] and iron oxide (E_B = 50–70 kJ/mol-H) [36]. With longitudinal butt-tensile restraint cracking (LB-TRC) testing, Shinozaki et al. [37] investigated the effect of oxygen on the mechanical integrity of HY-100 and HSLA-100 steels samples, welded with hydrogen contamination in the shielding gas. Longitudinal Bead – Tensile Restraint Cracking (LB-TRC) test was used to enable the investigators to impose mechanical tensile loading on a weld bead when the temperature reach 150° C during cooling after welding. At a hydrogen level of 4.7 ppm, HY-100 steel welds, which consistently revealed a martensitic microstructure, experienced a reduction of the critical stress for HAC as the oxygen content was increased up to 200 ppm. With increasing oxygen content, the fracture mode was altered from quasy-cleavage to intergranular. Intergranular failure occurred via oxide-matrix decohesion at prior austenite grain boundaries. These oxide trap sites may be too weak and consequently, the rate of hydrogen trapping may not be sufficiently fast to prevent accumulation of hydrogen at grain boundary areas of high stress concentration.

Several oxide inclusions, such as Al_2O_3 and $CaO\text{-}Al_2O_3$, are non-deformable. Within the regions of high stress concentration, these inclusions also act as a stress intensifier and promote a localized plastic deformation in steels [38,39]. Hydrogen concentration around the inclusion can be increased locally and the critical concentration for HAC can be reached earlier. In other inclusion situations, trapped hydrogen may relate to prevention of HAC by promoting decohesion and facilitate the formation of blunt crack at the inclusion-matrix interface. In this way, trapped hydrogen conversely could increase the critical stress for HAC because a crack initiation site is available without the need to fracture the oxide inclusions, otherwise sharp crack initiations are easily formed. Understanding of the relationship between inclusion-matrix decohesion and toughness as well as HAC needs to be further investigated.

The role of oxide inclusions in the HSLA-100 steel weld sample was thought to be overshadowed by the increasing formation of acicular ferrite or bainite structure as the oxygen content increase. An increase of critical stress with oxygen content, up to 638

ppm, was observed and thought to be a result of the formation of tougher microstructures. However, it has been known that, in the absence of hydrogen, the maximum toughness of weld metal usually occurs at an oxygen content of 250 ppm [40]. In this particular investigation, it is highly possible that the formation of acicular ferrite in HSLA-100 steel occurred at a higher temperature than the formation of martensite in HY-100 steel. In this situation, hydrogen capturing is more effective in HSLA-100 steel and contributes to the increase of critical stress for HAC. Reduction of diffusible hydrogen is faster in HSLA-100 steel than in HY-100 steel for the same welding cooling cycle.

Carbide Inclusions as Hydrogen Traps

TiC precipitates in microalloyed HSLA steel has been of great interest for many investigators due to the high binding energy (Eb= 98 kJ/mol-H) [28]. Stevens and Bernstein [41] had attempted to evaluated the mechanical response of TiC-containing HSLA steel. Unfortunately, they could not exclude the deleterious effect of sulfur or phosphorous segregation to grain boundaries, which occurred during annealing heat treatments that were intended to vary the density of TiC precipitates. The presence of small and finely distributed TiC precipitates were shown to improve the resistance to HAC, since they compensated for the loss of resistance to HAC due to the segregation of sulfur or phosphor. It was thought that, without the presence of such deep and innocuous trap sites, the fracture toughness of the hydrogen-charged HSLA steel would decrease significantly.

Besides TiC, VC inclusions have been investigated as hydrogen traps to prevent disbonding of austenitic stainless steel cladding from 2 ¼ Cr –1 Mo steel base plates [42]. Disbonding usually occurs at the interface of the two steel layers when a hydrogen-containing pressure vessel is cooled down from an elevated temperature. While disbonding in ordinary steel started to occur when the specimen was cooled down from 450° C and 14.7 Mpa hydrogen pressure, disbonding in VC modified steel was not observed even after cooling from 500° C and 19.6 Mpa (containing higher level of hydrogen). The role of VC was thought to be that of a hydrogen trap and alleviated localization of hydrogen at the cladding interface.

Quite recently a more comprehensive evaluation of VC particles has also been done through both hydrogen measurement and notched tensile testing [43]. Two similar classes of steel, AISI 4340 and ASTM A723 steels, were modified to obtain the same vanadium and carbon content. These modifications promoted the formation of VC particles, which were shown to significantly improve the resistance to HAC relative to the base steel compositions. The embrittlement index for AISI 4340 steel was decreased by the VC particles formation from 61.2 percent down to 22.2 percent. A smilar case was observed for the ASTM A723 steel (from 5.8 percent down to 3.8 percent). Quantitative evaluation of the binding energy of VC particles has not been reported. Extraction studies that were performed in this investigation showed that the particles do not release the trapped hydrogen during sample reheating at 200° C, which implies that these particles are irreversible traps.

Sulfide Inclusions as Hydrogen Traps

While sulfur content in steels has been reduced to improve mechanical properties, some papers have reported that a reduction of non-metallic inclusions, mainly sulfides, could increase the risk of HAC in the HAZ. Hirose, Araki and Kikuta [44] observed that, in quenched and tempered HSLA steels containing 10 ppm hydrogen, the critical stress for HAC increased with increasing sulfur content up to 300 ppm. The sulfur content was directly proportional to the MnS inclusion density, which was the main microstructural feature responsible for suppression of HAC. With the matrix of all the sample being martensite, these sulfides were thought not to reduce HAC by reducing the hardenability of steels. Instead, because of the fact that the apparent hydrogen diffusivity decreased with increasing MnS density, the above investigators concluded that MnS inclusions served as hydrogen trap sites, thus suppressing HAC. These investigators suggested that the presence of hydrogen at the interface of these inclusions did not become the initiation site for HAC because MnS inclusions are deformable. As a trap sites, manganese sulfide has been identified as a weak irrversible trap with a binding energy of 72 kJ/mol-H [45].

5. The Role of Retained Austenite as a Hydrogen Trap.

Austenite manifests a much larger solubility and much slower diffusivity of hydrogen than in ferrite. This phase, in the form of retained austenite, can behave as a three-dimensional hydrogen trap. Knowledge concerning retained austenite as an effective hydrogen trap has not been well established. Initially, retained austenite may assist in the accelerated reduction of diffusible hydrogen right after the formation of martensite. Hence, it can help reducing diffusible hydrogen without extensive dislocation assisted hydrogen transport. However, as the temperature drops, solubility of hydrogen in retained austenite decreases, and retained austenite begins to export hydrogen atoms to the adjacent martensite matrix. Furthermore, the slow diffusivity of hydrogen in this retained austenite may also increase the probability of HAC, since export of hydrogen atoms to the ferrite matrix would occur at low temperature, where the chance for HAC is high. The role of retained austenite, whether it helps to prevent or it increases the risk of HAC, strongly depends upon the welding thermal cycle, as well as upon the retained austenite density and its location with respect regions of high stress concentration. Theoretical predictions to determine the proper heat treatment for preventing HAC in high strength steeel welding should also include the effect of retained austenite, in addition to the previously mentioned factors (stress-assisted hydrogen diffusion, dislocation-assisted hydrogen transport, and hydrogen trapping).

Evaluations for HAC-related issues in steel welding such as diffusible hydrogen measurements involve quenching weld specimens in iced water and storing in liquid nitrogen or dry ice – acetone solutions after completion of the welding process. This procedure does not represent the actual welding situation in steel construction, since the weld sample transform completely to martensite when its temperature drops as low as -70° C. On the other hand, the slower cooling rate and much higher final welding temperatures in actual steel construction would yield significant amounts of retained austenite in many weldments. Investigations concerning retained austenite require better measurement techniques than the above mentioned conventional technique to get meaningful hydrogen concentrations as well as the appropriate mechanical responses.

6. Closure

In addition to the nominal amount of diffusible hydrogen, non-uniform distribution of hydrogen is a significant contributor to hydrogen cracking in high strength steel welding. This non-uniformity can be minimized when the martensite start temperature of the weld metal is slightly higher than that of the HAZ. Furthermore, localization of hydrogen at regions of high stress concentration should also be prevented by minimizing the amount of dislocation-assisted transport of hydrogen. Such a hydrogen transport may be facilitated by an extensive heat treatment imposed upon the weld joint. To avoid this, hydrogen traps may be incorporated, thus avoiding extensive heat treatment, while still reducing diffusible hydrogen concentration. Selection of hydrogen traps to prevent HAC requires further information than just their hydrogen trapping characteristics. Understanding the effect of these inclusions and their trapped hydrogen concentrations on the whole mechanical integrity of the weld joint is necessary. Finally, understanding the effect of retained austenite as a three-dimensional hydrogen trap with a temperature dependent trapping capacity should be carefully assessed, since actual welding of steel construction may involve a significant retained austenite volume fractions.

7. Acknowledgment

The authors acknowledge and appreciate the research support of the US Army Research Office and the Office of Naval Research.

8. References

1. N. Bailey, F.R. Coe, T.G. Gooch, P.M. Hart, N. Jenkins, and R.J. Pargeter, "*Welding Steel without Hydrogen Cracking*", 2nd Edition, Abington, 1993.
2. P.M. Hart, *Welding Journal*, Vol. 65, 1986, pp. 14-22s.
3. N.Yurioka and H.Suzuki, *Int. Mat. Rev.*, Vol. 35(4), 1990, pp. 216-249.
4. R. Wong, J. Blackburn, J. DeLoach, and R. DeNale, *in "Hydrogen Management in Steel Weldments"*, DSTO and WTIA, Oct. 1996, Melbourne, Australia, pp. 35-48.
5. V.F. Musiyachenko and S.B. Kasatkin, *Automatic Welding*, Sept.1985, pp. 22-26.
6. D.L. Olson, I. Maroef, C. Lensing, R.D. Smith, W.W. Wang, S. Liu, T. Wildeman, and M. Eberhart, *in "Hydrogen Management in Steel Weldments"*, DSTO and WTIA, Oct. 1996, Melbourne, Australia, pp. 1-19.
7. W.Wang, S. Liu, and D.L. Olson: in Proc. Intl. Conf. '*Offshore Mechanics and Arctic Engineering - Materials Engineering*', Vol. III, Florence, Italy, 1996, ASME, pp. 403-409.
8. J.P. Hirth: *Metal. Trans.*, 1980, **11A**, pp. 861-890.
9. S.A. Gedeon and T. Eagar: *Welding Journal*, 1990, pp. 213-220s
10. J. Vuik, *An Update of the State-of-the-art of Weld Metal Hydrogen Cracking*, IIW document, IXJ-175-92, 1992, American Council, AWS, Miami, FL
11. Th. Bollinghaus, H. Hoffmeister, and A. Dangeleit, "*A scatter Band for Hydrogen Diffusion Coefficients in Microalloyed and Low Carbon Structural Steels*", IIW Document IX-1767-94, 1994).
12. H. Granjon, "Cold Cracking in Welding of Steels", Intl. Symposium on Cracking and Fracture in Welds, Conf. Proc. Japan Welding Society, (1971), IB, 1.1.
13. B. Gravile, "*Hydrogen Cracking Sensitivity of HSLA Steels*", The Metallurgy, Welding and Qualification of Microalloyed (HSLA) Steel Weldments, (1990), pp. 127-150.
14 W.W. Wang, R. Wong, S. Liu, and D.L. Olson, in Conf. Proc of ' *Welding and Weld Automation in Shipbuilding*', Oct 29- Nov. 2, 1995, eds R.DeNale, TMS, Warrendale PA, 1996, pp. 17-31.
15. F. Matsuda et.al., *Trans. of JWRI*, Vol. 12 (2), 1983, pp. 75 - 85.
16. J.A. Donovan, *Metall. Trans. A*, Vol. 7, 1976, pp. 1677-1683.
17. J.A. Donovan, *Metall. Trans. A*, Vol. 7, 1976, pp. 145-149.
18 . M.R. Louthan, Jr., G.R. Caskey, Jr., J.A. Donovan, and D.E. Rawl, Jr., *Mat. Sci. and Eng.*, Vol. 10, 1972, pp. 357-368.
19. M. Kurkela and R.M. Latanision, *Sripta Metall.*, Vol. 13, 1979, pp. 927-932.
20. J.K. Tien, S.V. Nair and R.R., Jensen, in "*Hydrogen Effects in Metals*", eds. I.M Bernstein and A.W. Thompson, The Metall. Soc. of AIME, Pittsburgh, Pennsylvania, 1981, pp. 37-56.
21. S.V. Nair, R.R. Jensen, and J.K. Tien, *Metall. Trans. A*, Vol. 14, 1983, pp. 385-393.
22. J.K. Tien, A.W. Thompson, I.M. Bernstein and R.J. Richards, *Metall. Trans.A*, Vol. 7, 1976, pp. 821-829.
23. Y. Kikuta, in "*Hydrogen Effects in Metals*", eds. I.M. bernstein and A.W. Thompson, The Metall. Soc. of AIME, Pittsburgh, Pennsylvania, 1981, pp. 755-765.
24. Kikuta et. al., *Trans. Japan. Weld. Soc.*, Vol. 11 (2), 1980, pp. 36-44.
25. N. Yurioka and K. Kohira, "*A Numerical Analysis of the Diffusion and Trapping of Hydrogen in Steel Welds*", IIW Doc. IX-951-76, 1976.

26. N. Yurioka and S. Oshita, *"An Analysis of Effect of Microstructure, Strain and Stress on the Hydrogen Accumulation in HAZ"*, IIW Doc. IX-1161-80, 1980.
27. Grivnyak I, in *"Scientific Problems in Welding and Special Electrometallurgy Part 3"*, Kiev Naukova dumka, 1970, pp. 38-48.
28. G.M. Pressouyre and I.M. Bernstein, *Metall. Trans. A*, Vol. 9, 1978, pp. 1571-1580.
29. G.M Pressouyre and I.M. Bernstein, *Metall.Trans. A*, Vol. 12, 1981, pp. 835-844.
30. I.M. Bernstein and G.M. Pressouyre, in *"Hydrogen Degradation of Ferrous Alloys"*, ed. by R.A. Oriani, J.P. Hirth and M. Smialowski, Noyes Pub., 1985, pp. 641-685.
31. J.K. Tien, A.W. Thompson, I.M. Bernstein, and R.J. Richards, *Metall. Trans.* A, Vol.7, 1976, pp. 821-829.
32. G.M. Pressouyre and I.M. Bernstein, *Metall. Trans.A*, Vol. 12, 1981, pp. 835-844.
33 I.K. Pokhodnya, in Sem. Proc *'Hydrogen Management in Steel Weldments'*, eds. J.L. Davidson and D.L. Olson, DSTO and WTIA, Oct. 1996, Melbourne, Australia, pp. 141-181.
34. C.A. Lensing, I. Maroef, and D.L. Olson, *"Presentation at AWS Convention 1997"*, April 1997, Los Angeles.
35. K.Y. Lee, J.Y. Lee, and D.R. Kim, *Mat. Sci. Eng.*, Vol. 67, 1984, pp. 213-220.
36. J.L. Lee and J.Y. Lee, *Met. Trans. A*, Vol.17, 1986, pp. 2183-2186.
37. Shinozaki and T. North, *Metall. Trans. A*, Vol. 21, 1990, pp. 1287-1298.
38. E. Pickering, *JISI*, Vol. 189, 1958, p. 148
39. S. Rudnik, *JISI*, Vol.204, 1966, p. 374
40. D.J. Abson and R.J. Pargeter, Int. Mater. Rev., Vol. 31(4), 1986, pp. 141-194.
41. M.F. Stevens and I.M. Bernstein, *Metall. Trans. A*, Vol. 20, 1989, pp. 909-919.
42. J. Shimomura, Y. Nakano, S. Nakano, and S. Ueda, *ISIJ Int.*, Vol. 31(4), 1991, pp. 379-386.
43. G.L. Spencer and D.J. Duquette, " The Role of Vanadium Carbide in Reducing the Susceptibility to Hydrogen Embrittlement of High Strength Alloy Steels", US. Army Benet Laboratories, Watervliet, NY, (1997)
44. Y. Kikuta, T. Araki, and A. Hirose, *Trans. Japan Welding Society*, Vol. 19 (1), April 1988, pp. 60-65.
45. S.M. Lee and J.Y. Lee, Acta Metall., Vol. 35 (11), 1987, pp. 2695-2700.

9. Figures

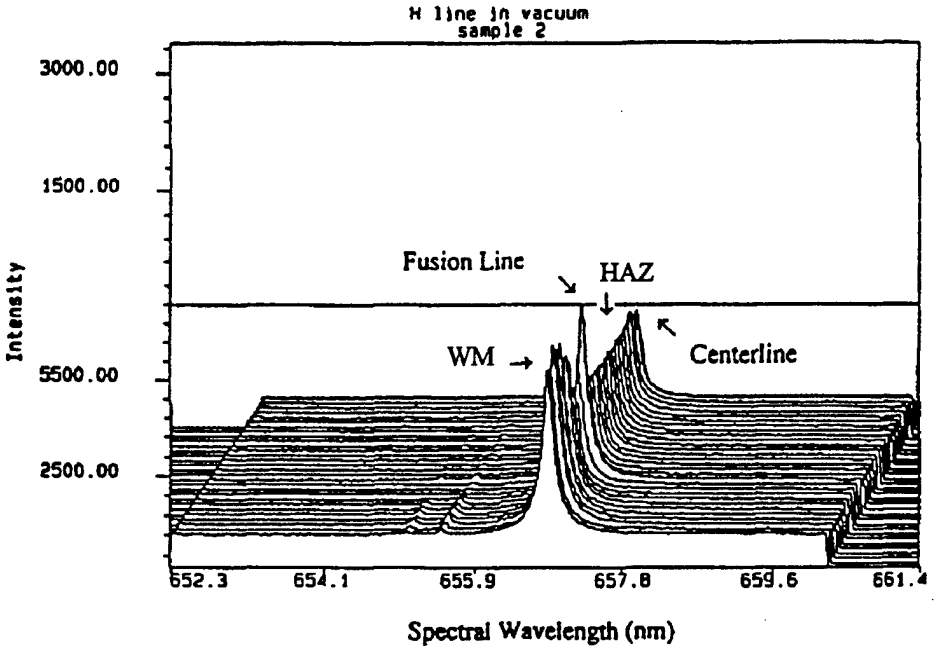

Figure 1. Non-uniform distribution of hydrogen across the center line of a weldment. Intensities of the hydrogen spectral emmission are proportional to the hydrogen concentration [6].

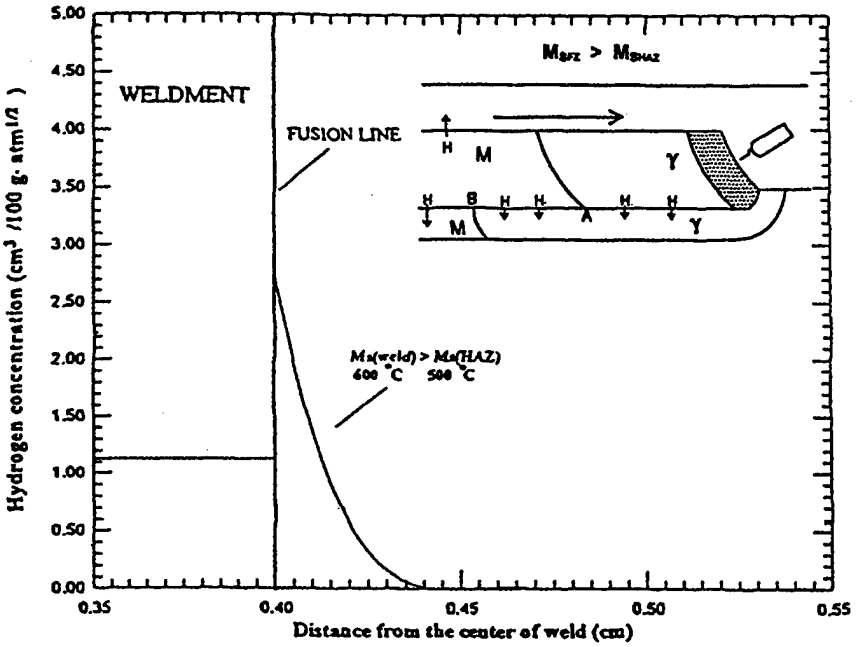

Figure 2. Hydrogen distribution across the fusion line of a steel weldment for Ms_{WM} (600° C) > Ms_{HAZ} (500° C) [14].

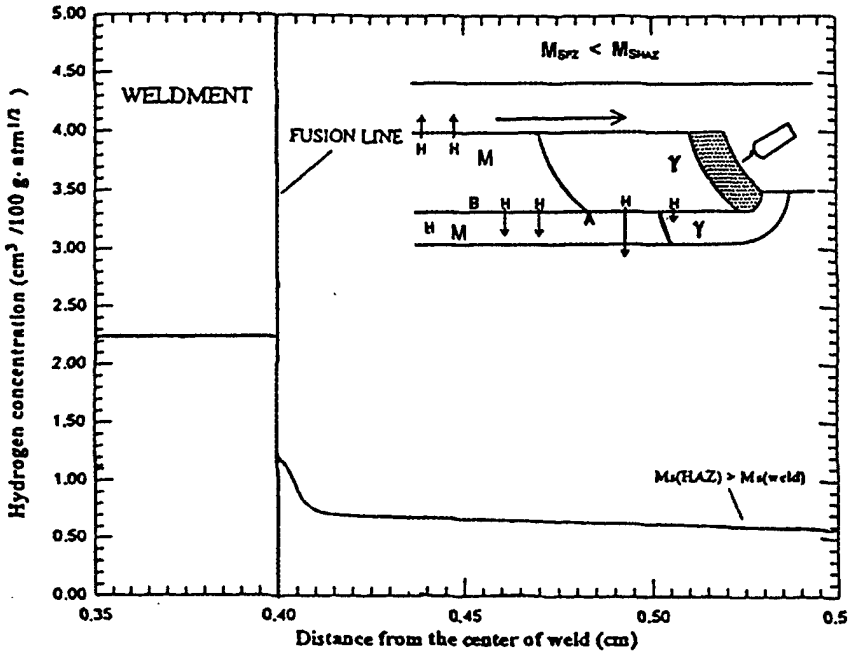

Figure 3. Hydrogen distribution across the fusion line of a steel weldment for Ms_{WM} (500° C) < Ms_{HAZ} (600° C) [14].

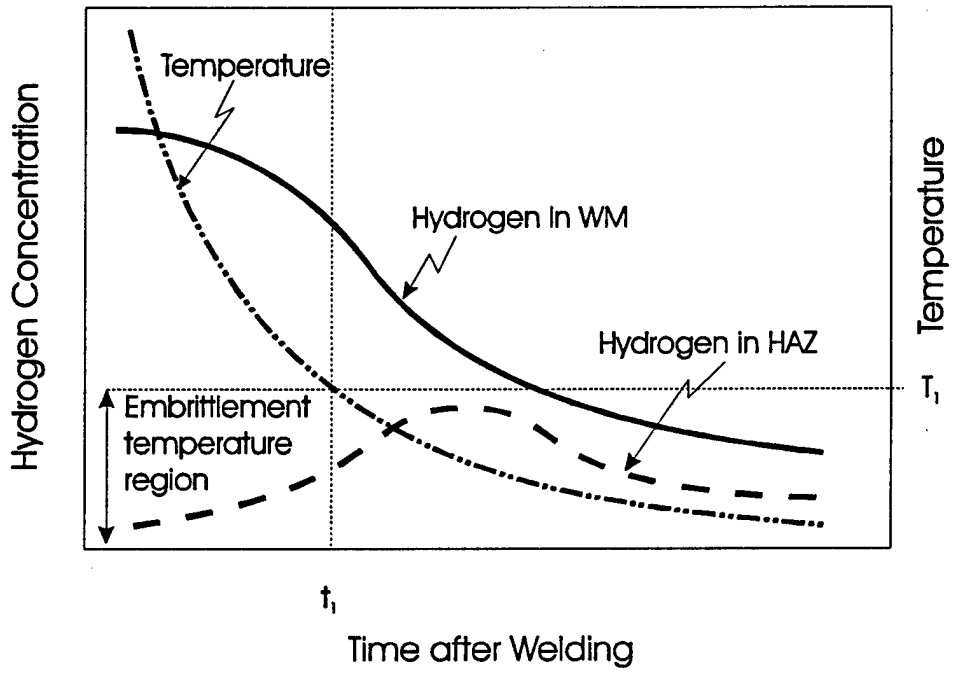

Figure 4. Variation of hydrogen concentration in the weld metal (WM) and the HAZ after completion of welding process [15]

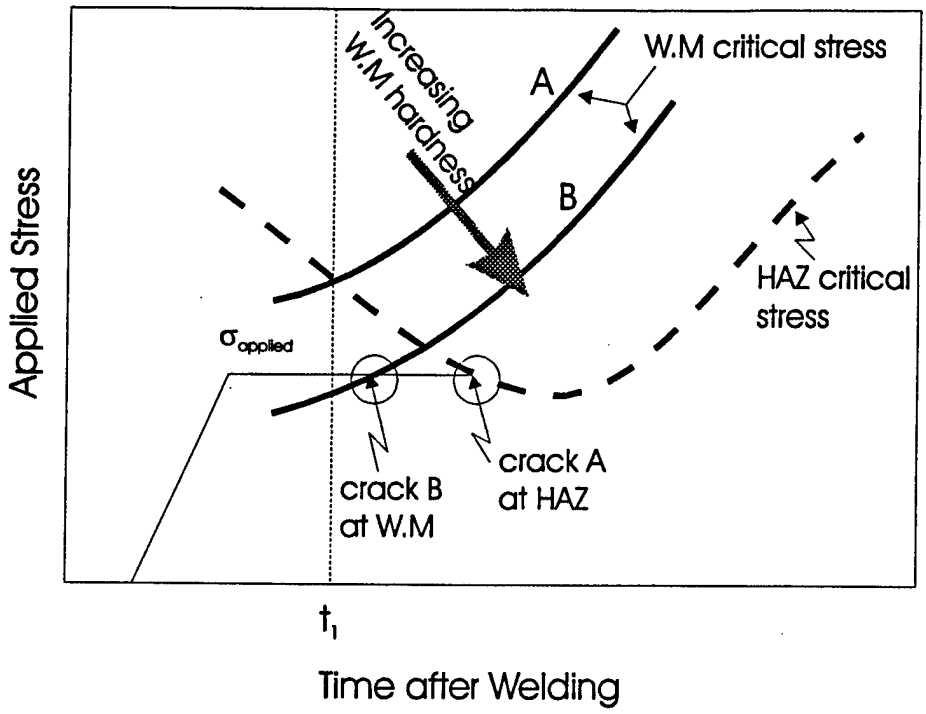

Figure 5. Variation in critical stress for HAC in weld metal (WM) and HAZ during cooling cycle. (A). low WM hardness: crack location is in HAZ. (B). high WM hardness: crack location is in WM [15].

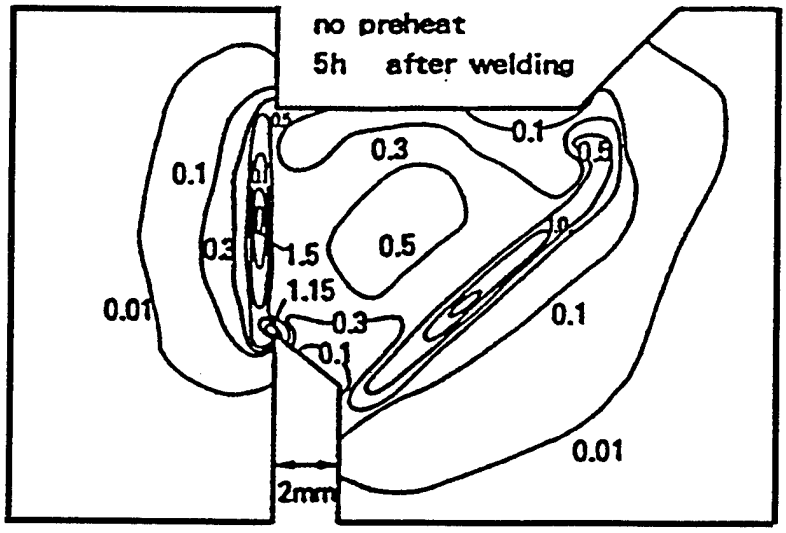

Figure 6. Distribution of hydrogen (non-dimensional concentration with respect to initial concentration in weld metal) in single bevel groove weld, 5 hrs. after welding [25,26]

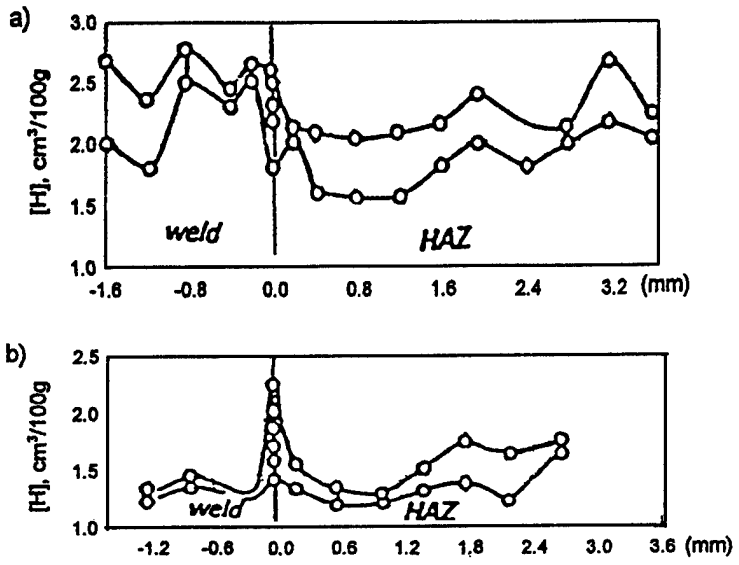

Figure 7. Distribution of hydrogen in a welded joint of 15Kh1M1F steel. (a). not heat treated after welding. (b). tempered at a high temperature (730° C) after welding [27].

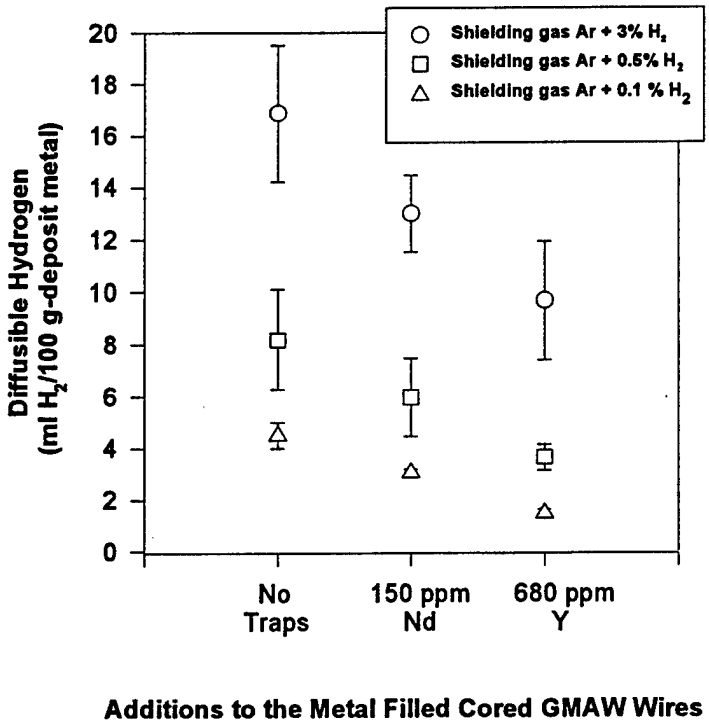

Figure 8. Effect of trap additions to the amount of diffusible hydrogen of weld samples welded with GMAW process at nominal heat input 1.5 kJ/mm [34].

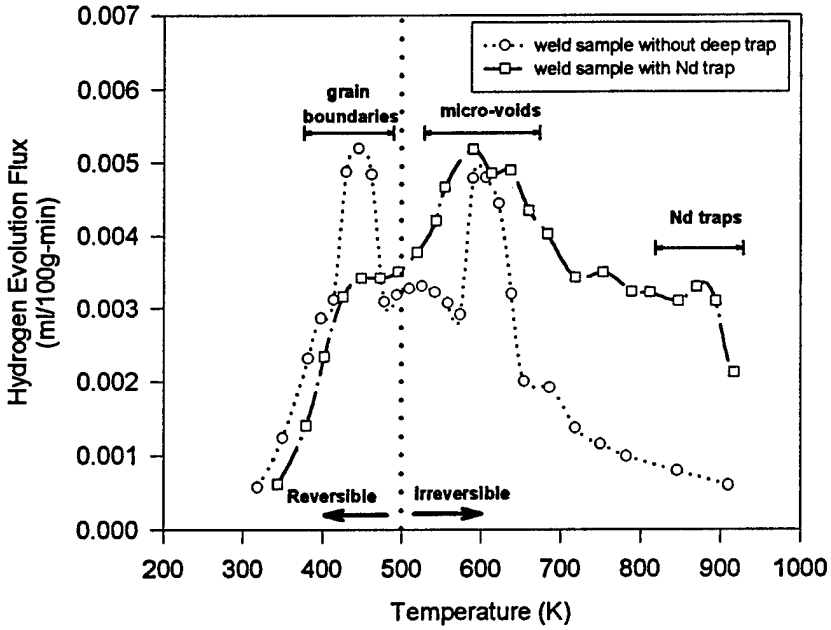

Figure 9. Hydrogen desorption at 4° C/min heating rate of iron weld sample free of deep traps and weld sample containing neodymium deep traps. The peak at 450 K is the hydrogen released from grain boundaries, at 600 K from micro-voids and at 873 K from neodymium associated trap sites [34].

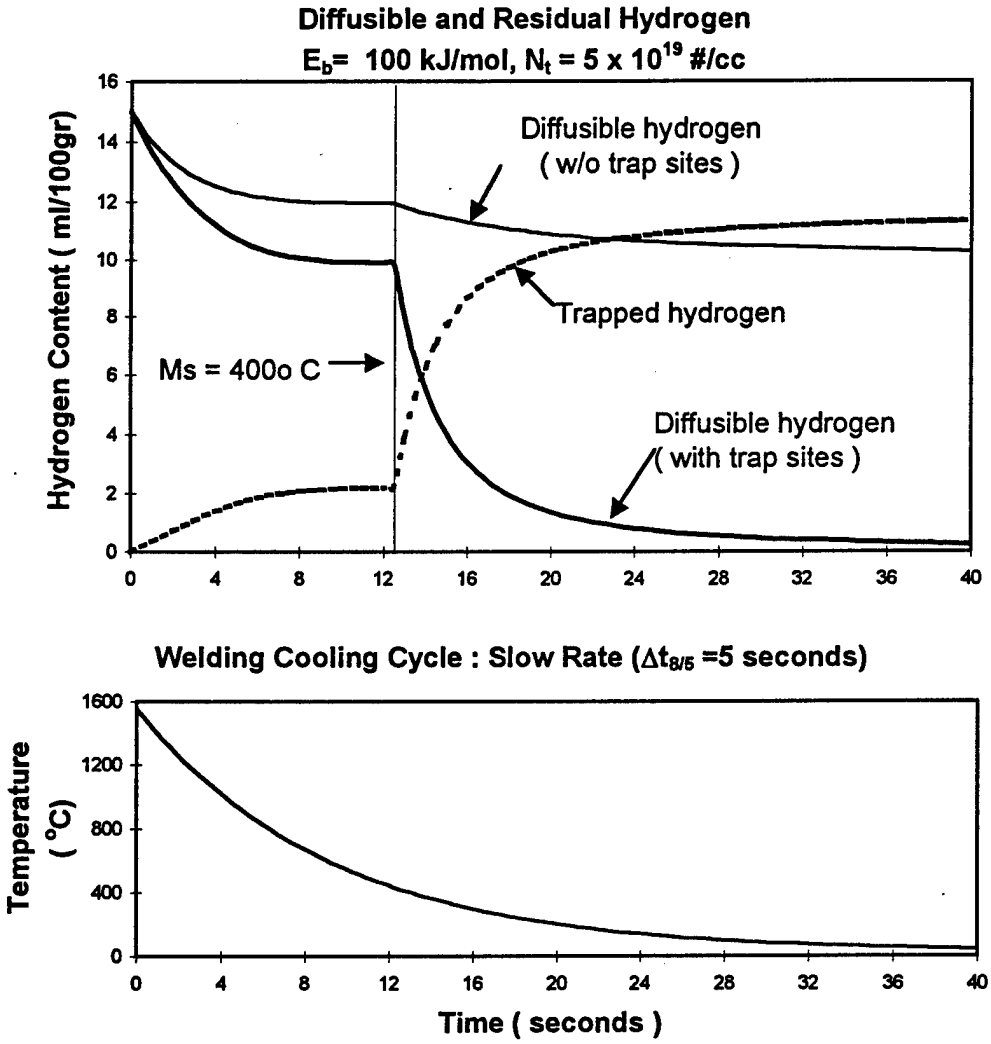

Figure 10. Theoretical evaluation on the performance of hydrogen trapping during welding cooling cycle. Initial diffusible hydrogen in the weld metal is 15 ml/100 g-deposit metal [6].

Appendix IV

Focus Officer Progress Report for the TTCP Project on Hydrogen Management in Steel Weldments for Defense Application.

"Reorganization of the Operating Tasks"

Hydrogen Management

Reorganization of the Operating Assignment Tasks

(November 25, 1997)

TTCP - Hydrogen Management

PROGRESS 1997

Significant progress has been made during 1997. The development of a new modified cruciform (WIC) test, which is very successful in detecting the propensity of transverse cracking in multipass welds, has been achieved (USA-NSWCCD and AUST-DSTO). Also a new life analysis procedure using a "fatigue intensity factor" has been developed which clearly differentiates between mechanical and hydrogen cracking affected life of steel components (USA-Army Benet Lab. and UK-Univ. of Cranfield).

The length of time necessary after repair welding before inspection for hydrogen cracking should be performed has been determined (CANADA-DREA). This repair welding information is essential to extend the life of high strength steel assemblies. Also hydrogen arc sensing during welding has been correlated to weld metal hydrogen content and shows potential of becoming an in-process hydrogen quality monitoring technique (USA USA-NSWCCD and USA-Penn. State Univ.).

An ultra low carbon bainitic (ULCB) welding wire composition which has shown very acceptable mechanical properties and welding performance has been developed and is being scaled up to production size heats for final evaluation (USA-NSWCCD). Both fluoride and weld metal hydrogen trapping additions to welding consumables have resulted in a significant reduction in weld metal diffusible hydrogen contents (USA-CSM). Similar success of the use of hydrogen traps in steel components for hydrogen management has been demonstrated (USA-Army Benet Lab.). Also analytical methods are being developed to evaluate the hydrogen content across the weld as well as the diffusible hydrogen content (USA-CSM). The hydrogen distribution is becoming a more serious issue with the use of steels of ever-increasing strength levels.

MILESTONES 1998

The significant milestones for the coming year will be the establishment of the worst case scenario for hydrogen cracking in fabrication which will be used to qualify welding consumables and practices and the development of testing criteria for measuring hydrogen cracking sensitivity in weld repair (USA-NSWCCD, AUST-DSTO, and AUST-ASC). The modeling of hydrogen cracking behavior in repair welds, which is an extension of the present work to thicker sections, will establish better guidelines for welding and inspection of higher strength steel repair welds (CANADA-DREA). The determination of the role of undermatching of the weld metal mechanical properties to that of the base metal in controlling hydrogen cracking will be established (USA-NSWCCD). The determination of the optimum content of fluoride and hydrogen trapping additions to the welding consumable to achieve reproducible low hydrogen weld deposits requiring less need for preheat and post weld heat treatments will be achieved(USA-CSM). A second Hydrogen Management in Steel Welding Conference and Workshop will be orgranized and conducted.

TASK 1

Research and Development of New Weld Hydrogen Cracking Tests

TASK 1

RESEARCH AND DEVELOPMENT OF NEW WELD HYDROGEN CRACKING TESTS

1. Longitudinal Restraint Cracking Test
   Australia-DSTO

2. Modified Gapped Bead on Plate Test
   Australia-DSTO

3. Modified WIC Test
   USA-NSWCCD

4. Measurement of K_{IEAC}
   USA-Army Benet Lab.-ARDEC

5. J-integral Fracture Toughness Test Procedures
   USA-Army Benet Lab.-ARDEC

6. Fatigue Life in Hydrogen Environments
   USA- Army Benet Lab.-ARDEC

7. To Survey Worst Case Scenario for Hydrogen Cracking in Fabrication
   Australia-DSTO
   Australia-ASC
   USA-NSWCCD

8. Develop Testing Criterion for Weld Repair
   Australia-DSTO
   Australia-ASC

9. Modeling of Electronic Bonding of Hydrogen in the Zone Ahead of Sub-critical Cracks in Ferrous Alloys
   USA-Army ARL
   USA-CSM
   Australia-DSTO

OPERATING ASSIGNMENT PTP1 - 013 (October 25, 1996)

HYDROGEN MANAGEMENT IN HIGH STRENGTH STEEL WELDMENTS FOR DEFENCE APPLICATIONS

Task 1 Research and Development of New Weld Metal Hydrogen Cracking Tests

Activity	Status	Results	Description	Organization
1. Longitudinal Restraint Cracking Test	completed	LRC tests found to be unconservative	The longitudinal restraint cracking (LRC) test was found to be unconservative. Effort has been redirected from this activity to the NSWC modified cruciform test (see Task 1 Activity 3).	Aust. - DSTO
2. Modified Gapped Bead on Plate Test	completed	Modified GBOP test was found to be unconservative despite the quench modification.	Despite the use of a "quench" to limit the removal of hydrogen, the modified GOP test was found to be unconservative.	Aust. - DSTO
3. Modified Weldability Test	in progress	Modified cruciform test successfully developed.	The NSWC modified cruciform test has been further modified by the use of 35mm plate and will be trialed using BIS 812 EMA steel. Modified WIC test being developed.	USA - NSWCCD Aust. - DSTO
4. Measurement of K_{IEAC}	in progress	See Description	K_{IEAC} tests were conducted on isothermally processed A723 steels at yield strength levels of 1275 Mpa and exhibited no significant difference in incubation times, crack growth rates, or K_{IEAC} threshold levels when compared to conventionally quenched and tempered A723 steels at identical yield strength levels. K_{IEAC} tests were conducted on quenched and tempered A723 Grade 2 steels at yield strength levels of 1130 Mpa, 1275 Mpa, 1330 Mpa, and 1380 Mpa. Hydrogen crack growth rates (da/dt) of the 1380 Mpa steel dramatically increased by approximately 1000 fold when compare to the 1130 Mpa steel.	USA - Army Benet Lab
5. J-integral fracture toughness test procedures	in progress	Small specimen J-Integral bend test has been develop and evaluated.	A simplified ASTM J-Ic fracture toughness bend test has been developed for testing small specimens from welds. An electric potential drop method is available for automated tests of H-cracking threshold or H-affected fatigue crack growth. The effects of side-grooves, comp. and heat treat on J-Ic fracture toughness and cleavage behavior of steel is being measured.	USA - Army Benet Lab

Task 1 (continued) Research and Development of New Weld Metal Hydrogen Cracking Tests

Activity	Status	Results	Description	Organization
6. Fatigue life in hydrogen environments	in progress	fatigue life test and analysis methods are being studied	A new life analysis procedure using a "fatigue intensity factor" clearly differentiates between mechanical and hydrogen cracking affected life of steel (cannon) components. This work is being conducted jointly with U.Parker (Univ. of Cranfield, UK). Causes of hydrogen cracking and control measures for cannon components are being identified, including thermal damage and associated residual stress effects on fatigue life.	USA - Army Benet Lab
7. To survey worst case scenario for hydrogen cracking in fabrication	in progress	From fabrication experience determined the design detail and working environment that represents the greatest risk of cracking	As a basis for determining the most appropriate test procedure, seek descriptions of worst case scenarios for hydrogen cracking in fabrication. The descriptions are to be circulated for comment. This activity has had involvement from the Australian Submarine Corporation's welding manager. However, he is no longer with the ASC. From experience with Collins fabrication, greatest risk is with closed tanks. Cruciform joint designs have high restraint and pose an increased risk. Most cracking occur at repairs.	Aust. - DSTO Aust. - ASC USA - NSWCCD
8. Develop testing criterion for weld repair	initiated	A reproducible test for measuring hydrogen crack sensitivity	Test piece design will incorporate a cruciform joint design. A groove of 100 to 150 mm lengths would be prepared at the crown of each weld. The groove depth should be half the throat thickness. Welding to fill the groove should be performed using candidate procedures.	Aust. - DSTO Aust. - ASC
9. Modeling of Electronic bonding of hydrogen in the zone ahead of sub-critical cracks in ferrous alloys	in progress	application of new modeling approaches	Determine relative energies of interstitials to migrate into this zone. Characterize the intraplanar bonds when interstitials are present (eg. Establish if these interstitials change the nature of these bonds by promoting/hindering crack tip propagation in this zone)	US Army - ARL

Task 1: Hydrogen Cracking Tests

Activity 1: The Longitudinal Restraint Cracking Test

Australia-DSTO

The Longitudinal Restraint Cracking Test (LRC) has been applied experimentally as a multipass hydrogen cracking test.

Results: The LRC was found to be unconservative. No cracks developed in LRC tests that were conducted under conditions that were known to produce transverse hydrogen cracks in full-scale multipass welds. Future work needs to consider increasing the length of the weld to increase the longitudinal residual stress.

Status: completed

Task 1: Hydrogen Cracking Tests

Activity 2: Modified Gapped Bead on Plate Test

Australia-DSTO

The standard Gapped Bead on Plate (GBOP) test is known to be unconservative for determining safe welding parameters for multipass welding. Yield strength level stresses are developed in the weld metal of the GBOP test specimen, however, the hydrogen concentration of a single pass is less than that which accumulates in multipass welds. An attempt was therefore made to make the GBOP test conservative by immersing the test piece in ice water 30s after the welding was extinguished. The aim of the "quench" was to decrease the rate at which hydrogen could diffuse from the test weld. During laboratory scale preheat free welding tests only the first pass is preheat free. Thereafter the temperature of the small test piece is elevated by the previous pass or passes. Subsequent passes may then be deposited soon after the first, at an elevated interpass temperature or after the piece has cooled to some low pre-defined temperature. If time is allowed for the test piece to cool then hydrogen from earlier passes will have time to diffuse from the weld and the effects of hydrogen buildup will be reduced. If a pass is deposited soon after the previous pass then the previous pass will have effectively preheated the test piece and the test is not really a test of preheat free welding. While preheating by earlier passes will also occur in a full scale structure, the effect will be reduced by the greater heat sink offered by the surrounding parent metal.

Results: Despite the "quench" treatment the test was still found to be unconservative.

Status: completed

Task 1: Hydrogen Cracking Tests

Activity 3: Modified Cruciform Test

USA-NSWCCD

Design of a modified WIC test to rapidly assess highly weldable new materials for cracking, including hydrogen cracking. The modified cruciform test has been found successful in detecting the propensity for transverse cracking in multipass welds and weld metal embrittlement (via loss of ductility in all weld metal tensile specimens). Research on the development of new hydrogen cracking test by designing a modified WIC type of test is in progress. The major differences between present practice and the modified approach being investigated is that the modified approach will use thicker plate and modified joint design to increase the thermal severity of the test. A test fixture will be developed to restrain the specimen during the test. Previously the specimen was welded to the plate. This practice required additional work to remove and inspect the specimen.

The modified specimens are being designed to evaluate both the longitudinal and transverse cracking. The specimen contains transverse and longitudinal notches to facilitate hydrogen crack initiation. The procedure involves deposition of several layers of weld beads to develop high restraint typical of multipass welding. An interpass temperature equal to the preheat temperature under investigation is being used between sets of fillet weld passes. Metallographic specimens are removed after completion of welding to inspect for cracking. All weld metal tensile specimens are also removed and tested to evaluate ductility loss.

Results: Modified cruciform test successfully developed. NSWC modified cruciform test further modified to 35 mm plate. Modified WIC test being developed.

Plans: A document describing the modified cruciform test procedures using AWS B.4 format will be prepared.

Status: in progress

Completion: 1998, Q2

Task 1: Hydrogen Cracking Tests

Activity 4: Measurement of K_{IEAC} for Higher Strength Steels

USA-Army Benet Laboratory-ARDEC

K_{IEAC} tests on A723 steels at yield strength levels between 1130 and 1275 Mpa are being performed. K_{IEAC} test is also being used to investigate isothermally processed A723 steel.

Results: K_{IEAC} tests were conducted on isothermally processed A723 steels at yield strength levels of 1275 Mpa. The isothermally processed material tested exhibited no significant difference in incubation times, crack growth rates, or K_{IEAC} threshold levels when compared to conventionally quenched and tempered A723 steels at identical yield strength levels. K_{IEAC} tests were conducted on quenched and tempered A723 Grade 2 steels at yield strength levels of 1130 Mpa, 1275 Mpa, 1330 Mpa, and 1380 Mpa. Hydrogen crack growth rates (da/dt) of the 1380 Mpa steel dramatically increased by approximately 1000 fold when compare to the 1130 Mpa steel.

Status: completed

Plans: Additional K_{IEAC} and da/dt tests will be conducted using the bolt-loaded specimen on high strength Maraging 200 and AerMet 100 steels. Also, to develop in-situ crack growth capabilities using the instrumented bolt and potential drop techniques.

Status: in progress

Completion: 1998, Q2

Task 1: Hydrogen Cracking Tests

Activity 5: J-integral Fracture Toughness Test Procedures

USA-Army Benet Laboratory-ARDEC

J-integral fracture toughness test procedures for weld applications are being investigated with emphasis on simplified test methods suitable for small specimens cut from welds. Measurements of Jic fracture toughness for cleavage in as welded 4130 steel HAZ have been made for applications to armament components.

Results: A simplified ASTM J-Ic fracture toughness bend test has been developed for testing small specimens from welds. An electric potential drop method is available for automated tests of hydrogen cracking threshold or hydrogen affected fatigue crack growth.

Plans: The effects of side-grooves, composition and heat treat on J-Ic fracture toughness and cleavage behavior of steel is being measured.

Status: in progress

Completion: 1998, Q3

Task 1: Hydrogen Cracking Tests

Activity 6: Fatigue Life Analysis in Hydrogen Environments

USA-Army Benet Laboratory-ARDEC
UK-Univ. of Cranfield

A new analysis has been described for characterizing fatigue life, including local stresses and initial crack. This work is being conducted jointly with U. Parker (Univ. of Cranfield, U. K.).

Results: A new life analysis procedure using a "fatigue intensity factor" clearly differentiates between mechanical and hydrogen cracking affected life of steel (cannon) components.

Plans: Causes of hydrogen cracking and control measures for cannon components are being identified, including thermal damage and associated residual stress effects on fatigue life.

Status: in progress

Completion: 1998, Q3

Task 1: Hydrogen Cracking Tests

Activity 7: To Survey The Worst Case Scenarios for Hydrogen Cracking in Fabrication

Australia-DSTO
Australia-ASC
USA-NSWCCD

As a basis for determining the most appropriate test procedure, descriptions of worst case scenarios for hydrogen cracking in fabrication is being sought.

Results: From fabrication experience determined the design detail and working environment that represents the greatest risk of cracking.

Plans: Descriptions are being requested and will be circulated for comment.

Status: in progress

Completion: 1998, Q2

Task 1: Hydrogen Cracking Tests

Activity 8: Development of Testing Criteria for Weld Repair

Australia-DSTO
Australia-ASC

The progressive aging of existing Naval platforms has necessitated the development of hydrogen cracking tests for weld repair. This condition potentially represents a worst case scenario for hydrogen cracking susceptibility.

Results: A reproducible test for measuring hydrogen crack sensitivity.

Plans: Identify the worst case weld repair scenarios on Naval structures and develop a test plan which will evaluate the various hydrogen cracking testing procedures to assess these repairs.

Status: in progress

Completion: 1997, Q4

Task 1: Hydrogen Cracking Tests

Activity 9: Modeling of Electronic Bonding of Hydrogen in the Zone Ahead of Sub-critical Crack in (BCC) Ferrous Alloys

USA-Army ARL
USA-CSM
Australia-DSTO

This investigation will determine the relative energies of interstitials that can migrate to the zone of sub-critical crack in ferrous alloys. It will characterize the intra planar bonds when interstitials are present (e.g. establish if these interstitials change the nature of these bonds promoting/hindering crack tip propagation in the zone).

Results: There is evidence from prior calculations (CSM - Mark Eberhart) that much understanding can be determine as to the nature of hydrogen damage from these fundamental atomic scale calculations.

Plans: Establish a research team of internationally respected investigators, both theoretical and experimental scientists, and propose the scope and work statements for this project to be submitted to the appropriate funding agencies. Dr. Genrich Krasko, US Army Research Laboratory was proposed as primary Principal Investigator.

Status: Initiated

Completion: 1999, Q2

TASK 2

Influence of Welding Parameters and Hydrogen Content on Hydrogen Cracking

TASK 2

DETERMINE RELATIONSHIP BETWEEN WELDING PARAMETERS (INCLUDING HYDROGEN CONTENT) ON MULTIPLE PASS WELD TRANSVERSE CRACKING

1. Hydrogen Induced Subcritical Cracking
   Australia-DSTO

2. Hydrogen Cracking and Heat Input
   Australia-DSTO

3. Risk Evaluation of Hydrogen Cracking
   Australia-DSTO

4. Hydrogen Arc Sensing and Modeling to Predict Weld Metal Hydrogen Content
   USA-NSWCCD
   USA-Penn. State Univ.

5. Modeling of Hydrogen Cracking Behavior in a Repair Weld
   Canada-DREA

6. Eliminate Post Weld Heat Treatment by an Electrotransport Practice
   USA-CSM

7. Characterization of Undermatched Weldments
   USA-NSWCCD
   Australia-DSTO

8. Cracking Mapping in a T-Butt Joint
   Australia-DSTO

9. Hydrogen Contents in Multipass Welds
   UK-DERA

Task 2 Determine Relationship Between Welding Parameters (hydrogen content) on Multiple Pass Weld Transverse Cracking

Activity	Status	Results	Description	Organization
1. Hydrogen -induced subcritical cracking	in progress	Specimens have been prepared, tests to begin in Oct. '97.	All weld metal specimens have been prepared from E120-S submerged arc weld metal. However, progress on this activity has been limited. Consequently extra manpower was devoted to this activity. Testing will begin in Q4, 1997.	Aust. - DSTO
2. Hydrogen cracking and heat input	in progress	High heat input welds crack at lower 'critical hardness' levels than lower heat input welds.	A test matrix wad conducted to determine the effect of heat input on hydrogen induced cracking. It was found that the resistance to hydrogen induced cracking is higher at higher heat input but that at high HI and low preheat HIC may occur in weld metal with moderately low hardness levels.	Aust. - DSTO
3. Risk evaluation of hydrogen cracking	completed	No significant evidence of cracking	An experimental test section was welded using a wide range of welding techniques and procedures. Little evidence of cracking was found.	Aust. - DSTO
4. Hydrogen arc sensing and modeling to predict weld metal hydrogen content	in progress	Model is being developed to allow prediction of weld metal hydrogen content	The arc-sensing model will be extended to determine weld pool shape and time-temperature profiles associated with GMA welding. Currently, relationships between weld metal microstructures and toughness are being established. Hydrogen distribution and migration from the welding plasma to the solidified weld metal is being modeled. The model is being developed for GMA welding and will incorporate feed metal and resulting papilla characteristic of GMAW. The model utilized spectrographic data supplied by the hydrogen sensor to establish the initial hydrogen species in the plasma.	USA - NSWCCD

Task 2 (continued) Determine Relationship between Hydrogen Content and Multipass Weld Transverse Cracking

Activity	Status	Results	Description	Organization
5. Modeling of hydrogen cracking behavior in a repair weld	initiated	Extension of work to 12mm being considered	Determination of the length of time necessary after repair welding before inspection for hydrogen cracking should be performed	Canada - DREA
6. Eliminate Post weld heat treatment by a electrotransport practice	in progress	with use of homopolar generator it may be possible to treat thick section materials	The concept of using electrotransport to reduce diffusible hydrogen levels was evaluated using transport calculations. The application of electrotransport during the welding thermal cycle maybe useful in reducing hydrogen cracking susceptibility in large structural components. Discussions in progress with the electromechanics laboratory of Univ. of Texas.	USA - CSM
7. Characterization of undermatched weldments	in progress	potential for reduction or elimination of preheat	The use of undermatching weld metal may improve productivity of welding high strength steels by reduction or elimination of preheat	USA - NSWCCD
8. Crack Mapping in a T-butt joint (New Activity)	initiated	Serial 'sections' through a T-butt joint to map crack locations in the weld and HAZ	A T-butt joint was welded using conditions known to produce HIC. Three-dimensional cracking frequency is measured throughout the joint by milling down through the joint and inspecting at 2mm intervals.	Aust. - DSTO
9. Hydrogen Content in Multipass Welds	initiated	Extension of works to understand weld hydrogen contents	Determination of the influence of multiple thermal experience due to multipass welding on the resulting diffusible hydrogen content	UK - DERA

Task 2; Influence of Welding Parameters and Hydrogen Content on Hydrogen Cracking

Activity 1: The Relationship Between Hydrogen Content and The Susceptibility to Hydrogen Cracking

Australia-DSTO

An experimental technique has been developed to determine the relationship between the hydrogen induced sub-critical crack growth rate and both the microstructural constituents and diffusible hydrogen content.

Results: Specimens have been prepared, tests to begin Oct., '97.

Plans: The trial will be extended to include an E120S filler metal.

Status: in progress

Completion: 1998, Q3

Task 2: Influence of Welding Parameters and Hydrogen Content on Hydrogen Cracking

Activity 2: Hydrogen Cracking and Heat Input

Australia-DSTO

The influence of heat input on hydrogen cracking has been investigated for a submerged arc consumable.

Results: High heat input welds crack at lower 'critical hardness' levels than lower heat input welds.

Plans: work continuing

Status: in progress

Completion: 1998, Q3

Task 2: Influence of Welding Parameters and Hydrogen Content of Hydrogen Cracking

Activity 3: Risk Evaluation of Hydrogen Cracking

Australia-DSTO

Control of weld metal hydrogen cracking in a 690 MPa yield strength steel during Australian submarine construction is an essential requirement. To evaluate the risk of hydrogen cracking and embrittlement, an experimental submarine section (7.8 m diameter, 2,4 m long, containing five stiffening ring frames) was fabricated using "high" carbon equivalent electrodes (Pcm= 0.283 versus typical values of 0.26) and a wide range of welding procedures. The effect of carbon content on cracking risk was also examined. The welds were examined both non-destructively and destructively.

Results: No significant evidence of cracking was found. An increase in carbon content from 0.07 to 0.10 wt. Pct. was found to have little effect on yield stress. Assessment of welds in a test fabrication showed that a wide range of techniques and procedures could be used without a risk of cracking.

Status: completed

Task 2: Influence of Welding Parameters and Hydrogen Content on Hydrogen Cracking

Activity 4: Hydrogen Arc Sensing and Modeling to Predict Weld Metal Hydrogen Content

USA-NSWCCD
USA-Penn. State Univ.

The arc-sensing model will be extended to determine weld pool shape and time-temperature profiles associated with GMA welding. Currently, relationship between weld metal microstructures and toughness are being established.

Hydrogen distribution and migration from the welding plasma to the solidified weld metal is being modeled. The model is being developed for GMA welding and will incorporate feed metal and resulting papilla characteristic of GMAW. The model utilized spectrographic data supplied by the hydrogen sensor to establish the initial species in the plasma.

Results: Hydrogen emissions data was used to predict diffusible hydrogen test results using the Penn. State Univ. model. A cylindrical heat source has been developed for model development. The cylindrical heat source produced a papilla consistent with GMAW.

Plans: The weld pool shapes and resulting thermal profiles will be validated. The effect of variations in welding parameters will be evaluated.

Status: in progress

completion: 1998, Q4

Task 2: Influence of Welding Parameters and Hydrogen Content on Hydrogen Cracking

Activity 5: Modeling of Hydrogen Cracking Behavior in Repaired welds

Canada-DREA

The question of how long after repair welding inspection for hydrogen cracking should be delayed is being examined by modeling and experiments. Dr. Lalit Malik of Fleet Technology and Dr, Brian Graville of Graville Associates have received a DREA research contract to address this question. Numerical modeling is being done to estimate the temperature history, hydrogen diffusion/distribution and thermal/residual stresses generated as a result of a multipass repair weld. Experiments are being done to determine the critical local hydrogen concentration for causing cracking for a given stress and microstructure. Essentially the experiments will allow the model to be calibrated for crack prediction. Experiments and modeling will focus on 9 mm thick A517 grade F steel, welded with E11018 electrodes. The critical hydrogen content for causing cracking for a give stress and hydrogen content will be determined by: placing a Charpy V notch in the heat affected zone of a multipass single V weld; gouging out part of the top of the weld, and rewelding, (simulating a repair weld); heat treating, if necessary, to cause some redistribution of hydrogen; and loading the specimen and determining if and when, crack growth occurs.

Results: High group interest in this project. Work in progress. Published report on "Delayed Cracking in Naval Structural Steels", by L.N. Pussegoda, B.A. Granville, and L. Malik, Report No. CR97/420, National Defence Research and Development, Canada.

Status: in progress

Completion: 1998, Q2

Task 2: Influence of Welding Parameters and Hydrogen Content on Hydrogen Cracking

Activity 6: Use of electrotransport to Reduce Diffusible Hydrogen Content

USA-CSM

The concept of using electrotransport to reduce diffusible hydrogen levels was evaluated using transport calculations.

Results: The application of electrotransport during the welding thermal cycle may be useful in reducing hydrogen cracking susceptibility in small technical assemblies that might otherwise experience distortion or unacceptable microstructural changes as a result of conventional post weld heat treatment.

Due to the requirement of excessively high current, if electrotransport methods are to be applied to heavy section weldments, this technique initially appeared useful for only small weldments such as those found in precision assemblies. Discussions are in progress with the Center of Electromechanics of the Univ. of Texas to set an industrial demonstration project to illustrate that homopolar power sources can produce sufficient current and are portable enough to work in combination with the welding practice associated with heavy section weldments.

Status: in progress

Completion: 1998, Q3

Task 2: Influence of Welding Parameters and Hydrogen Content on Hydrogen Cracking

Activity 7: Characterization of Undermatched Weldments

USA-NSWCCD
Australia-DSTO

The use of undermatching weld metals may improve productivity of welding high strength steels by reduction or elimination of preheats.

Plans: The scope and work statements will be defined and work will proceed.

Status: in progress

Completion: 1998, Q4

Task 2: Influence of Welding Parameters and Hydrogen Content on Hydrogen Cracking

Activity 8: Crack Mapping in a T-butt joint

Australia-DSTO

A T-butt joint was welded using conditions known to produce HIC. Three-dimensional cracking frequency is measured throughout the joint by milling down through the joint and inspecting at 2mm intervals.

Results: Serial "sections" through a T-butt joint to map crack locations in the weld and HAZ

Plans: The results are being evaluated.

Status: in progress

Completion: 1998, Q4

Task 2: Influence of Welding Parameters and Hydrogen Content on Hydrogen Cracking

Activity 9: Hydrogen Content in Multipass Welds

UK-DERA

Determination of the influence of multiple thermal experiences due to multipass welding on resulting hydrogen content.

Plans: Searching for collaboration.

Status: initiated

Completion: 1999, Q4

TASK 3

Development of High Strength Steel Filler Metals

TASK 3

DEVELOP HIGH STRENGTH STEEL FILLER METALS TO BE USED WITHOUT PREHEAT

1. Preheat Free MMA and FCA Welding Consumables
   Australia-DSTO
   Australia-CISRO-DMT

2. Development of ULCB Wires
   USA-NSWCCD

3. ULCB Wire Evaluation
   USA-NSWCCD

4. Evaluation of ULCB MCAW Consumables
   USA-NSWCCD

5. Fluoride Additions to Control Weld Hydrogen Content
   USA-CSM

6. Austenite Decomposition Temperature as Hydrogen Cracking Indicator
   USA-CSM
   USA-NSWCCD

7. Multiple Pass Weld Metal Properties Cooperative Project
   Australia-CISRO
   USA-CSM

8. Reduction of Diffusible Hydrogen Through The Use of Weld Metal Traps
   USA-CSM
   USA-Lincoln Electric

9. Analytical Methods to Evaluate Weld Hydrogen Distribution
   USA-CSM
   USA-SUNY Albany

Task 3 Develop High Strength steel filler metals to be used without preheat.

Activity	Status	Results	Description	Organization
1. Preheat free MMA and FCA Welding Consumables	in progress	Excessive oxygen levels in experimental Ni-Mn-Mo weld metals have resulted in unsatisfactory toughness.	Satisfactory tensile results were obtained for experimental Ni-Mo-Mn, low C, FCA and MMA consumables. Charpy results were variable. For FCA Charpy results were satisfactory/ marginal with O slightly high at 0.04 wt%. For MMA weld metals, Charpy results were unsatisfactory with a high O level of 0.06 wt%. New iteration is focussing on higher Mn and lower O. New MMA chemistry has C ultralow at 0.01 wt%.	Aust. - DSTO
2. Development of ULCB Wires (80-130 ksi yield strength)	in progress	Quantit. relationships developed between composition, transform. temp., cooling rate, grain size, and resulting mechanical properties.	Chemical analyses, microstructural evaluation, transformation studies, and mechanical property assessments performed on several ULCB welds. Statistical evaluation of resulting data identified composition, cooling rate, transformation temperature, and grain size as factors controlling mechanical properties. Regression equations describing these relationships are being developed and refined.	USA - NSWCCD
3. ULCB Wire Evaluation (80 ksi yield strength)	in progress	Evaluation of 14 experimental solid wires is completed. Several wires have met requirements. Testing of new matrix of 4 experimental wires is underway.	Mechanical property and weldability evaluations of 4 experimental wires are underway. Wire designs were based on results obtained from previous 14 experimental wires. Explosion crack starter testing will be performed on the best of these four wires. If testing is successful, a prototype production heat will be produced and evaluated.	USA - NSWCCD
4. Evaluation of ULCB MCAW consumables	in progress	Continuation of ULCB wire investigation	This task will evaluate 4 MCAW wires produced to meet weld deposit chemistries specified by NSWCCD	USA - NSWCCD
5. Fluoride additions to control weld hydrogen content	initiated	Theo. & experimental evidence has demonstrated the use of fluoride addition and can achieve low diffusible H contents.	Use of fluoride and optimal amounts of oxygen introduced to the welding plasma to control weld hydrogen content is being evaluated.	USA - CSM

6. Austenite decomposition temperatures as hydrogen cracking indicator	in progress	Preliminary results suggest value of using M_S temperatures	M_S temperatures were shown to delineate cracking tendencies of high strength steels in hydrogen environment. The difference in MS temperatures of base metal and weld metal can indicate whether cracking will occur in the weld or HAZ. The successful application of MS temperatures as a cracking induces results from the large differences in hydrogen solubility and diffusion coeff. between ferrite (martensite) and austenite.	USA - CSM USA - NSWCCD
7. Multiple pass weld metal properties cooperative project	in progress	Information is being exchanged	A cooperative research project between CSIRO and CSM is in progress to better understand the influence of alloying additives on the microstructural and mechanical properties of weld metal for shielded arc welding processes. The work is proceeding at each institution and visitations have been made to share data, to discuss alloying and thermal processing models, and to design needed experiments.	Aust - CSIRO USA - CSM
8. Reduction of diffusible hydrogen through the use weld metal hydrogen traps	in progress	Yttrium ferroadditions can make significant reductions in diffusible hydrogen	The use of weld metal hydrogen traps to reduce the available diffusible hydrogen content is being investigated.	USA - CSM USA – Lincoln Elect.
9. Analytical method to evaluate weld hydrogen distribution	initiated	Methods to measure weld hydrogen distribution are being evaluated. A stick-on tape with an electronic sensor for measuring diffusible hydrogen appears possible.	A number of methods have been used to demonstrate that the weld hydrogen content is not uniform in its distribution but has localized high contents which should be of major concern to the integrity of high strength steel welds. These localized hydrogen contents are most likely the cause in the spread of the measured hydrogen cracking results in welds that have acceptably low measured diffusible hydrogen contents.	USA - CSM

Task 3: Development of High Strength Steel Filler Metals

Activity 1: Preheat Free MMA and Flux Cored Arc Welding Consumables

Australia-DSTO
Australia-CISRO-DMT

The review of the status of preheat free consumables is continuing. Experimental MMA and FCA consumables, each at two different composition levels have been received from DMT/CSRRO, Adelaide.

Results: The first batch of consumables has been received. The all weld metal compositions for the two FCA consumables were:

Elements (wt, pct.)	A (600-690 MPa yield)	B (700-800 MPa yield)
C	0.04	0.04
Mn	1.6	1.01
Si	0.16	0.17
Ni	2.9	5.6
Mo	0.54	0.73
Ti	0.004	0.005
Cr	0.01	0.27
Al	0.009	0.011

Excessive oxygen levels in experimental Ni-Mn-No weld metals have resulted in unsatisfactory toughness.

Plans: Evaluation of weld metal properties, viz. all weld metal tensile, transverse tensile, Charpy toughness and metallography is about to commence. The next stage involves a new iteration of consumable compositions after discussions with NSWCCD. Obtaining core material of very low carbon content (0.02 wt, pct.) has been identified as a critical issue and this need will be pursued concurrently with the new iteration of compositions.

Status: in progress

Completion: 1998, Q4

Task 3: Development of High Strength Steel Filler Metals

Activity 2: Development of Ultra Low Carbon Bainite (ULCB) Wires

USA-NSWCCD

Development of Ultra Low Carbon Bainite (ULCB) wires (80-130 ksi yield strength). Chemical analyses, microstructural evaluation, transformation studies, and mechanical property assessments were performed on several ULCB welds. Statistical evaluation of resulting data identified composition, cooling rate, transformation temperature, and grain size as factors controlling mechanical properties. Regression equations describing these relationships are being developed and refined.

Results: Welds have been fabricated with various shielding gases and welding thermal cycles to produce weld metal of various oxygen and nitrogen contents and grain sizes. Work is progressing in thoroughly characterizing these weld metals.

Plans: work in progress

Status: in progress

Completion: 1998, Q2

Task 3: Development of High Strength Steel Filler Metals

Activity 3: Ultra Low Carbon Bainite Wire (80 ksi yield strength) Evaluation

USA-NSWCCD

Evaluation of 14 experimental solid wires is completed. Several wires have met requirements. Mechanical property and weldability evaluation of 4 experimental wires is underway. Wire designs were based on results obtained from previous 14 experimental wires. Explosion crack starter testing will be performed on the best of these four wires. If testing is successful, a prototype production heat will be produced and evaluated.

Results: work is in progress.

Plans: continuation of mechanical property and weldability evaluations. Determination of optimal chemical compositions using neural network analysis is in progress.

Status: in progress

Completion: 1998, Q2

Task 3: Development of High Strength Steel Filler Metals

Activity 4: Evaluation of ULCB MCA Welding Consumables

USA-NSWCCD

This activity will evaluate four MCA welding wires produced to meet weld deposit compositions specified by NSWCCD.

Results: work initiating

Plans: four selected MCA wire compositions will be prepared into welding wire and evaluated.

Status: initiated

Completion: 1998, Q3

Task 3: Development of High Strength Steel Filler Metals

Activity 5: Use of Fluorine and Optimal Oxygen Additions to the Welding Plasma to Assist in Hydrogen Management

USA-CSM

The use of selected fluoride and oxide additions to welding consumables to promote a plasma chemistry that reduces the weld pool hydrogen content is being investigated.

Results: Effective use of the water and HF reactions in the plasma to reduce weld pool hydrogen content has been demonstrated. Various fluoride additions are being added to the electrode covering and the resulting welds are being evaluated. Fluorides are being carefully selected based on their physical stability and their predicted pyrochemical behavior.

Further characterization of the influence of specific fluoride additions on the resulting diffusible hydrogen content has been performed. With the determination of the most promising fluoride additions more extensive evaluation will be preformed to determine the optimum fluoride content and weld metal oxygen content necessary for various sets of welding parameters. Diffusible hydrogen contents have been dropped from 5 ml/100 gram of Fe to 1.5 ml/100 gram of Fe. A significant reduction. The best fluorides determined from present effect are $AlSiF_2$ and K_3AlF_6.

Status: in progress

Completion: 1998, Q3

Task 3: Development of High Strength Steel Filler Metals

Activity 6: Use of Austenitic Decomposition Start Temperatures to Predict Weld Hydrogen Distribution and Cracking Behavior

USA-CSM
USA-NSWCCD

A practice of comparing calculated austenitic decomposition start temperatures of the base metal and weld metal to predict the hydrogen distribution and cracking behavior of high strength steel welds has been demonstrated. The practice uses the differences of the calculated martensite temperatures to predict whether cracking will occur in the weld or heat affected zone. The successful application of this indicator results from the large differences in hydrogen solubility and diffusion coefficient between ferrite (martensite)and austenite.

Results: Preliminary results indicate that this analytical approach can qualitatively make predicts of weld hydrogen behavior.

Plans: Efforts to refine this proposed practice will proceed. Work will expand the range of steel compositions of both plate materials and welding consumables used in this analysis to achieve more quantitative correlation. The thermomechanical simulator (Gleeble) will be used to determine measured austenitic decomposition start temperatures for the various high strength steel plates and weld deposits (welding consumables) of interest. Efforts will be made to promote welding consumable manufacturers to test this proposed practice.

Status: in progress

Completion; 1998, Q3

Task 3: Development of High Strength Steel Filler Metals

Activity 7: Multipass Weld Metal Properties

Australia-CISRO
USA-CSM

A cooperative research project between CISRO and CSM is in progress to better understand the influence of alloying additives on the microstructural and mechanical properties of weld metal for flux and metal cored welding. The work is proceeding at each institution and visitations have been made to share data, to discuss alloying and thermal processing models, and to design needed experiments.

This project is a strategic study in which the influence of well controlled additions of alloying and microalloying elements to experimental gas-shielded cored welding wires will be investigated. Major aspects of the project include martensite of cored consumables from high purity materials and assessment of details of the welds from these consumables with regard to mechanical properties, microstructure development and influence of non-metallic inclusions.

Results: Consumables are being made and weld properties are being characterized. The following data is from CISRO efforts.

Status: work in progress

Conclusion: 1998, Q3

Task 3: Development of High Strength Steel Filler Metals

Activity 8: Use of Weld Metal Traps for Hydrogen Management

USA-CSM
USA-Lincoln Electric

The use of weld metal hydrogen traps to reduce the available diffusible hydrogen content is being investigated. From literature reported and theoretically calculated binding energy values calculations have been made to assist in the selection of the most promising ferroadditions to be added to welding consumables.

Results: Selected ferroadditions of various transition metals and rare earths were made by CSM. Lincoln Electric Company has made metal filled cored wires with these additions at various content levels. A reproducible method to introduce specific hydrogen content into the weld metal was developed to allow for the evaluation of this concept of hydrogen management. An analytical arrangement and procedures to measure the hydrogen evolution rate as a function of weldment have been set up. Efforts have begun to measure the effectiveness of the Lincoln Electric produced experimental (with trapping additions) consumables. Preliminary results have shown drops in the diffusible hydrogen content due to trapping. Lincoln Electric is currently working on analyzing the recovery of ferroaddition to the wire. As soon as this recovery is known, another set of experimental wires can be made. Yttrium ferroadditions have demonstrated the most significant reduction in diffusible hydrogen content.

Plans: The investigation will continue with a thorough hydrogen analysis of the Lincoln Electric prepared consumables. The weld metal microstructure will be characterized to determine the type, size, size distribution and amount of weld metal traps. It is anticipated that after this first phase is completed another set of experimental consumables will be made using the addition that demonstrated the most promise. The second set of consumables should allow for optimization of content of the consumable trapping addition, weld metal oxygen content, and alloying contents for a specific welding heat input range.

Status: in progress

Completion: 1998, Q3

Task 3: Development of High Strength Steel Filler Metals

Activity 9: Analytical Methods to evaluate Weld Hydrogen Distribution

USA-CSM
USA-SUNY-Albany

The hydrogen distribution in a weld becomes significantly more important as the acceptable diffusible hydrogen contents decrease.
With the ever increasing use of steels of higher strength analytical techniques need to be developed to measure hydrogen distribution across the weld. These localized hydrogen contents are most likely the cause in the spread of the correlation between the measured diffusible hydrogen contents and cracking tendencies. A number of methods are being explored to measure hydrogen distributions. These methods included laser induced breakdown spectroscopy (LIBS), hydrogen exposure to silver bromide coatings, laser ablated gas chromatography, hydrogen changing the electrical conductivity of W_3O coatings, and MeV ion Beam Analysis.

Results: Preliminary results have successfully measured hydrogen distributions. The W3O oxide coating conductivity concept shows promise of attaching adhesive electrical device to read diffusible hydrogen directly from welded components.

Plans: Efforts will be made to develop an analytical practice to supplement the information presently reported by the costly and time consuming diffusible hydrogen measurements.

Status: in progress

Completion: 1999, Q3

ID	Task ID#	Task Description	Old Task ID
1	1.0 Task 1	R&D of New Weld H-Cracking Tests	NA
2	1.1 Task 1 Activity 1	Longitudinal Restraint Cracking Test	Task 4-1
3	1.2 Task 1 Activity 2	Modified Gapped Bead on Plate Test	Task 4-2
4	1.3 Task 1 Activity 3	Modified WIC Test	Task 4-3
5	1.4 Task 1 Activity 4	Measurement of KIEAC	Task 4-4
6	1.5 Task 1 Activity 5	J-integral fracture toughness procedures	Task 4-5
7	1.6 Task 1 Activity 6	Fatigue life in H-environments	Task 4-6
8	1.7 Task 1 Activity 7	Worst case scenario for H-cracking in fabrication	NA
9	1.8 Task 1 Activity 8	Develop Testing criterion for weld repair	NA
10	1.9 Task 1 Activity 9	Modelling of electronic bonding of hydrogen	NA
11	2.0 Task 2	Weld param. on multi-pass transverse cracking	NA
12	2.1 Task 2 Activity 1	Hydrogen induced subcritical cracking	Task 67-1
13	2.2 Task 2 Activity 2	Hydrogen cracking and heat input	Task 67-3
14	2.3 Task 2 Activity 3	Risk evaluation of hydrogen cracking	Task 67-4
15	2.4 Task 2 Activity 4	Hydrogen arc sensing and modelling	Task 67-5
16	2.5 Task 2 Activity 5	H-cracking behaviour in a repair weld	NA
17	2.6 Task 2 Activity 6	electrotransport practice	Task A-6
18	2.7 Task 2 Activity 7	Charact. of undermatched weldments	NA
19	2.8 Task 2 Activity 8	Crack Mapping in T-Butt Joint	NA
20	2.9 Task 2 Activity 9	Hydrogen Content in Multipass Welds	NA
21	3.0 Task 3	HS-steel filler metals to be used without preheat	NA
22	3.1 Task 3 Activity 1	Preheat free MMA & FCA Welding Consumables	Task A-1
23	3.2 Task 3 Activity 2	Development of ULCB wires	Task A-2,3
24	3.3 Task 3 Activity 3	ULCB wire evaluation	NA
25	3.4 Task 3 Activity 4	Evaluation of ULCB MCAW consumables	NA
26	3.5 Task 3 Activity 5	Fluorite additions to control weld H-content	NA
27	3.6 Task 3 Activity 6	Aust. decomposition T as H-cracking indicator	Task 4-7

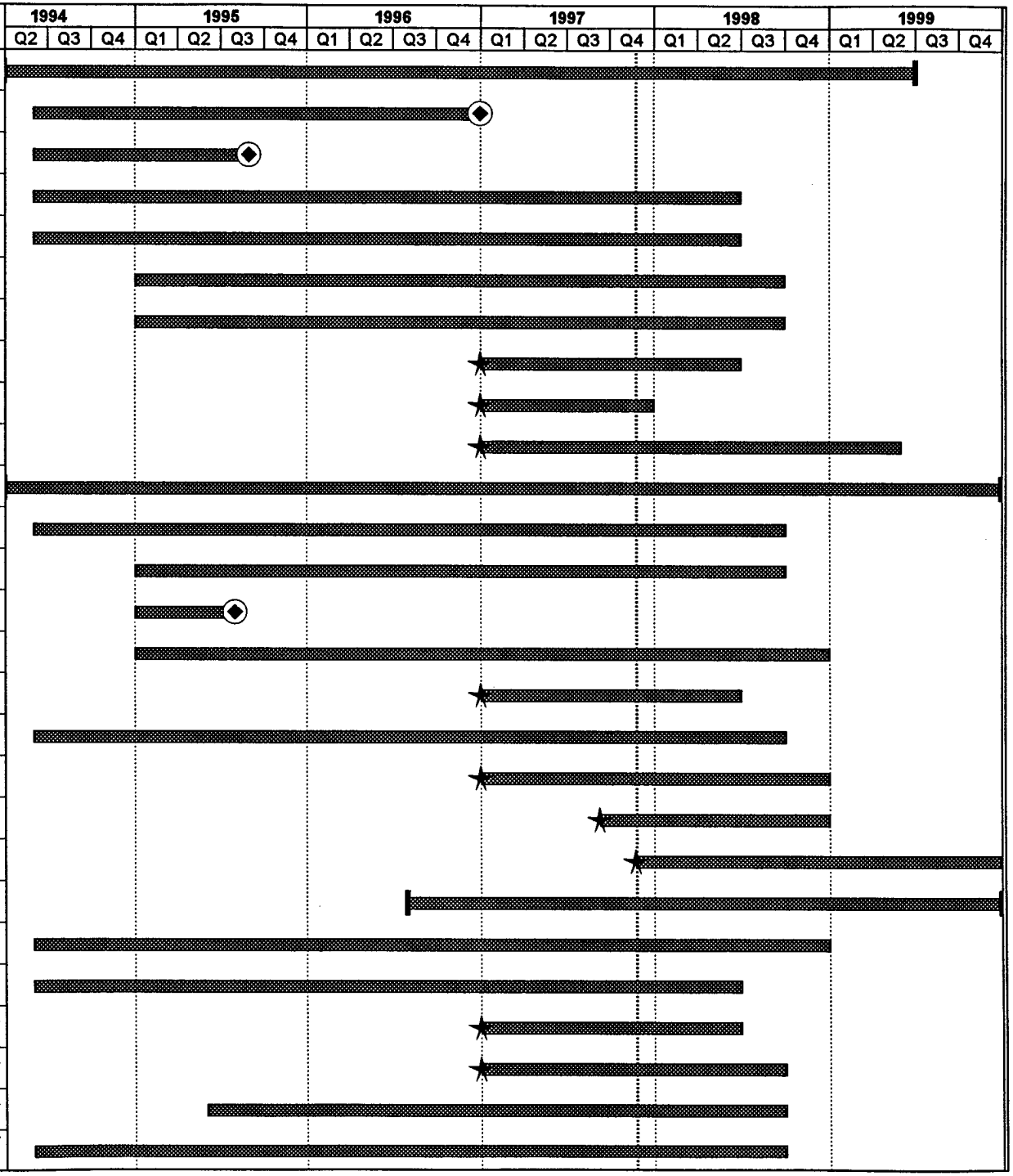

ID	Task ID#	Task Description	Old Task ID
28	3.7 Task 3 Activity 7	Multi-pass weld metal prop. cooperative project	Task 4-8
29	3.8 Task 3 Activity 8	Reduct. of Diff.-H thru the use weld metal H-traps	Task 67-8
30	3.9 Task 3 Activity 9	Anal. method to evaluate weld H-distribution